



University  
of Glasgow

McLeod, Faye Christine (2012) *The role of MeCP2 in activity-dependent brain processes*. PhD thesis.

<http://theses.gla.ac.uk/3747/>

Copyright and moral rights for this thesis are retained by the author

A copy can be downloaded for personal non-commercial research or study, without prior permission or charge

This thesis cannot be reproduced or quoted extensively from without first obtaining permission in writing from the Author

The content must not be changed in any way or sold commercially in any format or medium without the formal permission of the Author

When referring to this work, full bibliographic details including the author, title, awarding institution and date of the thesis must be given

# **The role of MeCP2 in activity-dependent brain processes**

Faye Christine McLeod  
BSc.

Thesis submitted in fulfilment of the requirements for the degree of Doctor of  
Philosophy

Institute of Neuroscience and Psychology  
College of Medical, Veterinary and Life Science  
University of Glasgow  
Glasgow, G12 8QQ  
UK

September 2012

© FC McLeod

## Abstract

Rett syndrome (RTT) is a neurodevelopmental disorder that is caused by mutations in the X-linked gene *MECP2* and results in cognitive impairment, epilepsy and motor dysfunction. Deletion or silencing of *Mecp2* in the brain of mice recapitulates many of the main phenotypes of the disorder and has been fundamental in understanding the actions of MeCP2 although the precise molecular function remains unknown. MeCP2 is classically thought to have a role in repressing gene transcription through recruitment of histone deacetylase proteins. Studies have also shown that *Mecp2* can be modified posttranslationally in response to neuronal activity.

The aim of this thesis was to investigate the activity-dependent alterations in MeCP2 and the association this has with levels of acetylated histone proteins, a marker of active gene transcription thus gaining a better insight into how neuronal activity affects the function of MeCP2. Furthermore at the network level, a second objective was to characterise the effects loss of functional MeCP2 has on the regulation of network circuitry in the brain and in particular the development of epileptiform activities. To study this I focussed on the hippocampus in wild-type and *Mecp2* mutant mice and *in vivo* administered the convulsant drug kainic acid (25mg/kg; IP) followed by seizure scoring and *in vitro* by application of various epileptogenic agents (kainic acid, bicuculline and 4-aminopyridine) to acute hippocampal slices. Having characterised the network properties, I then quantified protein alterations in phosphorylation of *Mecp2*, acetylated histone H3 and H4 and immediate early genes, c-Fos and Egr-1 in the hippocampus using western blot and quantitative immunohistochemistry techniques.

Based on a modified seizure scale (eight stages with lower being less severe), administration of kainic acid *in vivo* to *Mecp2*-deficient male mice resulted in a higher seizure score (mean =  $6 \pm 0.7$  vs.  $4 \pm 0.2$  units in wild-type) and more rapid onset (77% of mice show seizures after 10 minutes compared to 5% of wild-type mice). Field recording data collected *in vitro* following application of kainic acid to hippocampal slice from *Mecp2*-deficient mice show a significant increase in gamma power oscillation ( $1059 \pm 379\mu V^2$ ) compared to slices from WT mice ( $287 \pm 178\mu V^2$ ) which had a lower mean power. Application of bicuculline

revealed hippocampal slices from *Mecp2*-deficient mice had increased frequency of spontaneous epileptiform field events (1 $\mu$ M and 3 $\mu$ M bicuculline) and elevated duration of spontaneous and evoked epileptiform field events (10 $\mu$ M bicuculline). Similarly, 4-aminopyridine (4-AP) administration to hippocampal slices resulted in *Mecp2*-deficient mice displaying increased frequency of spontaneous field events (50 $\mu$ M 4-AP) and epileptic ictal-like events (88% of slices from *Mecp2*<sup>stop/y</sup> mice displayed these events compared to 43% of slices from WT mice). Furthermore there was an increase in spontaneous and evoked field events following application of 30 $\mu$ M and 10 $\mu$ M 4-AP.

Western blot experiments using hippocampal extracts from WT and *Mecp2*-deficient male mice treated with the convulsant drug kainic acid or saline (vehicle control) revealed *Mecp2* is highly phosphorylated at serine 421 (3.4  $\pm$  0.5 fold,  $p < 0.01$ ) upon induction of neuronal activity compared to saline controls but there was no change in histone H3 or H4 acetylated proteins. A complementary quantitative immunohistochemistry approach was used to assess variations in histone H3 or H4 acetylated proteins at the single cell level from heterozygous female mice (displaying a mosaic expression of *Mecp2*) treated with kainic acid or saline. These results revealed there was no difference in the levels of either acetylated histone H3 or H4 protein between *Mecp2* positive and negative nuclei. However there was a clear cell-autonomous effect in terms of a 5% reduction in the nuclear volume of *Mecp2*-deficient cells.

Quantification of immediate early gene signal in *Mecp2*<sup>+/-</sup> heterozygous female mice treated with kainic acid or saline using the same immunohistochemistry method showed there was no difference in the distribution of c-Fos intensities between *Mecp2* positive and negative nuclei following any treatment. However there was a greater proportion of *Mecp2*-deficient nuclei (~20%) expressing c-Fos under saline control conditions and following neuronal activity. Furthermore there was a reduction in the percentage of *Mecp2* negative nuclei in the top 25% of *Egr-1* intensities in the CA1 following three hours of neuronal activity (33.5  $\pm$  2.3% for *Mecp2* negative nuclei and 19.1  $\pm$  1.7% for *Mecp2* positive nuclei).

In summary my results show at the network level there is a reduction in seizure threshold and increase power of gamma oscillations in the hippocampus of *Mecp2*-deficient mice which could lead to a state of network hyperexcitability

and switch activities from physiological oscillatory rhythms to more pathological ones. An imbalance in inhibitory neuron regulation could partially contribute to alterations in network excitability to overall promote epileptogenesis. At the cellular level I report that Mecp2 can become phosphorylated following induction of neuronal activity but this is not associated with alterations in global histone acetylation. Nonetheless Mecp2-deficient cells display a reduction in nuclear volume and have alterations in c-Fos and Egr-1 levels following induction of neuronal activity. Overall my data contribute to the understanding of how the presence or absence of MeCP2 affects network excitability and how in turn neuronal excitability affects MeCP2 phosphorylation, histone acetylation and the activation of immediate early genes.

# Table of Contents

The role of MeCP2 in activity-dependent brain processes.....	1
Abstract .....	2
List of Tables.....	10
List of Figures .....	11
Acknowledgement .....	16
Authors Declaration .....	17
Definitions/Abbreviations .....	18
Chapter 1 .....	20
Introduction .....	20
1.1    General introduction .....	20
1.2    Control of gene expression in the brain .....	20
1.2.1    Transcription factors .....	21
1.2.1.1    CREB (cAMP response element binding protein) .....	22
1.2.1.2    NF- $\kappa$ B (Nuclear Factor- $\kappa$ B) .....	22
1.2.1.3    DREAM.....	23
1.2.2    Epigenetic mechanisms.....	24
1.2.2.1    Histone modifications.....	25
1.2.2.2    DNA methylation.....	26
1.3    MeCP2 and Rett syndrome.....	29
1.3.1    Rett Syndrome caused by mutations in <i>MECP2</i> .....	29
1.3.2    Clinical manifestations of RTT .....	29
1.3.3    Structure of MeCP2 protein and mutations.....	31
1.3.4    Occurrence in males .....	32
1.3.5    Mouse models of RTT .....	33
1.3.6    Neuropathology of RTT .....	38
1.3.6.1    RTT Patients.....	38
1.3.6.2    Neuronal pathology in RTT mouse models .....	38
1.3.6.3    Neuroglia pathology in RTT mouse models .....	40
1.3.7    Neurophysiological deficits in RTT.....	41
1.3.7.1    RTT patients.....	41
1.3.7.2    General abnormalities in RTT mouse models.....	42
1.3.7.3    Intrinsic and synaptic property deficits in RTT mouse models...	42
1.3.7.4    Long-term potentiation abnormalities in RTT mouse models....	44

1.4	Function of MeCP2.....	45
1.4.1	Transcriptional repressor .....	45
1.4.1.1	Altered gene expression .....	47
1.4.2	Regulation by activity .....	49
1.4.3	Transcriptional activator.....	51
1.4.4	Global regulator of chromatin structure.....	52
1.5	Aims .....	53
Chapter 2	.....	55
Materials and Methods	.....	55
2.1	Animal Models.....	55
2.1.1	Generation of the <i>Mecp2</i> knockout mouse models.....	55
2.1.2	Genotyping .....	56
2.1.2.1	DNA Extraction .....	56
2.1.2.2	PCR confirmation of genotypes .....	56
2.2	<i>In vitro</i> hippocampal slice experiments .....	59
2.2.1	Acute slice preparation .....	59
2.2.2	Extracellular recording.....	60
2.2.2.1	Bicuculline and 4-aminopyridine (4-AP) administration.....	60
2.2.2.2	Kainic acid administration.....	61
2.2.3	Data analysis .....	61
2.3	<i>In vivo</i> kainate experiments.....	62
2.3.1	Administration of anaesthesia and kainic acid.....	62
2.3.2	Seizure Score .....	62
2.3.3	Tissue preparation for protein analysis .....	65
2.4	Protein analysis .....	65
2.4.1	Western blot .....	65
2.4.1.1	Protein quantification.....	65
2.4.1.2	General method.....	66
2.4.1.3	7% gel electrophoresis .....	68
2.4.1.4	Analysis.....	69
2.4.2	Immunohistochemistry .....	70
2.4.2.1	General Method .....	70
2.4.2.2	Image Analysis.....	72
2.5	Statistical Analysis.....	76
2.6	General materials .....	76

2.6.1	Polymerase Chain Reaction (PCR) products .....	76
2.6.1.1	Primers .....	76
2.6.1.2	Enzymes .....	76
2.6.2	Solutions .....	77
2.6.2.1	Electrophysiology .....	77
2.6.2.2	General solutions .....	78
2.6.3	Drugs .....	79
Chapter 3	.....	80
Reduced seizure threshold and altered oscillatory properties in <i>Mecp2</i> knockout mice	.....	80
3.1	Introduction .....	80
3.2	Study Aim .....	81
3.3	Methods .....	82
3.4	Results.....	82
3.4.1	<i>Mecp2</i> -deficient mice have a heightened sensitivity to kainic acid-induced seizures <i>in vivo</i> .....	82
3.4.1.1	Kainic acid application to mice under anaesthesia .....	82
3.4.1.2	Kainic acid application to mice not under anaesthesia .....	83
3.4.2	Altered gamma network oscillations in the hippocampus of <i>Mecp2</i> <sup>stop/y</sup> mice. ....	84
3.4.3	Altered properties of bicuculline-induced epileptiform activity in the hippocampus of <i>Mecp2</i> <sup>stop/y</sup> mice.....	86
3.4.3.1	Spontaneous extracellular fEPSPs .....	86
3.4.3.2	Evoked extracellular fEPSPs.....	87
3.4.4	Altered properties of 4-aminopyridine-induced epileptiform activity in the hippocampus of <i>Mecp2</i> <sup>stop/y</sup> mice .....	89
3.4.4.1	Spontaneous extracellular fEPSPs .....	89
3.4.4.2	Evoked extracellular fEPSPs.....	92
3.5	Discussion .....	94
Chapter 4	.....	99
Relationship between <i>Mecp2</i> phosphorylation, histone acetylation and neuronal activity in wild-type and <i>Mecp2</i> -deficient mice	.....	99
4.1	Introduction .....	99
4.2	Study aim .....	100
4.3	Methods .....	101

4.4	Results.....	102
4.4.1	Increase in Mecp2 phosphorylation following application of kainic acid to WT mice .....	102
4.4.2	Modest histone H3 acetylation (H3Ac) alterations in WT and Mecp2-deficient mice after kainic acid treatment .....	103
4.4.3	Modest histone H4 acetylation (H4Ac) alterations in WT and Mecp2-deficient mice after kainic acid treatment .....	105
4.4.4	Anaesthetic effects on phosphorylation of Mecp2 and histone H3 and H4 acetylation.....	107
4.4.4.1	Robust increase in phosphorylation of Mecp2 .....	107
4.4.4.2	Modest alterations in histone H3 and H4 acetylation .....	109
4.5	Discussion .....	111
Chapter 5 .....		117
An investigation of histone protein levels in Mecp2 positive and negative neurons in the <i>Mecp2</i> <sup>+/-</sup> mosaic brain.....		117
5.1	Introduction .....	117
5.2	Study aim .....	118
5.3	Methods .....	118
5.4	Results.....	120
5.4.1	Nuclei deficient in Mecp2 display a 5% reduction in their nuclear volume 120	
5.4.2	Levels of histone H3 acetylation was unaltered between Mecp2 containing and Mecp2-deficient nuclei in the hippocampal formation .....	121
5.4.3	Levels of total histone H3 was unaltered between Mecp2 containing and Mecp2-deficient nuclei in the hippocampal formation.....	130
5.4.4	Levels of histone H4 acetylation was unaltered between Mecp2 containing and Mecp2-deficient nuclei in the hippocampal formation .....	138
5.4.5	Levels of total histone H4 was unaltered between Mecp2 containing and Mecp2-deficient nuclei in the hippocampal formation.....	146
5.5	Discussion .....	154
Chapter 6 .....		161
Altered regulation of immediate early genes levels in neurons deficient in Mecp2 in the <i>Mecp2</i> <sup>+/-</sup> mosaic brain.....		161
6.1	Introduction .....	161
6.2	Study aims .....	162

6.3	Methods .....	162
6.4	Results.....	165
6.4.1	<i>Mecp2</i> <sup>+/-</sup> mice display an increase in c-Fos expression following induction of neuronal activity compared to saline controls .....	165
6.4.2	Levels of c-Fos was unaltered between <i>Mecp2</i> positive and negative nuclei in the hippocampal formation .....	166
6.4.3	Greater proportion of <i>Mecp2</i> -deficient nuclei express c-Fos in the hippocampal formation .....	177
6.4.4	<i>Mecp2</i> <sup>+/-</sup> mice display an increase in Egr-1 expression following induction of neuronal activity compared to saline controls .....	180
6.4.5	Decreased levels of Egr-1 in <i>Mecp2</i> -deficient nuclei after kainic acid treatment in the hippocampal formation .....	181
6.5	Discussion .....	190
Chapter 7	.....	195
General discussion.....		195
7.1	Major and novel findings.....	195
7.1.1	Reduced seizure threshold and altered oscillatory properties in <i>Mecp2</i> knockout mice .....	195
7.1.2	No alteration in histone protein levels in <i>Mecp2</i> positive and negative neurons in the <i>Mecp2</i> <sup>+/-</sup> mosaic brain.....	196
7.1.3	Altered regulation of immediate early gene levels in neurons deficient in <i>Mecp2</i> in the <i>Mecp2</i> <sup>+/-</sup> mosaic brain .....	198
7.2	Significance of this study .....	199
7.3	Technical considerations and future studies .....	200
7.4	Summary .....	202
Appendix A .....		203
Nuclear preparation optimisation.....		203
Appendix B .....		203
Automated Script.....		204
References.....		211

## List of Tables

Table 1-1 Necessary criteria for classic RTT diagnosis.....	29
Table 1-2 Summary of the diverse <i>Mecp2</i> mouse models generated with global (whole body) and tissue specific expression of <i>Mecp2</i> .....	37
Table 2-1 Offspring generated from <i>Mecp2</i> knockout mouse models.....	55
Table 2-2 DNA extraction conditions .....	56
Table 2-3 Contents of each PCR reaction.....	57
Table 2-4 PCR conditions for both reactions .....	57
Table 2-5 Primary and secondary antibodies used for western blots .....	68
Table 2-6 Primary and secondary antibodies used for immunohistochemistry ...	71
Table 2-7 Primers used in PCR reactions.....	76
Table 2-8 Enzymes used in PCR reactions.....	77
Table 2-9 1 x Sucrose Artificial Cerebrospinal Fluid (sACSF).....	77
Table 2-10 1 x Recording ACSF .....	77
Table 2-11 Gel electrophoresis solutions .....	78
Table 2-12 General solutions used for western blotting .....	78
Table 2-13 General solutions used for immunohistochemistry .....	79
Table 2-14 Drugs.....	79

## List of Figures

Figure 1-1 Transcription factor modulation of gene transcription in response to neuronal activity .....	24
Figure 1-2 Epigenetic regulation of gene expression through histone modifications and DNA methylation .....	28
Figure 1-3 MeCP2 protein structure and common mutations types .....	31
Figure 1-4 Conventional function of MeCP2 as a transcriptional repressor .....	46
Figure 1-5 Activity-dependent phosphorylation of MeCP2.....	50
Figure 1-6 Activation of target genes. ....	52
Figure 1-7 Hypothesis of how MeCP2 controls gene expression in response to neuronal activity. ....	54
Figure 2-1 Genotype verification by PCR .....	58
Figure 2-2 Mouse brain orientation and hippocampal slice preparation. ....	60
Figure 2-3 Set-up used for monitoring the seizure scoring .....	63
Figure 2-4 Illustrated example of seizure score upon IP injection of kainic acid in mice .....	64
Figure 2-5 BSA curve fitting in a Bradford protein assay. ....	66
Figure 2-6 Analysis of western blots in Image J.....	69
Figure 2-7 Steps involved in the automated script. ....	73
Figure 2-8 Calculation of mean nuclei intensity from the script .....	74
Figure 2-9 Measurement of integrated density.....	75
Figure 3-1 Heightened sensitivity to kainate-induced seizures in <i>Mecp2<sup>stop/y</sup></i> mice .....	83
Figure 3-2 Increase seizure severity in <i>Mecp2<sup>-/y</sup></i> and <i>Mecp2<sup>+/-</sup></i> mice without anaesthesia .....	84
Figure 3-3 Gamma frequency network oscillations before and after kainic acid application. ....	85
Figure 3-4 Increased power of gamma frequency network oscillations in hippocampal slices from <i>Mecp2<sup>stop/y</sup></i> mice .....	86
Figure 3-5 Increased frequency and duration of bicuculline-induced spontaneous epileptiform activity in hippocampal slices from <i>Mecp2<sup>stop/y</sup></i> mice.....	87
Figure 3-6 Altered evoked fEPSP properties in hippocampal slices from <i>Mecp2<sup>stop/y</sup></i> mice in the presence of bicuculline. ....	89

Figure 3-7 Increased frequency and duration of 4-aminopyridine-induced spontaneous epileptiform activity in hippocampal slices from <i>Mecp2</i> <sup>stop/y</sup> mice .	91
Figure 3-8 Hippocampal networks from <i>Mecp2</i> <sup>stop/y</sup> mice have a greater propensity to display ictal-like events in response to 4-AP challenge. ....	92
Figure 3-9 Altered evoked fEPSP properties in hippocampal slices from <i>Mecp2</i> <sup>stop/y</sup> mice in the presence of 4-AP. ....	93
Figure 4-1 Subtle increase in pS421 Mecp2 protein levels in the hippocampus of WT mice following kainic acid treatment.....	<b>Error! Bookmark not defined.</b>
Figure 4-2 H3Ac levels in the hippocampus of WT and <i>Mecp2</i> <sup>stop/y</sup> mice are unaltered following kainic acid-induced epileptogenesis .....	105
Figure 4-3 H4Ac levels in the hippocampus of WT and <i>Mecp2</i> <sup>stop/y</sup> mice are unaltered between genotypes following kainic acid-induced epileptogenesis ..	106
Figure 4-4 Comparison of kainic acid seizure-mediated alterations in pS421 Mecp2 in presence and absence of anaesthesia. ....	107
Figure 4-5 Robust increase in pS421 Mecp2 levels in the hippocampus of WT mice without anaesthesia following kainic acid treatment. ....	108
Figure 4-6 50% of Mecp2 is phosphorylated in the hippocampus of WT mice after kainic acid treatment. ....	109
Figure 4-7 Increase in H3Ac levels after kainic acid administration in the hippocampus of <i>Mecp2</i> <sup>-/y</sup> mice without anaesthesia. ....	110
Figure 4-8 Altered H4Ac levels between genotypes in the hippocampus of WT and <i>Mecp2</i> <sup>-/y</sup> mice without anaesthesia. ....	111
Figure 5-1 5% reduction in nuclear volume in nuclei deficient in Mecp2.....	121
Figure 5-2 Unaltered H3AC levels in DG granule cell nuclei of the hippocampal formation between Mecp2 nuclei type under saline control conditions.....	123
Figure 5-3 Unaltered H3AC levels in CA1 pyramidal cell nuclei of the hippocampal formation between Mecp2 nuclei type under saline control conditions.....	125
Figure 5-4 Unaltered H3AC levels in DG granule cell nuclei of the hippocampal formation between Mecp2 nuclei type after kainic acid application .....	127
Figure 5-5 Unaltered H3AC levels in CA1 pyramidal cell nuclei of the hippocampal formation between Mecp2 nuclei type after kainic acid application .....	129

Figure 5-6 Unaltered total histone H3 levels in DG granule cell nuclei of the hippocampal formation between Mecp2 nuclei type under saline control conditions.....	131
Figure 5-7 Unaltered total histone H3 levels in CA1 pyramidal cell nuclei of the hippocampal formation between Mecp2 nuclei type under saline control conditions.....	133
Figure 5-8 Unaltered total histone H3 levels in DG granule cell nuclei of the hippocampal formation between Mecp2 nuclei type after kainic acid administration .....	135
Figure 5-9 Unaltered total histone H3 levels in CA1 pyramidal cell nuclei of the hippocampal formation between Mecp2 nuclei type after kainic acid application .....	137
Figure 5-10 Unaltered H4AC levels in DG granule cell nuclei of the hippocampal formation between Mecp2 nuclei type under saline control conditions.....	139
Figure 5-11 Unaltered H4AC levels in CA1 pyramidal cell nuclei of the hippocampal formation between Mecp2 nuclei type under saline control conditions.....	141
Figure 5-12 Unaltered H4AC levels in DG granule cell nuclei of the hippocampal formation between Mecp2 nuclei type after kainic acid application .....	143
Figure 5-13 Unaltered H4AC levels in CA1 pyramidal cell nuclei of the hippocampal formation between Mecp2 nuclei type after kainic acid application .....	145
Figure 5-14 Unaltered total histone H4 levels in DG granule cell nuclei of the hippocampal formation between Mecp2 nuclei type under saline control conditions.....	147
Figure 5-15 Unaltered total histone H4 levels in CA1 pyramidal cell nuclei of the hippocampal formation between Mecp2 nuclei type under saline control conditions.....	149
Figure 5-16 Unaltered total histone H4 levels in DG granule cell nuclei of the hippocampal formation between Mecp2 nuclei type after kainic acid application .....	151
Figure 5-17 Unaltered total histone H4 levels in CA1 pyramidal cell nuclei of the hippocampal formation between Mecp2 nuclei type after kainic acid administration .....	153

Figure 6-1 Example distribution of c-Fos fluorescent intensities and identification of background signal. ....	164
Figure 6-2 Time course of c-Fos protein expression in the hippocampal formation of <i>Mecp2</i> <sup>+/-</sup> female mice after application of kainic acid. ....	166
Figure 6-3 Unaltered c-Fos levels in DG granule cell nuclei of the hippocampal formation between <i>Mecp2</i> nuclei type under saline control conditions.....	168
Figure 6-4 Lack of c-Fos expression in <i>Mecp2</i> positive and negative nuclei in the CA1 region of the hippocampus under saline control conditions. ....	169
Figure 6-5 Unaltered c-Fos levels in DG granule cell nuclei of the hippocampal formation between <i>Mecp2</i> nuclei type following 0.5 hour of kainic acid application. ....	170
Figure 6-6 Unaltered c-Fos levels in CA1 pyramidal cell nuclei of the hippocampal formation between <i>Mecp2</i> nuclei type following 0.5 hour of kainic acid application.....	172
Figure 6-7 c-Fos expression is elevated following 3 hours of kainic acid induced seizures but is not different between <i>Mecp2</i> nuclei type in DG granule cell nuclei .....	174
Figure 6-8 c-Fos expression is elevated following 3 hours of kainic acid induced seizures but is not different between <i>Mecp2</i> nuclei type in CA1 pyramidal cell nuclei.....	176
Figure 6-9 Increased percentage of <i>Mecp2</i> negative nuclei expressing c-Fos in the DG of the hippocampal formation under saline control conditions. ....	178
Figure 6-10 Increased percentage of <i>MeCP2</i> negative nuclei expressing c-Fos in the DG of the hippocampal formation after 0.5 hour of kainic acid application. ....	179
Figure 6-11 Increased percentage of <i>Mecp2</i> negative nuclei expressing c-Fos in the CA1 of the hippocampal formation after 0.5 hour of kainic acid application. ....	180
Figure 6-12 Time course of Egr-1 protein expression in the hippocampal formation of <i>Mecp2</i> <sup>+/-</sup> female mice after application of kainic acid .....	181
Figure 6-13 Lack of Egr-1 expression in <i>Mecp2</i> positive and negative nuclei in the DG region of the hippocampal formation under saline control conditions.....	182
Figure 6-14 Unaltered Egr-1 levels in CA1 pyramidal cell nuclei of the hippocampal formation between <i>Mecp2</i> nuclei type under saline control conditions.....	183

Figure 6-15 Lack of Egr-1 expression in Mecp2 positive and negative nuclei in the DG region of the hippocampal formation following 0.5 hour of kainic acid treatment.....	184
Figure 6-16 Unaltered Egr-1 levels in CA1 pyramidal cell nuclei of the hippocampal formation between Mecp2 nuclei type following 0.5 hour of kainic acid administration.....	185
Figure 6-17 Egr-1 expression is elevated following 3 hours of kainic acid induced seizures but is not different between Mecp2 nuclei type in DG granule cell nuclei .....	187
Figure 6-18 Decreased Egr-1 levels in CA1 pyramidal cell nuclei deficient in Mecp2 following 3 hours of kainic acid administration .....	189
Supplementary Figure 1-1 Comparison of three cell lysate methods for western blot analysis .....	203

## Acknowledgement

Firstly I would like to thank my supervisors Dr Stuart Cobb and Professor Adrian Bird for all their help, support and guidance throughout my PhD. I would also like to thank my funding body SULSA who have given me the opportunity to undertake this PhD.

I am grateful to Dr Mark Bailey and Dr Imre Vida for their help and knowledge they have given me at different points throughout my PhD.

It is a pleasure to thank those whose contributions have made this thesis possible, namely Dr David Kelly for all his help and patience with me when writing the automated script; Dr Alastair Kerr for his help in data analysis and the two MRes students I supervised Robert Ganley and Svetlana-Alina Melcea.

Particularly I would like to thank the good friends I have made during my PhD who have been there from beginning to end including Rhiannon Thompson, Emma Brockett, Miranda Willis, Graham Lee, Paul Turko, Sam Booker and Jake Griffin. I also cannot forget my three amazing friends Katie, Laura and Claire; you have always been there for me, thanks guys!

Special thanks have to be given to my Glasgow work colleagues including Paul Ross, Dr Jonas Weng, Dr Rosie Spike and Dr Kamal Gadalla.

I would also like to thank my work colleagues in Edinburgh, notably Dr Pete Skene, Dr Jim Selfridge, Dr Jacky Guy and Dr Helene Cheval who have given me fantastic advice and help during my PhD.

And last but not least, nothing would have been possible without the constant support and love of my family, thank you guys so much. I especially want to thank my boyfriend Jack who has been my rock over the past year.

## Authors Declaration

I declare that the work presented in this thesis is entirely my own with all exceptions being clearly indicated or/and properly cited in the context.

Signature:.....

Faye McLeod

## Abbreviations

Ac	Acetylated
4-AP	4-aminopyridine
ACM	Astrocyte conditioned media
ADP	Adenosine diphosphate
AMPA	2-amino-3-(3-hydroxy-5-methyl-isoxazol-4-yl) propanoic acid
ANOVA	Analysis of variance
BDNF	Brain-derived neurotrophic factor
BP	Base pair
BSA	Bovine serum albumin
CA1	Cornu Ammonis area 1
CA3	Cornu Ammonis area 3
Ca <sup>2+</sup>	Calcium
CaM	Calcium/Calmodulin
CaMK	Calcium/calmodulin-dependent protein kinase
CaMKII	Calcium/calmodulin-dependent protein kinase II
CBP	CREB-binding protein
CM	Conditioned media
CNS	Central nervous system
CO <sub>2</sub>	Carbon dioxide
CpG	Cytosine-guanine dinucleotide
CREB	cAMP response element binding protein
CRH	Corticotrophin-releasing hormone
CTD	C-terminal domain
DAPI	4",6-diamidino-2-phenylindole
DG	Dentate gyrus
dH <sub>2</sub> O	Distilled water
ddH <sub>2</sub> O	Double distilled water
DNA	Deoxyribonucleic acid
DNMT	DNA methyltransferase
DPSS	Diode-pumped solid-state laser
DREAM	Downstream repressor element antagonist modulator
EEG	Electroencephalography
fEPSP	Field excitatory postsynaptic potential
GABA	γ-aminobutyric acid
GFAP	Glial fibrillary acidic protein
GFP	Green fluorescent protein
H1	Histone H1
H2A	Histone 2A
H2B	Histone 2B
H3	Histone 3
H3Ac	Histone H3 acetylation
H4	Histone 4
H4Ac	Histone H4 acetylation
HAT	Histone acetyltransferase
HDAC	Histone deacetylase
Het	Heterozygous
HPA	Hypothalamic-pituitary-adrenal
Hsp90	Heat shock protein 90
ID	Inter domain
IEG	Immediate early gene

KA	Kainic acid
LTD	Long term depression
LTP	Long term potentiation
L-VSCC	Long-lasting voltage sensitive calcium channels
MAPK	Mitogen-activated protein kinases
MBD	Methyl-CpG binding domain
Me	Methylated
MeCP1	Methyl-binding protein 1
<i>MECP2</i>	Human Methyl-binding protein 2 gene
<i>Mecp2</i>	Mouse Methyl-binding protein 2 gene
MeCP2	Human Methyl-binding protein 2 protein
<i>Mecp2</i>	Mouse Methyl-binding protein 2 protein
mEPSC	Miniature excitatory postsynaptic currents
mIPSC	Miniature inhibitory postsynaptic currents
N	Number
NBQX	2,3-dioxo-6-nitro-1,2,3,4-tetrahydrobenzo(f)quinoxaline-2,3-dione
NCS	Neuronal calcium signal
NeuN	Neuron nuclear antigen rbfox3
NF- $\kappa$ B	Nuclear factor- $\kappa$ B
NLS	Nuclear localisation signal
NMDA	N-methyl-D-aspartate
NTD	N-terminal domain
PB	Phosphate buffer
PBS	Phosphate buffer saline
PCR	Polymerase chain reaction
PFA	Paraformaldehyde
S421	Serine 421
S424	Serine 424
S80	Serine 80
SA	Saline
Sgk1	serum glucocorticoid-inducible kinase 1
Syn1	Synapsin1 promoter
SD	Standard deviation
SDS	Sodium dodecyl sulphate
SEM	Standard error of mean
RFP	Red fluorescent protein
RNA	Ribonucleic acid
rpm	round per minute
RTT	Rett syndrome
TBS	Tris buffered saline
TF	Transcription factor
TRD	Transcription repression domain
TrK	Tyrosine kinase
UV	Ultraviolet
Viaat	Vesicular inhibitory amino acid transporter
WT	Wild-type

# Chapter 1

## Introduction

### 1.1 General introduction

Epigenetic control of gene expression is important for normal development of the central nervous system (CNS) and mutations in genes that play an integral part of this process can cause various congenital diseases. Rett syndrome is a neurodevelopmental disorder caused by mutations in the X-linked gene *MECP2* (Amir et al., 1999) and leads to neurological deficits and severe mental retardation. A variety of mouse models have been generated which replicate the key phenotypes of this disorder (Chen et al. 2001; Guy et al. 2001) and the symptoms have even been reversed in gene reactivation studies (Guy et al., 2007). However the underlying function of MeCP2 and how its dysfunction/absence leads to Rett syndrome is still unclear. Activity-dependent transcription in the brain is important because it is required for experience-dependent synaptic changes which underlie maturation of neural networks (Dragunow et al., 2000). Studies have revealed that Mecp2 protein can be modified posttranslationally in response to neuronal activity (Zhou et al., 2006). Furthermore, it is now appreciated that some epigenetic mechanisms in the adult brain are amenable to external stimuli (Crosio et al., 2000). In this thesis I explore this phenomenon further at the cellular level by correlating activity-dependent changes in MeCP2 with alterations in histone acetylation, a recognised epigenetic mechanism. At the network level I attempt to characterise potential changes in network excitability as a result of MeCP2 deficiency thus gaining further insight into the role MeCP2 has in activity-dependent brain processes.

### 1.2 Control of gene expression in the brain

The brain is the most complex organ in the human body. There are many different neuronal cell types which have unique functions. The intricacy of neuronal networks is further enhanced with synapse and receptor location,

composition and interactions dictating the specificity of signalling pathways. Appropriate expression of genes throughout development and adulthood is important for neuronal identity and maintenance of these systems. Two key influences which play a significant role in regulating gene expression in the brain are transcription factors and epigenetic mechanisms.

### **1.2.1 Transcription factors**

Transcription factors (TFs) are regulatory proteins which can bind to short DNA sequences up- or downstream of genes and influence transcription in a positive or negative manner. The importance of these proteins is highlighted by their conservation between organisms and the increase in their numbers in proportion to the size of the genome (van Nimwegen, 2003). TFs function as part of a complex, and by binding to specific recognition sequences in DNA (regulatory elements) near a gene they can recruit multiple proteins to facilitate binding by RNA polymerase II, (RNA pol II) thus initiating transcription (Matsui et al., 1980). There are two types of regulatory elements, promoter elements that exert control near the gene promoter and enhancer elements which exert their effect at a distance. The transcription factor complement of a cell is crucial in the control of gene expression during development and in determining adult cell identity (reviewed by Collingwood et al., 1999).

During development and differentiation many TFs work together to regulate specific neuronal lineages, the acquisition of neuronal phenotypes as well as their own expression. This control is essential in the mature nervous system. TFs also play an important role in controlling gene expression under basal conditions and in response to external stimuli. Activity dependent control of neurite outgrowth and synapse formation and pruning is essential in maintaining a balance of inhibitory and excitatory synapses in the brain, and this is thought to occur through the regulation of gene expression (reviewed by West and Greenberg, 2011). There are two main classes of genes that are regulated by neuronal activity in the adult nervous system, immediate early gene TFs, which are general response factors in neurons, and neuronally enriched gene products, which have a specific function at synapses during development and plasticity. TFs can alter their function and localisation following activity-dependent signalling pathway activation to control expression of these genes. Examples of

how this is achieved in some well-studied TFs is shown in Figure 1-1 and explained in more detail below.

#### **1.2.1.1 CREB (cAMP response element binding protein)**

The transcription of certain genes can be detected within minutes following induction of neuronal activity; including immediate early genes such as *Fos* (Greenberg et al., 1986). This is aided by TFs such as CREB being prebound to gene promoters enabling them to quickly initiate gene transcription. Upon stimulus induced calcium entry via excitatory N-methyl-D-aspartate (NMDA) receptors and long-lasting voltage-sensitive calcium channels (L-VSCCs) in the brain, CREB bound to DNA at the calcium-response element (CRE) become phosphorylated at serine 133 (Shaywitz and Greenberg, 1999).

Calcium/calmodulin (CaM)-dependent protein kinase (CaMKs) results in rapid phosphorylation and mitogen-activated protein kinases (MAPKs) contributed to the sustained phosphorylation at later stages (Dolmetsch et al., 2001). This phosphorylation enables the recruitment of transcription coactivators such as CREB-binding protein (CBP) which activates transcription via histone acetylation (Chrivia et al., 1993). The CREB family are essential for neuronal survival and synaptic plasticity (Benito and Barco, 2010).

#### **1.2.1.2 NF- $\kappa$ B (Nuclear factor- $\kappa$ B)**

In comparison to CREB which is prebound to DNA and recruits co-factors, other TFs act through nuclear translocation. These responses are slower than prebound TFs and represent a later control of activity-regulated transcription. In many cells (except immune cells where it is constitutively active) NF- $\kappa$ B is detained in the cytosol in an inactive state through association with an inhibitor of NF- $\kappa$ B (I $\kappa$ B) (Meffert and Baltimore, 2005). Upon synaptic stimulation, phosphorylation of I $\kappa$ B results in degradation of this protein and nucleocytoplasmic shuttling of NF- $\kappa$ B into the nucleus of cells (Mercurio et al., 1997). As with CREB, NF- $\kappa$ B also requires CaMKII (calcium/calmodulin-dependent protein kinase II) pathway for activation through calcium influx into the cell (Meffert et al., 2003). NF- $\kappa$ B has a major role in injury and stress in the CNS which is analogous to its immune system role. However NF- $\kappa$ B is also postulated to function in specialised

signalling from the synapse to the nucleus which is important for synaptic plasticity (Meffert et al., 2003).

### **1.2.1.3 DREAM (Downstream repressor element antagonist modulator)**

Another mechanism by which TFs can exert their control over gene expression is through regulated DNA binding upon induction of neuronal activity and calcium influx into the cell. DREAM is a TF which belongs to the Neuronal Calcium Sensor (NCS) family of proteins which can bind calcium similar to the calcium effector protein CaM (Burgoyne, 2007). It is abundantly expressed in the CNS and interacts with DNA via a response element called downstream regulatory element (DRE) to repress transcription in the absence of calcium (Carrión et al., 1999). Calcium influx into the cell opposes this action resulting in a reduction in its affinity for DNA. DREAM has a role in vesicle trafficking and various forms of transcriptional control (reviewed by Burgoyne, 2007).

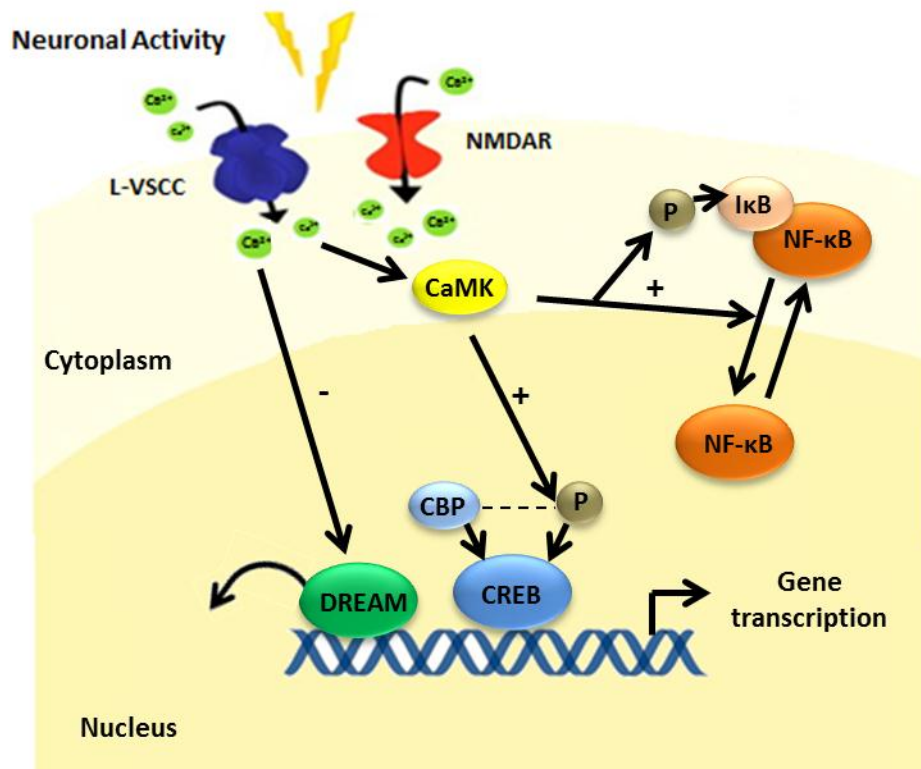


**Figure 1-1 Transcription factor modulation of gene transcription in response to neuronal activity**

Following neuronal activity, there are a variety of mechanisms in which transcription factors (TFs) can control gene expression. Firstly there is an influx of calcium (Ca<sup>2+</sup>) through long-lasting voltage-sensitive calcium channels (L-VSCC) or N-methyl-D-aspartate receptors (NMDAR) into the cytoplasm. This increase in calcium can negatively (-) regulate some TFs directly such as the repressor protein Downstream Repressor Element Antagonist Modulator (DREAM) by binding to it directly. This alters the affinity it has for DNA and releases it from DNA binding sites causing activation in gene expression. Alternatively elevated calcium levels can activate calcium/calmodulin-dependent protein kinase (CaMK) pathways which positively (+) regulate some TFs by phosphorylating those that are prebound to DNA such as cAMP response element binding protein (CREB). This enables them to recruit other co-factors including CREB-binding protein (CBP) in the case of CREB to activate gene transcription. Furthermore CaMKII can also positively regulate the translocation of TFs into the nucleus. For example Nuclear Factor-κB (NF-κB) is bound to an inhibitor protein (IκB) in the cytoplasm but phosphorylation of this protein enables NF-κB to shuttle into the nucleus and regulate gene expression. This diagram is modified from Zhou et al. 2006.

### 1.2.2 Epigenetic mechanisms

In conjunction with TFs, epigenetic mechanisms also play an important role in regulating gene expression in the brain. The term epigenetics can be defined as ‘the structural adaptation of chromosomal regions so as to register, signal or perpetuate altered activity states’, (Bird, 2007). In other words, the focus is on chromosomes and genes where mechanisms are in place to control heritable gene expression states without changing the underlying DNA sequence. These

changes are important in cellular differentiation throughout life, which allow cells to maintain different characteristics despite containing the same genomic material. It is now appreciated that epigenetic regulatory networks are not static and play an essential role in cell development, homeostasis and ageing (Dulac, 2010; Mehler, 2008). Their ability to respond to environmental stimuli makes these processes imperative to the correct function of neuronal networks in the CNS. Two major epigenetic mechanisms which contribute to alterations in gene expression are histone modifications and DNA methylation which regulate the availability of TF binding sites on DNA. A summary of these mechanisms are shown in Figure 1-2 and explained in more detail below.

### **1.2.2.1 Histone modifications**

Chromatin is a complex of DNA, histones and non-histone proteins in the nucleus. The basic component of chromatin is the nucleosome which contains four core histones - H2A, H2B, H3 and H4. Two copies of each of these histones assemble to form an octamer core around which DNA wraps. This aids in DNA packing within the nucleus, regulates access of TFs and cofactors, and assists in DNA repair. The shape of chromatin can be condensed (heterochromatin) resulting in compact DNA which is unable to be transcribed. Alternatively, chromatin can be in a more open form (euchromatin) enabling access of gene transcription machinery. This is facilitated by posttranslational modifications on the N-terminal tails of histones proteins, by histone modifying enzymes, which alters their affinity for DNA (reviewed by MacDonald and Roskams, 2009). Importantly histone modifying enzymes cannot access their substrates unless targeted by prebound DNA activators or repressors. There are at least eight types of modifications that occur on histone residues including acetylation, methylation, phosphorylation, ubiquitylation, SUMOylation, ADP (adenosine diphosphate) ribosylation, deimination and proline isomerisation (reviewed by Kouzarides, 2007). Histone acetylation, methylation and phosphorylation are amongst the well-studied modifications. Methylation of histone H3 and H4 at lysine and arginine residues is mediated by methyltransferase enzymes which can mono-, di- or trimethylate histone tail residues. The functional consequences of methylation depend on the specific amino acid modified. For example, methylation of lysine 4 on histone H3 is associated with active gene

transcription but methylation of lysine 9 on histone H3 is associated with repression of transcription (Noma K et al., 2001).

In contrast to methylation of histone residues, phosphorylation and acetylation can be regulated by neuronal activity (Crosio et al., 2000). Histone H3 can be phosphorylated at a number of serine residues and phosphorylation of histone H3 at serine 10 has been shown to be involved in chromosome condensation during mitosis (Wei et al., 1999). This residue can also be phosphorylated upon induction of neuronal activity and correlates with activation of immediate early genes (Crosio et al., 2000). Furthermore MAPKs signalling pathways have been linked to the phosphorylation at this residue (Cheung et al., 2000; Chwang et al., 2006). Finally acetylation of histone H3 and H4 can be regulated by histone acetyl transferase (HAT) and histone deacetylase (HDAC) enzymes which activate genes by the addition of acetyl groups to lysine residues or repress genes by removal of acetyl groups from lysine residues respectively. Acetylation at lysine residue 5, 8, 12 and 16 for histone H4 (Clarke et al., 1993) and lysine residue 9 and 14 for histone H3 (Roh et al., 2005) have been identified as key regulatory sites which are amenable to stimulus induction (reviewed by Riccio, 2010).

#### **1.2.2.2 DNA methylation**

Another important epigenetic mechanism is DNA methylation which contributes to the stability of gene expression states (reviewed by Jaenisch and Bird, 2003). For example DNA methylation is involved in genomic imprinting in which some genes will only express the maternal or paternal allele specifically (Li et al., 1993). However recent studies have shown that DNA methylation is amenable to stimulus-dependent regulation in the mature nervous system too which results in demethylation of DNA. For instance, seizure events in the hippocampus result in reduced DNA methylation at the promoter regions of neuronally enriched gene products (Ma et al., 2009). DNA methylation is catalysed by DNA methyltransferase (DNMTs) enzymes which modify DNA bases to add a methyl group to carbon-5 of the cytosine pyrimidine ring; principally at CpG dinucleotides (cytosine and guanine separated by a phosphate). There are two types of DNMTs - maintenance (Dnmt1) and *de novo* (Dnmt3a and Dnmt3b) DNMTs. The former is important during DNA replication to preserve methylation patterns in replicated cells (Yoder et al., 1997) and the latter has a role in

targeting unmethylated CpG dinucleotides (Okano et al., 1999). The significance of DNA methylation during development is highlighted by the lethality experienced in knockout DNMT mice (Okano et al., 1999).

The effect of DNA methylation on gene expression is mainly mediated indirectly, through the binding of proteins to methylated CpG dinucleotides - specifically methyl binding domain proteins (MBDs) which repress transcription. The first MBD discovered was methyl-CpG binding protein 1 (MeCP1; Meehan et al., 1989) and the second was methyl-CpG binding protein 2 (MeCP2; Lewis et al., 1992). MeCP2 has a more simplistic protein structure than MeCP1 and the identification of an MBD sequence (required for recruitment to methylated DNA) in its structure enabled the identification of four more MBD proteins - MBD1, MBD2, MBD3 and MBD4 (Hendrich and Bird, 1998). Recruitment of HDAC proteins is the most common method for repression of gene transcription employed by all MBDs, except MBD4 which has role in DNA repair (Hendrich et al., 1999), and is mediated by a transcriptional repression domain (TRD) in their protein structure (reviewed by Bird and Wolffe, 1999).

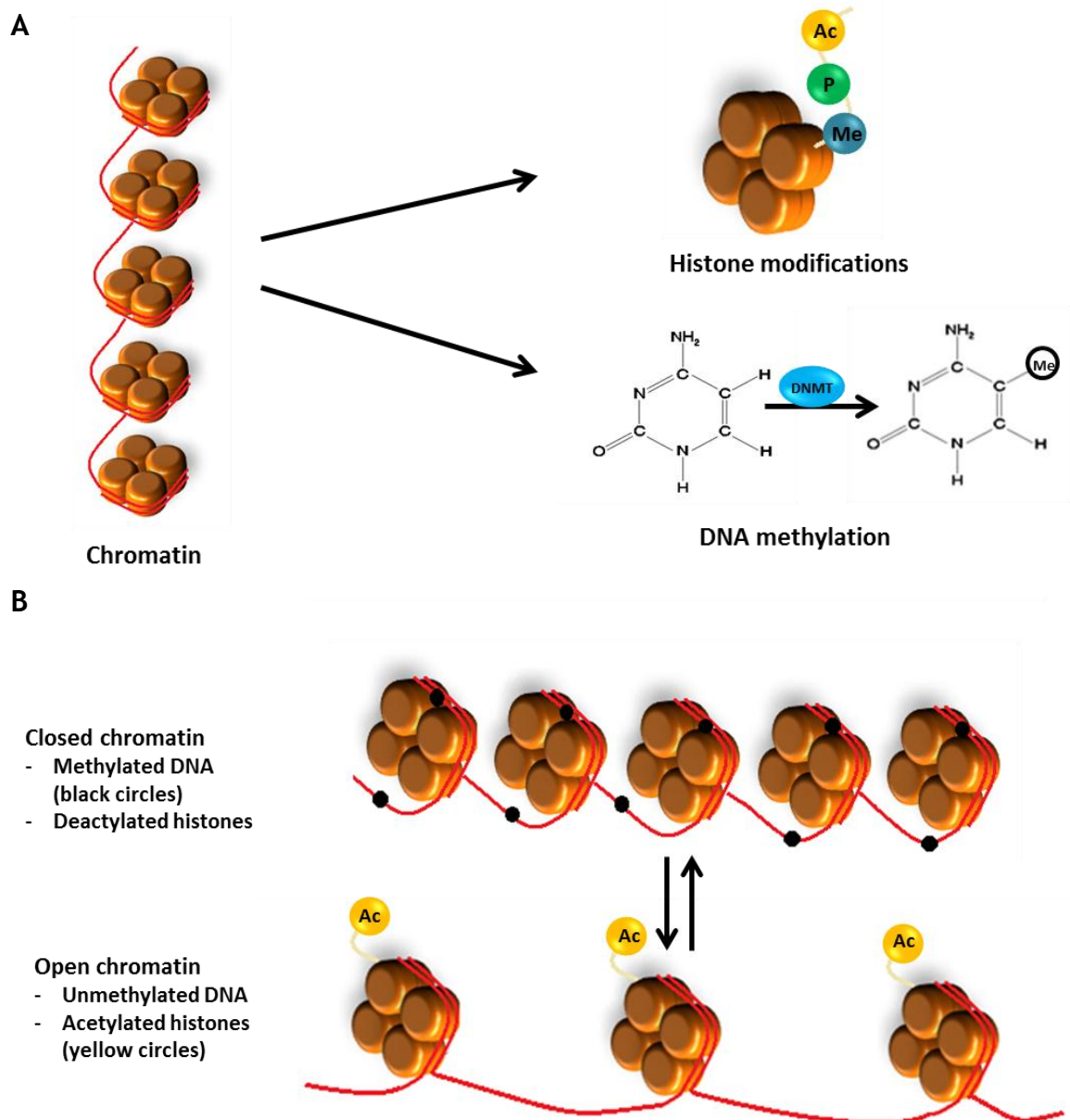


**Figure 1-2 Epigenetic regulation of gene expression through histone modifications and DNA methylation**

(A) Chromatin is a complex of DNA (red) wrapped around a histone (orange) octamer (two copies of each core histone – H2A, H2B, H3 and H4) in the nucleus. Modifications to the histone tails can change the accessibility of chromatin to transcriptional machinery through alterations such as the enzymatic addition of acetyl (Ac, yellow), phospho (P, green) or methyl (Me, blue) groups thus altering gene expression (histone modifications). Furthermore addition of a methyl group to carbon-5 of the cytosine pyrimidine ring (chemical structure) by methyltransferase enzymes (DNMTs) can also modify the chromatin structure typically leading to repression of genes (DNA methylation). (B) Example of how these epigenetic mechanisms can alter chromatin to regulate gene expression. Closed chromatin has methylated DNA (black circles) and deacetylated histone tails which typically lead to repression of gene transcription. However a more open chromatin structure has unmethylated DNA and acetylated histones to aid activation of gene expression.

## 1.3 MeCP2 and Rett syndrome

### 1.3.1 Rett Syndrome caused by mutations in *MECP2*

Rett Syndrome (RTT, OMIM 312750) is a sporadic neurodevelopmental disorder that affects roughly 1 in every 10,000 female live births and is the second leading cause of all mental retardation in girls (Neul et al., 2010). The restriction of the disease to females suggested an X-linked dominant mode of inheritance, with the mutation presumed to be lethal in males (Xiang et al., 1998). However, due to the unpredictable occurrence of RTT, it was hard to map the locus on the chromosome. From the use of genetic linkage studies and the investigation into rare family cases with RTT, the most probable location was indicated as Xq28 (Amir et al., 1999). Subsequently, following further gene sequencing analysis into plausible disease-causing mutations of candidate genes in this locus, it was found that a mutation in *MECP2* was the cause of RTT (Amir et al., 1999). This was surprising as MeCP2 had no previous known involvement in the CNS or brain development and is in fact a widely expressed transcriptional regulator involved in epigenetic mechanisms as described above.

### 1.3.2 Clinical manifestations of RTT

RTT was first identified as a distinct disorder based on clinical studies carried out by Dr Andreas Rett in 1966 (Rett, 1966), and Dr Bengt Hagberg in 1983 (Hagberg et al., 1983). The necessary criteria for diagnosis often found in classic forms of RTT (Neul et al., 2010) are displayed in Table 1-1.

**Table 1-1 Necessary criteria for classic RTT diagnosis**

Classic RTT diagnostic criteria
1. Partial or complete loss of purposeful hand skills
2. Partial or complete loss of purposeful spoken language
3. Gait abnormalities
4. Stereotypical hand movements
5. Period of regression followed by recovery or stabilization

In classic RTT a stage progression of the disorder is speculated (Hagberg 2002), although some variable overlap is still present. Initially after birth, sufferers appear to develop normally for about 6-18 months with some even learning to

walk and talk. Subsequently, signs of RTT slowly begin to appear. Foremost is a decrease in the average circumference of the head, advancing to full developmental stagnation by the age of three consisting of stunted growth, weight loss and muscle hypotonia. Patients then enter a period of rapid regression where autistic features become more prevalent such as avoidance of eye contact, communication dysfunction and lack of social interaction. During this time sufferers can also lose vital hand skills and develop stereotypic movement (e.g. claspings of hands); experience psychomotor abnormalities; encounter breathing abnormalities such as protracted inspirations and profound mental retardation. One of the most challenging symptoms is the high risk of seizure development ranging from mild to severe epilepsy (Chahrour and Zoghbi 2007; Hagberg 2002).

By the age of 4 onwards, patients commonly reach the stationary stage where signs of improvement may become evident in social behaviour. Nonetheless, the risk of suffering from scoliosis and decreased bone mineral density is increased due to a continual loss in weight; anxiety levels are heightened and further autonomic abnormalities can manifest such as cardiac irregularities. Reaching teenage years, the intensity of seizures begins to reduce but most patients enter a late motor deterioration phase where motor function depreciates further, often leading to immobility. However, it is still possible for patients to live beyond early adulthood although the risk of further disability is greatly enhanced with sudden death occurring in 25% of cases commonly from autonomic dysfunction (Chahrour and Zoghbi 2007; Hagberg 2002; Hagberg 2005)

The age of onset and the development of symptoms are known to vary between each patient ranging from severe to mild cases. This leads to development of atypical forms of RTT in which a regression stage is required for the diagnosis. There are three distinct variant forms of RTT - the preserved speech variant, the congenital variant and the early seizure variant. The first of the three has mutations in *MECP2* in the majority of cases however the latter two are rarely associated with *MECP2* mutations (Neul et al., 2010).

### 1.3.3 Structure of MeCP2 protein and mutations

Around 95-97% of classical RTT cases are caused by mutations in *MECP2* (Neul et al., 2008) and in 50-70% of atypical RTT cases (Percy et al., 2007). A vast majority of these mutations have now been identified and are compiled regularly in comprehensive databases ([www.mecp2.org.uk](http://www.mecp2.org.uk); RettBase: <http://mecp2.chw.edu.au/>). The structure of the MeCP2 protein and the typical mutations that arise can be observed in Figure 1-4.

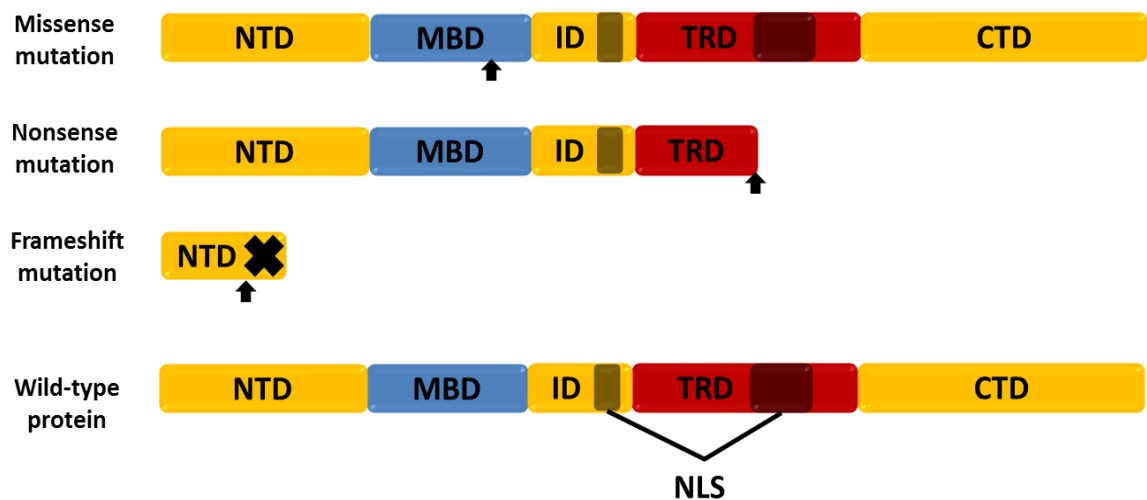


**Figure 1-3 MeCP2 protein structure and common mutations types**

Representative diagram showing the basic structure of the MeCP2 protein (wild-type protein) and the common mutation types (missense, nonsense and frameshift) that occur in RTT. The wild-type protein contains several functionally distinct domains including the N-terminal domain (NTD), methyl binding domain (MBD), inter domain (ID), transcriptional repressor domain (TRD), C-terminal domain (CTD) and the nuclear localisation signals (NLS). Black arrows under each mutation type give a hypothetical situation of where each mutation could occur and the effect. Missense mutations are a type of point mutation result in a single nucleotide change which typically leaves the entire protein intact. Nonsense mutations are a type of point mutation which results in a single nucleotide change leading to a premature stop codon and the formation of a shortened protein. Frameshift mutations are insertions or deletions of a number of nucleotides that lead to a loss of the open reading frame. They terminate at the first stop codon (end of X in diagram) causing a truncated protein.

*MECP2* is comprised of four exons but due to alternative splicing exon can be differentially expressed giving rise to two isoforms of the protein. They differ only at their N-termini with exons three and four remaining unchanged (Mnatzakanian et al., 2004). There are three known functional domains in the latter two exons, the methyl-CpG binding domain (MBD), the transcription repression domain (TRD) and a nuclear localisation signal (NLS). More than 600 mutations are known (RettBase: <http://mecp2.chw.edu.au/mecp2/>), and the majority occur in the exons coding for these domains. As identified in 1999, the

basic spectrum of mutations includes missense, nonsense and frameshift mutations (Amir et al., 1999).

Frameshift mutations arise from the addition or loss of DNA bases which change the reading frame of a gene (three bases that code for an amino acid). These types of mutation can occur over the entire length of the protein but are clustered at the C-terminal region and usually result in a non-functional product. Nonsense mutations arise from a single nucleotide change which prematurely signals the cell to stop building a protein. The majority of these occur within the MBD and TRD producing a shortened protein that might be functional or not. Missense mutations arise from a change in one DNA base pair resulting in the substitution of one amino acid for another. The bulk of mutations typically occur in the MBD with the rest of the protein left intact (Free et al. 2001; Yusufzai and Wolffe 2000).

Around 70% of all cases are eight missense and nonsense mutations (R106, R133, T158, R168, R255, R270, R294 and R306) and C-terminal deletions account for about 10% (Christodoulou et al. 2003; Moretti and Zoghbi 2006). It was found that mutations in the NLS region or causing premature stop codons cause more severe symptoms than missense mutations. In comparison, C-terminal deletions appear to produce a milder outcome (Smeets et al., 2005). In general, *MECP2* mutations are not conserved. Consequently depending on the type of *MECP2* mutation inherited, the symptoms developed in each patient will differ.

#### **1.3.4 Occurrence in males**

Following the discovery of mutations in *MECP2* causing RTT, it was questioned whether the disorder was indeed restricted to girls. After genetic testing, males were found to exhibit similar symptoms to those seen in classic RTT (Jan et al., 1999) or other disorders such as mental retardation and encephalopathy, but most males with this mutation will die within the first year of life. Males with mutations in the gene can show a similar phenotype to females in the rare case of concurrent Klinefelter syndrome, in which the presence of an extra chromosome leads to males having one functional copy of the gene (Schwartzman et al. 1999).

*MECP2* is an X-linked gene in which RTT females are heterozygous for the WT or mutant *MECP2* allele. Due to X-chromosome inactivation, in which one of the two copies of the X- chromosome in each cell will become inactive, female RTT patients have a cell population that is mosaic for expression of the mutant allele. The inactivation is a random and independent process from cells in the embryo with the majority inherited from the paternal germ line (Trappe et al., 2001). It is therefore uncommon for males to inherit the disorder but those that do will have a declined chance of survival due to mutations in *MECP2* being on all of their X chromosomes. Although inactivation is generally balanced in women, determination of the severity of the phenotype will ultimately depend on the number of cells that are affected and the mutation type.

### 1.3.5 Mouse models of RTT

To enable research into RTT and its pathology the use of mouse models which closely mimic the disorder is required. Table 1-2 summarises all the current mouse models that have contributed significantly to understanding the RTT phenotype. After the discovery of *MECP2* as the dominant cause of RTT, gene targeting procedures were used to create mice in which *Mecp2* was knocked out in order to recapitulate the phenotype (Chen et al. 2001; Guy et al. 2001). Although RTT predominantly affects females, the majority of models are of hemizygous male mice. This is because heterozygous female mice have a variable phenotype, resulting from random X-chromosome inactivation causing differences in the percentage of cells expressing *Mecp2*, and delayed symptom onset (six to nine months) making them difficult to study. In comparison, the onset of symptoms in male mice is consistent and rapid (roughly seven weeks) making this a more useful model for studies of the disorder.

Constitutive knockouts generated by both Chen et al and Guy et al in 2001 produced *Mecp2* knockout mouse models that had a remarkable similarity in phenotypes to the human condition. Using Cre-*loxP* technology, the mice created by Guy et al lacked exon three and four of the *Mecp2* gene therefore preventing *MECP2* expression altogether (*Mecp2*<sup>-/y</sup>). Alternatively, Chen et al used Cre-*loxP* technology to only delete exon three of the *Mecp2* gene but the symptoms generated were still very similar (*Mecp2*<sup>1lox/y</sup>). In the former model, male mice appeared normal until the third postnatal week before they began to

show symptoms including uncoordinated gait, less spontaneous movements, hind limb claspings, irregular breathing, wearing of the teeth and varied body weight. The severity of symptoms increased with age resulting in death of hemizygous male mice around postnatal week eight (Guy et al., 2001). The Chen et al model was comparable with symptoms in mice arising around postnatal week four which included abnormal gait, body tremors, hind limb claspings, loss of body weight and irregular breathing (Chen et al., 2001). Conversely in 2002, a male mouse model with a truncated *Mecp2* mutation (premature stop codon positioned after codon 308; *Mecp2*<sup>308/y</sup>) was generated which produced a milder RTT phenotype - longer survival (up to a year), normal body weight and fertile mice (Shahbazian et al., 2002). This model enables the study of male mice with RTT symptoms over longer experimental periods.

Since the development of these constitutive knockouts and truncation model, several other mouse models have been generated which has increased the knowledge of RTT pathology further. A conditional knockout of *Mecp2* using a nestin-Cre transgene generated a mouse model in which *Mecp2* was deleted in the brain (Guy et al., 2001). Animals in this model displayed an identical phenotype to constitutive knockouts with both showing neurological symptoms at six weeks of age and heterogeneous females displaying abnormalities after a few months. Furthermore, other studies have also shown deleting *Mecp2* using a neuron-specific promoter (microtubule-binding-protein, Tau) prenatally (Luikenhuis et al., 2004) and inactivating *Mecp2* postnatally using an inducible Cre-ESR/Lox system in the whole brain at 3, 11 and 20 weeks after birth (Cheval et al., 2012) can generate Rett-like phenotypes. These latter three studies highlight the importance of MeCP2 function in the brain with a specific role for MeCP2 in mature neurons.

Following the replication of RTT phenotypes in the brain, recent studies have focused on deleting *Mecp2* in specific neurons to see which cell type contribute to RTT pathology. The use of Cre-*loxP* technology to remove *Mecp2* from Sim1-expressing neurons in the hypothalamus (Fyffe et al., 2008) and aminergic neurons (Samaco et al., 2009) produced mice that were dysfunctional in social and feeding behaviours or displayed either motor dysfunction and aggression respectively. Viral-mediated basolateral amygdala-specific deletion of *Mecp2* (AAV-CreGFP; *Mecp2*<sup>2lox/y</sup>) generated mice with heightened anxiety levels

(Adachi et al., 2009). Furthermore using a bacterial artificial chromosome containing the *Viaat* (vesicular inhibitory amino acid transporter) promoter to target Cre dependent deletion of *Mecp2* in neurotransmitter  $\gamma$ -aminobutyric acid (GABA) secreting neurons (*Viaat-Mecp2<sup>-/y</sup>*), produced several Rett-like features including repetitive behaviours, motor dysfunction, respiratory dysfunction and weight loss (Chao et al., 2010). These studies demonstrate that *Mecp2* plays an important role in many neuronal subtypes.

Imperative to understanding the functioning of MeCP2 in the brain and specific cell types, was the development of a transgenic mouse that had a two-fold overexpression of MeCP2 (*Mecp2<sup>Tg1/y</sup>*) compared to wild-type (WT) levels (Collins et al., 2004). Initially the mice appeared to have enhanced motor learning and synaptic plasticity but after 20 weeks they developed seizures, displayed diminished mobility and around 30% died within the first year. The same group also showed that by removing the endogenous allele, thus reducing *Mecp2* levels to normal, the effects observed were reduced. Furthermore, overexpression of a *Mecp2* transgene in the brain using the Tau-promoter generated mice with severe motor impairments (Luikenhuis et al., 2004). These findings demonstrate tightly controlled levels of MeCP2 protein are required for appropriate regulation of target genes and functioning of cells.

A landmark study in which conditionally silenced *Mecp2* was reactivated postnatally demonstrated the feasibility of reversing the disorder in RTT patients (Guy et al., 2007). Endogenous *Mecp2* was silenced in the mouse by insertion of a lox-stop cassette (*Mecp2<sup>Stop/y</sup>*) which can be conditionally activated through Cre-mediated deletion of the cassette (tamoxifen-inducible Cre transgene). Small repeated doses of tamoxifen injections caused reversal of most phenotypes seen in male and female symptomatic mice and prolonged their lifespan. These findings suggest that the dysfunction caused by MeCP2 absence is not permanent and that the majority of phenotypes can be rescued. One theory behind this is the proposal that MeCP2 target sites are characterised by conserved DNA methylation patterns and thus when *Mecp2* is reintroduced into a knockout mouse, read-through of the predefined patterns can occur and enable normal functioning (Guy et al., 2007). Partial reversal of RTT symptoms has also been observed with re-expression of *Mecp2* specifically in prenatal (Luikenhuis et al., 2004) and postnatal neurons (Giacometti et al., 2007).

Furthermore, re-expression of *Mecp2* in astrocyte specific cells in the brain using a Cre transgene driven by the human astrocytic glial fibrillary acidic protein (*hGFAP*) promoter (*Mecp2*<sup>Stop/y</sup>- *hGFAPcreT2*) improves locomotion, anxiety levels, respiratory dysfunction and prolonged lifespan (Lioy et al., 2011). These studies show that targeting neurons in the brain can reverse RTT symptoms and astrocytes contribute an essential part to RTT pathology.

**Table 1-2 Summary of the diverse *Mecp2* mouse models generated with global (whole body) and tissue specific expression of *Mecp2***

Model name	<i>Mecp2</i> <sup>1lox/y</sup>	<i>Mecp2</i> <sup>-/y</sup>	<i>Mecp2</i> <sup>Tg1/y</sup>	<i>Mecp2</i> <sup>308/y</sup>	<i>Mecp2</i> <sup>Stop/y</sup>	<i>Sim1-Cre</i> ; <i>Mecp2</i> <sup>2lox/y</sup>	AAV- <i>CreGFP</i> ; <i>Mecp2</i> <sup>2lox/y</sup>	<i>PET1-Cre</i> ; <i>Mecp2</i> <sup>2lox/y</sup>	<i>Viaat</i> - <i>Mecp2</i> <sup>-/y</sup>	<i>Cre ESR</i> <sup>T</sup> ; <i>Mecp2</i> <sup>1lox/y</sup>	<i>Tau-Mecp2</i> ; <i>Mecp2</i> <sup>1lox/y</sup>	CAGGS LSL <i>Mecp2</i> ; <i>Mecp2</i> <sup>-/y</sup>	<i>Mecp2</i> <sup>Stop/y</sup> - hGFAPcreT2	
Location	Global					Non-global								
Cell-type	N/A	N/A	N/A	N/A	N/A	Hypothalamus	Amygdala	Aminergic Neurons	GABAergic neurons	Brain – 3, 11 and 20 weeks old	Postmitotic neurons	Mature CNS neurons (P0-P30)	Astrocytes	
Objective	Deletion of <i>Mecp2</i> in all cells	Deletion of <i>Mecp2</i> in all cells	Duplicate <i>Mecp2</i> in all cells	Truncate <i>Mecp2</i> in all cells	Re-expression of <i>Mecp2</i> 3-4 weeks postnatal	Deletion of <i>Mecp2</i> in the hypothalamus	Deletion of <i>Mecp2</i> in the amygdala	Deletion of <i>Mecp2</i> in aminergic neurons	Deletion of <i>Mecp2</i> in GABAergic neurons	Deletion of <i>Mecp2</i> in the brain at 3, 11 and 20 weeks old	Deletion/re-expression of <i>Mecp2</i> in postmitotic neurons	Re-expression of <i>Mecp2</i> in mature CNS neurons	Re-expression of <i>Mecp2</i> in astrocytes	
Result	RTT phenotype	RTT phenotype	RTT phenotype	Milder RTT phenotype	Rescue RTT phenotype	Social and feeding behaviour dysfunction	Anxiety phenotype	Motor dysfunction and aggression	Develop several RTT-like phenotype	RTT phenotype	Prevent phenotype	Partial rescue of RTT phenotype	Improve RTT phenotype	
Ref	Chen et al, 2001	Guy et al 2001	Shahbazian et al, 2002	Luikenhuis et al, 2004	Guy et al, 2007	Fyffe et al, 2008	Adachi et al, 2009	Samaco et al, 2009	Chao et al, 2010	Cheval et al, 2012	Luikenhuis et al, 2004	Giacometti et al, 2006	Liroy et al, 2011	

## 1.3.6 Neuropathology of RTT

### 1.3.6.1 RTT Patients

Before the development of *Mecp2* mouse models, studies performed to understand the pathology of RTT were done on human post-mortem subjects. Brain autopsies of RTT patients revealed a smaller brain size (Schultz et al., 1993) with reduced neuronal cell size and increased cell packing density in many brain regions including the cerebral cortex, hypothalamus and hippocampus (Bauman et al., 1995). There have also been reports of impaired dendritic growth and complexity of pyramidal cells in the frontal and motor cortices (Armstrong et al., 1995), and reduced synaptic spine density in pyramidal neurons in the hippocampus (Chapleau et al., 2009) and frontal cortex (Belichenko et al., 1994). Consistent with this reduction of neuronal complexity, the density of a number of excitatory neurotransmitter including NMDA, 2-amino-3-(3-hydroxy-5-methyl-isoxazol-4-yl) propanoic acid (AMPA) and metabotropic glutamate receptors in the frontal cortex was reduced in older RTT patients but higher in younger patients (Blue et al., 1999). However, at the macroscopic level there appears to be no major neuronal degeneration or malformations present in the brains of RTT patients.

### 1.3.6.2 Neuronal pathology in RTT mouse models

This phenomenon of alteration in dendritic and axonal growth is consistent in animal models of the disease. Adult *Mecp2* knockout mice have been shown to exhibit abnormal neuronal growth, especially with respect to dendrite formation. For example, knockout mice have thinner dendrites and reduced spine number in pyramidal neurons of the somatosensory cortex at six weeks of age (Fukuda et al., 2005). The same group also showed delayed maturation of postsynaptic densities (Fukuda et al., 2005). More recently, neural stem cells from the dentate gyrus (DG) of the hippocampus in knockout and WT animals were found to proliferate at the same rate and have a comparable cell density (Smrt et al., 2007). This suggests that MeCP2 is not important for early neurogenesis. Further evidence shows that immature neurons in the same area of knockout animals exhibit horizontal and short processes, typical attributes of new neurons during differentiation, indicating impairment in maturation (Smrt et al., 2007).

Additional work studying the morphology of dendrites and axons in two mouse models of RTT (*Mecp2*<sup>-/y</sup> and *Mecp2*<sup>308/y</sup>) supports the previous findings with extensive deformities in the motor cortex, CA1 (Cornu Ammonis Area 1) and fascia dentata of the hippocampus found (Belichenko et al., 2009b). Dendrites were swollen, had diminished spine head area and reduced spine density. Equally axons displayed disrupted organisation of their processes. Intriguingly the changes observed in the dendrites varied extensively between neighbouring neurons (Belichenko et al., 2009b). More work carried out on neuronal cultures transfected with mutant *MECP2*, confirmed the latter findings of decreased spine densities in CA1 region of the hippocampus. Interestingly the effects observed in CA3 (Cornu Ammonis area 3) neurons were milder (Chapleau et al., 2009). Furthermore a recent study has shown that postnatal loss of *Mecp2*, specifically at five (late juvenile stage) or ten (adult stage) weeks displayed smaller brains, increased neuronal density, retraction of dendritic arbour and reduction in spine density in the hippocampus (Nguyen et al., 2012). They also showed reduction in excitatory synaptic proteins including receptor (NMDA and AMPA) and vesicle proteins. Overall, the above data suggest that MeCP2 is important in mature neuron development, specifically with respect to dendrites with subsequent effects on synapse and circuit formation.

The above studies suggest that mutations in MeCP2 could have a cell autonomous effect on morphology. However further work carried out on dendritic morphology has revealed that neurons carrying the mutant *Mecp2* gene could affect neighbouring cells as well (Belichenko et al., 2009). With X-chromosome inactivation, if mutant cells have a direct influence on adjacent neurons which are positive for MeCP2, inevitably there would be some neuropathological effects. Belichenko et al examined dendritic spines in the motor cortex and found a decrease in spine density, head size and increases in spine neck length, spots and long spines in both *Mecp2*-deficient and *Mecp2* positive neurons from heterozygous female mice in comparison with cells from female WT mice. This suggests that *Mecp2* mutant cells are having deleterious effects on nearby neurons in a non-cell autonomous manner. However, *Mecp2*-deficient cells in heterozygous female mice displayed an increase in dendritic swellings or narrowings whereas *Mecp2* positive cells in heterozygous female mice did not signifying that some effects are restricted to *Mecp2* negative cells (Belichenko et

al., 2009a). Overall, effects such as these will be an important factor to consider when investigating synaptic dysfunction and other pathological impairments associated with mutations in *Mecp2*.

### 1.3.6.3 Neuroglia pathology in RTT mouse models

In agreement with the previous work, Ballas et al also claim to see a non-cell autonomous influence of *Mecp2* deficiency on dendritic morphology, however most interestingly this discrepancy involves glia cells (Ballas et al., 2009). Even though MeCP2 is widely expressed throughout the body, the results from neuron specific conditional knockouts, suggested that neuronal deficiency of MeCP2 caused the majority of RTT phenotypes (Guy et al., 2001;

Luikenhuis et al., 2004). Glia cells were not considered to express any MeCP2 (Kishi and Macklis, 2004); however most recent studies contradicted this. For example, non-neuronal cells in the embryo have been shown to express *Mecp2* and that deficiencies in *Mecp2* causes impairment in growth (Nagai et al., 2005). More recently, Ballas et al used an antibody that bound to the C terminus of *Mecp2*, in combination with improved immunostaining, to show that the protein is present in all types of glia in rat and mouse brain (Ballas et al., 2009).

Subsequently, *Mecp2* deficiency in astrocytes (the most abundant glial cell) was investigated by co-culturing WT and *Mecp2* mutated hippocampal neurons in astrocyte conditioned media (ACM) from WT or *Mecp2* mutated astrocytes. The ACM from mutant astrocytes failed to support normal neuronal growth of WT or mutant hippocampal neurons but mutant neurons grown in WT ACM displayed normal dendritic morphology (Ballas et al., 2009). Collectively, this work highlights the importance of MeCP2 in glia cells for normal neuronal function. The toxicity effect that astrocytes appear to have on neighbouring neurons could be mediated by a reduction in certain secreted factors that are fundamental for dendritic morphology or by secretory factors that have a more lethal effect on neurons.

Conversely, another study using conditioned media (CM) from another type of glia cell, microglia (present in macrophages), have shown that hippocampal neurons treated with this CM from *Mecp2*-deficient microglia but not astrocytes exhibit dysfunctional dendritic morphology and abnormalities in postsynaptic

glutamate components (Maezawa and Jin, 2010). They identified glutamate as the toxic secretory factor mediating these effects due to the presence of elevated glutamate levels in microglia from *Mecp2*-deficient mice and blockage of glutamate inhibiting the toxic effects. Furthermore the transplantation of WT microglia into the bone marrow of *Mecp2*-deficient mice (irradiated for mutant microglia) in a recent study (Derecki et al., 2012) resulted in arrest of RTT like pathology including increased lifespan, reduced respiratory abnormalities, increased body weight and improved motor function. Overall the above studies show glia cells, especially microglia, have a significant influence on neuropathology of RTT.

### **1.3.7 Neurophysiological deficits in RTT**

Despite obvious alterations in dendritic morphology, the full extent of abnormalities resulting from MeCP2 deficiency is still not clear. Considering normal brain function is based on a balance between excitatory and inhibitory neurotransmission, any factors that disturb this equilibrium will result in aberrant brain development. Alterations in synaptic output can interfere with information coding in neural circuits and potentially long-term plasticity. Subsequently, a variety of studies have performed a more functional approach to understand the neuronal basis of MeCP2 dysfunction.

#### **1.3.7.1 RTT patients**

The development of epilepsy in ~70-80% of RTT patients is a prominent phenotype (Hagberg, 2002) with the severity of seizures appearing to fall in late adolescence (Steffenburg et al., 2001). Furthermore RTT patients with epilepsy appear to have greater motor dysfunction and cognitive impairment thus highlighting the significance of this phenotype (Kim et al., 2012).

Electroencephalography (EEG) is a useful tool for studying epilepsy allowing characterisation of the events and the ability to determine the specific region of the brain from which seizures arise. Although there are no characteristic EEG patterns in RTT patients (Glaze, 2005), the EEG is still invariably abnormal. For example, epileptiform discharges are common during sleep (Aldrich et al., 1990), prominent rhythmical theta activity (Niedermeyer et al., 1997) and loss of developmental features associated with EEGs including the loss of a dominant

rhythm that usually occurs in the visual cortex at ages 1-4 years (Glaze et al., 1987).

### **1.3.7.2 General abnormalities in RTT mouse models**

As with neuropathological deficits, studies in mouse models of RTT have been advantageous in investigating the neurophysiological deficits in RTT and thus giving insight into the function of MeCP2. In contrast to RTT patients, constitutive *Mecp2* knockout mice do not display a prominent epileptic phenotype (Chen et al., 2001; Guy et al., 2001). However, the male mouse model with a truncated *Mecp2* mutation develop spontaneous myoclonic seizure (Shahbazian et al., 2002) and overexpression of *Mecp2* in mice cause frequent clonic seizures to occur in older (~one year) animals (Collins et al., 2004). These studies suggest that specific mutation types and levels of MeCP2 predispose the development of abnormal neuronal activity in the brain. Although *Mecp2*-deficient mice display abnormalities in EEG activity including spontaneous epileptiform discharges in the cortex (D’Cruz et al., 2010; Colic et al., 2011), dysfunction of cortical delta slow wave activity which usually occurs during sleep (Wither et al., 2012) and gamma and beta band abnormalities in response to auditory stimulation (Liao et al., 2012). Collectively these suggest there is an alteration in network circuitry in *Mecp2*-deficient mice.

### **1.3.7.3 Intrinsic and synaptic property deficits in RTT mouse models**

To investigate these discrepancies in circuitry, other studies have focused on whether a dysfunction in excitatory and inhibitory input to the brain is present in *Mecp2*-deficient mice as these are important factors for regulating neuronal circuitry. The majority of these studies have performed electrophysiological *in vitro* brain slice experiments or culture preparations to investigate the differences in intrinsic and synaptic properties in neurons between WT and *Mecp2*-deficient mice. Firstly, despite the morphological differences in soma size, the intrinsic membrane properties between genotypes are similar. For example, CA3 and CA1 pyramidal neurons in the hippocampus (Zhang et al., 2008), pyramidal neurons in layer V of the somatosensory cortex (Dani et al., 2005) and cortical layer II/III pyramidal (Wood et al., 2009) all showed comparable resting membrane potentials, input resistance and firing patterns

between WT and mutant mice. A lack of change in intrinsic excitability suggests that the physiology of cells in *Mecp2*-deficient mice is normal.

Despite similarities in intrinsic properties, there are documented alterations in both excitatory and inhibitory synaptic properties between WT and *Mecp2*-deficient mice. Whole-cell recordings from *Mecp2* mutant mice coronal brain slices detected a reduction in spontaneous action potential firing in layer V of the somatosensory cortex (Dani et al., 2005). They attributed this to impaired quantal neurotransmitter release from excitatory synapses as spontaneous miniature excitatory postsynaptic currents (mEPSCs) were smaller in mutant mice and no difference was seen in spontaneous miniature inhibitory postsynaptic currents (Dani et al., 2005). Complementary to this work, another group performed experiments in the middle cortical layers of *Mecp2*-knockdown neurons and detected a significant reduction in local excitatory input pathways and unaltered synaptic inputs (Wood et al., 2009). Moreover, another study recorded a reduction in spontaneous mEPSC frequency in hippocampal dissociated cultures but no change in miniature inhibitory postsynaptic currents (mIPSC) properties when compared with WT cultures (Nelson et al., 2006). Further experiments conducted using hippocampal cultures have also shown that neurons grown from *Mecp2*-deficient mice show a reduction in evoked EPSC amplitude and spontaneous mEPSC frequency whereas doubling the levels of *Mecp2* results in an increase in these parameters (Chao et al., 2007). Collectively, all these studies suggest that loss of MeCP2 manifests abnormalities in excitatory neurotransmission leading to a reduction in excitatory synaptic strength and an imbalance in synaptic output which could be linked to aberrant presynaptic transmission properties in mutant animals.

Alterations in inhibitory synaptic properties have also been proposed in *Mecp2*-deficient mice. Whole-cell patch clamp recordings in the brain stem of *Mecp2* knockout mice have revealed impairments in GABAergic synapses (Medrihan et al., 2008). A reduction in the frequency of mIPSPs was observed which is the opposite to some of the studies described above (Dani et al., 2005). There are two inhibitory components in the brain stem, glycine- and GABA<sub>A</sub>- receptor mediated currents and it is therefore important to distinguish the specific pathways affected in RTT. No disparity was observed in glycinergic events but isolation of GABAergic currents demonstrated a similar trend as before with a

decrease in frequency in knockout mice. This data suggests abnormalities with presynaptic components in GABAergic interneurons (Medrihan et al., 2008). Furthermore whole-cell recordings from the CA3 region of the hippocampus in *Mecp2*-deficient mice show elevated spontaneous IPSCs (Zhang et al., 2008). This was accompanied by a decrease in spontaneous EPSCs amplitude leading to the reduced basal inhibitory rhythmic activity also documented in the CA3 (Zhang et al., 2008). Finally recordings from the thalamus reveal alterations in the number and frequency of quantal GABAergic events in excitatory and inhibitory neurons (Zhang et al., 2010). More recently, mEPSC amplitude and frequency were unchanged but mIPSC quantal size reduced in striatal neurons from mice in which *Mecp2* was deleted from GABAergic neurons (Chao et al., 2010). These data suggest that MeCP2 is also required for the normal development of GABAergic circuits and loss of MeCP2 disrupts inhibitory neurotransmission.

It is evident from the above experiments performed on *Mecp2* knockout mice that an alteration in synaptic output is present. However, identification of the underlying components involved has caused some controversy. Possible explanations for varied results could be region or pathway specific differences or even variability caused by the different ages of the animals studied. A combination of both inhibitory and excitatory deficits is also plausible. Considering glutamatergic neurons can synapse onto GABAergic interneurons, discrepancies in either constituent would directly affect the other and therefore contribute to overall changes in synaptic activity. Moreover all the work thus far has emphasised the importance of a balance between inhibitory and excitatory transmission for appropriate MeCP2 function which may be complementary to the morphological deficits observed.

#### **1.3.7.4 Long-term potentiation abnormalities in RTT mouse models**

Long term potentiation (LTP), is a form of synaptic plasticity and typically consists of a prolonged increase in synaptic transmission strength requiring NMDA receptor activation. Several studies, involving various mouse models of RTT, have demonstrated deficits in synaptic plasticity in symptomatic *Mecp2* knockout mice through impairment in LTP at the Schaffer-collateral to CA1 pyramidal cell synapse (Asaka et al., 2006). To specify which synaptic elements are affected, Asaka et al did further work on paired-pulse facilitation (PPF) properties of

hippocampal neurons which is an assessment of presynaptic function. *Mecp2* knockout animals had lower PPF values compared to wild-type controls implying that deficits observed in excitatory neurotransmission may be linked to presynaptic function (Asaka et al., 2006). Another study found a reduction in LTP in the CA1 region of the hippocampus from symptomatic -mildly symptomatic *Mecp2*-deficient mice and that the LTP response became saturated, indicative of a 'ceiling' effect (Weng et al., 2011). This suggests that a reduction in LTP could be associated with synapses from *Mecp2*-deficient mice already operate close to a maximal effect. Furthermore, decreases in LTP in the CA1 region of the hippocampus, motor and sensory cortex were also observed in mice expressing a truncated form of *Mecp2* (Moretti et al., 2006). In contrast, LTP was enhanced in *Mecp2* overexpressing mice (Collins et al., 2004). These results highlight the critical role for tightly regulated MeCP2 levels and that there are age dependent alterations in excitatory synaptic plasticity.

In conjunction with deletion or overexpression of *Mecp2* in neurons, deletion in specific neurons also recapitulates deficits in LTP. For example deletion of *Mecp2* from GABAergic neurons results in an a reduction in fEPSP (field excitatory post synaptic potential) slope which becomes saturated upon a continual increase in stimulus (Chao et al., 2010), Furthermore, impairments in long term depression (LTD), the other synaptic plasticity phenomenon (a long-lasting decrease in synaptic strength), have also been documented in *Mecp2* mutant mice. Low frequency stimulation in the CA1 region of the hippocampus in symptomatic *Mecp2*-deficient mice failed to elicit LTD (Asaka et al., 2006) and mice with a truncated form of *Mecp2* had an impairment in LTD (Moretti et al., 2006). Collectively dysfunction in LTP and LTD could be the result of alterations in excitatory synaptic transmission or GABAergic mediated control of excitatory synaptic plasticity. This is evident upon the onset of RTT symptoms thus highlighting the important role MeCP2 has in the maturing nervous system.

## **1.4 Function of MeCP2**

### **1.4.1 Transcriptional repressor**

Before the discovery of *MECP2* as the primary cause of RTT (Amir et al., 1999), MeCP2 was shown to repress gene transcription upon binding to methylated DNA

(Nan et al., 1997). As mentioned previously, MeCP2 is a methyl binding domain protein which binds to DNA following the addition of a methyl group to carbon-5 of the cytosine pyrimidine ring (DNA methylation); principally at CpG dinucleotides (cytosine and guanine separated by a phosphate). Once bound, the proteins are traditionally thought to recruit a large repressor complex and chromatin remodelling proteins such as HDAC proteins which suppresses gene transcription by chromatin compaction (Jones et al., 1998). Figure 1-5 below demonstrates how MeCP2 is postulated to function and what might happen following mutations of this protein.

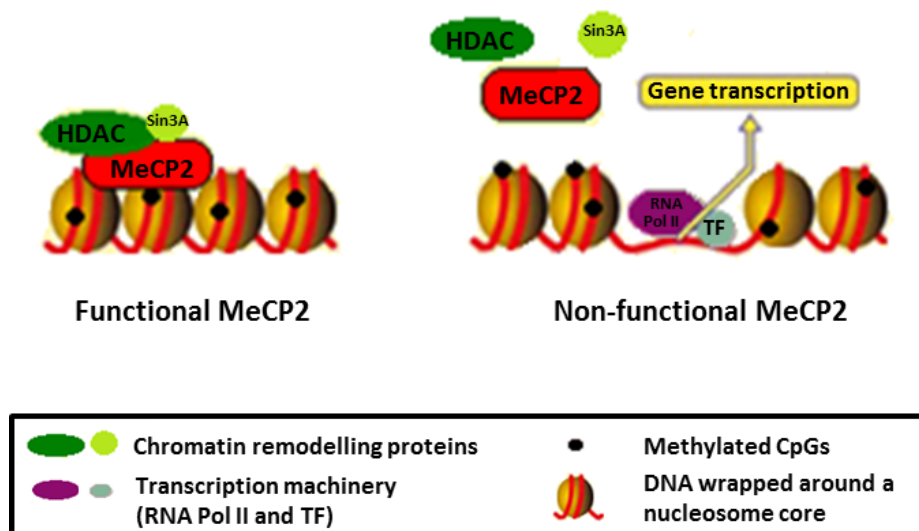


**Figure 1-4 Conventional function of MeCP2 as a transcriptional repressor**

The left diagram represents how MeCP2 is postulated to function by binding to methylated DNA and recruitment of downstream genes through recruitment of chromatin remodelling proteins such as HDAC. The right diagram is a hypothetical situation of what might happen if there was a mutation in MeCP2. The protein would become non-functional potentially inhibiting the binding of MeCP2 to DNA and thus transcription of genes. This diagram is modified from McIntyre et al., 2007.

MeCP2 binds to methylated DNA through interaction with the methyl-CpG-binding domain and recruits transcription factors and chromatin remodelling proteins, such as Sin3A, HDAC and methyl transferases, through the transcriptional repression domain (Jones et al., 1998; Nan et al., 1997). However, it is suggested the transcriptional repression of MeCP2 could be chromatin independent too by means of inhibiting the basal transcriptional machinery through interaction with general transcription factor IIB (Kaludov and Wolffe, 2000). Furthermore, repression is also thought to occur by MeCP2-mediated chromatin remodelling. This involves MeCP2 acting to form a loop of

inactive, methylated chromatin which regulates gene expression by containing deacetylated histones which condense the DNA and restrict transcription (Horike et al., 2005). Either way, mutations in *MECP2* could affect any area of these processes resulting in a partially functioning protein or a complete breakdown in operation. Consequently, the progression of aberrant gene expression was expected with mutations in MeCP2 and a role as a transcriptional repressor.

#### 1.4.1.1 Altered gene expression

Since MeCP2 is postulated to a repressor of gene expression it would be expected that its absence would lead to increased expression of downstream genes. General gene expression profile analysis has reported that less than 5% of genes show considerable differences in regulation (Tudor et al., 2002). One reason for this might be that MeCP2 regulates different sets of genes in diverse cell types, therefore whole brain studies would fail to produce accurate results. However several target genes have been identified. Firstly through the use of chromatin immunoprecipitation (ChIP) and mouse models expressing different gene types, brain-derived neurotrophic factor (*Bdnf*) was first discovered as a target of MeCP2 (Chen et al., 2003). In knockout mice they found a two-fold increase in the *Bdnf* exon IV-specific mRNA compared to WT and suggest that neuronal activity regulates BDNF in a promoter specific manner whereby MeCP2 is released from a BDNF promoter upon depolarisation. BDNF is a member of the neurotrophin family that are classified as secretory proteins involved in neuronal survival and differentiation during early brain development therefore highlighting a potential role for MeCP2 in regulating this process. Conversely, mice lacking *Mecp2* have been shown to have a reduction in *Bdnf* protein levels in the cortex (Chang et al., 2006). However as levels of BDNF are controlled by neuronal activity the overall decline in cortical neuronal activity seen in *Mecp2* knockout mice could explain this occurrence.

Other targets of MeCP2 include imprinted genes, such as *DLX5*. Parental imprinting involves epigenetic marks such as methylation being placed on certain genetic loci during early embryonic development causing the silencing (imprinting) of expression of a specific gene on one parental chromosome only (LaSalle, 2007). *Dlx5* and neighbouring gene *Dlx6* reside on chromosome six and regulate the production of GABAergic neurons in the brain. These genes appear

to be up-regulated in *Mecp2* knockout mice but have unmethylated CpG islands (Horike et al., 2005). However, *Mecp2* binds to methylated sequences and forms a silent chromatin loop (compact DNA) between the two genes which regulates *Dlx5* expression. *Mecp2*-deficient mice have active chromatin and wider loops resulting in greater access to the *Dlx5* region and a subsequent increase in expression (Horike et al., 2005), however other studies have contradicted this process. Schüle et al analysed the imprinting of the *Dlx6* gene using real time quantitative reverse-transcriptase polymerase chain reaction assays for the expression of *Dlx5* and *Dlx6* in the forebrain of mutated mice and found that there was no significant difference between control and mutated samples. Similar results were found in human cell lines (Schüle et al., 2007). This suggests that *DLX5* and *DLX6* are not imprinted in humans and are unlikely to be modulated by MeCP2 thereby questioning their role in RTT and highlighting the importance of specificity in brain cell type for the clarification of results.

Glucocorticoid genes, including corticosterone (McGill et al., 2006), and glucocorticoid-inducible genes, serum glucocorticoid-inducible kinase 1 (*Sgk1*) and FK506-binding protein 51 (*Fkbp5*; Nuber et al., 2005) have also been shown to be upregulated in *Mecp2* mutant mice. Normally, activation of the hypothalamic-pituitary-adrenal (HPA) axis via corticotrophin-releasing hormone (CRH) leads to the release of a steroid hormone corticosterone from the adrenal cortex into the bloodstream whereby it can moderate stress levels (Bale et al., 2002). In a study containing truncated *Mecp2* mice, there was elevation in corticosterone levels, which suggests increased HPA axis activity giving rise to an amplified response to stress. A considerable over-expression of the *Crh* gene in areas of the brain essential for behavioural and physiological responses to stress is reported such as the hypothalamus and central nucleus of the amygdala (McGill et al., 2006). Furthermore, another study using *Mecp2*-deficient mice and cDNA microarrays, has also reported an increase in the expression of two glucocorticoid-inducible genes *Sgk1* and *Fkbp5* (Nuber et al., 2005). Methylated CpG sites are present in these regions and MeCP2 is speculated to bind the regulatory regions of these genes and modulate their function. *Sgk1* is involved in neurotransmission, for example through sodium and potassium channel activation and is therefore likely to be involved in a various aspects of neuronal communication, and thus development. *Fkbp5* encodes a glucocorticoid

receptor-regulating co-chaperone of Hsp90 (heat shock protein 90), a chaperone involved in steroid hormone signalling (Nuber et al., 2005). Consequently modulation of neuronal maturation and transmission could be indirectly affected by MeCP2.

### **1.4.2 Regulation by activity**

Corresponding with the hypothesis of repression is the concept of neuronal activity regulating gene expression profiles (Zhou et al., 2006). At an early age, sensory experience is thought to play an important part in synaptic organization of the brain. Considering that RTT symptoms first become prominent at the same time as synapses are being intensively pruned in response to environmental stimuli, it is possible that inappropriate connectivity due to irregular experience-dependent synaptic modifications may be a cause of pathology.

Membrane depolarization together with a calcium influx into the cell has been linked to phosphorylation of MeCP2 and the activation of downstream target genes (Chen et al., 2003). Using a phospho-site-specific antibody, phosphorylation of MeCP2 specifically at amino acid residue S421 in the brain has been connected with dissociation from methylation sites and activation of genes associated with dendritic growth and spine maturation (Zhou et al., 2006). Figure 1-6 demonstrates this in more detail.

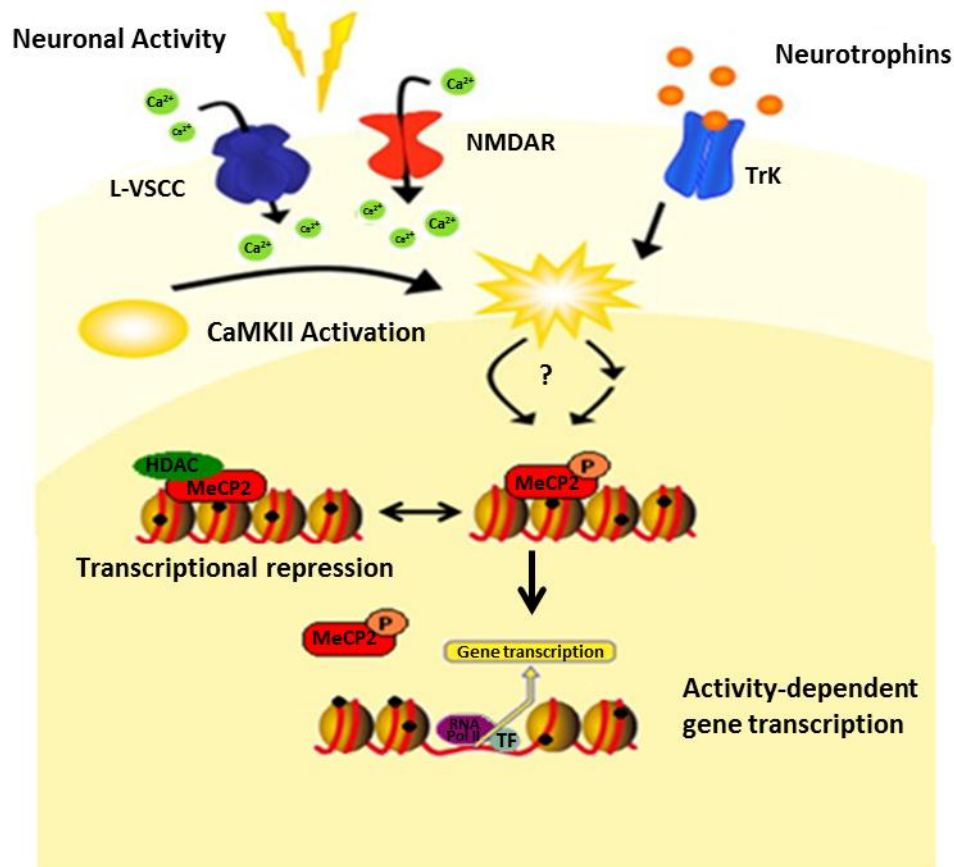


#### Figure 1-5 Activity-dependent phosphorylation of MeCP2

Upon induction of neuronal activity, calcium influx into the cell via long-lasting voltage sensitive calcium channels (L-VSCCs) or N-methyl-D-aspartate receptors (NMDAR) activates a calcium/calmodulin-dependent protein kinase II (CaMKII) which phosphorylates MeCP2 at S421. Alternatively neurotrophins, such as BDNF binding to tyrosine kinase (Trk) receptors, can also trigger the phosphorylation of MeCP2 via calcium independent mechanisms. This results in detachment from methylated DNA sites (black dots) and activation of gene transcription. This diagram is adapted from McIntyre et al., 2007 and Zhou et al., 2006.

It is possible that some missense *MECP2* mutations could lead to a deficiency in the ability of MeCP2 to be phosphorylated in response to activity. This could lead to abnormal regulation of neuronal connectivity and maturation and could explain some of the milder Rett phenotypes seen in some patients. More recently, phosphorylation of Mecp2 at a different site, serine 80 (S80), is thought to be negatively regulated by neuronal activity whereby dephosphorylation occurs upon membrane depolarisation (Tao et al., 2009). It is suggested that S80 phosphorylation is associated with MeCP2 function in resting neurons and S421 phosphorylation in depolarised neurons thus altering gene transcription from a repressed to activated state respectively (Tao et al., 2009). Mutations in *MECP2* at either of these regions would interfere with this process leading to altered gene expression. Overall, these findings suggest a role for activity-dependent regulation of MeCP2.

### 1.4.3 Transcriptional activator

It is hypothesised that in addition to MeCP2's role as a transcriptional repressor it could also be involved in activation of genes (Chahrour et al., 2008; Yasui et al., 2007). Using a ChIP-on-chip approach, Yasui and colleagues carried out an epigenomic binding analysis of known or implemented MeCP2 gene targets and discovered that 62.6% of MeCP2-bound promoters were actively expressed. In addition they found the binding sites for MeCP2 to be mainly non-methylated. These results clearly challenge the previous theory of transcriptional repression however given the study was performed using neuroblastoma cells, the data may not truly reflect the product observed in normal neuronal tissue.

Nonetheless in agreement with this work was a study carried out by Chahrour et al the following year (Chahrour et al., 2008). They decided to analyse the gene expression profiles in the hypothalamus of mice that have no *Mecp2* present or those that have double the amount in the hope of deciphering more information into the molecular mechanism of MeCP2. Through the use of microarray analysis, a variety of genes were found to be altered in both cases. Surprisingly around 85% of these genes appeared to be activated not repressed. ChIP work with the antibody for *Mecp2* confirmed that *Mecp2* bound to the promoter region of six of the activated genes (*Sst*, *Oprk1*, *Mef2c*, *Gamt*, *Gprin1* and *A2bp1*). The same group also identified *Mecp2* to bind to the promoter region of the transcriptional activator CREB1 and also associate with this protein at the promoters of activated target gene (Chahrour et al., 2008). Figure 1-7 demonstrates how this might occur.

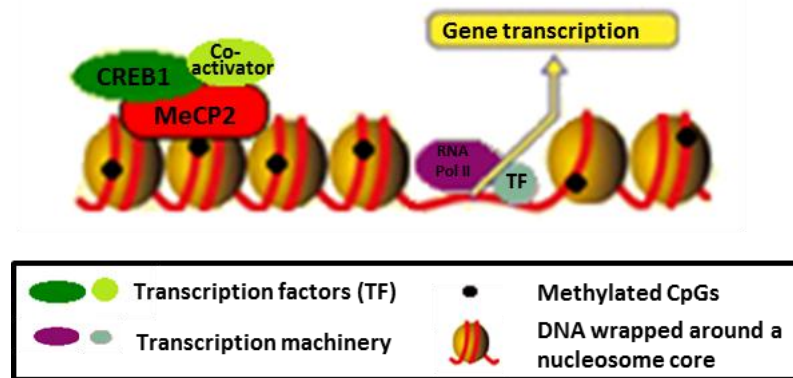


**Figure 1-6 Activation of target genes.**

MeCP2 is postulated to bind methylated DNA and recruit transcriptional activator proteins such as CREB1 at the promoters of active target genes thereby activating gene transcription. This diagram is adapted from McIntyre et al., 2007.

This data supports the idea that MeCP2 has a role in activating target genes and not just repressing them. In this instance, one explanation for these results might be that MeCP2 is repressing a transcriptional repressor therefore activation of the targets of this repressor would occur. Another explanation is that the changes observed might be secondary to the physiological properties of the hypothalamus. In any case these results propose a more complex mechanism of transcriptional regulation by MeCP2 with a variety of genes being either positively or negatively regulated.

#### 1.4.4 Global regulator of chromatin structure

More recently, MeCP2 has been hypothesized to have a genome wide function (Skene et al., 2010). Using ChIP analysis, *Mecp2* was found to bind methylated regions of DNA in neurons globally throughout the entire genome and not at defined gene promoters. Consistent with this, the same group identified the levels of *Mecp2* to be comparable to that of histone octamers, quantified as one molecule of *Mecp2* to every two nucleosomes. Furthermore they also found that *Mecp2* can globally alter the chromatin state with a two fold increase in histone H3 acetylation levels found in *Mecp2*-deficient mice compared to WT controls (Skene et al., 2010). This data suggests that MeCP2 might have a genome wide effect on chromatin structure rather than control the expression of specific genes.

## 1.5 Aims

The overall theme of this thesis is to explore the interactions between neuronal activity, the putative transcriptional repressor MeCP2 and levels of histone protein acetylation. My hypothesis is that neuronal activity modulates MeCP2 and that this is in turn linked to alterations in histone acetylation. As histone acetylation is related with a more open chromatin state (reviewed by MacDonald and Roskams, 2009), MeCP2 may link neuronal activity with the regulation of gene transcription. This proposed interaction is shown in cartoon format in Figure 1-8. In addition to the actions of neuronal activity on MeCP2 signalling, I am also interested the reverse relationship, that of how functional MeCP2 may in turn impact on neuronal activity. For this I pay particular emphasis on how MeCP2 may regulate excitability at the level of the neuronal network. This has significance in RTT in which lack of functional MeCP2 may have network excitability consequences.

Thus, the specific research questions can be stated as follows:

- i. How does the presence or absence of functional MeCP2 affect neuronal network level activity and excitability in the brain?
- ii. How does neuronal network activity affect putative MeCP2 regulation of histone acetylation and immediate early gene activation?

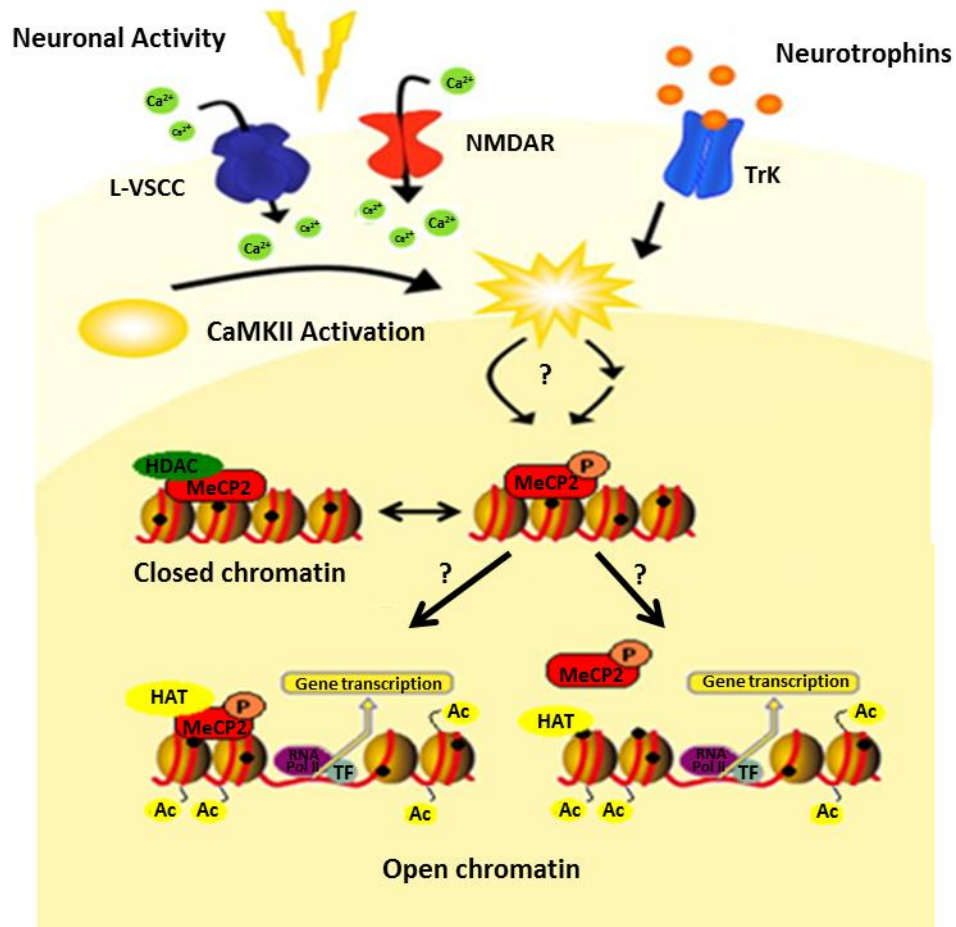


**Figure 1-7 Hypothesis of how MeCP2 controls gene expression in response to neuronal activity.**

Under basal conditions, MeCP2 could bind methylated DNA (black dots) and repress downstream genes through recruitment of histone deacetylase proteins (HDACs) which lead to a closed chromatin state. However upon induction of neuronal activity, MeCP2 becomes phosphorylated (P) which could activate downstream genes through recruitment of histone acetyltransferase proteins (HATs). These proteins acetylate (Ac) lysine residues on histone tails and result in an open chromatin structure which enables transcriptional machinery to enter start transcribing genes. This diagram is adapted from McIntyre et al., 2007 and Zhou et al., 2006.

## Chapter 2

### Materials and Methods

#### 2.1 Animal Models

##### 2.1.1 Generation of the *Mecp2* knockout mouse models

Two mice models were used in which *Mecp2* was either silenced or knocked out. The first model used Cre-*loxP* technology to delete exon 3 and 4 of the endogenous mouse *Mecp2* gene to create a structural knockout mouse (Guy et al, 2001). The second model used the insertion of a *lox-Stop* cassette into intron 2 of the mouse *Mecp2* gene to create a functional knockout mouse (Guy et al, 2007). When heterozygous (Het) females are mated with wild-type (WT) males, a mixture of offspring is generated in a ratio of 1:1:1:1 as summarised in Table 2-1.

**Table 2-1 Offspring generated from *Mecp2* knockout mouse models**

Female	WT male ( <i>Mecp2</i> <sup>+/y</sup> )				
<i>Mecp2</i> <sup>+/-</sup> (Guy et al, 2001)	Sex	Female	Female	Male	Male
	Genotype	WT ( <i>Mecp2</i> <sup>+/+</sup> )	Het ( <i>Mecp2</i> <sup>+/-</sup> )	WT ( <i>Mecp2</i> <sup>+/y</sup> )	Hemizygous ( <i>Mecp2</i> <sup>/y</sup> )
<i>Mecp2</i> <sup>stop/+</sup> (Guy et al, 2007)	Sex	Female	Female	Male	Male
	Genotype	WT ( <i>Mecp2</i> <sup>+/+</sup> )	Het ( <i>Mecp2</i> <sup>stop/+</sup> )	WT ( <i>Mecp2</i> <sup>+/y</sup> )	Hemizygous ( <i>Mecp2</i> <sup>stop/y</sup> )

Both models were housed at the University of Glasgow. Heterozygous females (*Mecp2*<sup>+/-</sup> and *Mecp2*<sup>stop/+</sup>) were bred on an inbred C57BL6/J background to generate offspring as mentioned above. Mice aged 6-10 weeks from these colonies were used in all experiments. However a subset of experiments were conducted using heterozygous female mice aged 10-13 weeks engineered to express a *Mecp2*-EGFP fusion by a targeted gene knock-in in mouse ES cells (generated in Adrian Bird's laboratory at the University of Edinburgh; *Mecp2*<sup>tm3.1Bird</sup>, Jackson Laboratories stock no. 014610). *Mecp2* status was detected in cells by the presence or absence of fluorescence in living or fixed cells. These heterozygous females (*Mecp2*<sup>GFP/+</sup>) were produced by breeding

*Mecp2*<sup>+/-</sup> females with *Mecp2*<sup>GFP/y</sup> males (supplied by Adrian Bird's laboratory) on a C57BL6/J background.

Offspring genotypes from all colonies were determined by Polymerase Chain Reaction (PCR). Mice were housed in groups with littermates, maintained on a 12 hour light/dark cycle and provided with food and water *ad libitum*. Experiments were carried out in accordance with the European Communities Council Directive (86/609/EEC) and a project license with local ethical approval under the UK Animals (Scientific Procedures) Act (1986).

## 2.1.2 Genotyping

### 2.1.2.1 DNA Extraction

DNA samples were taken from mouse ear samples and placed into pre-labelled 200µl PCR tubes (Fisher Scientific, UK) with 20µl of a DNareleasy reagent (Anachem Ltd, UK). Each sample was then positioned into a GeneAmp thermal cycler (PCR system 9700; Applied Biosystems, UK) and run under the following conditions stated in Table 2-2.

**Table 2-2 DNA extraction conditions**

Temperature (°C)	Duration (mins)
75	5
96	2
20	hold

### 2.1.2.2 PCR confirmation of genotypes

Extracted DNA was diluted in autoclaved dH<sub>2</sub>O (1/10) before two sets of PCR reactions were carried out on each DNA sample to enable characterisation of genotype. The first reaction contained primers that would anneal to the WT *Mecp2* allele (forward primer = P5, reverse primer = P7) and the second reaction include primers that would anneal to the *Mecp2* knockout allele (forward primer = P5, reverse primer = P6). All primers were designed by Guy et al, 2001. The contents of each PCR reaction (placed in separate labelled PCR tubes) is summarised in Table 2-3.

**Table 2-3 Contents of each PCR reaction**

Reagent	WT <i>Mecp2</i> allele	<i>Mecp2</i> knockout allele
Thermo-start HP PCR master mix	13µl	13µl
Autoclaved water	9µl	9µl
Forward Primer	P5 1µl (0.4µM)	P5 1µl (0.4µM)
Reverse Primer	P7 1µl (0.4µM)	P6 1µl (0.4µM)
DNA sample	2 µl (5-10ng)	2 µl (5-10ng)
<b>Final Volume</b>	26µl	26µl

These two PCR reactions were subsequently run under identical conditions on a GeneAmp thermal cycler (PCR system 9700) as stated in Table 2-4.

**Table 2-4 PCR conditions for both reactions**

Step	Temperature (°C)	Time
Initial de-naturation	94	15 minutes
<b>X 35 cycles</b>		
De-naturation	94	45 seconds
Annealing	61	45 seconds
Extension	72	45 seconds
<b>Final extension</b>		
Final extension	72	10 minutes
Hold	4	infinity

Finally the PCR products from each PCR reaction were mixed with 3µl of 5 x DNA loading dye and separated according to their size by gel electrophoresis on a pre-made 0.8% agarose gel at 110 volts for one hour. Upon completion, separated PCR products were visualised using an UV transilluminator (UV-TM-40; Upland, USA; wavelength 254nm) and photographed using Canon digital camera (PC1192; Japan) to confirm genotype status. An example of such a gel is shown in Figure 2-1.

As discussed previously, in order to distinguish the genotype of each DNA sample two PCR reactions were performed. The first lane of each sample was loaded with the PCR product from the WT *Mecp2* allele (producing a 416bp band) and

the second lane was loaded with the PCR product from the *Mecp2* knockout allele (generating a 470bp band). WT mice (male and female) were identified by the presence of a band only in the WT *Mecp2* allele lane, a hemizygous male would only generate a band in the *Mecp2* knockout allele lane, and a heterozygous female mouse would display a band in both lanes.

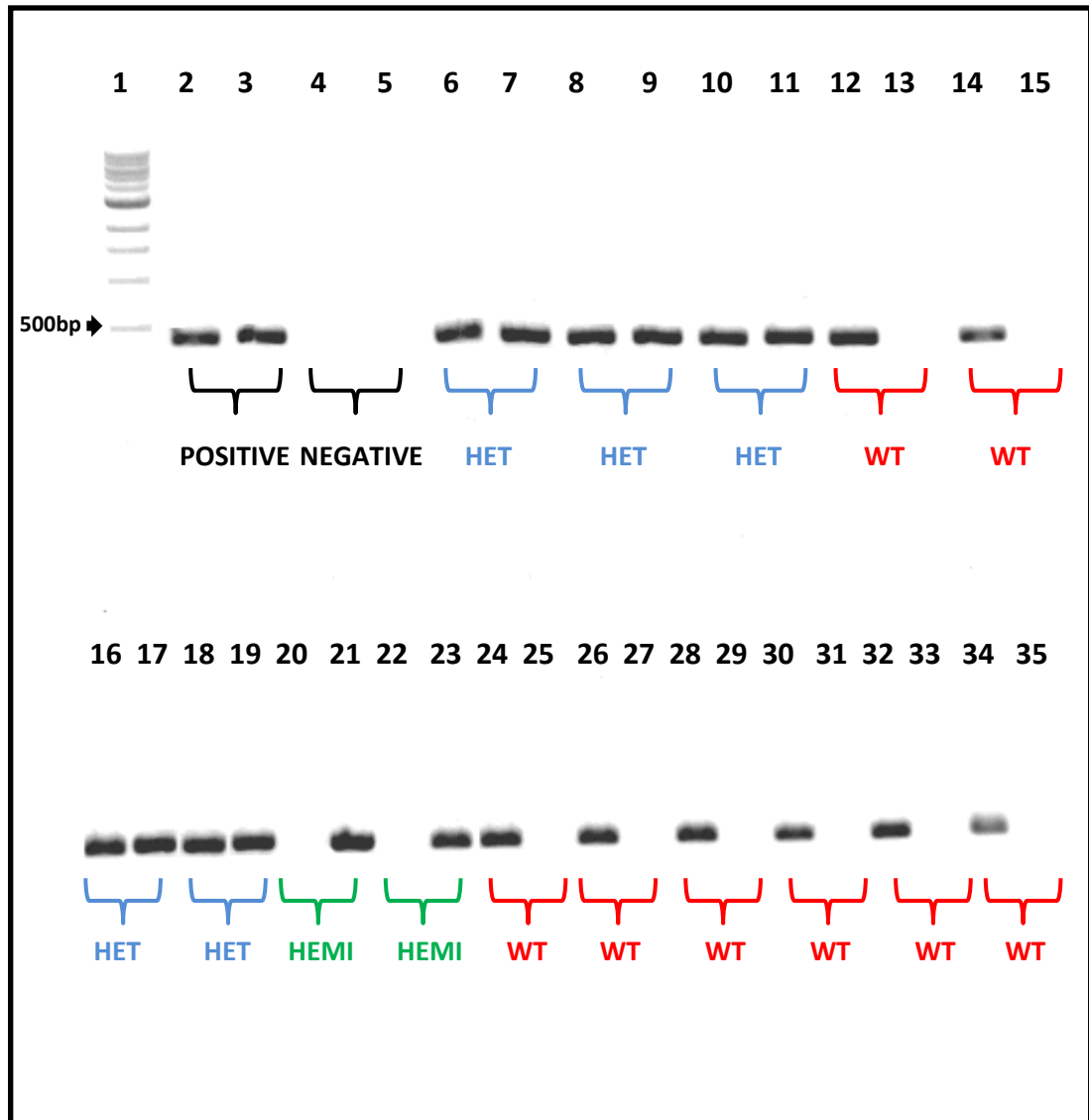


### Figure 2-1 Genotype verification by PCR

Representative gel image showing the genotypes of mice that were verified by PCR. Each DNA sample from a mouse is represented by two lanes (two PCR reactions) – the first identifies the WT *Mecp2* allele and the second identifies the *Mecp2* knockout allele. Heterozygous (Het) female mice (blue) contain a band in both lanes (e.g. DNA sample in lane 6 and 7), WT mice (red) have a band in the first lane only (e.g. DNA sample in lane 12 and 13) and hemizygous (hemi) male mice (green) contain a band in the second lane only (e.g. DNA sample in lane 20 and 21). The genotype of a known heterozygous female mouse is used as a positive control for the PCR reaction (lane 2 and 3) and a sample with no DNA is used as a negative control (lane 4 and 5). A 1kb DNA ladder (New England Biolabs, UK) is loaded in lane 1.

## 2.2 *In vitro* hippocampal slice experiments

### 2.2.1 Acute slice preparation

*Mecp2<sup>stop/y</sup>* mice and their wild-type litter mates were culled by cervical dislocation, followed by decapitation; all conducted under Schedule 1 procedures under the Home Office Animals (Scientific Procedures) act 1986. The brain was quickly removed and transferred to ice-cold, oxygenated (95% O<sub>2</sub>, 5% CO<sub>2</sub>) sACSF. Next the cerebellum and a small section of the frontal cortex were removed before the brain was hemisected down the midline. The two hemispheres were then placed on the side that was just cut and the inside dorsal part of the brain was cut away as show in Figure 2-2. Subsequently this region of each hemisphere was fixed with cyanoacrylate glue (Loctite, UK) onto the stage of a vibratome (Leica VT1200S; Leica Microsystems, Germany). Transverse tissue slices (400µm) were cut and the hippocampus removed from the adjoining tissue. Slices were immediately transferred to a submerged chamber perfused with oxygenated (95% O<sub>2</sub>, 5% CO<sub>2</sub>) sACSF maintained at 34°C. After 30 minutes, slices were either kept at 21°C in the same chamber (for later use) or placed directly into an interface chamber kept at 34°C where they were left to equilibrate for a further 30-60 minutes before recording commenced. This chamber was oxygenated with Recording ACSF containing at a flow rate of 5-6ml/minute.

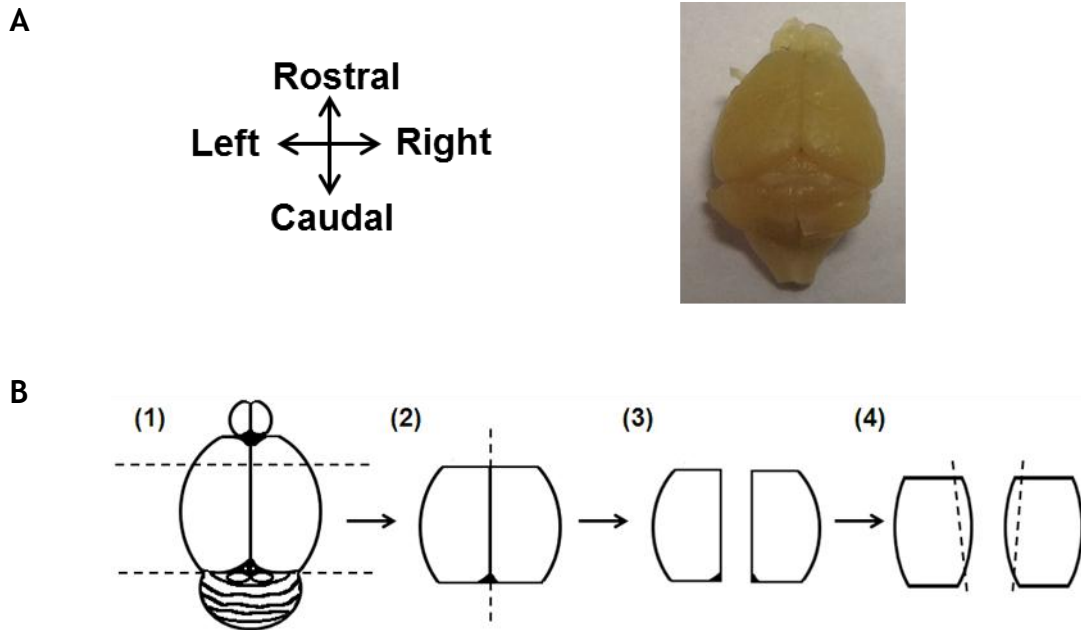


**Figure 2-2 Mouse brain orientation and hippocampal slice preparation.**

(A) Birds eye view of a real mouse brain and anatomical orientations. (B) Schematic diagram of how the brain is dissected in preparation for obtaining transverse hippocampal slices: (1) the frontal cortex and cerebellum are removed; (2)–(3) the brain is hemisectioned down the midline and (4) then the two hemispheres are placed on their side that was just cut and an incision is made into the inside dorsal part of each brain section. This region of each hemisphere is then fixed with cyanoacrylate glue onto a vibratome.

## 2.2.2 Extracellular recording

### 2.2.2.1 Bicuculline and 4-aminopyridine (4-AP) administration

Recording glass microelectrodes were made from standard walled (1.2mm O.D. x 0.69mm I.D.) borosilicate glass capillaries (Harvard Apparatus, UK) and pulled on a Flaming/Brown micropipette puller (Model P-87, Sutter Instrument Co., USA) with a tip resistance of ~1-5M $\Omega$ . Stimulating electrodes were made from bipolar tungsten wire (World Precision Instruments, USA) to which current was delivered through an isolated current stimulator box (Model D52A, Digitimer Ltd, UK). Recording electrodes were filled with ACSF and positioned in the stratum radiatum of area CA1 whilst stimulating electrodes were positioned in the Schaffer-collateral afferent fibres (axons from pyramidal cells in the CA3 region) to record field excitatory postsynaptic potentials (fEPSPs).

Recordings were amplified (10X) using an Axoclamp 2A amplifier (Molecular Devices, USA) in bridge mode, filtered (100 kHz) with a Brownlee Model 440 Signal Processor (Brownlee Precision Co, USA) and digitized at 10 kHz (Digidata 1322A, Axon Instruments) onto two PC hard discs using WinWCP data acquisition

software (John Dempster, University of Strathclyde; Glasgow, UK) and Axoscope software (Molecular devices, USA). A Hum Bug 50/60Hz noise eliminator (Quest Scientific, UK) was also used to reduce background electrical noise (50Hz). All recordings used a stimulus protocol comprised of pulses that were 10ms apart. Stimulus intensity for each experiment was determined at the start by obtaining an input-output curve for each slice though increasing the stimulating current pulse in 0.2 increments from a low current pulse ( $-0.02\text{mA}$ - $0.32\text{mA}$ ) to the point a maximal fEPSP was generated. The current pulse equating to half of this maximal response was then used for the entire experiment. Subsequently, evoked fEPSPs and spontaneous fEPSPs were monitored simultaneously during a 10 minute baseline and following either bicuculline (Abcam, UK) or 4-aminopyridine (Sigma Aldrich, UK) administration. An input-output curve was also performed at the end of each experiment.

#### **2.2.2.2 Kainic acid administration**

ACSF-filled glass microelectrodes were placed in the CA3 stratum radiatum. Recordings were amplified (10X) with the signal low pass filtered at 100Hz as before. The signal was amplified by a further 1000X using the Brownlee model 440 instrumentation amplifier and digitized at 4kHz onto PC hard disk using Axoscope software (Molecular devices). Following two minute baseline recording, kainic acid (Abcam; 400nM) was administered for one hour before a further two minute recording was taken from each slice in the chamber (up to six). Subsequently, NBQX ( $5\mu\text{M}$ ) was co-applied and additional two minute recordings were collected. Gamma oscillations were identified as high frequency field potential oscillations and confirmed offline using power spectrum and autocorrelation analysis.

#### **2.2.3 Data analysis**

For extracellular bicuculline and 4-AP experiments event analysis was conducted offline using Christoph Schmidt-Hieber's Stimfit 0.9 software (evoked EPSPs; <http://www.stimfit.org/>) and Clampfit 9.0 software (spontaneous EPSPs; Molecular devices, USA). Event analysis for extracellular kainic acid experiments was conducted using Axograph X software (Molecular devices) offline. Fast Fourier Transform (FFT) was used on each two minute recording to create a

power spectrum of gamma oscillations formed by averaging segments of 1024 data points. Total power was calculated as the area under each power spectrum between 20-80Hz and peak frequency was taken as the dominant peak in this region. Samples were defined as epileptic and removed if moderate levels of spontaneous spiking events were detected in the baseline recording. Epileptiform baselines were defined as greater than 30 events in a two minute trace.

## **2.3 *In vivo* kainate experiments**

### **2.3.1 Administration of anaesthesia and kainic acid**

*Mecp2<sup>stop/y</sup>*, *Mecp2<sup>-/y</sup>*, *Mecp2<sup>+/-</sup>*, *Mecp2<sup>GFP/-</sup>* mice and their WT littermates (male and female) were injected with kainic acid (Abcam; 25 mg/Kg IP in 0.9% saline) or 0.9 % saline (vehicle control). Each mouse was weighed just before the start of each experiment and the appropriate dose to be given was calculated. For most experiments, mice were maintained under light isoflurane anaesthesia (2.5-3%) to reduce suffering. This involved mice being placed into a transparent, sealed plastic box with a constant and controlled supply of isoflurane added (5%). Once mice were unconscious (lying still with only breathing movements) kainic acid or saline was then given. A subset of experiments was also conducted in the absence of anaesthesia in which mice were injected with either kainic acid or saline and then placed into the same transparent plastic box (Figure 2-3).

### **2.3.2 Seizure Score**

Initial seizure scoring of mice that were given kainic acid was carried out in real time by observing the animals and logging the score every five minutes for three hours. In addition, all experiments were captured by a video camera, positioned below the transparent plastic box, which was connected to a computer. This set-up is shown in Figure 2-3. Furthermore, every mouse was marked with a different coloured strip on their tail to allow easy identification during the experiment.

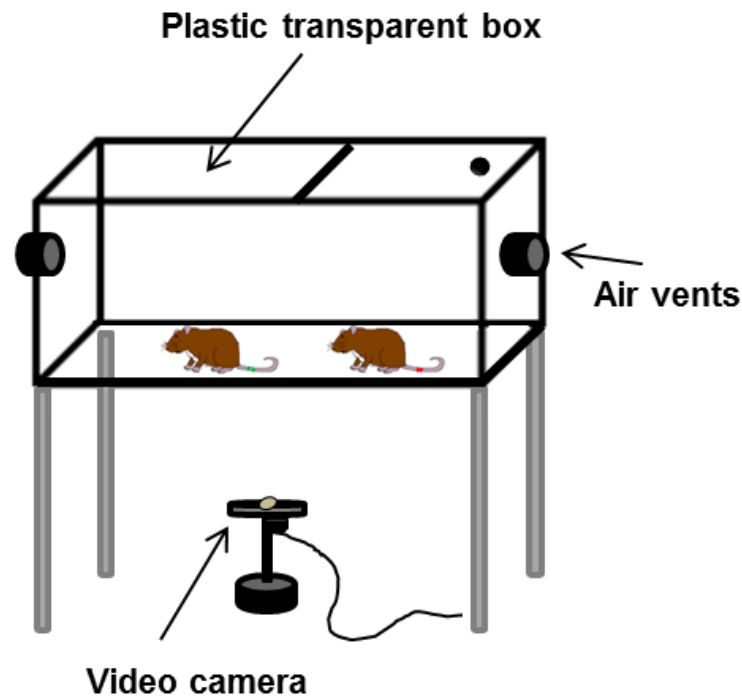
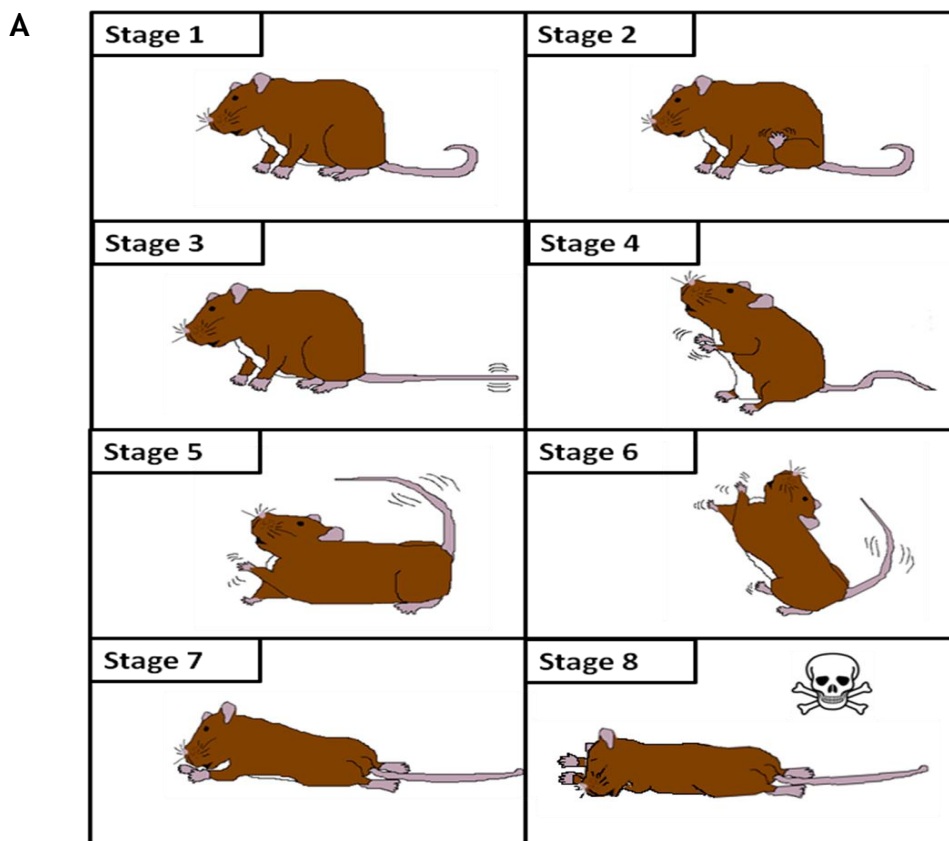


**Figure 2-3 Set-up used for monitoring the seizure scoring**

The set-up used for monitoring seizure scoring consists of a plastic transparent box with a video camera placed underneath which is connected to a computer. When the mice are under anaesthesia, the air vents are kept connected to the isoflurane. All mice have a different colour stripes on their tails to identify them during scoring.

Seizure score was modified into eight stages from a previously documented scale (Racine, 1972) and an illustrated example of the seizures developed with and without anaesthesia can be seen in Figure 2-4. To ensure a roughly even number of animals was in each group, mice were genotyped before conducting the experiments. As all experiments were carried out by the same person, the seizure scoring of mice was not performed blind. Seizures comprised of fast breathing and erratic twitches in the early stages before development of tail shaking, forelimb clonus (front paw shaking) and ultimately full tonic-clonic seizures in the later stages of epilepsy.



**B**

Stage	Without anaesthesia	With anaesthesia
0	Normal exploratory activity	Lying still with controlled breathing
1	Hunched/immobile behaviour with fast breathing	Lying still with fast breathing
2	Generalised spasm/twitch or scratching behaviour	Lying down with generalised spasm/twitch
3	Tail extension (with or without shake)	Lying down with tail extension (with or without shake)
4	Forelimb clonus (forepaw shake)	Lying down with forelimb clonus
5	Forelimb clonus plus tail shake (one time)/ loss of balance	Lying down with forelimb clonus plus tail shake (one time)
6	Continuous forelimb clonus plus tail shake (>2)/ hyperactive seizures	Continuous forelimb clonus plus tail shake (>2)
7	Full body extension (full tonic extension)	Full tonic-clonic seizures/ hyperactive seizures
8	Death	Death

**Figure 2-4 Illustrated example of seizure score upon IP injection of kainic acid in mice**  
 (A) Diagrammatic examples of the eight seizure score stages (amended from (Racine, 1972)). Note, the examples are from mice without anaesthesia. (B) Descriptive explanation of each illustrated seizure stages with and without anaesthesia. Seizures comprised of fast breathing and erratic twitches in the early stages before they develop tail shaking, forelimb clonus (front paw shaking) and ultimately full tonic-clonic seizures in later stages. Animals with anaesthesia exhibit almost identical phenotypes to mice administered kainic acid without anaesthesia except they are lying flat from being unconscious.

### **2.3.3 Tissue preparation for protein analysis**

Following kainic acid-induced seizures, mice were handled in two manners. For western blot analysis, mice were killed by cervical dislocation and decapitation. The hippocampi were then quickly removed from each hemisphere and placed in 1.5ml eppendorf tubes (Greiner bio-one, UK) before being snap frozen in liquid nitrogen to be stored at  $-20^{\circ}\text{C}$  for later use. For tissues required for immunohistochemistry, mice were anaesthetised with sodium pentobarbital (Euthatal) at a dose of 100 mg/kg body weight (Merial Animal Health Ltd., Harlow, UK) in preparation for intracardiac perfusion. Subsequently having confirmed no reflexes were present in the mice, the chest of each mouse was opened up to expose the heart and a perfusion needle was inserted into the left ventricle. A small cut was made in the right atrium of the heart and saline solution was flushed through the animal briefly to clear blood vessels. Finally 300ml of 4% paraformaldehyde (PFA) in 0.1M PB (pH 7.5) was perfused through the needle to fix the mouse. At the end of the process the mouse would be completely rigid with an almost clear liver. Whole brains were subsequently removed, post-fixed overnight in the same fixative at  $4^{\circ}\text{C}$  then transferred to 30% sucrose (Fisher Scientific) in 0.1 PBS. Brains were cut into blocks and coronal brain sections ( $30\mu\text{M}$ ) were cut on a vibratome (Leica VT1000 microtome, Leica Microsystems) and then placed in a solution of 50% ethanol (BDH Laboratories, UK) dissolved in  $\text{dH}_2\text{O}$  for 30 minutes to aid future antibody penetration. Finally sections were washed three times in 0.3M PBS and placed in 100% glycerol (Sigma-Aldrich) to be stored at  $-20^{\circ}\text{C}$  and used for immunohistochemistry.

## **2.4 Protein analysis**

### **2.4.1 Western blot**

#### **2.4.1.1 Protein quantification**

Hippocampal extracts for western blot analysis were homogenised in 500 $\mu\text{l}$  cell lysate buffer by grinding in a 1.5ml eppendorf tube (Greiner bio-one) with a plastic pestle (Sigma-Aldrich, Z359947) with no removal of tissue. Optimisation of this nuclear preparation method is shown in Appendix A (Supplementary Figure 1-1). A Bradford protein assay was then used to normalise the protein

content of the hippocampal lysates. This was achieved by comparing each hippocampal lysate against a standard curve of known protein content - Bovine Serum Albumin (BSA; Sigma-Aldrich) dissolved in dH<sub>2</sub>O to obtain a concentration range including (in mg/ml) 0, 0.25, 0.50, 1, 1.5 and 2. Each hippocampal lysate (diluted 1/100) and BSA standard was mixed with diluted (1:1 in dH<sub>2</sub>O) Bio-Rad protein assay dye reagent (Bio-Rad laboratories, UK). Subsequently each standard and hippocampal lysate was pipetted twice into a 96-well plate and the absorbance measured with an Opsys MR plate reader (Dynex Technologies, UK) using Revelation Quicklink software (Dynex Technologies, version 4.25) at a wavelength of 595nm. The average reading of the blank wells (0mg/ml BSA) was subtracted from the other standards and the standard curve plotted using a linear curve fit. An example of this curve fitting and absorbance calculation is observed in Figure 2-5.

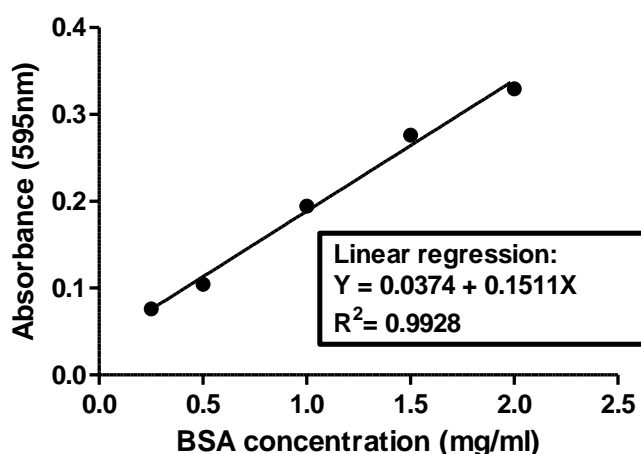


**Figure 2-5 BSA curve fitting in a Bradford protein assay.**

An example of a BSA standard curve used for quantifying the protein content of unknown hippocampal lysates. A linear regression is used to determine the line of best fit and calculate absorbance of the unknown samples.

Finally, once read the measurements for each hippocampal lysate, taken from the Revelation Quicklink software, were multiplied by 100 to compensate for the dilution factor applied at the start.

#### 2.4.1.2 General method

Hippocampal lysates of known protein content were made up to equal working concentrations using appropriate volumes of ddH<sub>2</sub>O. Samples were then thoroughly mixed with 4x lithium dodecyl sulfate (LDS) sample buffer (Life

Technologies, UK) at a ratio of 2/3 protein to 1/3 LDS before being boiled for 5 minutes to shear genomic DNA. Equal amounts (20µg) of each sample and Prestained Protein Ladder (Fermentas, UK) were electrophoresed through a 4-12% Bis-Tris NuPAGE gel (Life Technologies) in 20 X NuPAGE MOPS running buffer (diluted 1/20, Life technologies) at 120V for two hours. Proteins were then transferred using Transfer buffer to polyvinylidene difluoride (PVDF) membranes (Life Technologies) for 90 minutes at 30V, 220mA. Membranes were rinsed in ddH<sub>2</sub>O and soaked in Ponceau red (Sigma-Aldrich) for five minutes to check transfer efficiency.

Subsequently, membranes were placed in blocking solution containing 5% (w/v) dried skimmed milk powder (Marvel), diluted in Tris buffered saline (TBS) for one hour and probed over night at 4°C with primary antibodies (Table 2-5) in the same blocking solution. The only exception was the primary antibody anti-pS421 MeCP2 which was incubated in a solution containing 5% (w/v) bovine serum albumin (Sigma-Aldrich) diluted in TBS. The next day, handling of the membranes differed depending on the exposure technique. With exposure to enhanced chemiluminescence (ECL), membranes were washed three times in TBS containing 0.1% Tween-20 (TBST; Sigma-Aldrich) for 10 minutes each before incubation with horseradish peroxidase (HRP)-conjugated secondary antibodies (Table 2-5) in blocking solution for one hour at room temperature. Following three more washes in TBST, membranes were incubated in Immobilon Western Chemiluminescent HRP Substrate (Millipore, UK) using equal quantities of luminol and peroxide solution for five minutes on a shaker. Finally membranes were placed into a cassette and developed using x-ray films (Kodak, UK) on a Kodak X-OMAT 2000 processor with the exposure time varied depending on the antibody used. In each case the aim was to achieve an optimal balance between signal-background ratios.

Conversely, membranes exposed to an infrared scanner were washed three times for 15 minutes each in TBST before being blocked for 30 minutes in 5% milk blocking solution. Fluorescent secondary antibodies (Table 2-5) were applied to the same solution for one hour in the dark. Membranes were washed four times in TBST (five minutes each) in the dark then a further five times in TBS to remove any Tween-20. Finally, results were visualised using an Odyssey Infrared Imaging Systems scanner (LI-COR Biosciences, USA).

**Table 2-5 Primary and secondary antibodies used for western blots**

Antibody	Dilution	Supplier
<b>Primary</b>		
Mouse anti-MeCP2	1/1000	Sigma- Aldrich
Rabbit anti-MeCP2	1/1000	Millipore
Rabbit anti-pS421 MeCP2	1/2000	Gift from Greenberg lab in the USA
Mouse anti-NeuN	1/2000	Millipore
Rabbit anti-acetyl-Histone H4	1/5000	Millipore
Rabbit anti-acetyl-Histone H3	1/10,000	Millipore
Rabbit anti-Histone H3	1/20,000	Abcam
Rabbit anti-c-Fos	1/1000	Millipore
Rabbit anti-Egr-1	1/1000	Santa Cruz Biotechnology, USA
Mouse anti-GAPDH	1/2000	Santa Cruz Biotechnology
<b>Secondary</b>		
Goat anti-Rabbit IgG HRP (ECL)	Range 1/5000-1/20,000, depending on primary	Millipore
Goat anti-Mouse IgG HRP (ECL)	1/5000	Millipore
IRDye 800CW Goat anti-Rabbit IgG (infrared)	Range 1/5000-1/10,000, depending on primary	LI-COR
IRDye 800CW Goat anti-Mouse IgG (infrared)	1/5000	LI-COR

#### 2.4.1.3 7% gel electrophoresis

To resolve Mecp2 (75kDa in weight) and quantify absolute levels of phosphorylated Mecp2 protein, 7% gels were used for electrophoresis in some experiments to resolve the higher weight protein. 7% polyacrylamide resolving and stacking gels were prepared as stated in the general material section in this chapter and 60-80µg of hippocampal lysates were run in Tris-glycine buffer overnight (4° C) slowly at 15mA. The gel was kept running until the 55kDa band on the Prestained Protein Ladder ran off the gel. The gel was then cut at the appropriate size and the western blot performed as described above. Mecp2 was immunostained with the rabbit anti-MeCP2 antibody from Millipore and visualised by ECL.

#### 2.4.1.4 Analysis

The x-ray films developed from ECL were scanned onto a computer in colour using a flat-bed HP Scanjet 4400c scanner and protein intensity quantified using the analysis of gels option in Image J software (<http://rsbweb.nih.gov/ij/>) as shown in the example in Figure 2-6. This involved images being converted into grayscale and, using the rectangular selection tool, large rectangles were drawn around each band of interest in turn. Subsequently, a profile plot was created for each selected area and a straight line was drawn at the base of each peak, from one side to the other to enclose the area of the peak (the tails to either side of the peak were the background signal). Finally, using the wand tracing tool to select each peak, the size could be expressed as a percentage of the total size of all the measured peaks. If a loading control was present the percentage value of the protein of interest was divided by the loading control (NeuN) percentage to get a relative intensity.

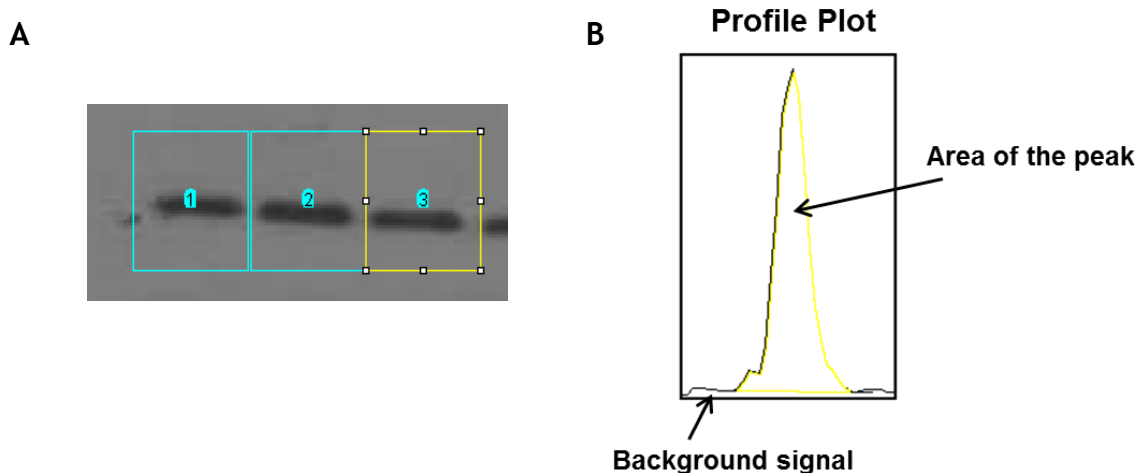


**Figure 2-6 Analysis of western blots in Image J**

(A) Rectangles are drawn around the bands of interest and (B) a profile plot is then created for each band. A line is drawn at the base of each peak to enclose the area of each peak with tails on either side encompassing the background signal. Each peak is selected (yellow) and the size calculated.

Probing for Mecp2 run on a 7% gel, highlighted two bands around 75 kDa in some hippocampal lysate samples (the top band = phosphorylated Mecp2 and the bottom band = unmodified MeCP2). To quantify the total levels of phosphorylated Mecp2, the percentage value of the top band was divided by the sum of the percentage values of both bands together to give a percentage difference.

Membranes scanned using an infrared scanner were analysed using Odyssey Infrared Imaging System version 3 (LI-COR Biosciences). A box was drawn around each fluorescent bands of interest and an integrated intensity measurement was determined. No background subtraction was needed as the software compensated for this already in the intensity outputs. Subsequently, the intensity readings of each main protein of interest were divided by their respective loading control (NeuN) to account for gel loading variations. Finally, most western blots contained two genotype (WT or *Mecp2<sup>stop/y</sup>*) and treatment (saline or kainic acid) group replicates on the one gel to minimise inter-gel variability. To enable comparison of results, integrated intensities of each main protein of interest were divided by the average of the WT saline group and plotted as fold change relative to this group.

## 2.4.2 Immunohistochemistry

### 2.4.2.1 General Method

Free-floating coronal brain sections from *Mecp2<sup>+/-</sup>* and *Mecp2<sup>GFP/-</sup>* mice were washed three times (10 minutes each) in 0.3M NaCl buffered saline (PBS) at room temperature and blocked using 15% (w/v) normal goat serum in 0.3M PBS with 0.3% Triton-X-100 for one hour at room temperature. Sections were then incubated with primary antibodies (Table 2-6) in 0.3M PBS with 0.3% Triton-X-100 (Sigma-Aldrich) at 4°C for two-three days. Subsequently sections were rinsed three times in 0.3M PBS before incubation with fluorescent secondary antibodies (Table 2-6) in 0.3M PBS with 0.3% Triton-X-100 (in the dark) overnight at 4°C. Sections were then washed a final three times in 0.3M PBS in the dark prior to incubation with the nuclei marker 4', 6-diamidino-2-phenylindole (DAPI, Sigma-Aldrich; dissolved in dH<sub>2</sub>O to make a 20mg/ml stock; 1/1000 working dilution) in 0.3M PBS for 30 minutes at room temperature. Finally sections were mounted in Vectashield (Vector labs, UK) on coverslips and optical image stacks collected on a Leica SP5 Confocal microscope (Leica Microsystems) equipped with diode (405nm), argon (488nm), diode pumped solid-state (DPSS; 561nm) and red helium-neon (633nm) lasers.

**Table 2-6 Primary and secondary antibodies used for immunohistochemistry**

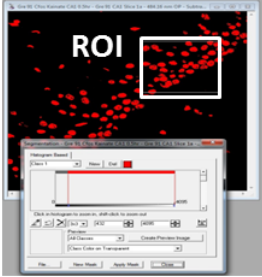
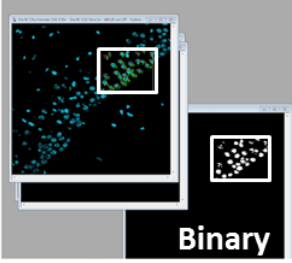
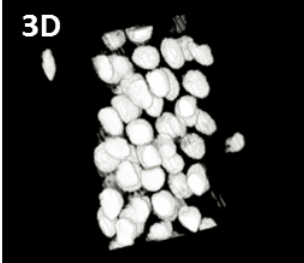
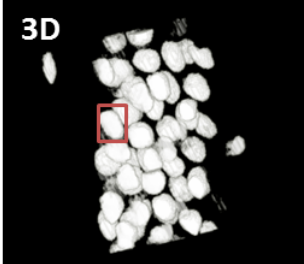
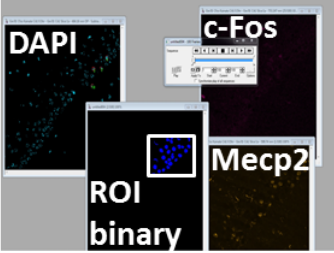
<b>Antibody</b>	<b>Dilution</b>	<b>Supplier</b>
<b>Primary</b>		
Mouse anti-MeCP2	1/500	Sigma-Aldrich
Rabbit anti-pS421 MeCP2	1/2000	Gift from Greenberg lab in the USA
Rabbit anti-acetyl-Histone H4	1/100	Millipore
Rabbit anti-acetyl-Histone H3	1/200	Millipore
Rabbit anti-Histone H3	1/100	Abcam
Mouse anti-Histone H4	1/200	Abcam
Rabbit anti-c-Fos	1/4500	Millipore
Rabbit anti-Egr-1	1/100	Santa Cruz Biotechnology
<b>Secondary</b>		
Alexa fluor 488 goat anti-rabbit	1/500	Life Technologies
Alexa fluor 488 goat anti-mouse	1/500	Life Technologies
Alexa fluor 546 goat anti-mouse	1/500	Life Technologies
Alexa fluor 647 goat anti-rabbit	1/500	Life Technologies

Additionally, before sections were probed with primary antibodies, rabbit anti-Histone H3 and rabbit anti-Histone H4, they had to undergo an antigen retrieval step. This involved, rinsing the free floating coronal brain sections three times (for 10 minutes each) in 0.1M phosphate buffer (PB) before transferring to 10mM sodium citrate buffer preheated to and maintained at 80°C in a water bath for 30 minutes. Retaining the sections in the same solution, they were allowed to cool to room temperature then washed three times in 0.1M PB. Subsequently, sections were blocked using 2% (w/v) dried skimmed milk power (Marvel) in 0.1M PB containing 0.3% Triton X-100 for one hour. Sections were then be incubated for two-three days with rabbit anti-Histone H3 and rabbit anti-Histone H4 primary antibodies in 0.3M PBS with 0.3% Triton-X-100 (Sigma-Aldrich) at 4°C and the immunohistochemistry continued as described above.

### 2.4.2.2 Image Analysis

All images stacks (protein of interest, Mecp2 and DAPI) were taken on a Leica SP5 Confocal microscope (Leica Microsystems) and saved using LAS AF acquisition software (Leica Microsystems). At least two optical image stacks were taken for each hippocampal formation region (CA1 and DG) from every brain section (minimum of two per animal). All images were captured as a Z-series (15uM in depth) using a Z-step of 0.25uM, zoom factor 1, pinhole airy 1, 63x objective lens, image size 1024 x 1024 pixels, 0.48uM pixel size and in 12 bit to improve the intensity measurement accuracy. A subset of optical image stacks was also taken on a 20x objective lens. Detector gain and offset differed depending on which protein of interest was being investigated but were kept constant throughout imaging of all the replicates of that protein. The cells of interest were in the pyramidal cell layer of the hippocampus and using the antibodies from table 2-14, the nuclei of each pyramidal cell becomes brightly immunostained.

Following image capture, cells were then analysed either manually or with an automated script. The automated script was developed in Image-Pro Plus 7.0 (Media Cybernetics, UK) to quantify cell intensity differences between Mecp2 positive and negative nuclei. The script was developed by Dr David Kelly at the University of Edinburgh and an annotated detailed version of the computer programming involved in this is described in Appendix B. In addition, a simplified step by step explanation of how the Macro works is provided in Figure 2-7.

<p><b>Step 1 – Subtract background</b></p>	<p><b>Step 2 – Select and threshold ROI</b></p>
	
<p>An area on the DAPI image is selected with no objects present, the intensity measured and the maximum intensity deleted from the DAPI image.</p>	<p>Select region of interest (ROI) that contains DG or CA1 cell body layer nuclei. The image is then thresholded to highlight the nucleus.</p>
<p><b>Step 3 – Create binary image</b></p>	<p><b>Step 4 – Create 3D image</b></p>
	
<p>Every layer of the ROI z-stack is gone through to create a binary (black and white) mask of the selected nuclei which is combined altogether at the end.</p>	<p>3D image is created of nuclei in ROI based on the binary image. The 3D image is watershed split to separate touching objects and object size filters are applied.</p>
<p><b>Step 5 – Select nuclei one at a time</b></p>	<p><b>Step 6 – Obtain measurements</b></p>
	
<p>A single nuclei is extracted from the 3D image one at a time to determine if the nuclei is completely formed (e.g. not cut in half) and volume of nuclei.</p>	<p>Binary mask outline of nuclei created based on volume. This outline is applied to the original MeCP2 and protein of interest (e.g. c-Fos) images to obtain MeCP2 status and intensity.</p>

**Figure 2-7 Steps involved in the automated script.**

Six steps are highlighted which explain in general how the automated script works to quantify nuclei measurements using all three image stacks (DAPI, MeCP2 and protein of interest). The DAPI image is turned into a 3D thresholded binary mask which is reapplied to the original MeCP2 and protein of interest image to determine the presence or absence of MeCP2 and nuclei intensity respectively. The scale (in pixels) is taken from the original DAPI image.

Importantly, during steps five and six the automated script stops at each selected nuclei in the ROI of the DAPI image before any measurements were taken enabling the user to manually check that the nucleus was intact. If the nucleus was incomplete it was discarded from the analysis at this point and the script proceeded to the next nucleus. This was done because nuclei in the image could have been cut in half due to being positioned at the boundary of the confocal stack or more usually they were incompletely thresholded. At this stage of the process the user is blind to whether the nucleus of this cell is positive or negative for Mecp2. Once the nucleus was accepted the script proceeded to create a 2D binary mask outline of that nucleus based on the 3D volume. This outline is applied segment by segment to the original protein of interest image stack to determine the mean nuclei intensity. Figure 2-8 describes in more detail exactly how mean nuclei intensity was determined from the script.

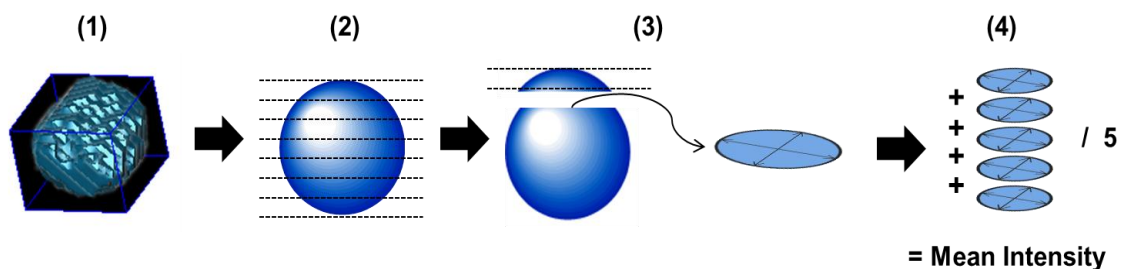


**Figure 2-8 Calculation of mean nuclei intensity from the script**

(1) A 3D nuclei is transferred back into a 2D binary image. A region of interest is created to enable accurate positioning of that nucleus on the original confocal image. (2) The image is split into the original segments of the image stack and (3) an average intensity is taken of each segment. (4) Finally all average intensities are added together and divided by the total number of segments (e.g. 5) to obtain the mean intensity for that nucleus.

Subsequently, the script identified the Mecp2 status from the same nuclei in the Mecp2 image. Mecp2 positive cells were determined by the mean intensity being >250 grey scale units in three consecutive segments of the Mecp2 image. Volume measurements were calculated from the 3D image before all measurements for each cell (mean intensity, Mecp2 status and volume) were exported automatically to an excel file. Volume measurements were important as afterwards the mean intensity for each nucleus was multiplied by the volume to obtain an integrated density value. Figure 2-9 demonstrates the significance of this in greater detail.

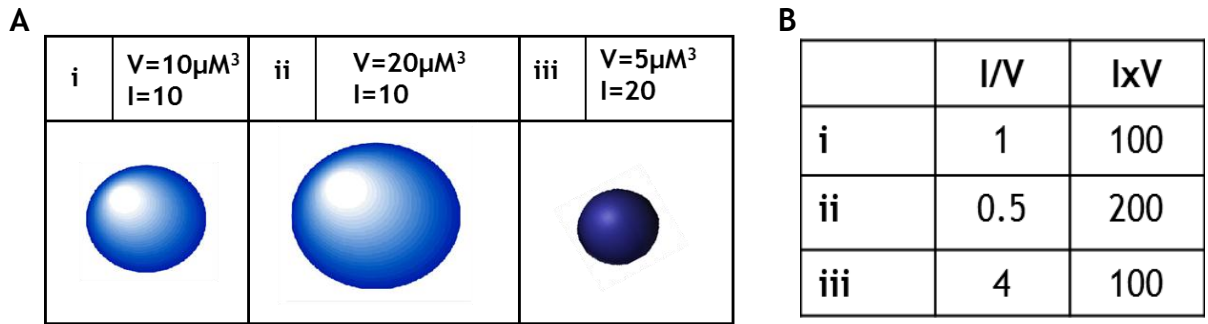


**Figure 2-9 Measurement of integrated density**

(A) Example of nuclei with different volumes ( $V$ ) and fluorescent intensities ( $I$ ) (i-iii). (B) Measurement of the integrated density in two manners – dividing or multiplying by the volume. Note the importance of the latter calculation where the volume is taken into consideration in the correct manner and the data not skewed. For example in (iii) the cell is bright due to the small size of the nuclei. Dividing by the volume amplifies this result which is incorrect. Multiplying by the volume takes the size of the nuclei into account and an accurate integrated density is obtained.

Finally, as *Mecp2* positive nuclei were in the same image stack as *Mecp2* negative nuclei, the difference between the two nuclei types can be accurately determined. In order to avoid the problem of determining which parameter (stack, section or animal) to normalise the data to when quantifying intensities, a chi-square test was performed. A chi-square analysis was performed to determine whether there was a change in the distribution of *Mecp2* positive and negative nuclei above the median intensity value. However if only some of the nuclei had the phenotype in the population then this would result in a dilution effect if all nuclei were considered. Therefore the percentage difference in nuclei types that were in the upper quartile intensity values was also determined.

In addition, optical image stacks were also analysed manually using Image J software to quantify the difference between the total number of nuclei immunostained for a specific protein of interest in *Mecp2* positive and negative nuclei. The Macro did not obtain an accurate measurement of the total number of nuclei in each section as nuclei were removed from the analysis for being incomplete. The z-stack was flattened for the protein of interest in a given image and all the nuclei that were positive for that protein counted. The counts for these nuclei were then overlaid onto the *Mecp2* immunostained image and the proportion of nuclei that were positive or negative for *Mecp2* calculated. Additionally the total number of DAPI immunostained nuclei and *Mecp2* positive nuclei were counted (from flattened z-stacks) in some images regardless of the

protein of interest to compare the proportion of Mecp2 positive to negative nuclei in each image.

## 2.5 Statistical Analysis

All data was expressed as mean  $\pm$  SEM and analysed using Graphpad Prism software (GraphPad, USA) or Minitab Statistical software (Minitab, USA). For parametric data normality of the data was confirmed using a Box-Cox Transformation or Johnson Transformation when necessary. Subsequently a Student's unpaired t-test, Log-rank test, two-way ANOVA with Tukeys *post hoc* test and three-way ANOVA with Tukeys *post hoc* test was used where appropriate. Non parametric tests were also performed using a Mann Whitney U test and chi-squared test. Statistical significance was accepted at  $p < 0.05$  and the following abbreviations were used throughout: ns = no significant difference, \* =  $p < 0.05$ , \*\* =  $p < 0.01$  and \*\*\* =  $p < 0.001$ .

## 2.6 General materials

### 2.6.1 Polymerase Chain Reaction (PCR) products

#### 2.6.1.1 Primers

The primers used in PCR reactions are listed in Table 2-7.

**Table 2-7 Primers used in PCR reactions**

Primer	Nucleotide Sequence 5'-3'	Supplier
P7 (416bp)	GGCTTGCCACATGACAAGAC	Sigma-Aldrich
New P6 (470bp)	TCCACCTAGCCTGCCTGTACTTTG	Sigma-Aldrich
New P5 (416bp)	TGGTAAAGACCCATGTGACCCAAG	Sigma-Aldrich

#### 2.6.1.2 Enzymes

The enzymes used in PCR reactions are listed in Table 2-8.

**Table 2-8 Enzymes used in PCR reactions**

Enzyme	Supplier
DNAreleasey™	Anachem Ltd
2X Thermo-Start™ High performance PCR Master Mix	Fisher Scientific

## 2.6.2 Solutions

### 2.6.2.1 Electrophysiology

Solutions used for electrophysiology experiments are listed in Table 2-9 and Table 2-10.

**Table 2-9 1 x Sucrose Artificial Cerebrospinal Fluid (sACSF)**

Salt	Concentration (mM)	Quantity (g/L dH <sub>2</sub> O)	Supplier
NaCl	87	5.084	BDH Laboratories
KCl	2.5	0.186	BDH Laboratories
NaHCO <sub>3</sub>	25.0	2.100	Fisher Scientific
NaH <sub>2</sub> PO <sub>4</sub>	1.25	0.195	BDH Laboratories
Glucose	25.0	4.504	Fisher Scientific
Sucrose	75.0	25.673	Fisher Scientific
Pyruvate	1	7 (mls)	Sigma-Aldrich
Ascorbate	1	0.5 (ml)	Sigma-Aldrich
MgCl <sub>2</sub>	7	0.110	BDH Laboratories
CaCl <sub>2</sub>	0.5	0.198	BDH Laboratories

**Table 2-10 1 x Recording ACSF**

Salt	Concentration (mM)	Quantity (g/L dH <sub>2</sub> O)	Supplier
NaCl	124	72.47	BDH Laboratories
KCl	3	2.24	BDH Laboratories
NaHCO <sub>3</sub>	26	21.84	Fisher Scientific
NaH <sub>2</sub> PO <sub>4</sub>	1.25	1.95	BDH Laboratories
MgSO <sub>4</sub>	1	2.46	BDH Laboratories
Glucose	10	18.02	Fisher Scientific
CaCl <sub>2</sub>	2	2 (mls)	BDH Laboratories

### 2.6.2.2 General solutions

Solutions used in all DNA or protein gel electrophoresis can be observed in Table 2-11. All chemicals listed in this section were supplied from BDH Laboratories or Sigma-Aldrich unless otherwise stated.

**Table 2-11 Gel electrophoresis solutions**

Solution	Chemical Components
<b>1 x Tris-borate-EDTA (TBE)</b>	90mM Trizma base, 90mM Orthoboric acid and 2mM EDTA.
<b>5 x DNA loading buffer</b>	0.5% SDS (w/v), 0.25% Xylene cyanol (w/v), 0.25% Bromophenol blue (w/v) and 1.5% Ficoll® 400 (w/v) in 3x TBE.
<b>Ethidium Bromide</b>	10mg/ml in H <sub>2</sub> O
<b>Agarose gel</b>	0.8% (w/v) agarose in 0.5M TBE buffer containing 200 ng/ml ethidium bromide
<b>1.5M Tris pH 8.8</b>	27 g Tris-base, 2 ml HCl and 150 ml dH <sub>2</sub> O
<b>1M Tris pH 6.8</b>	3 g Tris-base, 50 ml dH <sub>2</sub> O and adjust to pH 6.8 with HCl
<b>7% (w/v) acrylamide resolving gel</b>	40% Acrylamide (7mls; 29:1 Bio-Rad laboratories, UK), 1.5M Tris pH 8.8 (10mls), dH <sub>2</sub> O (23mls), 20% SDS (200µl), Temed (20µl) and 10% APS (200µl)
<b>4.3% (w/v) acrylamide stacking gel</b>	40% Acrylamide (1.29 mls), 1M Tris pH 6.8 (3 mls), dH <sub>2</sub> O (7.71mls), 20% SDS (60µl), Temed (6µl) and 10% APS (75µl)
<b>1 x Tris-glycine buffer</b>	50mM Tris-base, 400mM Glycine

General solutions used for western blotting are listed in Table 2-12.

**Table 2-12 General solutions used for western blotting**

Solution	Chemical Components
<b>Cell lysate buffer</b>	20mM HEPES, 10mM KCl, 1mM MgCl <sub>2</sub> , 0.5mM DTT, 0.1% Triton X-100, 20% Glycerol, 2mM PMSF, 5mg/ml Aprotinin, 5mg/ml Leupeptin and 10mM Sodium Butyrate
<b>Transfer buffer</b>	20X NuPAGE Transfer Buffer (50mls; Life Technologies, UK), Methanol (100mls) and 850ml dH <sub>2</sub> O
<b>Tris Buffered Saline (TBS)</b>	20mM Tris-HCL (pH8.0), 137mM NaCl
<b>Blocking solution</b>	5% (w/v) dried skimmed milk powder (Marvel) diluted in TBS

General solutions used for immunohistochemistry are listed in Table 2-13.

Table 2-13 General solutions used for immunohistochemistry

Solution	Chemical Components
0.2M Phosphate Buffer (PB)	Solution A: 18.72 g of NaH <sub>2</sub> PO <sub>4</sub> (2H <sub>2</sub> O) in 600mls dH <sub>2</sub> O. Solution B: 42.45g of Na <sub>2</sub> HPO <sub>4</sub> in 1500mls dH <sub>2</sub> O. Add 560mls solution A to 1440mls of solution B and adjust to pH 7.4.
0.3M NaCl buffered saline (PBS)	100mls 0.2M PB, 900ml dH <sub>2</sub> O and 36g NaCl.
10mM sodium citrate buffer	2.94g of Tri-sodium citrate, 1000ml dH <sub>2</sub> O and adjust to pH 8.5.
4% Paraformaldehyde (PFA)	40g of Paraformaldehyde, 500ml 0.2M PB, 400mls dH <sub>2</sub> O and a few drops of 1M NaOH

### 2.6.3 Drugs

The drugs used in experiments are documented in Table 2-14.

Table 2-14 Drugs

Drug	Final Concentration	Quantity	Supplier
Saline	0.9%	0.9g of NaCl dissolved in dH <sub>2</sub> O	BDH Laboratories
Kainic acid (10mg)	25mg/kg	Worked out from a 1mg/ml stock (dissolved in 0.9% saline)	Abcam
Kainic acid (1mg)	400nM	34µl from 4.69M stock added to 366ml ACSF	Abcam
NBQX (1mg)	5µM	333µl from a 3mM stock added to 199.68ml ACSF	Abcam
Bicuculline (1mg)	0.1, 1, 3 and 10µM	1µl, 10µl, 30µl and 100µl respectively from a 10mM stock added to 100mls ACSF.	Abcam
4-aminopyridine	1, 3, 10, 30 and 50µM	1µl, 3µl, 10µl, 30µl and 50µl respectively from a 100mM stock added to 100mls ACSF.	Sigma-Aldrich

## Chapter 3

# Reduced seizure threshold and altered oscillatory properties in *Mecp2* knockout mice

### 3.1 Introduction

A major phenotype in RTT is the propensity for 70-90% of patients to develop epilepsy (Hagberg et al., 2002) with diverse seizure types ranging from complex partial to myoclonic seizures (Steffenburg et al. 2001; Kim et al. 2012). RTT patients have an age-related onset with frequency and severity of seizures declining in late adolescence (Steffenburg et al. 2001). Some authors report no significant clinical difference between patient genotypes (Cardoza et al., 2011) but a recent large scale study suggests that seizures may indeed vary by mutation type, with T158M (74%) and R106W (78%) mutations being most frequently associated with epilepsy (Glaze et al., 2010). Abnormalities in EEG recordings are also detected in RTT patients such as epileptiform discharges (Ishizaki et al., 1989) and slow oscillatory theta activity (Hagne et al. 1989; Niedermeyer et al. 1997). This could lead to an overall state of cortical hyperexcitability. Whilst the EEG is invariably abnormal at some stage, there is no characteristic or diagnostic EEG pattern for RTT (Glaze, 2005).

EEG recordings from *Mecp2* knockout mice display abnormal spontaneous rhythmic discharges of 6-9 Hz in the somatosensory cortex in awake but immobile mice, and increased peak frequency of theta rhythm in the hippocampus (D'Cruz et al., 2010); similar findings are observed in RTT patients. More recently, event related potentials (ERPs), brain activations that occur during certain behavioural tasks, were measured in *Mecp2*<sup>-/-</sup> mice and found to be altered in amplitude and latency of these events compared to WT controls; parameters that can reflect the strength and timing of cognitive processes (Goffin et al., 2012). This study also investigated the oscillations using passive EEG recordings and found an increase in high gamma (70-140 Hz) in *Mecp2*<sup>-/-</sup> mice compared to controls - activity that can be associated with epilepsy in the EEG before and during seizures (Goffin et al., 2012). Combining these EEG

findings in mice and RTT patients, it would suggest that disruption of MeCP2 causes alterations in network excitability.

Limitations exist in the use of EEG recordings *in vivo*. For example, intersubject variability and stage of disease process can vary and data outputs are complex. Further experiments have also been conducted *in vitro* which has tried to investigate this disparity in network circuitry in greater detail. Considering that a precise regulation of excitatory (Glutamatergic) and inhibitory (GABAergic) input is essential for normal brain function, any discrepancies in the balance of these factors could cause alterations in the properties of neuronal network circuitry. *Mecp2*-deficient mice show reduced spontaneous inhibitory postsynaptic potentials in the CA3 of the hippocampus attributed to decreased levels of spontaneous glutamate receptor-mediated synaptic currents (Zhang et al., 2008). Additionally, voltage sensitive dye studies revealed increased amplitude and spatiotemporal spread of neuronal depolarisations in the CA1 of the hippocampus. Isolation of the CA1 eliminated these differences suggesting alterations in network excitability originate from the CA3 (Calfa et al. 2011). Collectively these studies propose that an imbalance in inhibitory neuron regulation in the hippocampus render the entire network prone to hyperexcitability. Mice with no *Mecp2* in GABA releasing neurons also recapitulate many RTT features (Chao et al., 2010) therefore suggesting a role for MeCP2 in regulation of inhibitory input.

### **3.2 Study Aim**

In this study the aim was to investigate whether there were alterations in seizure threshold in *Mecp2*-deficient mice. The specific research questions in this chapter were to:

- i. Investigate the effects of kainic acid administration (a convulsant drug) on seizure development in WT and *Mecp2*-deficient mice.
- ii. Investigate further possible alterations in hippocampal network properties/excitability using a range of epileptogenic agents *in vitro*.

### 3.3 Methods

To investigate the epileptic phenotype *in vivo*, the convulsant drug kainic acid (25 mg/Kg IP in 0.9% saline) or saline (vehicle control) was injected into 6-10 week old symptomatic male *Mecp2<sup>stop/y</sup>* mice and their WT litter mates to monitor and analyse their seizure score. Seizure scores were amended from a previous documented scale (Racine, 1972) described in greater detail in chapter 2. Most experiments were carried out with the mice under light (2.5-3%) isoflurane anaesthesia but a subset of experiments were performed on male *Mecp2<sup>-/y</sup>*, female *Mecp2<sup>+/-</sup>* mice and their WT litter mates (aged 6-10 weeks) without anaesthesia.

Network excitability was examined *in vitro* by application of bicuculline, 4-aminopyridine and kainic acid to hippocampal slices from *Mecp2<sup>stop/y</sup>* mice and their WT litter mates as described in chapter 2. Subsequently, field excitatory postsynaptic potentials (fEPSPs) and gamma oscillations were recorded from the CA1 and CA3 regions of the hippocampus respectively to characterise network properties in both genotypes.

### 3.4 Results

#### 3.4.1 *Mecp2*-deficient mice have a heightened sensitivity to kainic acid-induced seizures *in vivo*

##### 3.4.1.1 Kainic acid application to mice under anaesthesia

To systematically examine the susceptibility of mice lacking *Mecp2* to develop seizures, we challenged male *Mecp2<sup>stop/y</sup>* mice (functional *Mecp2* knockout) and their WT littermates with the convulsant drug kainic acid (25mg/Kg) or vehicle (saline). Whilst none of the mice showed spontaneous seizure-like activity under homecage conditions or prior to drug application, kainic acid resulted in the rapid development of seizure activity (comprising of fast breathing, erratic twitches, tail shaking, limb clonus, and tonic-clonic seizures) in both *Mecp2<sup>stop/y</sup>* and WT mice. However, semi-quantitative scoring of mice based on a modified Racine scale (Chapter two) revealed that the proportion of mice displaying overt epileptiform signs is greater in *Mecp2<sup>stop/y</sup>* mice (100% of *Mecp2<sup>stop/y</sup>* mice develop seizures within three hours post treatment in contrast to 80% of WT).

Moreover, the onset of seizure activity was more rapid in *Mecp2*<sup>stop/y</sup> mice (Figure 3-1A;  $p < 0.001$ , log rank test;  $n = 20$  WT and 13 *Mecp2*<sup>stop/y</sup>) and the overall seizure profile (Figure 3-1B) and maximal seizure score (mean =  $6 \pm 0.7$  vs  $4 \pm 0.2$  units in WT; Figure 3-1C;  $p > 0.01$ , unpaired t-test) are greater in *Mecp2*<sup>stop/y</sup> mice.

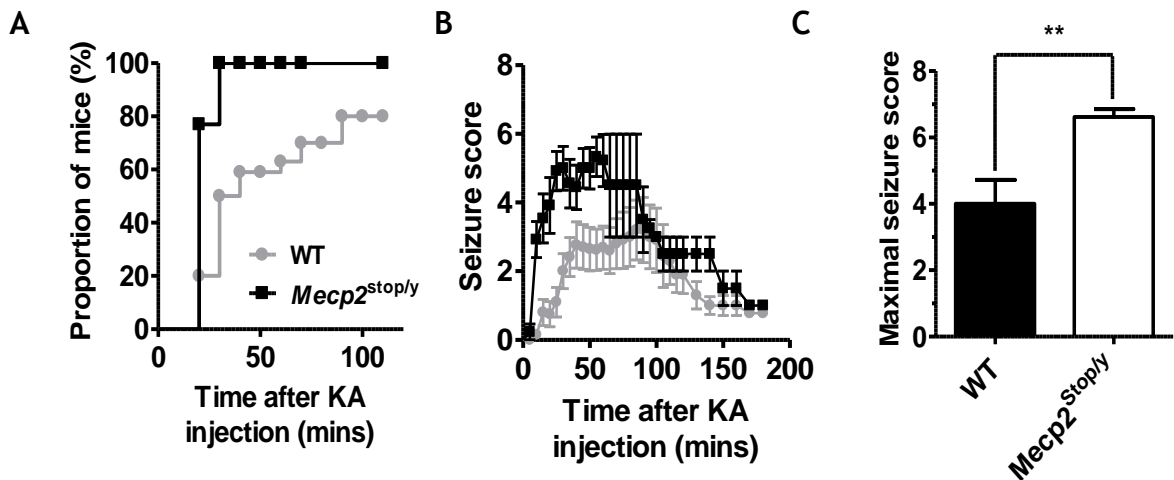


**Figure 3-1 Heightened sensitivity to kainate-induced seizures in *Mecp2*<sup>stop/y</sup> mice**  
 Plot showing the proportion of WT (grey circles) and *Mecp2*<sup>stop/y</sup> mice (black squares) displaying overt seizures following administration of kainic acid (KA, 25 mg/Kg, IP). *Mecp2*<sup>stop/y</sup> mice show a quicker onset of seizures ( $p < 0.001$ , Log-rank test,  $n = 20$  WT and 13 *Mecp2*<sup>stop/y</sup>). (B) Time plot showing mean seizure score over 3 hours post-KA application (same symbols as in A). (C) Bar graph showing maximal seizure score in WT and *Mecp2*<sup>stop/y</sup> mice ( $n =$  same as above;  $p < 0.01$ , unpaired t-test). All data expressed as mean  $\pm$  SEM. Note all mice were under anaesthesia.

### 3.4.1.2 Kainic acid application to mice not under anaesthesia

To omit the variable of anaesthesia, kainic acid was also applied to *Mecp2*-deficient mice without anaesthesia. Maximal seizure score was quantified and an increase in seizure severity was observed in *Mecp2*<sup>-/y</sup> mice ( $6 \pm 0.8$  units) when compared to their male WT littermates ( $2 \pm 0.2$  units; Figure 3-2A;  $p > 0.01$ , unpaired t-test;  $n = 6$  mice for each genotype). This disparity was also observed in heterozygous female mice ( $6 \pm 0.4$  units; *Mecp2*<sup>-/+</sup>) when compared to female WT littermates ( $3 \pm 1$  units; Figure 3-2B;  $p > 0.05$ , unpaired t-test;  $n = 5-8$  mice for each genotype).

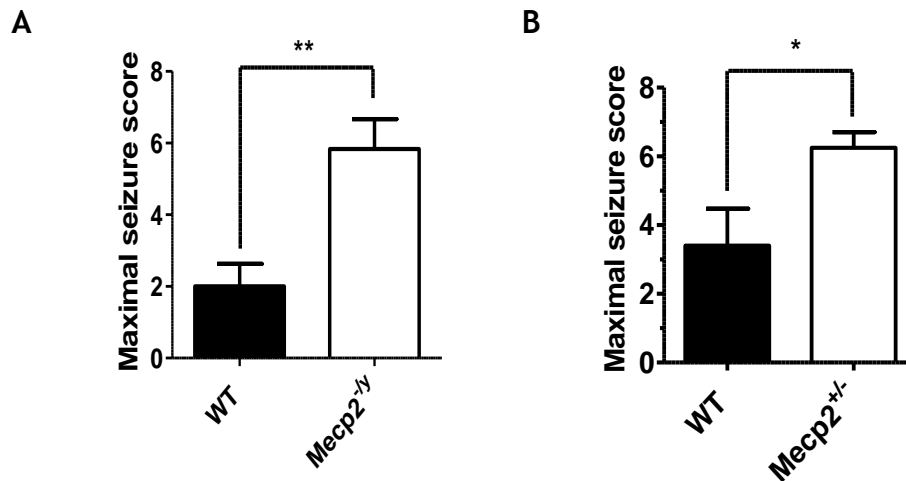


**Figure 3-2 Increase seizure severity in *Mecp2<sup>-ly</sup>* and *Mecp2<sup>+/-</sup>* mice without anaesthesia**  
 (A) Column plot comparing the maximal seizure score in WT male to *Mecp2<sup>-ly</sup>* mice without anaesthesia. An increase in seizure severity is observed in *Mecp2<sup>-ly</sup>* mice ( $p < 0.01$ , unpaired t-test,  $n = 6$  mice for each genotype). (B) Plot showing the maximal seizure score in *Mecp2<sup>+/-</sup>* female mice compared to their WT littermates without anaesthesia. A greater seizure score is present in *Mecp2<sup>+/-</sup>* mice ( $p < 0.05$ , unpaired t-test,  $n = 5-8$  mice for each genotype). All data expressed as mean  $\pm$  SEM.

### 3.4.2 Altered gamma network oscillations in the hippocampus of *Mecp2<sup>stop/ly</sup>* mice.

These *in vivo* studies have shown that *Mecp2*-deficient mice have a heightened sensitivity to kainic acid-induced seizures. One possible contributing factor to this could be alterations in the propensity of neuronal networks in *Mecp2*-deficient mice to generate synchronous forms of network activity such as hippocampal gamma oscillations. In response to nanomolar concentrations of kainic acid, the hippocampus is capable of generating rhythmic oscillations, particularly in the gamma band (20-80Hz) which are considered to represent 'physiological' forms of network oscillation but may result in pathological hypersynchrony if excessive (Fisahn, 2005). Therefore, in order to test this theory we applied kainic acid (400nM) to hippocampal slices from *Mecp2<sup>stop/ly</sup>* mice and their WT littermates. Under control (WT slices) conditions, kainic acid resulted in the appearance of regular gamma network oscillations (Figure 3-3Ai). The activity was network driven and completely eliminated by addition of the AMPA/kainate receptor blocker, NBQX (5 $\mu$ M; Figure 3-3Aii). This kainic acid-induced oscillatory activity was further examined by power spectrum analysis which showed dominant frequency at ~30-40Hz (Figure 3-3Aiv). Under the same experimental conditions, slices from *Mecp2<sup>stop/ly</sup>* mice appeared to have more prominent and higher gamma oscillations compared to WT slices (Figure 3-3Bi-iv).

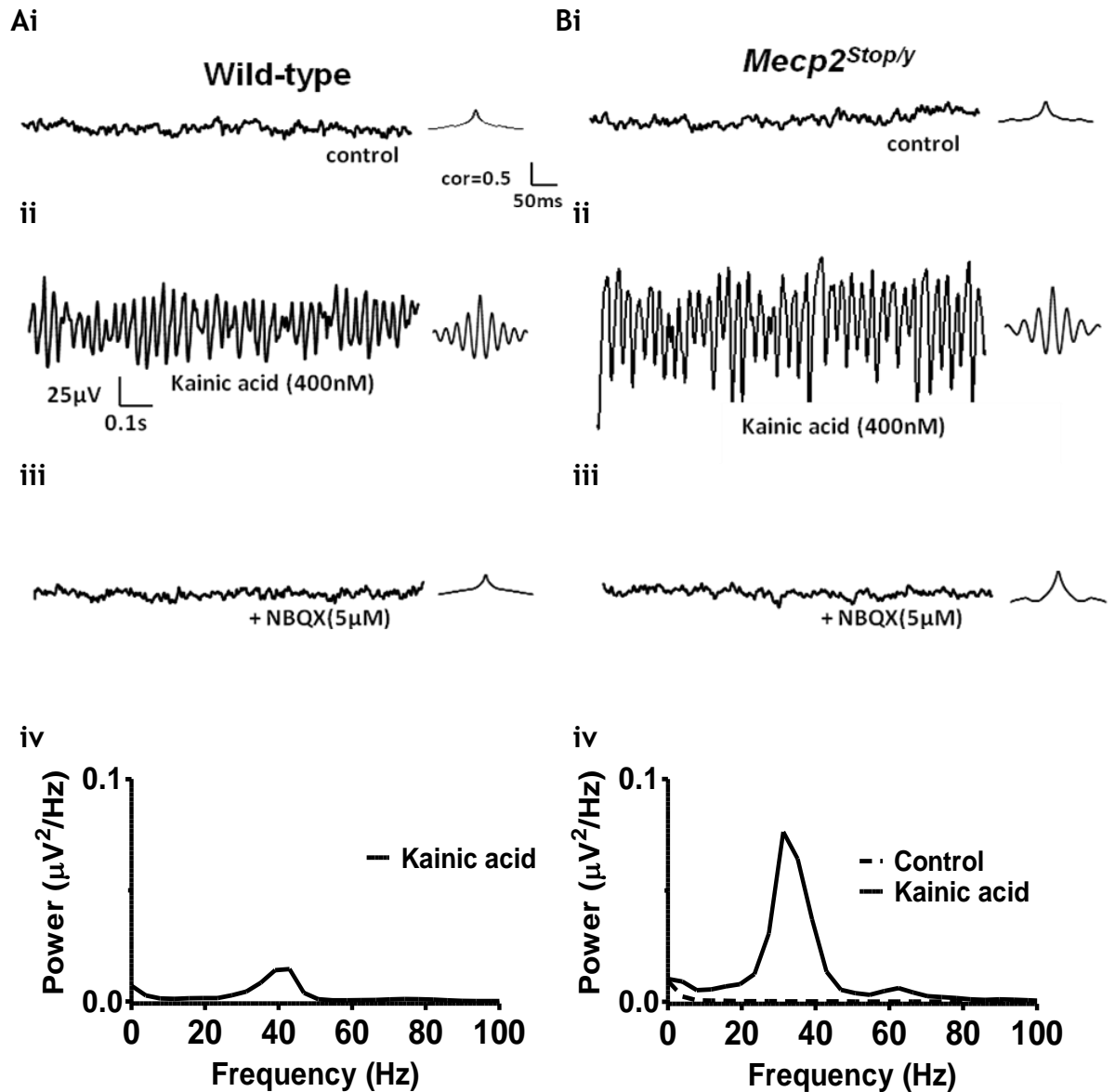


**Figure 3-3 Gamma frequency network oscillations before and after kainic acid application.** (A) Representative extracellular field potential traces from WT hippocampus showing (i) baseline quiescence prior to application of kainic acid (400nM) following which (ii) trace becomes dominated by a gamma frequency (~30-40Hz) oscillation. This network oscillation was abolished following administration of the kainate receptor antagonist NBQX (5µM). (iv) Power spectrum from same experiments showing oscillation with a dominant frequency at ~40Hz. Inserts at end of each trace are corresponding autocorrelation plots which reveal the presence of regular oscillation in kainic acid-treated slices. (B) Similar representative data plots from a *Mecp2*<sup>stop/y</sup> mouse hippocampal slice. Note the more prominent and higher power gamma frequency oscillation relative to the WT traces. All data expressed as mean  $\pm$  SEM and scale bars: voltage traces, 25µV, 0.1 s; correlation=0.5, 50 ms.

These observations were confirmed by power spectrum analysis from all the pooled data. Slices from *Mecp2*<sup>stop/y</sup> mice displayed a higher mean power ( $1059 \pm 379\mu\text{V}^2$ ) compared to slices from WT mice ( $287 \pm 178\mu\text{V}^2$ ) which had a lower mean power (Figure 3-4A-B; Mann-Whitney U test; n=14-26 slices for each genotype). Furthermore there was a significant difference in mean power between control and kainic acid treatment for each genotype (Figure 3-4B;  $p < 0.05$ , Mann-Whitney U test). However, no difference was observed between

genotypes when quantifying the dominant frequency of each oscillatory activity after 60 minutes of kainic acid treatment with a WT slice frequency of  $33 \pm 1.7\text{Hz}$  and  $35 \pm 2.1\text{Hz}$  for *Mecp2*<sup>stop/y</sup> slices (Figure 3-4C;  $p=0.579$ , Mann-Whitney U test).

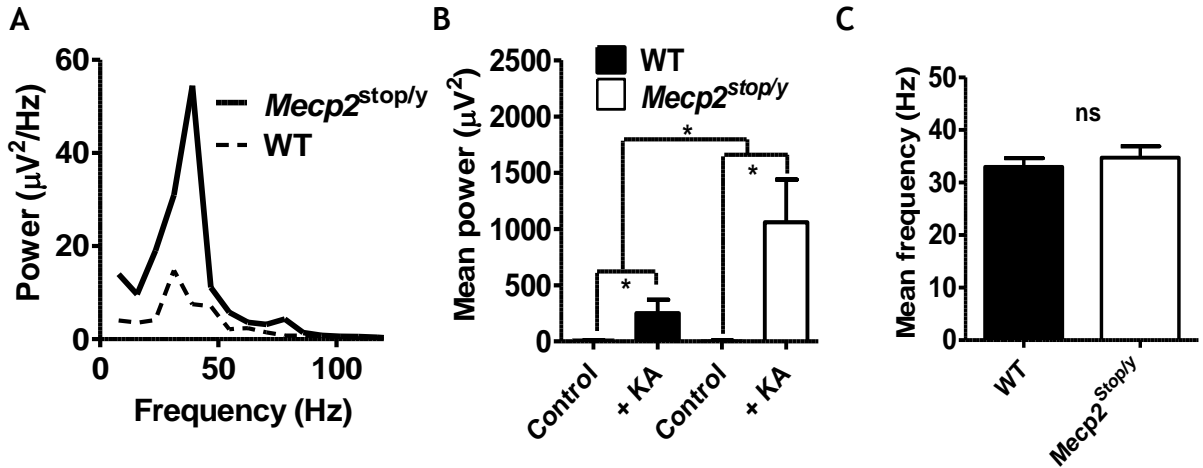


**Figure 3-4 Increased power of gamma frequency network oscillations in hippocampal slices from *Mecp2*<sup>stop/y</sup> mice**

(A) Pooled data showing average power spectra from WT (n=26 slices from 9 mice) and *Mecp2*<sup>stop/y</sup> samples (n=14 slices from 6 mice). (B) Column plot showing mean oscillatory power before and following kainic acid (KA) application in WT and *Mecp2*<sup>stop/y</sup> samples revealing a significant difference in mean power between treatment ( $p < 0.05$ , Mann-Whitney U test, n=14-26 slices per genotype) and genotype ( $p < 0.05$ , Mann-Whitney U test). (C) Plot showing dominant frequency which did not differ between genotypes ( $p = 0.579$ , Mann-Whitney U test, same n as above). All data expressed as mean  $\pm$  SEM.

### 3.4.3 Altered properties of bicuculline-induced epileptiform activity in the hippocampus of *Mecp2*<sup>stop/y</sup> mice.

#### 3.4.3.1 Spontaneous extracellular fEPSPs

Considering fast spiking GABAergic interneurons are important for the generation of gamma oscillations in the hippocampus (Traub et al., 2003) and previous studies have suggested an important role for *Mecp2* in the regulation of inhibitory input (Chao et al. 2010; Zhang et al. 2008) I applied the GABA<sub>A</sub> receptor antagonist bicuculline to hippocampal slices from *Mecp2*<sup>stop/y</sup> mice and their WT littermates. Extracellular field recordings obtained from the stratum radiatum in area CA1 in response to bicuculline (10 $\mu\text{M}$ ) administration showed characteristic spontaneous epileptiform bursting activity (Figure 3-5A). Slices from *Mecp2*<sup>stop/y</sup> mice showed a greater frequency of these bursting events at low doses (0.1-1 $\mu\text{M}$ ) of bicuculline (Figure 3-5B-C;  $p < 0.05$ , two-way ANOVA with Tukeys *post hoc* test; n=18-22 slices for each genotype). Subsequently, analysis

of the duration of these spontaneous epileptiform bursts revealed the duration was longer in slices from *Mecp2*<sup>stop/y</sup> mice (713 ± 47ms) compared to WT controls (383 ± 55ms) after application of 10µM bicuculline (Figure 3-5D;  $p < 0.001$ , two-way ANOVA with Tukeys *post hoc* test).

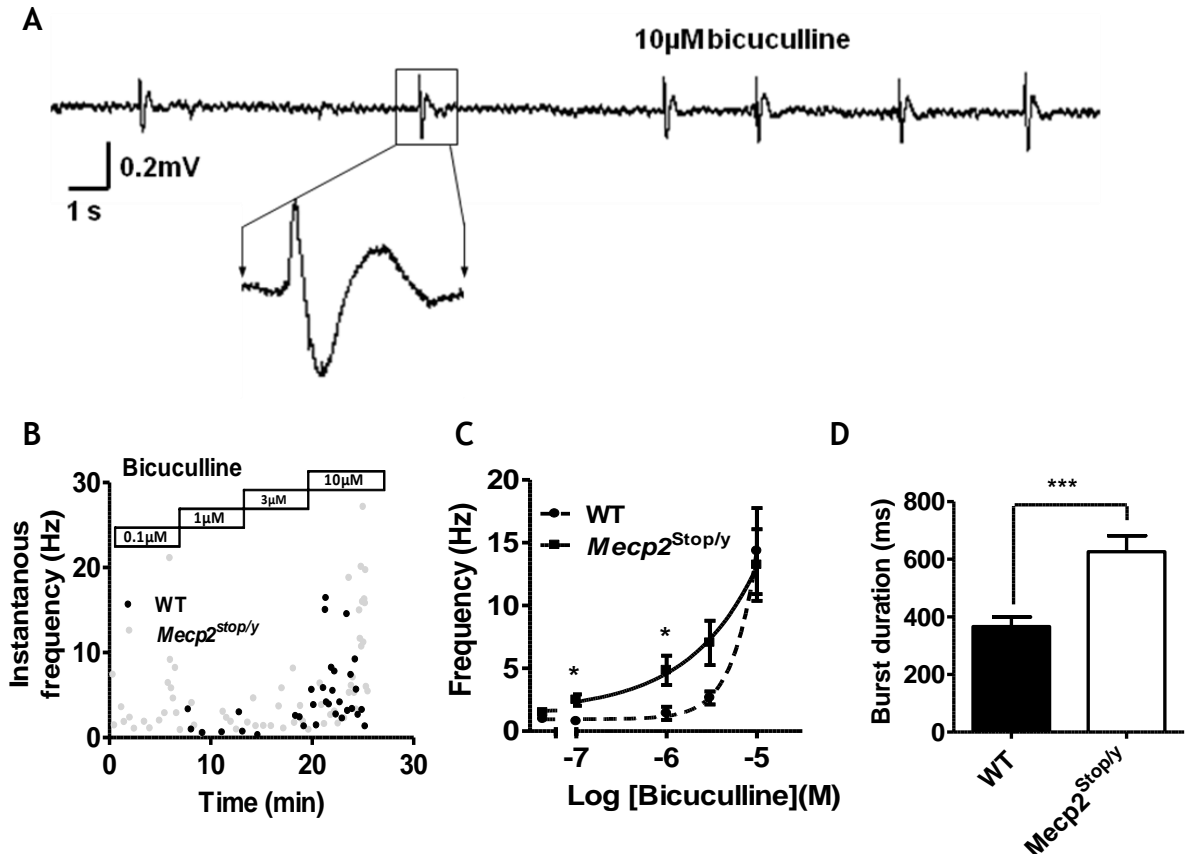


**Figure 3-5 Increased frequency and duration of bicuculline-induced spontaneous epileptiform activity in hippocampal slices from *Mecp2*<sup>stop/y</sup> mice**

(A) Representative extracellular fEPSP recording in area CA1 showing characteristic spontaneous epileptiform bursting activity in response to application of the GABA<sub>A</sub> receptor antagonist bicuculline (10µM). Insert shows individual burst event. (B) Scatter plot showing instantaneous burst frequency in representative recordings from WT (black symbols) and *Mecp2*<sup>stop/y</sup> (grey symbols) slices in response to increasing bath concentration of bicuculline (0.1-10 µM). (C) Plot showing frequency of epileptiform bursting in response to increasing bath concentrations of bicuculline. There is a significant difference in burst frequency between genotypes at 0.1-1 µM concentrations ( $p < 0.05$ , two-way ANOVA with Tukeys *post hoc* test,  $n = 18$  slices, from 5 WT mice and  $n = 22$  slices from 5 *Mecp2*<sup>stop/y</sup> mice). (D) Plot showing increased duration of spontaneous epileptiform events ( $p < 0.001$ , two-way ANOVA with Tukeys *post hoc* test) in slices from *Mecp2*<sup>stop/y</sup> mice in the presence of 10 µM bicuculline (same  $n$  as above). Scale bar: 0.2 mV, 1s and all data expressed as mean ± SEM.

### 3.4.3.2 Evoked extracellular fEPSPs

Evoked extracellular fEPSPs recorded in stratum radiatum of area CA1 showed characteristic polyspikes behaviour when delivered in the presence of bicuculline (10µM; Figure 3-6A). Quantification of the average number of these polyspike events that occur following synaptic stimulation revealed *Mecp2*<sup>stop/y</sup> mice (2.9 ± 0.5) had the propensity to develop a greater number of post-

stimulated burst events at the highest concentration of bicuculline (10 $\mu$ M) compared to WT littermates ( $0.9 \pm 0.2$ ; Figure 3-6B;  $p < 0.001$ , two-way ANOVA with Tukeys *post hoc* test;  $n = 12$  slices per genotype;  $n = 18-22$  slices for each genotype). Additionally, the duration of evoked fEPSPs was longer in *Mecp2<sup>stop/y</sup>* slices ( $416 \pm 66$ ms) compared to WT ( $83 \pm 25$ ms) at 10 $\mu$ M bicuculline (Figure 3-6C;  $p < 0.001$ , two-way ANOVA with Tukeys *post hoc* test). Finally the input-output relationship between stimulus intensity and rise rate (60-80% of the initial slope of evoked fEPSP) during baseline control conditions and after 10 $\mu$ M bicuculline in *Mecp2<sup>stop/y</sup>* and WT slices was calculated. There was a trend towards *Mecp2<sup>stop/y</sup>* slices having higher rise rate values in both treatment groups compared to WT slices (Figure 3-6D;  $p < 0.001$  for an overall genotype affect, general linear model with genotype, treatment and stimulus as factors and Tukeys *post hoc* test).

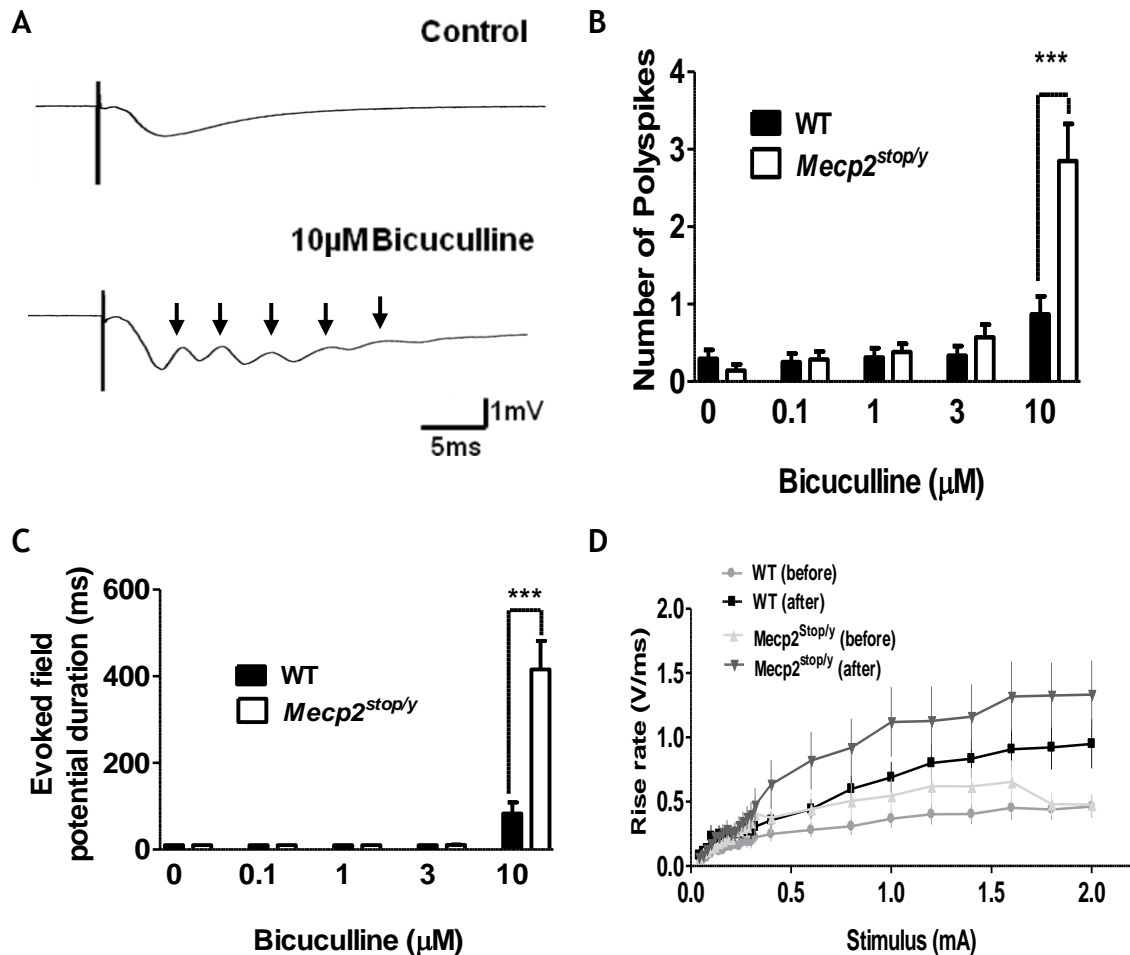


**Figure 3-6 Altered evoked fEPSP properties in hippocampal slices from *Mecp2<sup>stop/y</sup>* mice in the presence of bicuculline.**

(A) Representative fEPSP recordings in area CA1 showing characteristic polyspikes (arrows) in the presence of bicuculline (10 $\mu$ M) following synaptic stimulation. (B) Plot showing number of polyspikes present in response to increasing bath concentrations of bicuculline (0.1-10  $\mu$ M). There was a significant difference in polyspike number between genotypes at 10  $\mu$ M concentrations ( $p < 0.001$ , two-way ANOVA with Tukeys *post hoc* test,  $n = 18$  slices, from 5 WT mice and  $n = 22$  slices from 5 *Mecp2<sup>stop/y</sup>* mice). (C) Plot showing increased duration of evoked fEPSP (3 and 10  $\mu$ M;  $p < 0.05$ , two-way ANOVA with Tukeys *post hoc* test) in slices from *Mecp2<sup>stop/y</sup>* mice in the presence of increasing bicuculline concentrations (same  $n$  as above). (D) Input-output relationship between stimulus intensity and rise rate (60-80% of the initial slope of evoked fEPSP) during control conditions and after 10  $\mu$ M bicuculline in both genotypes. Note the trend towards higher rise rate values in *Mecp2<sup>stop/y</sup>* mice (same  $n$  as above,  $p < 0.001$  for an overall genotype affect, general linear model with genotype, treatment and stimulus as factors and Tukeys *post hoc* test.) Scale bar: 1 mV, 5s and all data expressed as mean  $\pm$  SEM.

### 3.4.4 Altered properties of 4-aminopyridine-induced epileptiform activity in the hippocampus of *Mecp2<sup>stop/y</sup>* mice

#### 3.4.4.1 Spontaneous extracellular fEPSPs

In contrast to bicuculline-induced disinhibition of networks, the potassium channel blocker 4-aminopyridine (4-AP) promotes epileptiform activity via neuronal depolarization and strengthening glutamateric signalling (Traub and Jefferys, 1994). To further evaluate hippocampal network excitability, I applied

the potassium channel blocker 4-AP to hippocampal slices from *Mecp2<sup>stop/y</sup>* mice and their WT littermates. Extracellular field potential recordings were taken from the stratum radiatum in area CA1 of the hippocampus which showed characteristic spontaneous epileptiform bursting activity following application of 50 $\mu$ M 4AP (Figure 3-7A). No difference in the frequency of these epileptiform bursting events was observed between genotypes upon incremented concentrations of 4AP except at the highest concentration administered (Figure 3-7B-C; 50  $\mu$ M,  $p < 0.05$ , two-way ANOVA with Tukeys *post hoc* test;  $n = 12$  slices per genotype). Subsequently quantification of the duration of the spontaneous epileptiform burst events revealed that the duration was longer in slices from *Mecp2<sup>stop/y</sup>* mice ( $203 \pm 24$ ms) compared to WT controls ( $134 \pm 24$ ms) upon application of 50 $\mu$ M 4-AP (Figure 3-7D;  $p < 0.05$ , two-way ANOVA with Tukeys *post hoc* test).

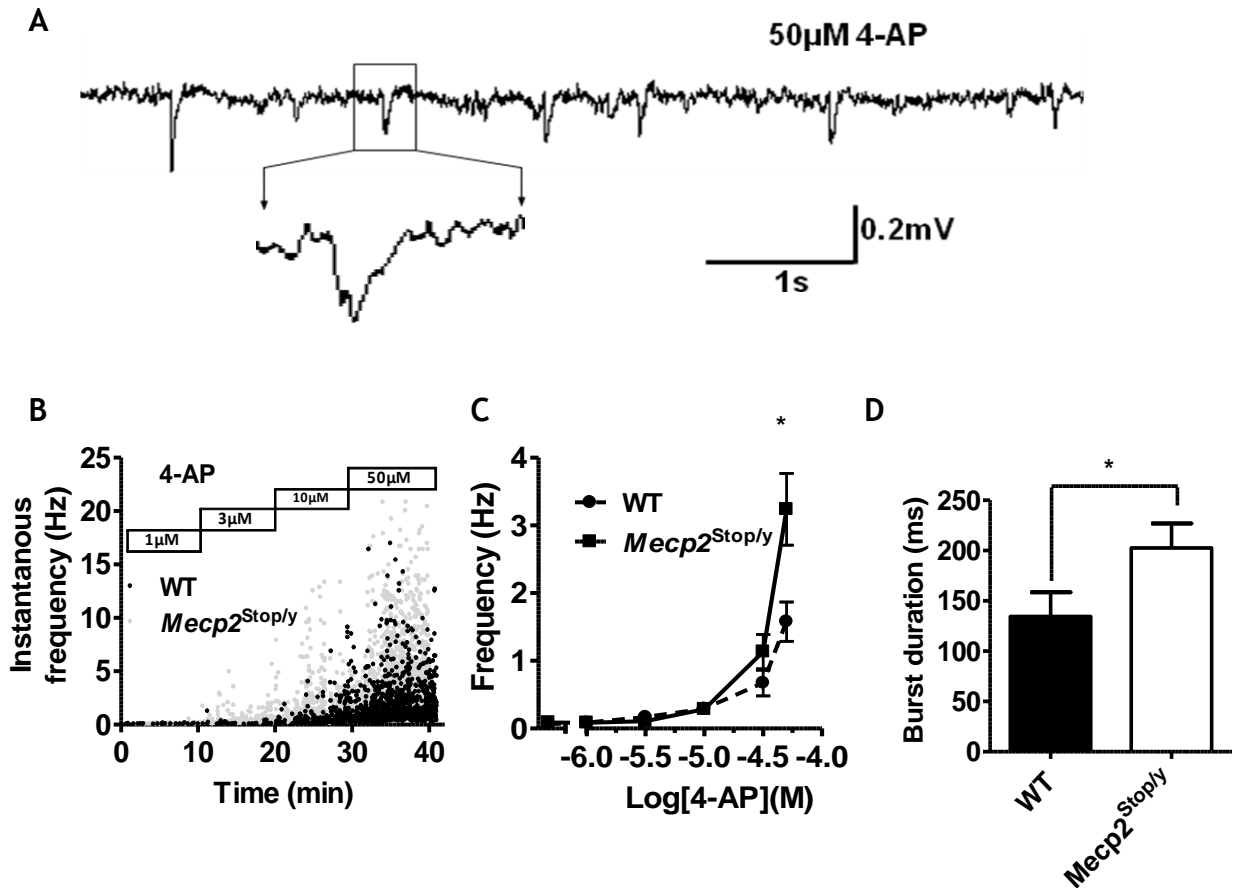


**Figure 3-7 Increased frequency and duration of 4-aminopyridine-induced spontaneous epileptiform activity in hippocampal slices from *Mecp2<sup>stop/y</sup>* mice**

(A) Representative extracellular fEPSP recording in area CA1 showing characteristic spontaneous epileptiform bursting activity in response to application of the potassium channel blocker 4-aminopyridine (4-AP, 50  $\mu$ M). Insert shows individual burst event. (B) Scatter plot showing instantaneous burst frequency in representative recordings from WT (black symbols) and *Mecp2<sup>stop/y</sup>* (grey symbols) slices in response to increasing bath concentration of 4-AP (1-50  $\mu$ M). (C) Plot showing pooled epileptiform burst frequency data in response to increasing bath concentrations of 4-AP. There was a significant difference in burst frequency between genotypes at the highest concentration tested (50  $\mu$ M,  $p < 0.05$ , two-way ANOVA with Tukeys *post hoc* test,  $n = 12$  slices per genotype). (D) Plot showing increased duration of spontaneous epileptiform bursts ( $p < 0.05$ , two-way ANOVA with Tukeys *post hoc* test) in slices from *Mecp2<sup>stop/y</sup>* mice in the presence of 50  $\mu$ M 4-AP (same  $n$  as above). Scale bar: 0.2 mV, 1 s and all data expressed as mean  $\pm$  SEM.

In addition to an increase in the frequency and duration of epileptiform bursting activity after 50  $\mu$ M 4-AP administration in slices from *Mecp2<sup>stop/y</sup>* mice, these slices also had an increased propensity to display ictal-like events (distinctive epileptic events; Figure 3-8B). These events are characterised by a high frequency discharge followed by train of burst-like events (Figure 3-8Aiii). 88% of slices from *Mecp2<sup>stop/y</sup>* mice displayed these events compared to 43% of slices from WT mice (Figure 3-8B;  $p < 0.05$ , chi-squared test;  $n = 3$  from a total of 7 slices for WT and  $n = 8$  from a total of 9 slices for *Mecp2<sup>stop/y</sup>* mice).

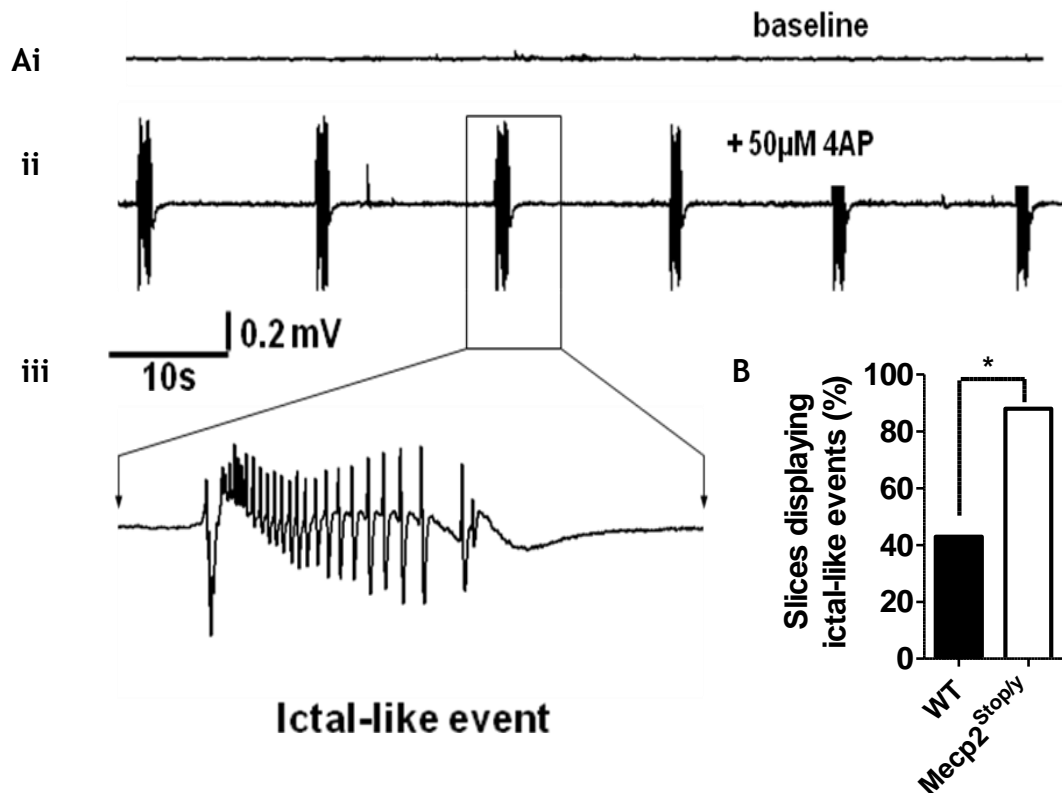


**Figure 3-8 Hippocampal networks from *Mecp2*<sup>stop/y</sup> mice have a greater propensity to display ictal-like events in response to 4-AP challenge.**

(Ai) Representative fEPSP recording from a *Mecp2*<sup>stop/y</sup> hippocampus displaying typical baseline quiescence. (ii) Subsequent application of 4-AP (50 μM) results in the appearance of characteristic ictal-like events (high frequency discharge followed by train of burst-like events) as shown in insert (iii). (B) Column plots showing that the occurrence of ictal-like is more commonly observed in slices from *Mecp2*<sup>stop/y</sup> mice compared to WT ( $p < 0.05$ , chi-squared test,  $n=3$  from a total of 7 slices for WT and  $n=8$  from a total of 9 slices for *Mecp2*<sup>stop/y</sup> mice). Scale bar: 0.2 mV, 10 s and all data expressed as mean  $\pm$  SEM.

#### 3.4.4.2 Evoked extracellular fEPSPs

Evoked extracellular fEPSPs recorded in stratum radiatum of area CA1 in the presence of 4-AP (50 μM) resulted in the appearance of characteristic polyspike behaviour in response to synaptic stimulation (Figure 3-9A). Quantification of the average number of these polyspikes that occur showed that slices from *Mecp2*<sup>stop/y</sup> mice ( $2.6 \pm 0.3$ ) have a greater mean number of post-stimulus burst events when tested at the highest concentration of 4-AP (50 μM) compared to WT littermates ( $1.8 \pm 0.2$ ; Figure 3-9B;  $p < 0.05$ , two-way ANOVA with Tukeys *post hoc* test;  $n=12$  slices per genotype). Additionally, the duration of evoked EPSPs was longer in *Mecp2*<sup>stop/y</sup> slices (30 μM =  $25 \pm 6$  ms; 50 μM =  $93 \pm 12$  ms) compared to WT slices (30 μM =  $10 \pm 0.4$  ms; 50 μM =  $15 \pm 3$  ms) in the presence of incremented concentrations of bicuculline (Figure 3-9C;  $p < 0.05$ , two-way ANOVA with Tukeys *post hoc* test). Finally, Figure 3-9D shows the input-output relationship between stimulus intensity and rise rate (60-80% of the initial slope of evoked fEPSP) during baseline control conditions and after 50 μM 4-AP in

*Mecp2*<sup>stop/y</sup> and WT slices. No significant difference between genotypes was present (general linear model with genotype, treatment and stimulus as factors and Tukeys *post hoc* test).

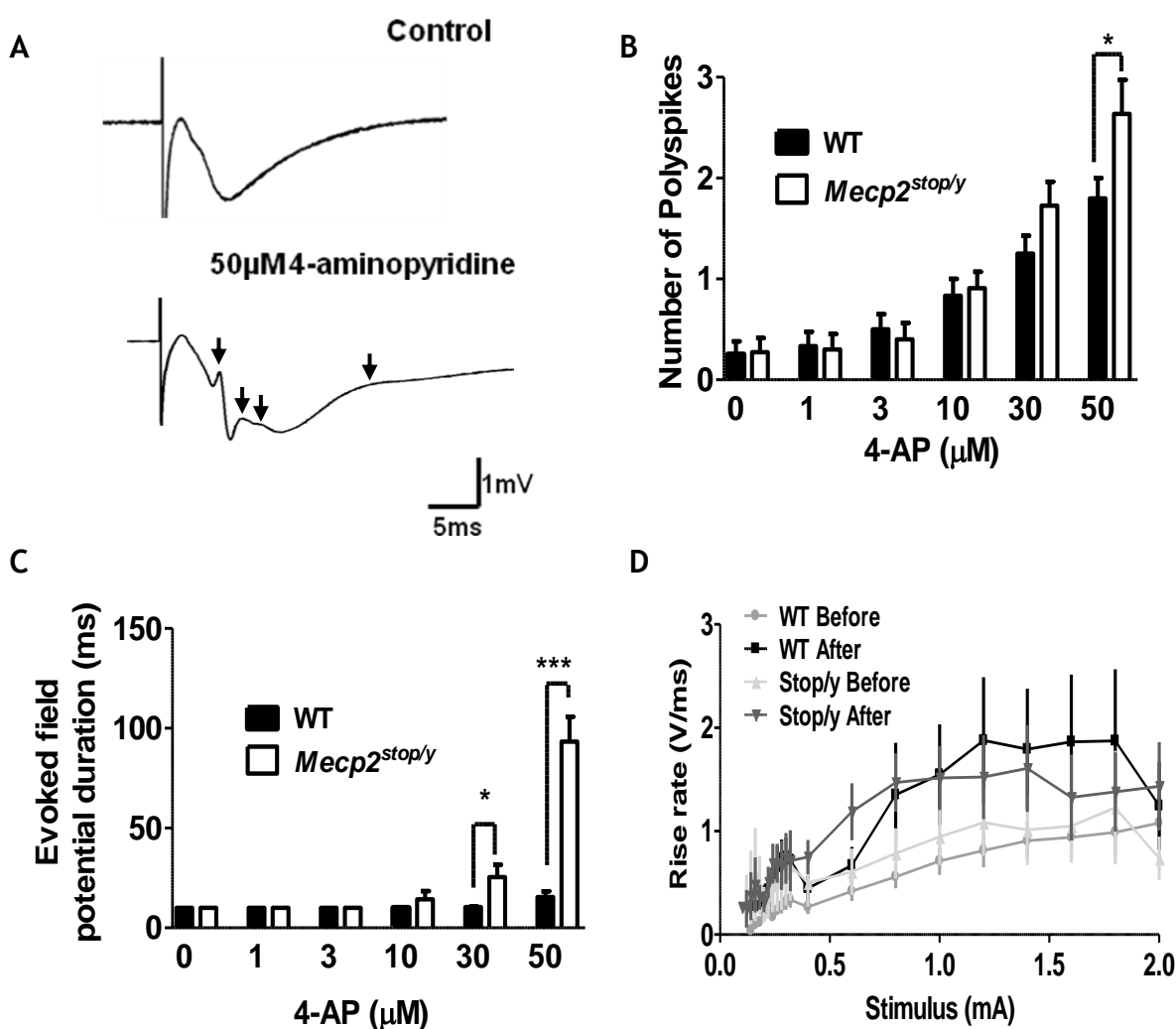


**Figure 3-9 Altered evoked fEPSP properties in hippocampal slices from *Mecp2*<sup>stop/y</sup> mice in the presence of 4-AP.**

(A) Representative evoked fEPSP recordings in area CA1 showing characteristic polyspikes (arrows) in the presence of 4-AP (50µM) following synaptic stimulation. (B) Plot showing number of polyspikes present in response to increasing bath concentrations of bicuculline (1-50µM). There was a significant difference in polyspike number between genotypes at 50 µM concentration ( $p < 0.05$ , two-way ANOVA with Tukeys *post hoc* test,  $n = 12$  slices per genotype). (C) Plot showing an increased duration of evoked fEPSP ( $p < 0.05$ , two-way ANOVA with Tukeys *post hoc* test) in slices from *Mecp2*<sup>stop/y</sup> mice in the presence of 30-50 µM 4-AP (same  $n$  as above). (D) Input-output relationship between stimulus intensity and rise rate (60-80% of the initial slope of evoked fEPSP) during control conditions and after 50µM 4-AP in both genotypes. No significant difference between genotypes is present (same  $n$  as above,  $p > 0.05$ , general linear model with genotype, treatment and stimulus as factors and Tukeys *post hoc* test.). Scale bar: 1 mV, 5s and all data expressed as mean  $\pm$  SEM.

### 3.5 Discussion

Epilepsy is a prominent feature of Rett syndrome (RTT) patients (Hagberg et al., 2002) which can be very difficult to treat as the types of seizures patients exhibit vary widely (Steffenburg et al. 2001). Moreover, a recent study has highlighted the importance of MeCP2 in epilepsy generation as the levels of MeCP2 mRNA are up-regulated in intractable temporal lobe epilepsy (Tao et al., 2012). This current study focused on the factors which contribute towards network excitability and seizure development in RTT. Using a mouse model in which *Mecp2* is silenced by the addition of a STOP cassette (Guy et al., 2007), I have found a reduced seizure threshold and altered network oscillatory properties in *Mecp2*-deficient mice, and suggest that these alterations could have a profound influence on epilepsy generation.

The hippocampus is a focal point in epilepsy generation (Chang and Lowenstein, 2003) and has a well described circuitry making it an ideal area of the brain to study seizure development. The application of kainic acid, an ionotropic glutamate receptor agonist, *in vivo* to mice is a common model used to investigate epilepsy which can lead to neurochemical and histopathological changes within the hippocampus (Sperk et al., 1983a). Furthermore, whilst an epileptic phenotype has previously been observed in *Mecp2* mutant mice, the seizure phenotype of RTT mouse models has not been fully characterised. Therefore the application of kainic acid to WT and *Mecp2*<sup>stop/y</sup> mice enabled me to systematically examine the propensity of mice lacking *Mecp2* to develop seizures. I found that the proportion of mice displaying overt epileptiform signs was greater and the onset of seizures more rapid in *Mecp2*<sup>stop/y</sup> mice which suggest they have a heightened sensitivity to seizure induction and potentially a lower seizure threshold (Figure 3-1). This data may explain the clinical predisposition that RTT patients have to the development of epileptic seizures. Furthermore, this propensity for seizure generation was also observed in *Mecp2*<sup>+/-</sup> heterozygous female mice (which display a mosaic expression to *Mecp2*) and *Mecp2*<sup>-/y</sup> male mice when compared to their WT littermates (Figure 3-2) in the absence of anaesthesia suggesting that the differences were genuine and not due to the confounding variability in the effects of anaesthesia.

To investigate the contributing factors to heightened sensitivity observed *in vivo*, I applied kainic acid (400nM) to hippocampal slices *in vitro* from WT and *Mecp2*<sup>stop/y</sup> mice male mice. In response to nanomolar concentrations of kainic acid, the hippocampus is capable of generating rhythmic oscillations, particularly in the gamma band (20-80Hz; Fisahn, 2005). Gamma oscillations are synchronous network activities in the brain and can be associated with cognition, consciousness and synaptic plasticity (Traub et al., 1998). In our studies, mice deficient in *Mecp2* exhibited more powerful gamma oscillations (Figure 3-3 and Figure 3-4A-B) than their WT litter-mates after the addition of kainic acid; however the mean frequency in these oscillations was not significantly different between genotypes (Figure 3-4C). Oscillation frequency is mediated by the net excitation of interneurons and by the kinetics of the inhibitory postsynaptic potentials between them (Whittington et al., 1995). The fact that I do not see a difference in the dominant frequency is surprising as this has a major impact on the maintenance of gamma oscillations and studies in *Mecp2* mutant mice have shown abnormalities in mIPSC properties (Chao et al., 2010; Medrihan et al., 2008). However my results still suggest that an overall disruption in neuronal network circuitry is present. Furthermore an increase in oscillatory power was also observed recently in a mouse model of RTT through electroencephalography (EEG) recordings (Goffin et al., 2012) in which an increase in the high gamma frequency range (70-140Hz) was observed. However, the major differences in this study compared to my results were that I observed a power increase below 40Hz and my experiments were conducted *in vitro* compared to *in vivo*.

The balance between excitation and inhibition is essential for the generation and maintenance of physiological oscillations, therefore an imbalance in this regulation may be responsible for aberrant gamma oscillations seen in this study. However the exact disruption at the network level cannot be determined by these results alone. As the observed power of these oscillations was increased, it can be concluded that either there is a decrease in inhibitory action or an increase in excitation throughout the network. Previous studies have demonstrated that a selective removal of *Mecp2* in GABAergic neurons of the brain recapitulates many of the symptoms of RTT (Chao et al., 2010). Additionally, fast spiking GABAergic interneurons are important for the generation of gamma oscillations in the hippocampus. They are stimulated by

high frequency ectopic spiking of the principal cells axon plexus which results in their activation, this activity then feeds back onto the principal cells modulating their firing activity (Traub et al., 2003). Consequently it is possible that the observed increase in oscillatory power can be explained by a reduction in GABAergic inhibition in as shown in various papers documenting such a phenomenon in *Mecp2*-deficient mice (Chao et al., 2010; Medrihan et al., 2008; Zhang et al., 2008; Zhang et al., 2010).

To investigate the involvement of GABAergic inhibition in epileptogenesis in the hippocampus of *Mecp2*-deficient mice, I applied bicuculline (10 $\mu$ M), a GABA<sub>A</sub> receptor antagonist to hippocampal slices from *Mecp2*<sup>stop/y</sup> mice and their WT littermates. I found an increase in the frequency of spontaneous epileptiform bursting activity at low doses of bicuculline (0.1-1 $\mu$ M) in the CA1 region in slices from *Mecp2*<sup>stop/y</sup> mice compared to WT controls (Figure 3-5A-C.). *Mecp2*<sup>stop/y</sup> mice also showed an increase in the duration of spontaneous (Figure 3-5D) and evoked (Figure 3-6C) epileptiform bursts and a greater number of polyspikes (Figure 3-6A-B) in the presence of 10 $\mu$ M bicuculline. These results suggest *Mecp2*<sup>stop/y</sup> mice are more likely to develop epileptiform activity and that even in the absence of inhibition there are still excitability differences between genotypes, potentially from excitatory input. Additionally, *Mecp2*<sup>stop/y</sup> mice had the propensity to have higher rise rate values of fEPSPs, even without bicuculline application (Figure 3-6D). This result could imply that *Mecp2*-deficient mice have alterations in basal synaptic transmission. Other studies using *Mecp2* mutant mice have shown conflicting results on this topic with some showing an enhancement in basal synaptic in the hippocampus (Moretti et al., 2006) and alterations in basal inhibitory rhythms (Zhang et al., 2008) but others showing no difference (Asaka et al., 2006; Weng et al., 2011). Collectively, my data suggests there is a disruption of network excitability in *Mecp2*<sup>stop/y</sup> mice. The increase in frequency of spontaneous events and longer duration of evoked field potentials at low doses of bicuculline suggests there is a reduced threshold for the initiation of epileptiform activity.

More specifically, this data implies that mice deficient in *Mecp2* could have a disruption in GABAergic mediated control of network circuitry or that the principal cells in the hippocampus are more excitable. Other studies have shown that *Mecp2-deficient* mice have reduced spontaneous inhibitory postsynaptic

potentials in the CA3 of the hippocampus (Zhang et al., 2008). They also applied bicuculline to *Mecp2*-null slices and found prolonged evoked field potentials in the CA3, similar to our findings in the CA1, which suggest altered inhibitory rhythms are present in the hippocampus. Furthermore a recent study using voltage sensitive dyes within the hippocampus revealed an increase in amplitude and spatiotemporal spread of neuronal depolarisations in the CA1. Isolation of this region eliminated these differences thus proposing alterations in network excitability originate from the CA3 (Calfa et al., 2011). The results of the above two studies propose an imbalance in inhibitory neuron regulation in the hippocampus rendering the overall circuitry prone to hyperexcitability.

To further characterise the hyperexcitability phenotype I observed in hippocampal slices from *Mecp2*-deficient mice, I also applied the potassium channel blocker 4-AP to slices from *Mecp2*<sup>stop/y</sup> mice and their WT littermates. As with bicuculline, a more substantial increase in the frequency of spontaneous epileptiform bursting activity and duration of spontaneous epileptiform bursts was found in the CA1 of *Mecp2*<sup>stop/y</sup> mice (Figure 3-7). Additionally the duration of evoked epileptiform events (Figure 3-8C), the number of polyspikes (Figure 3-8A-B) and the occurrence of high frequency discharges followed by a train of burst-like events (ictal-like events; Figure 3-9) was greater in *Mecp2*<sup>stop/y</sup> mice in the presence of 30-50 $\mu$ M 4-AP. Overall these data suggest there are alterations in neuronal network circuitry in *Mecp2*-deficient mice whereby they are more likely to develop seizures, there is an increase in the strength of the seizures and there is a greater diversity in seizure type in the presence of 4-AP. It also indicates the *Mecp2*<sup>stop/y</sup> mice could be sensitive to changes in ionic conductance in cells, important for cell function and communication.

Altered receptor composition at the synapse in cells deficient in *Mecp2* could ultimately render the cells more susceptible to changes in ionic conductance. Indeed, reduced synapse size (Moretti et al., 2006), reduced NMDA receptor subunits (Maliszewska-Cyna et al., 2010) and decreased dendritic branching and spine number (Chapleau et al., 2009) have all been documented in mouse models of RTT which suggest morphological changes at the synapse could be an important factor in the hyperexcitability phenotype observed. Interestingly, in my lab one of my colleagues has shown that single cell recordings from principal CA1 neurons in the hippocampus of female WT and *Mecp2*<sup>+/-</sup> mice have no

significant differences between either their intrinsic or evoked properties (Louise Williams; unpublished data). However, heterozygous female mice do exhibit heightened sensitivity to kainic acid-induced seizures (Figure 3-2B) which suggests that at the cellular level excitability in *Mecp2*-deficient neurons is unaltered and that hyperexcitability differences are the consequence of the activity of the whole network.

In summary, I report a reduction in seizure threshold and increased power of gamma oscillations in *Mecp2*-deficient mice which ultimately leads to a state of hyperexcitability at the network level. My results suggest there could be a switch from a physiological oscillatory rhythm to a more pathological hypersynchrony. Furthermore, an imbalance in inhibitory neuron regulation in the hippocampus could partially contribute towards this disruption in network excitability and seizure development in these mice. Seizures are particularly common, debilitating and damaging aspect of RTT (Glaze et al., 2010). As such, application of my kainic acid seizure challenge model may be beneficial in future studies testing novel pharmacological and genetic approaches therapies in RTT (Cobb et al., 2010, Gadalla et al., 2011) to establish whether putative benefits extend into the epilepsy domain of the phenotype.

## Chapter 4

# Relationship between Mecp2 phosphorylation, histone acetylation and neuronal activity in wild-type and Mecp2-deficient mice

### 4.1 Introduction

Mecp2 is one of the most abundant nuclear proteins in neurons (Skene et al., 2010). However, the mechanisms by which MeCP2 regulates gene expression in the brain and leads to the abnormalities stated in chapter 3 remains ambiguous. A number of proposed theories have been put forward including the ability of Mecp2 to regulate the transcription of both inactive and active genes (Chahrour et al., 2008) through binding of methylated and unmethylated DNA respectively (Nikitina et al., 2007). Recently Mecp2 was shown to bind predominantly at methylated CpGs (Skene et al., 2010) thus considering methylated DNA is associated with a condensed chromatin state (reviewed by MacDonald and Roskams, 2009) this would imply a significant role in gene silencing.

The capability of Mecp2 to act as a repressor is facilitated by the recruitment of chromatin remodelling proteins such as histone deacetylases (Nan et al., 1998). Histones are the main protein component of nucleosomes around which DNA is wrapped. There are four core histones - H2A, H2B, H3 and H4 in which two copies of each of these histones assemble to form one octameric nucleosome and function to pack DNA into the nucleus. Unpacking and packing of DNA for gene regulation is facilitated by various posttranslational modifications at residues on histone tails, including methylation, acetylation, phosphorylation and ubiquitination (reviewed by Kouzarides, 2007). Among the core histones, H3 and H4 are the principal targets of these modifications (Turner, 1991). Acetylation and deacetylation of lysine residues are well studied modifications with the former being associated with active genes and the latter with silenced (reviewed by MacDonald and Roskams, 2009). The balance of this enzymatic process is pivotal for normal gene regulation in which a reduction in one protein

leads to an increase in the other. Consequently mutations in *MECP2* could alter the stability of this system resulting in dysregulation of important genes.

Activity-dependent regulation of gene expression plays an important role in postnatal neuronal maturation (reviewed by West and Greenberg, 2011). The ability of *Mecp2* to become phosphorylated upon membrane depolarization (Chen et al., 2003) suggests that MeCP2 could play a crucial role in linking neuronal activity with control of gene expression. Using a phospho-site-specific antibody, phosphorylation of *Mecp2* specifically at amino acid residue serine 421 in the brain has been connected with dissociation from methylation sites and activation of genes (Zhou et al., 2006). An increase in histone acetylation would be predicted in this occurrence. Furthermore phosphorylation at a different site, serine 80 is thought to be negatively regulated by neuronal activity whereby dephosphorylation occurs upon membrane depolarisation. It is suggested that S80 phosphorylation is associated with MeCP2 function in resting neurons and S421 phosphorylation in depolarised neurons thus altering gene transcription from a repressed to activated state respectively (Tao et al., 2009). Other phosphorylation sites (Tao et al., 2009) are likely to be involved and could act as post-translational markers. Mutations in *MECP2* at these sites could disrupt this regulatory process, and lead to changes in chromatin proteins involved in the control of gene expression.

## 4.2 Study aim

In this study, the aim was to investigate the interactions between neuronal activity, MeCP2 phosphorylation and histone (H3 and H4) acetylation in order to understand how they work together to regulate gene expression. The specific aims were to:

- i. Confirm the effect of neuronal activity on the phosphorylation of *Mecp2* at serine 421 (pS421 *Mecp2*) in the hippocampus of WT mice using the convulsant drug kainic acid.
- ii. Investigate whether there are differences in acetylated histone (H3 and H4) protein levels in the hippocampus of WT and *Mecp2*-deficient mice

under basal conditions and following kainic acid-induced neuronal activity.

### 4.3 Methods

To induce neuronal activity, 25mg/kg kainic acid or saline was applied intraperitoneally to symptomatic *Mecp2*<sup>stop/y</sup> male mice (under light isoflurane anaesthesia; 2.5-3%), *Mecp2*<sup>-/y</sup> male mice (not under anaesthesia) and their WT littermates aged 6-10 weeks as described in chapter two. At the end of each experiment, the mice were culled by cervical dislocation and decapitation before the hippocampus was removed and snap frozen in liquid nitrogen.

Hippocampal samples from each animal were homogenized in cell lysate buffer and protein levels quantified using a Bradford assay. Proteins were electrophoresed through a 4-12% Bis-Tris NuPAGE gel or 7% acrylamide gel (for absolute levels of phosphorylated Mecp2) and a western blot was performed as stated in chapter two to evaluate alterations in phosphorylated MeCP2 and histone (H3 and H4) acetylated protein levels between samples. Proteins were probed overnight with primary antibody rabbit anti-acetyl-Histone H3 (acetylated on lysines 9 and 14; 1/10000), rabbit anti-acetyl-Histone H4 (acetylated on lysines 5, 8, 12 and 16, 1/5000), rabbit anti-pS421 MeCP2 (1/2000), rabbit anti-MeCP2 (1/1000) or mouse anti-NeuN (1/2000) as a loading control. Subsequently, anti-rabbit HRP-conjugated secondary (for anti-MeCP2 primary only) or anti-rabbit and anti-mouse fluorescent secondary antibodies secondary antibodies were applied to membranes and results visualized and analysed using ECL or Odyssey infrared imaging systems respectively as described in chapter two. To normalise to a common measure in every western blot and enable comparison of results, integrated intensities of each main protein of interest were divided by the average of the WT saline group. This gave a fold change of integrated intensity relative to WT saline as plotted in each graph.

## 4.4 Results

### 4.4.1 Increase in Mecp2 phosphorylation following application of kainic acid to WT mice

Phosphorylation of Mecp2 following addition of 50mM KCl to cultured rat cortical neurons was the first evidence that MeCP2 could be subject to posttranslational modifications following neuronal activity (Chen et al., 2003). Later, the same group discovered that phosphorylation of Mecp2 at serine 421 (pS421 Mecp2) was important in regulating Mecp2 derepression at the BDNF promoter (Zhou et al., 2006). A significant increase in phosphorylation at this site is present in specific brain regions, including the striatum, following psychostimulant administration (Mao et al., 2011) and in mesolimbocortical brain regions after amphetamine application (Hutchinson et al., 2012). Therefore, to investigate the effects of neuronal activity on pS421 MeCP2 levels, I applied the convulsant substance kainic acid *in vivo* to WT mice and quantified the levels of phosphorylation in the hippocampus by western blot. Experiments were conducted with mice under light isoflurane anaesthesia (2.5-3%) to minimize the discomfort of the mice. There was a  $1.5 \pm 0.3$  fold increase in pS421 Mecp2 levels (fold difference compared to saline controls) following half an hour kainic acid treatment and  $2.6 \pm 0.8$  fold increase following three hours of kainic acid treatment (Figure 4-1;  $p < 0.05$ , unpaired t-test,  $n = 6-8$  mice for each genotype at every time point). However the effects observed following kainic acid treatment were quite variable and did not achieve significance. Additionally not all hippocampal samples display Mecp2 phosphorylation as can be observed in one of the samples after three hours (lane 3) of kainic acid treatment (Figure 4-1).

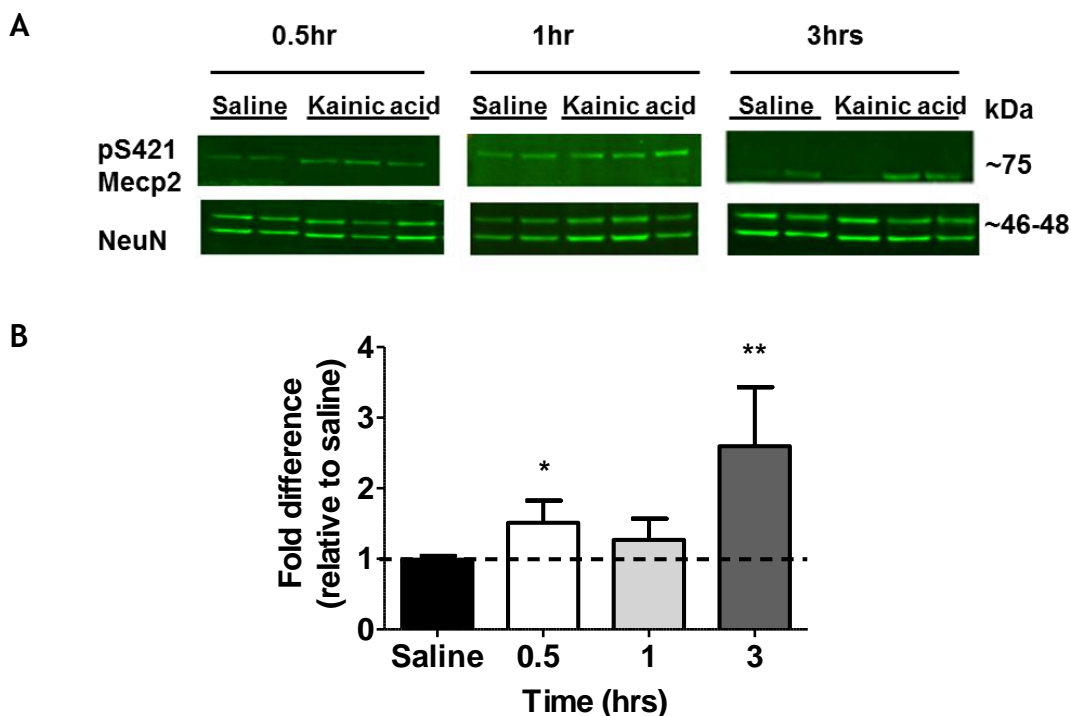


**Figure 4-1 Subtle increase in pS421 Mecp2 protein levels in the hippocampus of WT mice following kainic acid treatment**

(A) Representative western blot comparing pS421 Mecp2 protein levels 0.5, 1 and 3 hours after kainic acid (KA) administration to saline (SA) controls. Note the modest increase and variable phosphorylated levels (B) Bar plot showing pooled data ( $p < 0.05$  at 30 minutes,  $p < 0.01$  at 3 hours, unpaired t-test,  $n = 6$  to 8 mice for both genotypes at every time point). Data expressed as mean  $\pm$  SEM. Note experiments were conducted with mice under anaesthesia.

#### 4.4.2 Modest histone H3 acetylation (H3Ac) alterations in WT and Mecp2-deficient mice after kainic acid treatment

Induction of neuronal activity through administration of kainic acid can increase the phosphorylation of Mecp2. However, this does not explain how MeCP2 might regulate gene expression. One proposed theory was that the dissociation of DNA bound Mecp2 from the BDNF promoter and subsequent elevation in BDNF levels upon phosphorylation of Mecp2 at pS421 (Zhou et al., 2006 but see recent publication Cohen et al., 2011) could result as a consequence of increased histone acetylation levels. Additionally, under basal conditions, whole mouse brain homogenates from Mecp2-deficient mice appear to have elevated levels of histone H3 acetylation (H3Ac) on a global scale (Skene et al., 2010). Therefore, under basal conditions when neuronal activity is low, MeCP2 could repress gene expression by binding at methylated DNA sites and recruiting histone deacetylases proteins to remove acetyl groups from lysine residues at histone H3 tails. Upon neuronal activity, MeCP2 could dissociate from DNA methylation sites thus enabling histone acetyltransferases enzymes to add acetyl groups to lysine

residues at histone H3 tails and enable gene activation. To test this hypothesis, I applied saline or evoked kainic-acid- induced seizures in WT and *Mecp2*<sup>stop/y</sup> mice (under light isoflurane anaesthesia; 2-5-3%) and quantified the levels of H3Ac in the hippocampus by western blot.

Samples were assessed at a number of different time points following the initiation of kainic acid or saline treatment (0.5, 1 and 3 hours). A representative blot of H3Ac protein levels produced after three hours of kainic acid treatment can be observed in Figure 4-2A. Quantification of results after three hours showed no difference was observed between any treatment or genotype (Figure 4-2B;  $p > 0.05$ , two-way ANOVA with Tukeys *post hoc* test;  $n = 5$  to 8 for both genotypes and drug treatment groups). Furthermore, no significant change was observed in H3Ac protein levels in either genotype at any of the earlier 0.5 hour and 1 hour time points (Figure 4-2C;  $p > 0.05$ , two-way ANOVA with Tukeys *post hoc* test).

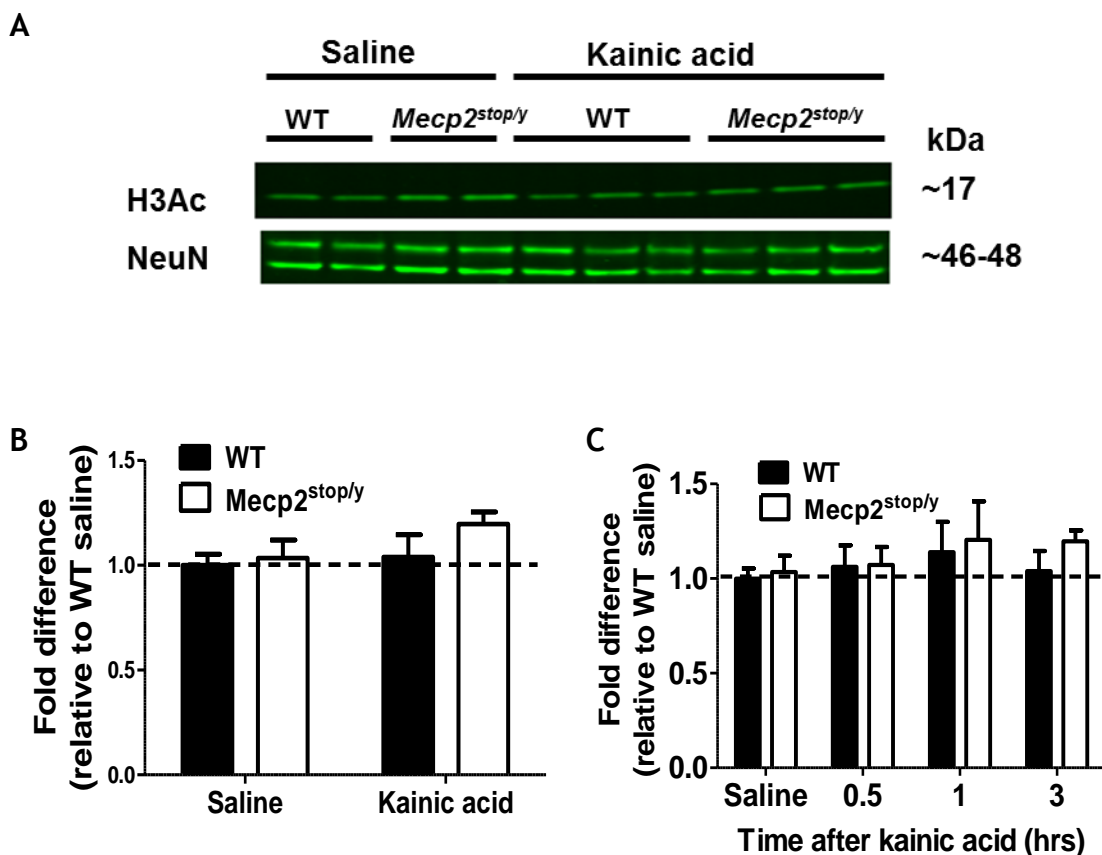


**Figure 4-2 H3Ac levels in the hippocampus of WT and *Mecp2<sup>Stop/y</sup>* mice are unaltered following kainic acid-induced epileptogenesis**

(A) Representative blot comparing H3Ac levels in WT and *Mecp2<sup>stop/y</sup>* mice before and after 3 hours of kainic acid treatment. (B) Quantification of H3Ac before and 3 hours post kainic acid administration reveal no significant change in acetylated protein levels in either WT or *Mecp2<sup>stop/y</sup>* mice ( $p > 0.05$ , two-way AVOVA with Tukeys *post hoc* test;  $n = 5$  to  $8$  for both genotypes and drug treatment groups). (C) Pooled data showing H3Ac levels at a range of time points (0.5, 1 and 3 hours) post kainic acid treatment. No significant change in either genotype is revealed at any other time point ( $p > 0.05$ , two-way AVOVA with Tukeys *post hoc* test). Data expressed as mean  $\pm$  SEM. Note experiments were conducted with mice under anaesthesia

#### 4.4.3 Modest histone H4 acetylation (H4Ac) alterations in WT and *Mecp2*-deficient mice after kainic acid treatment

Histone H4 protein is another core component of nucleosomes, forming histone H3-H4 tetramers (Xu et al., 2010). Therefore, interactions can occur between the two histones potentially including modifications of their lysine residues. A previous report has shown application of kainic acid to WT mice result in an acute increase in histone h4 acetylation (H4Ac) after three hours (Sng et al., 2006). To assess whether MeCP2 has any influence on H4Ac levels, I applied saline or evoked kainic-acid- induced seizures in WT and *Mecp2<sup>stop/y</sup>* mice (under light isoflurane anaesthesia; 2-5-3%) and quantified the levels of H4Ac in the hippocampus by western blot. A representative blot showing H4Ac levels after three hours of kainic acid can is shown in Figure 4-3A.

Quantification at this time point showed there was no difference in H4Ac protein between WT and *Mecp2*<sup>stop/y</sup> mice, however there was an overall significance in treatment towards an increase in H4Ac levels in both genotypes following kainic acid administration (Figure 4-3B;  $p < 0.05$ , two-way ANOVA with Tukeys *post hoc* test,  $n = 5$  to 8 for both genotypes and drug treatment groups). Analyse of H4Ac protein levels at the earlier 0.5 hour and 1 hour time points, revealed that there was no significant change in either genotype (Figure 4-3B;  $p > 0.05$ , two-way ANOVA with Tukeys *post hoc* test).

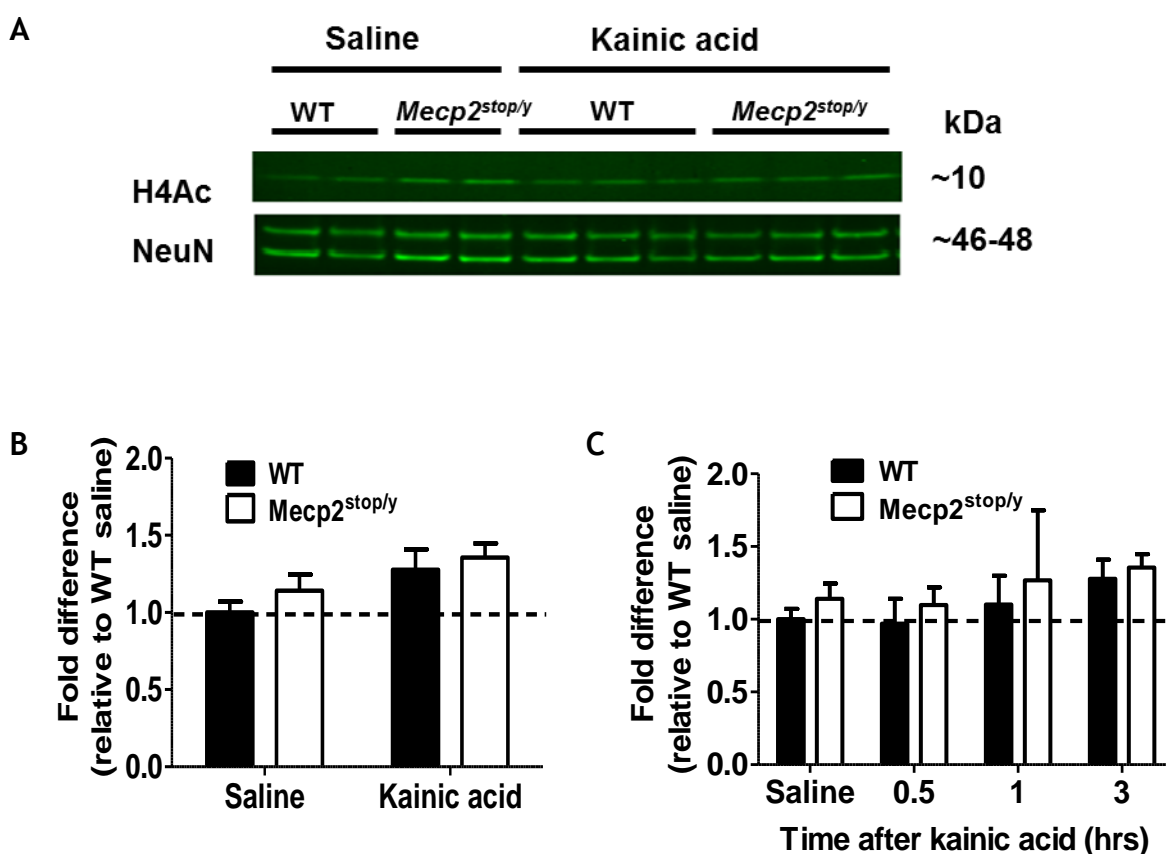


**Figure 4-3 H4Ac levels in the hippocampus of WT and *Mecp2*<sup>stop/y</sup> mice are unaltered between genotypes following kainic acid-induced epileptogenesis**

(A) Representative blot comparing histone H4 acetylation (H4Ac) levels in WT and *Mecp2*<sup>stop/y</sup> mice before and after 3 hours of kainic acid treatment. (B) Quantification of H4Ac before and post 3 hours kainic acid administration. No difference was apparent between genotypes but there was an overall significance in treatment towards an increase in H4Ac ( $p < 0.05$ , two-way ANOVA with Tukeys *post hoc* test,  $n = 5$  to 8 for both genotypes and drug treatment groups). (C) Pooled data comparing H4Ac levels post kainic acid treatment at a range of time points (0.5, 1 and 3 hours). No significant change in either genotype is revealed at any other time point ( $p > 0.05$ , two-way ANOVA with Tukeys *post hoc* test,  $n =$  same as above for all time points). Data expressed as mean  $\pm$  SEM. Note experiments were conducted with mice under anaesthesia.

#### 4.4.4 Anaesthetic effects on phosphorylation of Mecp2 and histone H3 and H4 acetylation

##### 4.4.4.1 Robust increase in phosphorylation of Mecp2

General anaesthesia was administered throughout in most experiments for animal welfare reasons. However, it is known to suppress overall activity in the brain (White and Alkire, 2003, Peltier et al., 2005) and this may have an impact on molecular pathways involved in neuronal activity such as the phosphorylation of MeCP2. To investigate the variable effects of pS421 Mecp2 levels following kainic acid treatment in WT mice under anaesthesia, a small number of experiments were conducted in the absence of anaesthesia and the results compared. As seen in Figure 4-4, the initial observations show that basal pS421 Mecp2 levels were similar in mice with and without anaesthesia. Additionally, mice administered kainic acid but that did not display any overt seizure as indicated by lack of erratic twitches, tail shaking, forelimb clonus and full tonic-clonic seizures had comparable levels of basal pS421 Mecp2 to saline treated mice. Conversely a prominent increase in pS421 Mecp2 protein levels was present in mice without anaesthesia after three hours of kainic acid treatment compared to the variable levels of pS421 Mecp2 protein in mice under anaesthesia.

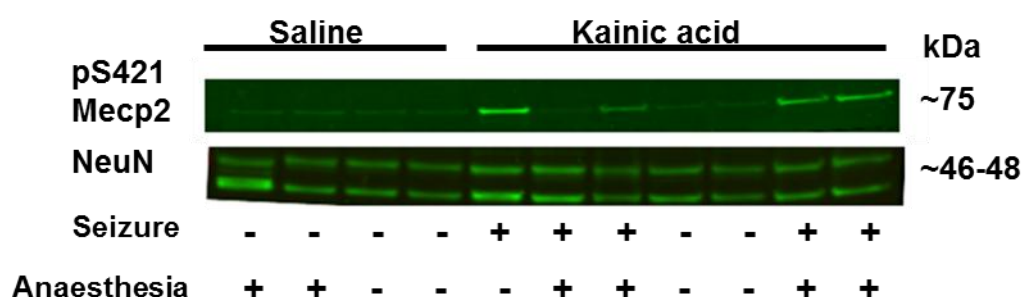


**Figure 4-4 Comparison of kainic acid seizure-mediated alterations in pS421 Mecp2 in presence and absence of anaesthesia.**

Representative western blot comparing the phosphorylation of Mecp2 levels (pS421 Mecp2) in WT mice with anaesthesia and without. Application of kainic acid (for 3 hours) without anaesthesia produces a robust increase in phosphorylation levels in the presence of an epileptic seizure compared to hippocampal samples under anaesthesia. Note mice that did not display a seizure have weak Mecp2 phosphorylation levels at serine 421.

Subsequently, more replicates of WT mice treated with saline or kainic acid without anaesthesia was performed and levels of pS421 Mecp2 quantified to confirm these observations. A robust increase was observed in pS421 Mecp2

levels ( $3.4 \pm 0.5$  fold) after three hours of kainic acid treatment (Figure 4-5A-B;  $p < 0.01$ , unpaired t-test,  $n = 6$  mice for both drug groups). All principal cells in the hippocampus showed high levels of pS421 Mecp2 immunoreactivity when immunostained at three hours following administration of kainic acid compared to saline control treated (Figure 4-5C). Only a few cells were weakly labeled for pS421 Mecp2 under control (saline treated) conditions. However full quantitative analysis was not performed on these images.

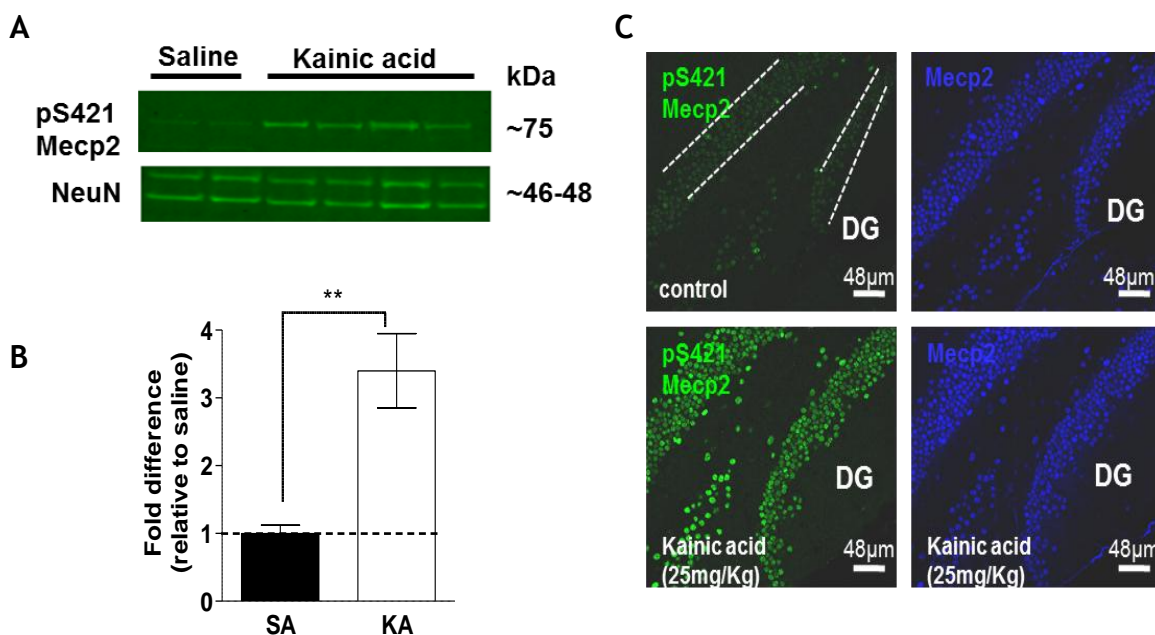


**Figure 4-5 Robust increase in pS421 Mecp2 levels in the hippocampus of WT mice without anaesthesia following kainic acid treatment.**

(A-B) Representative western blot and bar plot showing a robust increase in pS421 Mecp2 protein levels in WT mice at three hours following kainic acid (KA) treatment in the absence of anaesthesia when compared with saline (SA) controls ( $p < 0.01$ ; unpaired t-test,  $n = 6$  mice for both drug groups). (C) WT brain sections immunostained for pS421 Mecp2 and total Mecp2 in control (saline) and kainic acid treatment (3hrs) in the dentate gyrus (DG) of the hippocampus. Note all pyramidal cells are immunostained strongly with pS421 Mecp2 following kainic acid. Data expressed as mean  $\pm$  SEM and scale bar:  $50\mu\text{M}$ .

To access the total amount of MeCP2 that becomes phosphorylated in response to neuronal activity, hippocampal protein samples from mice treated with saline and kainic acid for three hours (not under anaesthesia) were run on a low percentage gel to separate out Mecp2 and any modified bands that were present. As observed in Figure 4-6A, two Mecp2 bands appeared in all samples treated with kainic acid. The upper band represented phosphorylated Mecp2, as previously described by Chen et al, 2003 who performed a similar experiment on rat cortical neurons and found that alkaline phosphatase treatment of their nuclear preparation eliminated this band (Chen et al., 2003). Quantification of this upper band in relation to the total levels of Mecp2 (lower band) showed a

50 ± 7% increase in the levels of phosphorylated Mecp2 after kainic acid treatment compared to only a 5 ± 0.5% increase in saline controls (Figure 4-6B;  $p < 0.01$ , unpaired t-test,  $n = 5$  mice for each drug treatment group).

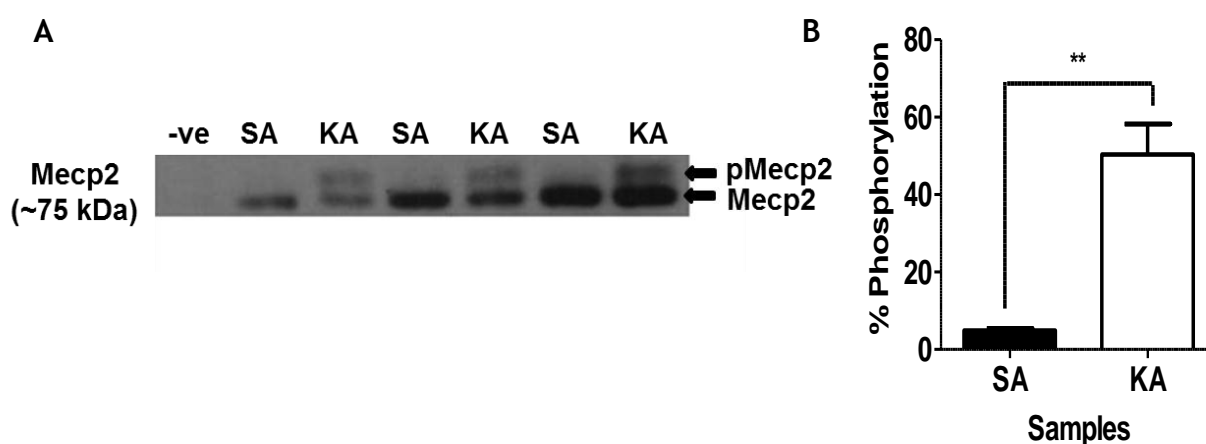


**Figure 4-6 50% of Mecp2 is phosphorylated in the hippocampus of WT mice after kainic acid treatment.**

(A) Representative blot showing the total levels of phosphorylated Mecp2 in the hippocampus of WT mice (upper band; Mecp2 is the lower band) before and after kainic acid treatment. SA = saline hippocampal samples, KA = kainic acid hippocampal samples and -ve = negative control (no Mecp2 staining). (B) Plot showing a 50% increase in phosphorylated Mecp2 levels in kainic acid treated samples ( $p < 0.01$ , unpaired t-test,  $n = 5$  mice for each drug treatment group). Data expressed as mean ± SEM.

#### 4.4.4.2 Modest alterations in histone H3 and H4 acetylation

To confirm that the negative results for histone acetylation above were not as a result of any confounding effects of anaesthesia, the levels of acetylation were measured in the small number of experiments not conducted under anaesthesia. A representative western blot showing relative H3Ac protein changes before and after three hours of kainic acid treatment in both WT and Mecp2-deficient mice is shown in Figure 4-7A. Quantification showed there was no difference in the levels of H3Ac before and after kainic acid treatment in WT mice (Figure 4-7B;  $p > 0.05$ , two-way ANOVA with Tukeys *post hoc* test;  $n = 6$  mice for each genotype and drug treatment group). Mice that lack Mecp2 showed no difference in their H3Ac levels compared to WT mice under control conditions but appeared to have greater levels (0.5 fold) following kainic acid treatment in relation to WT ( $Mecp2^{-/-} = 1.3 \pm 0.06$ ; WT =  $0.8 \pm 0.09$ ; Figure 4-7B;  $p < 0.01$ , two-way ANOVA with *post hoc* test). This significance could be attributed to the slight decline observed in H3Ac in WT mice after kainic acid treatment.

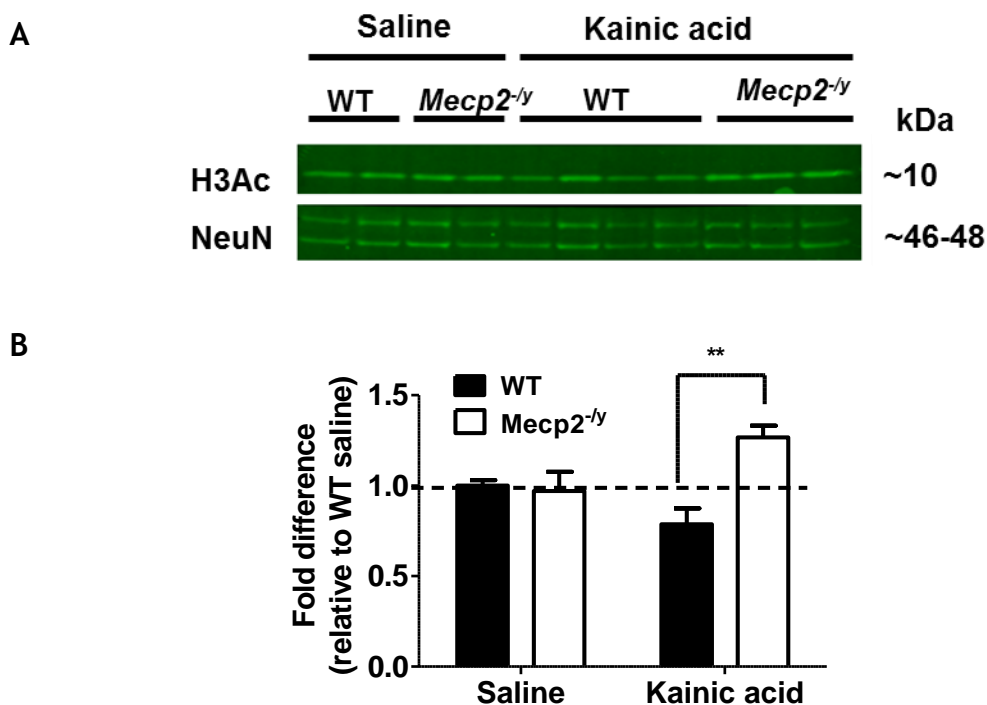


**Figure 4-7 Increase in H3Ac levels after kainic acid administration in the hippocampus of *Mecp2<sup>-/-</sup>* mice without anaesthesia.**

(A) Representative blot comparing H3Ac in WT and *Mecp2<sup>-/-</sup>* mice before and after 3 hours of kainic acid treatment without anaesthesia. (B) Pooled data showing a 0.5 fold increase ( $p < 0.01$ , two-way ANOVA with Tukeys *post hoc* test,  $n = 6$  mice for both genotypes and drug treatment groups) in *Mecp2<sup>-/-</sup>* mice compared to WT mice after kainic acid treatment. Data expressed as mean  $\pm$  SEM.

Levels of H4Ac were also determined in mice that were administered saline and kainic acid in the absence of anaesthesia. A representative western blot of H4Ac protein changes before and after three hours of kainic acid treatment in both WT and *Mecp2*-deficient mice is shown in Figure 4-8A. Quantification of the pooled data (Figure 4-8B) showed that there was no difference in H4Ac levels in WT mice following kainic acid treatment. Furthermore, although mice deficient in *Mecp2* appeared to have greater levels of H4Ac under control conditions when compared to WT, this did not achieve statistical significance ( $p = 0.27$ ). However, there was an overall significance in H4Ac between genotypes (Figure 4-8B;  $p < 0.05$ , two-way ANOVA with Tukeys *post hoc* test;  $n = 6$  mice for both genotypes and drug treatment groups).

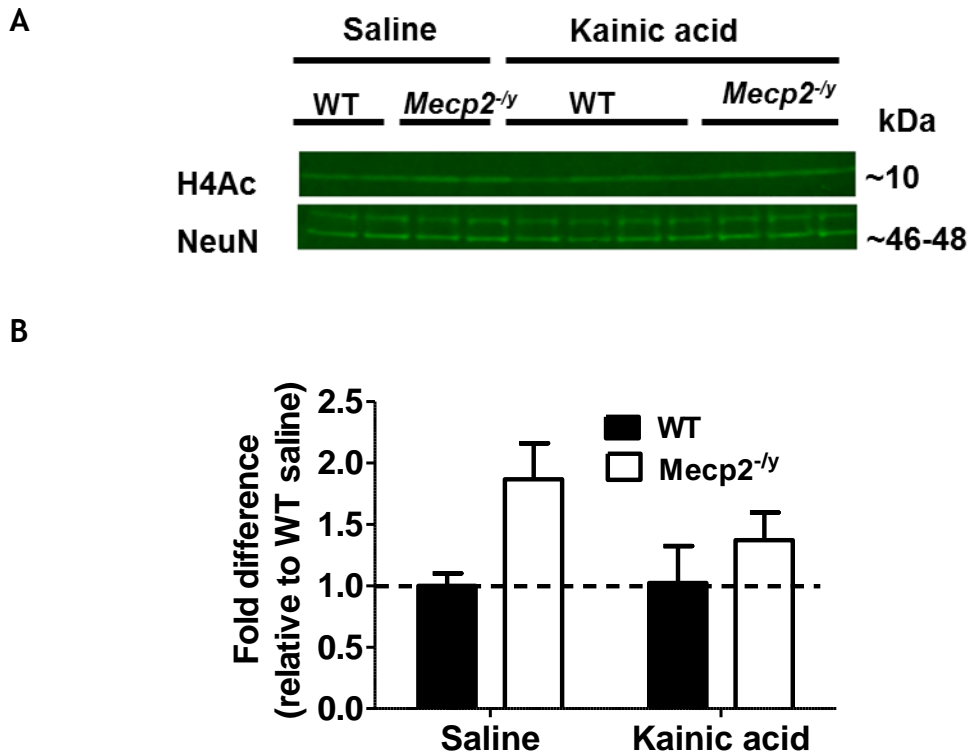


**Figure 4-8 Altered H4Ac levels between genotypes in the hippocampus of WT and *Mecp2<sup>-/-</sup>* mice without anaesthesia.**

(A) Representative blot comparing H4Ac in WT and *Mecp2<sup>-/-</sup>* mice before and after 3 hours of kainic acid treatment without anaesthesia. (B) Pooled data showing an overall significance in H4Ac between genotypes ( $p < 0.05$ , two-way AVOVA with Tukeys *post hoc* test,  $n = 6$  mice for both genotypes and drug treatment groups). Data expressed as mean  $\pm$  SEM.

## 4.5 Discussion

The function of MeCP2 was originally thought to be as a transcriptional repressor and that loss of function mutations in the protein would result in an over expression of genes it regulated and lead to the phenotype associated with RTT. However the last 10 years has seen this model challenged and other mechanisms have been put forward, for example, a role as a transcriptional activator (Chahrour et al., 2008), global transcriptional repressor (Skene et al., 2010) or regulator of chromatin looping (Horike et al., 2005). One of the most interesting findings in this period was the discovery that MeCP2 could be dynamically regulated by neuronal activity (Chen et al., 2003). In experiments described in this chapter, I have tried to investigate the possible effects of neuronal activity on the posttranslational modifications of MeCP2 and link this to potential alterations in histone acetylation. It was hoped that this would gain further insight into how MeCP2 regulates gene expression. Overall the main finding of the current study was to demonstrate that phosphorylation of MeCP2 was not linked to any alterations in histone acetylation (H3Ac or H4Ac) in WT mice

following kainic acid treatment. However studies performed in *Mecp2*-deficient mice (*Mecp2*<sup>stop/y</sup> and *Mecp2*<sup>-/y</sup>) show that lack of *Mecp2* may result in alterations in the regulation of histone acetylation under basal conditions and following kainic acid-induced neuronal activity.

More specifically, I have shown that *Mecp2* can be phosphorylated at residue serine 421 in the hippocampus (Figure 4-1 and Figure 4-5) and that ~50% of *Mecp2* molecules are phosphorylated (Figure 4-6) following kainic-acid induced seizures. Importantly, the presence of a seizure was required to obtain an increase in phosphorylation. Levels of pS421 *Mecp2* from mice that did not display any seizure like activity were extremely weak and comparable to control (saline) treated mice (Figure 4-4). These results suggest that MeCP2 can be posttranslationally modified and that high levels of MeCP2 are phosphorylated upon induction of neuronal activity. However it should be noted that the seizures generated following application of kainic acid do represent excessive neuronal activity. It is not clear which sites other than serine 421 are important in the activity dependent regulation of MeCP2. Recently, using a similar electrophoresis method to separate *Mecp2* as I did in Figure 4-6, a study also established two *Mecp2* bands from epileptic mouse brains which they subjected to mass spectrometry (Tao et al., 2009). They identified other sites on *Mecp2* that can become phosphorylated including serine residues 149, 164, 421 and 424. The latter two residues were only observed in the upper band that was produced in epileptic samples suggesting that these two phosphorylation sites were important upon induction of neuronal activity.

The Tao group also discovered phosphorylation at serine 80 was important in resting neurons which could become dephosphorylated upon neuronal activity (Tao et al., 2009). Knockin mouse models were created with mutations at either serine 80 or 421 and producing opposing behaviours with the latter displaying decreased motor control and the former increased locomotor control (Tao et al., 2009). This suggests that phosphorylation at specific residues sites on MeCP2 could have differing effects on MeCP2 function. These findings correlate with another recent study which highlights the specific site of phosphorylation on MeCP2, duration and type of the stimuli and exact gene being investigated are important for determining whether MeCP2 acts as a repressor or activator of gene transcription (Gonzales et al., 2012). Additionally, they could explain why

another study found that mutating both serine 421 and 424 in *Mecp2* enhanced *Mecp2* occupancy at the *Bdnf* promoter and increased transcription in the hippocampus (Li et al., 2011) whereas the original work on phosphorylation at serine 421 identified a reduction in *Bdnf* transcription in cortical neurons (Zhou et al., 2006).

Furthermore, phosphorylation of MeCP2 at specific residues and binding of MeCP2 to specific gene promoters, as mentioned in the previous studies, could potentially explain why I was unable to associate any alterations in phosphorylation with an increase in histone H3 or H4 acetylation in WT mice (Figure 4-2, 4-2, 4-7 and 4-8). My original theory focussed on MeCP2 having a role as transcriptional repressor and recruiting histone deacetylase proteins to silence genes when neurons were quiescent (Nan et al., 1998). Subsequently, upon neuronal activation MeCP2 could dissociate away from these genes resulting in gene activation, aided by histone acetylation. However my data did not support this model. As the developing brain is constantly responding to various activity-dependent inputs (reviewed by West and Greenberg, 2011), differential posttranslational modifications of MeCP2 and the type of external stimuli could determine the specific targets and function of MeCP2 in various brain regions throughout development.

Conflicting with the idea of MeCP2 as a regulator of specific ‘target genes’, recent ChIP-seq analysis has established that the pan-MeCP2 antibody and phosphorylated *Mecp2* are strongly associated with methylated DNA (silenced genes) throughout the entire genome regardless of whether any neuronal activation is present (Cohen et al., 2011). They also discovered that the induction of activity-dependent genes such as BDNF remains unaltered following phosphorylation at serine 421. These results suggest that there is a weaker association with phosphorylated MeCP2 and genes that are actively transcribed and interestingly contradicts the original findings from this group in which they reported an increase in the transcription of BDNF with phosphorylation of *Mecp2* (Zhou et al., 2006). The results obtained in this chapter, in which I could not show evidence for any increase in acetylation with elevated *Mecp2* phosphorylation levels is in support of this finding as lack of actively transcribed genes is usually associated with a condensed chromatin state and thus less histone acetylation (reviewed by MacDonald and Roskams, 2009).

Regardless of whether MeCP2 has a more specific or global role in the regulation of gene expression, how MeCP2 reacts and adapts to changes in neuronal activity in its immediate environment will be similar for both. For example accurate timing of events will be important for proper MeCP2 regulation of genes and histone deacetylase proteins it interacts with. As many transcriptional responses are dynamic and transient, there will be a rapid change in the levels of acetylated and deacetylated histone in order to restore gene expression to basal levels. Reversal of deacetylated proteins can occur in 5-8 minutes but acetylation can be reversed more rapidly, ~1.5 minutes (Katan-Khaykovich and Struhl, 2002). Any disruption to this tightly controlled process could lead to alterations in gene expression. Interestingly although I did not detect an increase in histone acetylation in WT mice following induction of neuronal activity with the convulsant drug kainic acid I observed a significant elevation in H3Ac following induction of neuronal activity in *Mecp2*-deficient mice (Figure 4-7). This could suggest the mechanisms and timing by which *Mecp2* regulates gene expression under dynamic processes is disrupted as more acetylated histone proteins were present than in WT conditions.

The speed at which histone proteins become acetylated and deacetylated may also contribute to the lack of acetylation observed in WT mice in this chapter. As previous studies have shown a continuous increase in H4Ac in the hippocampus following kainic acid administration from 0.5-3 hours (Sng et al., 2006), I based my experimental design around these time points. However as the histone acetylation turns over quickly (Katan-Khaykovich and Struhl, 2002), I could be missing early changes in histone acetylation. Alternatively, the time it takes for kainic acid to induce neuronal activity in cells and thus alter acetylation and deacetylation levels could take longer than the time points analysed (0.5-3 hours) therefore centring the time after kainic acid administration could mean I have missed later events, although this is unlikely as I observe seizures within minutes of administering kainic acid without anaesthesia. Additionally, other experimental variables that could be contributing to the lack of increase in histone acetylation could be the lysine residues that the H3Ac antibody and H4Ac antibody bind to do not become acetylated. Although the antibodies used in this study bind regions on histone tails that are associated with active euchromatin (lysine residue 5, 8, 12 and 16 for H4Ac, Clarke et al., 1993; lysine residue 9 and

14 for H3Ac, Roh et al., 2005), some histone acetyltransferase (HAT) enzymes which acetylate lysine amino acids can be quite specific in terms of the individual lysine residues and particular histones. For example, a specific type of HAT Gcn5 preferentially acetylates lysine 14 of histone H3 and lysine 8 and 16 of histone H4 (Kuo et al., 1996). This could mean that depending on which HAT kainic acid induced neuronal activity activates, the binding to all acetylated residues might be weakening the effect if the acetylation is more specific. However the antibody used by Sng et al, 2006 mentioned above was same H4Ac antibody I used in my experiments binding to all four lysine residues and they still observed elevated histone acetylation levels in WT mice following kainic acid treatment.

There are other experimental differences from the Sng et al, 2006 group that might account for why my results contradict theirs. Firstly, since the strain of mouse can differentially influence cellular responses following kainic acid-induced seizures (Schauwecker and Steward, 1997), the fact that my mice were on a C57BL6/J background compared to their Std-ddY mice could have an effect. Secondly, the method used for extracting nuclear proteins in the paper was significantly different to mine. My method was optimised in the first instance by homogenising whole hippocampal lysates without losing any protein to obtain a clear nuclear MeCP2 protein band (Appendix A, Supplementary Figure 1-1). However the above study used a more complex approach including sonication and precipitation of samples to obtain histone proteins. My method may not be sensitive enough to detect changes in histone acetylation or potentially Sng et al are removing too much of their protein in their nuclear preparation thus their findings are not accurate.

Finally, another major experimental variable that could have been influencing my results was anaesthesia. At the recommendation of the vet, I applied volatile isoflurane to the mice before kainic acid or saline was administered to minimise the stress to the mice. However, anaesthesia is known to suppress overall activity in the brain (White and Alkire, 2003, Peltier et al., 2005) which may impact on activity-dependent alterations in cellular pathways such as the phosphorylation of MeCP2. Indeed only a subtle and variable increase in phosphorylation of Mecp2 was observed in WT mice that were administered kainic acid under anaesthesia (Figure 4-1). In comparison, samples from

unanaesthetised WT mice showed a robust increase in phosphorylation of Mecp2 with all principal cells in the hippocampus strongly immunoreactive for pS421 Mecp2 (Figure 4-4 and Figure 4-5). It is possible then that the dampening effect of anaesthetic administration could be minimizing the extent of phosphorylation. Isoflurane anaesthetics bind to a variety of target proteins in the brain including GABA<sub>A</sub> receptors, glycine receptors (Harrison et al., 1993), AMPA and NMDA receptor mediated ion channels (Carlà and Moroni, 1992) and two-pore potassium channels (Patel et al., 1999). The overall effect is to alter the balance of excitation and inhibition in the brain and dampen activity. Although the effects of anaesthetic are evident on phosphorylation of Mecp2, alterations in histone acetylation were less pronounced. The results in both the presence and absence of anaesthesia showed only subtle differences and it is possible that the excitability threshold for phosphorylation of MeCP2 and histone acetylation is different and thus the strength of neuronal activity applied could have a differential effect on their activity.

In conclusion, my work and the above studies on phosphorylation of MeCP2 highlight the complex role neuronal activity has on controlling MeCP2 and gene expression. In this chapter I have shown that induction of neuronal activity using the convulsant drug kainic acid leads to an increase in the phosphorylation of Mecp2 but was not linked to any alterations in histone acetylation (H3Ac or H4Ac) in WT mice following kainic acid treatment. This could be due to histone acetylation and phosphorylation of MeCP2 at specific target genes. The effect could be getting diluted as I am looking at global changes in histone acetylation in the hippocampus. Future experimental approaches studying this phenomenon over specific gene locus using ChIP and antibodies against pS421 MeCP2 and acetylated histones could help explore this theory. The experiments performed on Mecp2-deficient mice in this chapter show that lack of Mecp2 may result in alterations in the regulation of histone acetylation following kainic acid-induced neuronal activity. However, this result is still quite subtle and variable leading to controversy in the results. Designing a study with a higher degree of specificity and resolution will enable a more definitive judgment to be made on the differences in histone acetylation between WT and Mecp2-deficient mice.

## Chapter 5

# An investigation of histone protein levels in *Mecp2* positive and negative neurons in the *Mecp2*<sup>+/-</sup> mosaic brain

### 5.1 Introduction

In the previous chapter I investigated the influence of neuronal activity on the posttranslational modifications of *Mecp2* and levels of histone acetylation in WT and *Mecp2*-deficient mice. I demonstrated that neuronal activity can lead to the phosphorylation of MeCP2 at serine 421 in WT mice but the changes in histone acetylation levels, as measured by western blot, in both WT and *Mecp2*-deficient mice were subtle and highly variable. The inconsistencies in histone measures could be partially due to the confounding actions of anaesthetic administration which may have dampened neuronal activity and prevented the occurrence of clear effects on histone acetylation. Another contributing factor could be the sensitivity of the assay being used to determine effects and, in particular, the difficulty of detecting very subtle changes in histone acetylation by western blot. To overcome this, another approach was devised and refined to investigate the potential relationship between MeCP2 and histone acetylation in neurons.

For a more accurate assessment of MeCP2 influence on histone acetylation levels, I utilised female mice heterozygous for *Mecp2* null mutation, a more accurate model of RTT in girls (Chen et al. 2001; Guy et al. 2001). As *MECP2* is an X-linked gene random X-chromosome inactivation at the cellular level results in inactivation of either the WT or mutant allele. Therefore, the female RTT patients or heterozygous mice will have a cell population that is mosaic for expression of the mutant allele. This phenomenon in heterozygous female mice creates a valuable internal standard by which quantitative immunofluorescence imaging can be used to compare differences in cells that express the mutant gene with those that have a normal copy. Normally there are variables associated with quantitative immunofluorescence imaging that make it difficult to compare the fluorescence intensity between two different samples (e.g. brain

sections/mice) accurately. For example, if I was observing the fluorescence intensity of histone acetylation in brain sections from WT and *Mecp2*-deficient mice, variables from the immunostaining process such as the amount of antibody that can penetrate the tissue and differential fixation in the mice (more or less crosslinking) could introduce unknown variability in to the results. However, as I am comparing the effects of two cells within the same section, most variables are minimised as the ratio difference between *Mecp2* positive and negative nuclei in theory should be consistent. Furthermore there is power in this analysis to look at many cells from specific regions at once therefore highlighting any subtle differences that are present.

## 5.2 Study aim

A dominant hypothesis is that MeCP2 regulates gene expression through influencing histone protein acetylation. In this study my aim was to investigate the relationship between *Mecp2* levels and the levels of histone H3 and H4 acetylation using an immunohistochemistry based method in *Mecp2*<sup>+/-</sup> heterozygous mice. The specific aims were to:

- i. Determine whether there is any difference in histone H3 and H4 acetylation and total levels of histone H3 and H4 in nuclei positive and negative for *Mecp2* protein in the hippocampal formation.
- ii. Investigate the effect neuronal activity has on the regulation of these histone proteins in nuclei positive and negative for *Mecp2* in the hippocampal formation.

## 5.3 Methods

Kainic acid (25mg/kg) or saline (controls) was applied intraperitoneally to pre-symptomatic *Mecp2*<sup>GFP/-</sup> female mice aged 10-13 weeks (in the absence of anaesthesia) and monitored for seizure score over a three hour period. At the end of each experiment, mice were culled humanely by overdose of sodium pentobarbital (Euthatal) and fixed by intracardiac perfusion as described in chapter two. The brains were removed, post-fixed in the same fixative and coronal brain sections (30µm spanning) cut on a vibratome ready for

immunohistochemistry. This technique was performed as stated in chapter two, whereby brain sections underwent an antigen retrieval step before incubation with primary antibodies rabbit anti-acetyl-Histone H3 (acetylated on lysines 9 and 14, 1/200), rabbit anti-acetyl-Histone H4 (acetylated on lysines 5, 8, 12 and 16, 1/100), rabbit anti-Histone H3 (1/100) and mouse anti-Histone H4 (1/200) for two-three days. All histone H4 antibodies were incubated on the same brain sections. Afterward, fluorescent secondary antibodies (Alexa fluor 546 goat anti-mouse and Alexa fluor 647 goat anti-rabbit) were added to sections overnight in the dark. Subsequently, sections were incubated with the nuclei marker DAPI (20mg/ml stock; 1/1000 working dilution) for 20 minutes then mounted onto coverslips. At least two random and non-overlapping image stacks of the hippocampal formation in the DG and CA1 region for each section were collected on a Leica SP5 Confocal microscope equipped with diode (405nm), argon (488nm), diode pumped solid-state (DPSS; 561nm) and red helium-neon (633nm) lasers.

Differences in all histone protein intensities between Mecp2 positive and negative nuclei were quantified using a custom written (Dr David Kelly, University of Edinburgh) automated script in Image-pro Plus 6.0 described in detail in chapter two. The script determined three parameters for every nucleus in the image stack: 1. the mean intensity for that particular histone antibody, 2. the nuclei volume and 3. whether Mecp2 was present or not. In order to avoid the problem of determining which parameter (stack, section or animal) to normalise the data to when quantifying intensities, a chi-square test was performed. For each histone protein, the chi-square test derived whether there was a change in the distribution of Mecp2 positive and negative nuclei above the median or in the upper quartile intensity values.

Firstly the histone protein intensities for each nucleus in the section were ranked in order from highest to lowest. The number of Mecp2 positive and negative nuclei with histone intensities above the median or in the upper quartile was then calculated, these were referred to as the **observed** values. If the histone intensities of both nuclei types are normally distributed then it is expected that 50% of each nuclei type would have histone intensities above the median and 25% of each nuclei type would have histone intensities in the upper quartile. For example if there were 60 nuclei in total and 40 nuclei were

negative for *Mecp2* and 20 nuclei positive for *Mecp2*, then you would expect 20 *Mecp2* negative and 10 *Mecp2* positive nuclei to be above the median histone intensity. Furthermore you would expect 10 *Mecp2* positive nuclei and 5 *Mecp2* negative nuclei above the upper quartile histone intensity. Collectively these were referred to as the **expected** values. A chi-square analysis then determined if the **observed** value for each nuclei type significantly differed from the **expected** value. If a difference was present, this could indicate that there was a relationship between *Mecp2* levels and levels of that specific histone protein. The statistics were done on the raw number counts and not percentages of *Mecp2* positive and negative nuclei to ensure that sections with smaller numbers of nuclei do not disproportionately affect the overall chi-squared value. Percentages were summarised at the end to obtain the magnitude of any affect present.

## 5.4 Results

### 5.4.1 Nuclei deficient in *Mecp2* display a 5% reduction in their nuclear volume

Measurement of nuclear volume is essential for accurately calculating nuclear protein abundance. To investigate whether there were any differences in architecture of *Mecp2* positive and negative nuclei, the volume of each nucleus was quantified from 3D images in which DAPI labelling was used to detect the nucleus. Analysis was performed from three different mice under saline control conditions in the hippocampal formation (DG and CA1). The micrograph in Figure 5-1A shows a representative image of DAPI immunostained nuclei co-localised with *Mecp2* positive nuclei. Three dimensional reconstructions of DG granule nuclei revealed the nuclear volume to be smaller in *Mecp2*-deficient nuclei ( $195.4 \pm 1.6\mu\text{m}^3$ ) compared to neighbouring *Mecp2* containing nuclei ( $204.5 \pm 2.3\mu\text{m}^3$ ). This corresponded to a 5% reduction in nuclear volume (Figure 5-1Bi-ii;  $p < 0.001$ , unpaired t-test,  $n = 177-243$  nuclei from three mice). A similar effect was observed in pyramidal nuclei in the CA1 whereby nuclear volume was smaller in *Mecp2*-deficient nuclei ( $328.4 \pm 4.3\mu\text{m}^3$ ) compared to *Mecp2* positive nuclei ( $344.8 \pm 5.4\mu\text{m}^3$ ). This also equated to a 5% reduction in nuclear volume in this area (Figure 5-1Ci-ii;  $p < 0.05$ , unpaired t-test,  $n = 89-179$  nuclei from three mice).

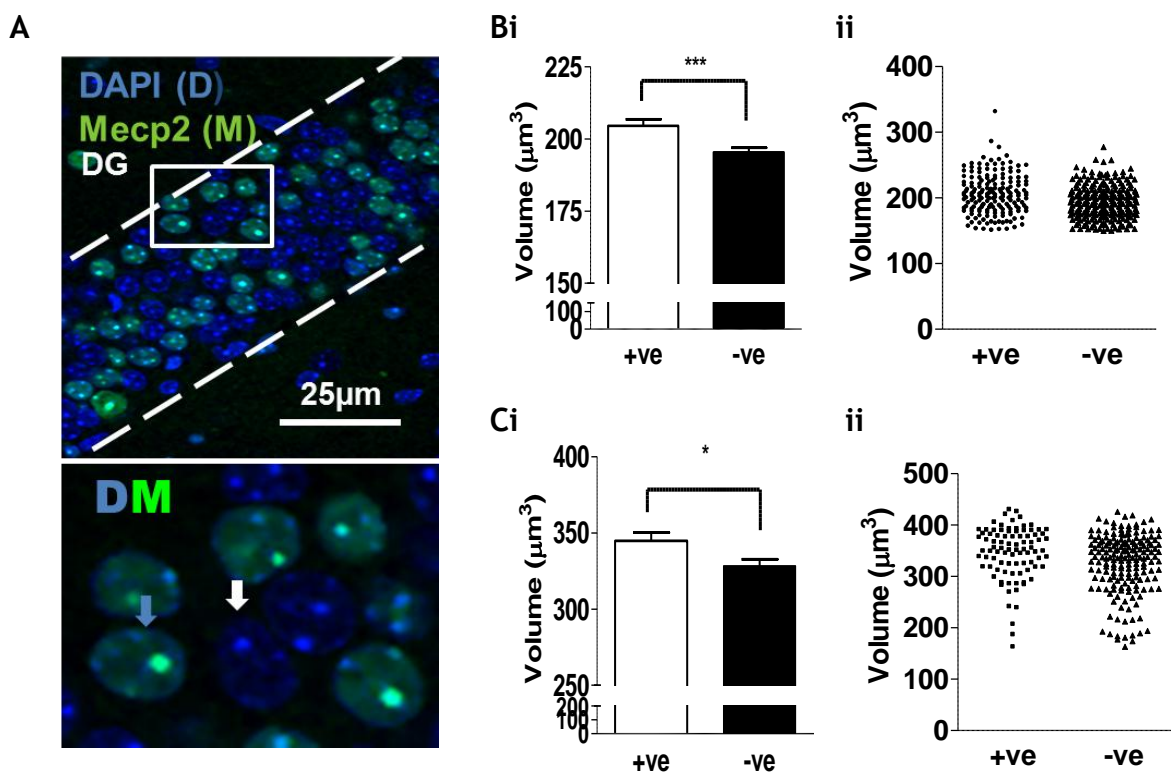


**Figure 5-1 5% reduction in nuclear volume in nuclei deficient in Mecp2**

(A) Example micrograph showing DAPI immunostained nuclei (and co-localised Mecp2 positive nuclei) in the DG of the hippocampal formation used to create the 3D images for volume measurements. The white box shows the location of nuclei in the bottom higher magnification image. White arrows highlight nuclei which do not contain Mecp2 and blue arrows indicate those that do. (Bi) Bar graph of nuclei volume in the DG showing a 5% decrease in volume in nuclei that lack Mecp2 compared to those that do not ( $p < 0.001$ , unpaired t-test,  $n = 177-243$  nuclei from three mice). The spread of this data is shown in the scatter plot (Bii). (Ci) Quantification of nuclei volume in the CA1 displaying a 5% reduction in nuclei deficient in Mecp2 ( $p < 0.05$ , unpaired t-test,  $n = 89-179$  nuclei from three mice). The spread of this data is expressed in the scatter plot (Cii). Data expressed as mean  $\pm$  SEM in the bar graphs. Scale bar = 25µM; +ve = positive nuclei and -ve = negative nuclei.

#### 5.4.2 Levels of histone H3 acetylation was unaltered between Mecp2 containing and Mecp2-deficient nuclei in the hippocampal formation

Three dimensional reconstructions of CA1 and DG nuclei in the hippocampal formation revealed the nuclear volume to be smaller by 5% in Mecp2-deficient nuclei compared to neighbouring Mecp2 containing nuclei. This could affect the measures of mean intensity of histone proteins; therefore all mean intensity values for each nucleus were multiplied by their volume measurement to compensate and obtain an integrated density value. Previously I observed no change in histone H3 acetylation (H3Ac) levels between *Mecp2*<sup>-y</sup> male mice and their WT littermates in the hippocampus under saline control conditions (Chapter 4). To investigate the effect of H3Ac in similar conditions at the single

cell level, I determined whether there was a difference in the distribution of H3Ac intensities in nuclei positive and negative for *Mecp2* from heterozygous female mice. In Figure 5-2, a representative micrograph can be observed of nuclei immunostained with H3Ac and *Mecp2* status displayed through fluorescence of the EGFP fusion protein in the DG of the hippocampal formation (Figure 5-2A). There was no difference in the observed and expected number of *Mecp2* negative nuclei above the median H3Ac intensity value. (Figure 5-2B;  $p=0.905$ , chi-square test;  $n = 7$  sections from three mice). Therefore the percentage of *Mecp2* positive ( $46.5 \pm 1.3\%$ ) and negative nuclei ( $53.1 \pm 2\%$ ) above the H3Ac median intensity value (Figure 5-2Di) were not different as the chi-square value indicated no significance.

Furthermore, to determine if a subset of the population of nuclei varied in H3Ac protein levels, the number of nuclei that were positive or negative for *Mecp2* in the top 25% (in the upper quartile) of H3Ac intensities was measured. Similarly, there was no difference in the observed number of *Mecp2* negative nuclei in the upper quartile H3Ac intensity values and the expected number of top 25% *Mecp2* negative nuclei (Figure 5-2C;  $p=0.766$ , chi-square test). As this chi-square statistic was not significant, there was no difference in the percentage of *Mecp2* positive nuclei ( $22.9 \pm 1.1\%$ ) in the upper quartile H3Ac intensity values compared to *Mecp2* negative nuclei ( $28.9 \pm 2.5\%$ ; Figure 5-2Dii).

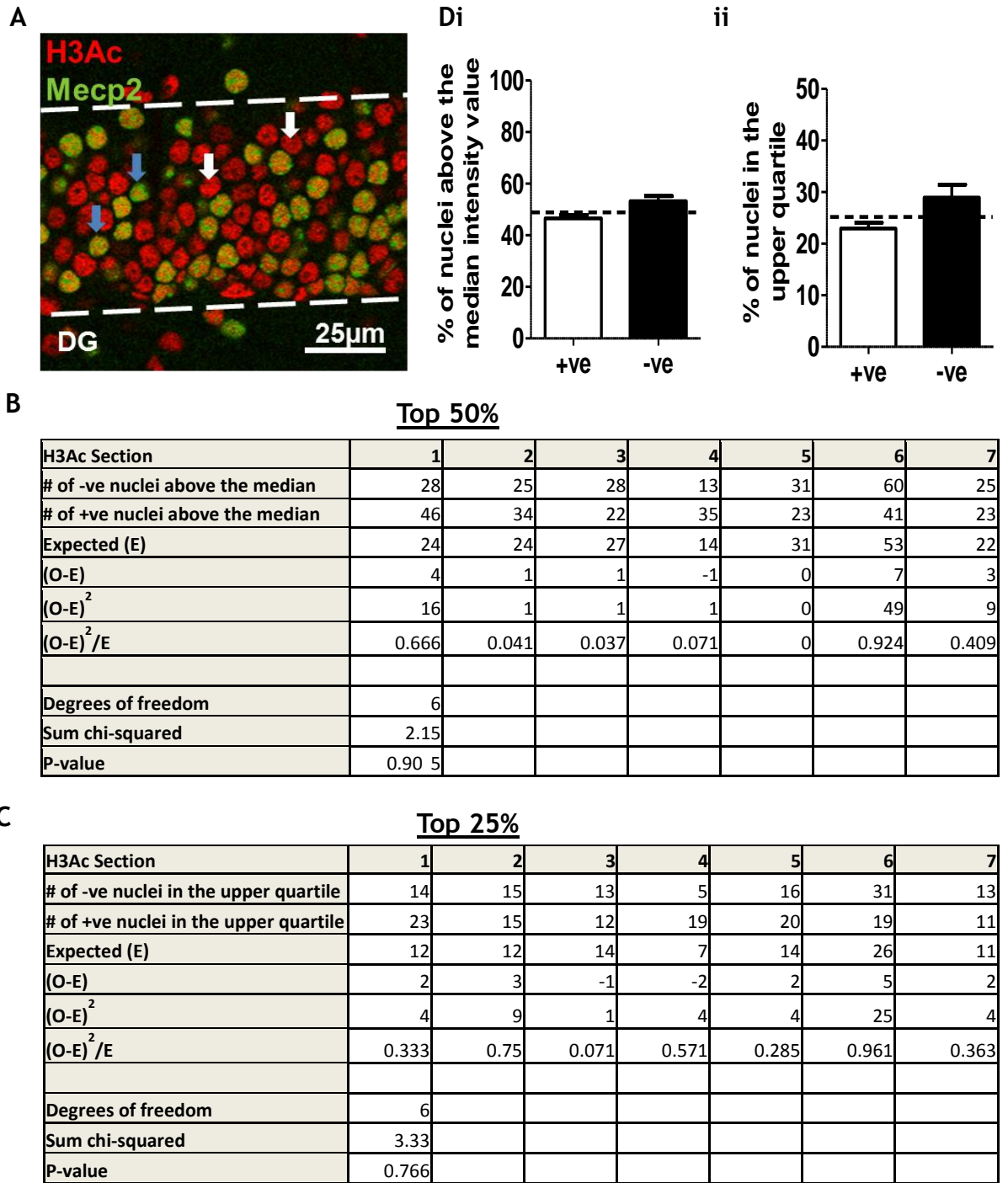


**Figure 5-2 Unaltered H3Ac levels in DG granule cell nuclei of the hippocampal formation between Mecp2 nuclei type under saline control conditions**

(A) Representative image of DG granule cell nuclei immunostained for H3Ac and Mecp2 status displayed through fluorescence of the EGFP fusion protein. White arrows highlight example nuclei which do not contain Mecp2 and blue arrows indicate those that do. (B-C) Tables showing the number of Mecp2 positive and negative nuclei above the overall median (B) and upper quartile (C) for H3Ac intensity values from sections used for chi-square analysis. Chi-square statistic is derived from the expected and observed number of Mecp2 negative nuclei present. The number of observed nuclei was not different to the expected number in both cases ( $p=0.905$  for (B) and  $p=0.766$  (C), chi-square test,  $n = 7$  sections from 3 mice). (Di-ii) Summary plots showing the percentage of each nuclei type above the median (Di) and in the upper quartile (Dii) H3Ac intensity values. Data expressed as mean  $\pm$  SEM in the bar graphs. Scale bar = 25 $\mu$ m; +ve = positive nuclei and -ve = negative nuclei.

To verify the distribution of H3Ac intensities the investigation was extended by conducting a similar analysis in hippocampal area CA1. In Figure 5-3, a representative micrograph of nuclei immunostained with H3Ac and Mecp2 status displayed through fluorescence of the EGFP fusion protein in the CA1 of the hippocampal formation is shown (Figure 5-3A). Quantification revealed there was no difference in the observed and expected number of Mecp2 negative nuclei above the median H3Ac intensity value (Figure 5-3B;  $p=0.92$ , chi-square test;  $n = 10$  sections from three mice). As this chi-square statistic was not significant, there was no difference in the percentage of Mecp2 positive nuclei ( $43.5 \pm 2.5\%$ ) above the median H3Ac intensity values compared to Mecp2 negative nuclei ( $53.7 \pm 1.8\%$ ; Figure 5-3Di). Any slight deviations in percentage were thus likely due to random chance.

Additionally there was no difference in the observed and expected number of Mecp2 negative nuclei in the upper quartile H3Ac intensity values although a small increase in the number of observed Mecp2 negative nuclei was seen in 7 out of 10 sections (Figure 5-3C;  $p=0.42$ , chi-square test). This would account for the percentage of nuclei in the upper quartile H3Ac intensity values in Mecp2 positive nuclei ( $19.8 \pm 2.1\%$ ) to be lower than Mecp2 negative nuclei ( $28.9 \pm 1.7\%$ ) however as the chi-square statistic was not significant and the difference in actual numbers was small, this trend was negligible (Figure 5-3Dii).

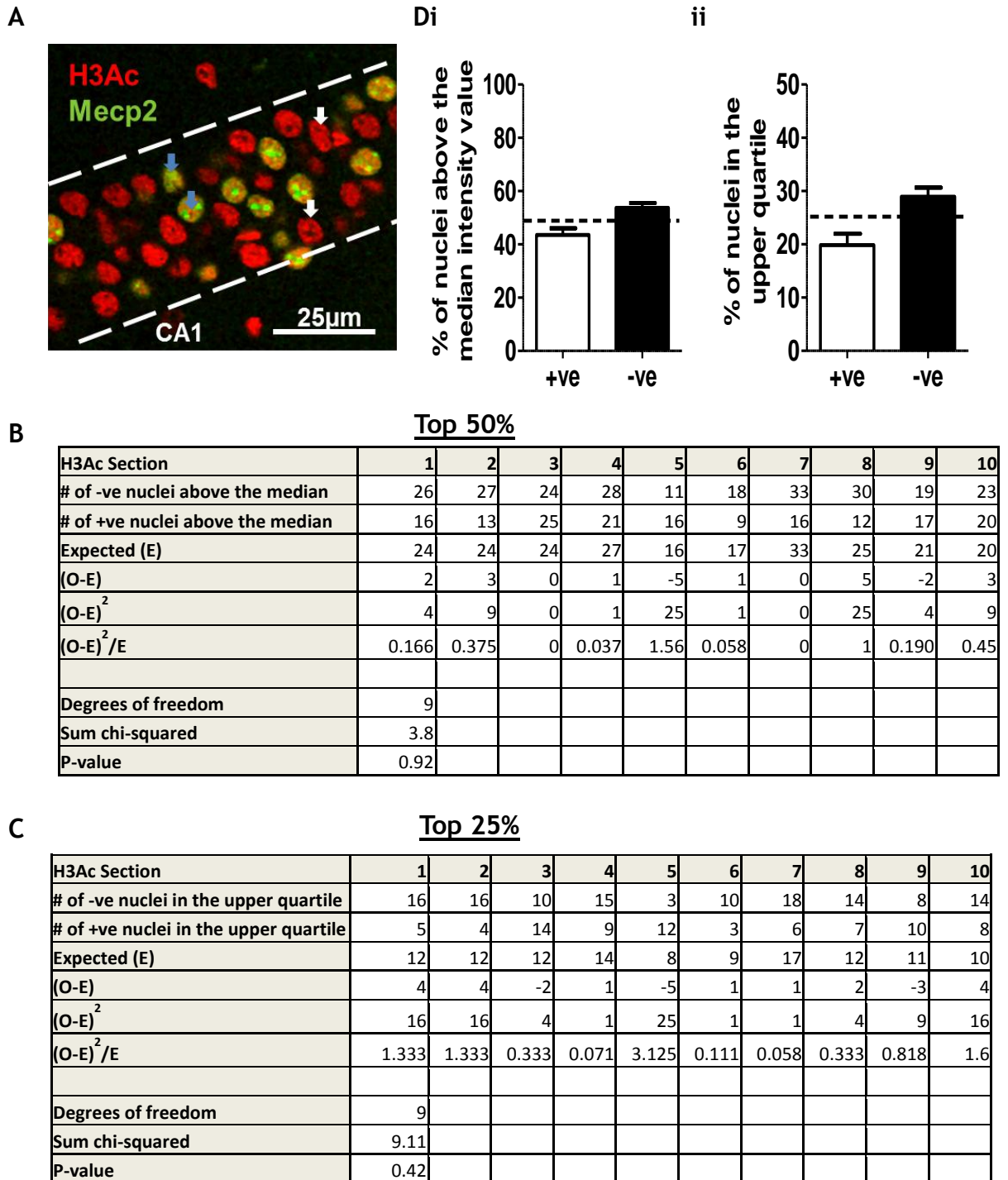


**Figure 5-3 Unaltered H3AC levels in CA1 pyramidal cell nuclei of the hippocampal formation between Mecp2 nuclei type under saline control conditions**

(A) Representative image of CA1 pyramidal cell nuclei immunostained for H3Ac and Mecp2 status displayed through fluorescence of the GFP fusion protein. White arrows highlight example nuclei which do not contain Mecp2 and blue arrows indicate those that do. (B-C) Tables showing the number of Mecp2 positive and negative nuclei above the overall median (B) and upper quartile (C) for H3Ac intensity values from sections used for chi-square analysis. Chi-square statistic is derived from the expected and observed number of Mecp2 negative nuclei present. The number of observed nuclei was not different to the expected number in both cases ( $p=0.92$  for (B) and  $p=0.42$  (C), chi-square test,  $n = 10$  sections from 3 mice). (Di-ii) Summary plots showing the percentage of each nuclei type above the median (Di) and in the upper quartile (Dii) H3Ac intensity values. Data expressed as mean  $\pm$  SEM in the bar graphs. Scale bar = 25 $\mu$ M; +ve = positive nuclei and -ve = negative nuclei.

In Chapter 4, I observed a 0.5 fold increase in H3Ac protein levels as revealed by western blot in the hippocampus of *Mecp2*<sup>-ly</sup> male mice compared to their WT littermates following three hours of neuronal activity. To determine the regulation of H3Ac under similar conditions using my refined method of quantification, I investigated whether there was a difference in the proportion of *Mecp2* positive and negative nuclei with H3Ac following the induction of neuronal activity by application of the convulsant drug kainic acid. A representative micrograph of the nuclei immunostained with H3Ac and *Mecp2* status displayed through fluorescence of the EGFP fusion protein in the DG of the hippocampal formation following induction of neuronal activity is shown in Figure 5-4A. Chi-square analysis revealed that there was no difference in the number of observed *Mecp2* negative nuclei above 50% (Figure 5-5B;  $p=0.99$ , chi-square test;  $n= 15$  sections from four mice) or 25% (Figure 5-4C;  $p=0.99$ , chi-square test) of the highest H3Ac intensities and expected numbers. Chi square tests thus confirmed that there was no significant difference in the percentage of *Mecp2* positive above the median ( $47.9 \pm 2.1\%$ ) and upper quartile ( $25.8 \pm 1.3\%$ ) H3Ac intensity values compared to *Mecp2* negative nuclei ( $51.1 \pm 1.3\%$  for above median;  $24.7 \pm 1.3\%$  for in the upper quartile).

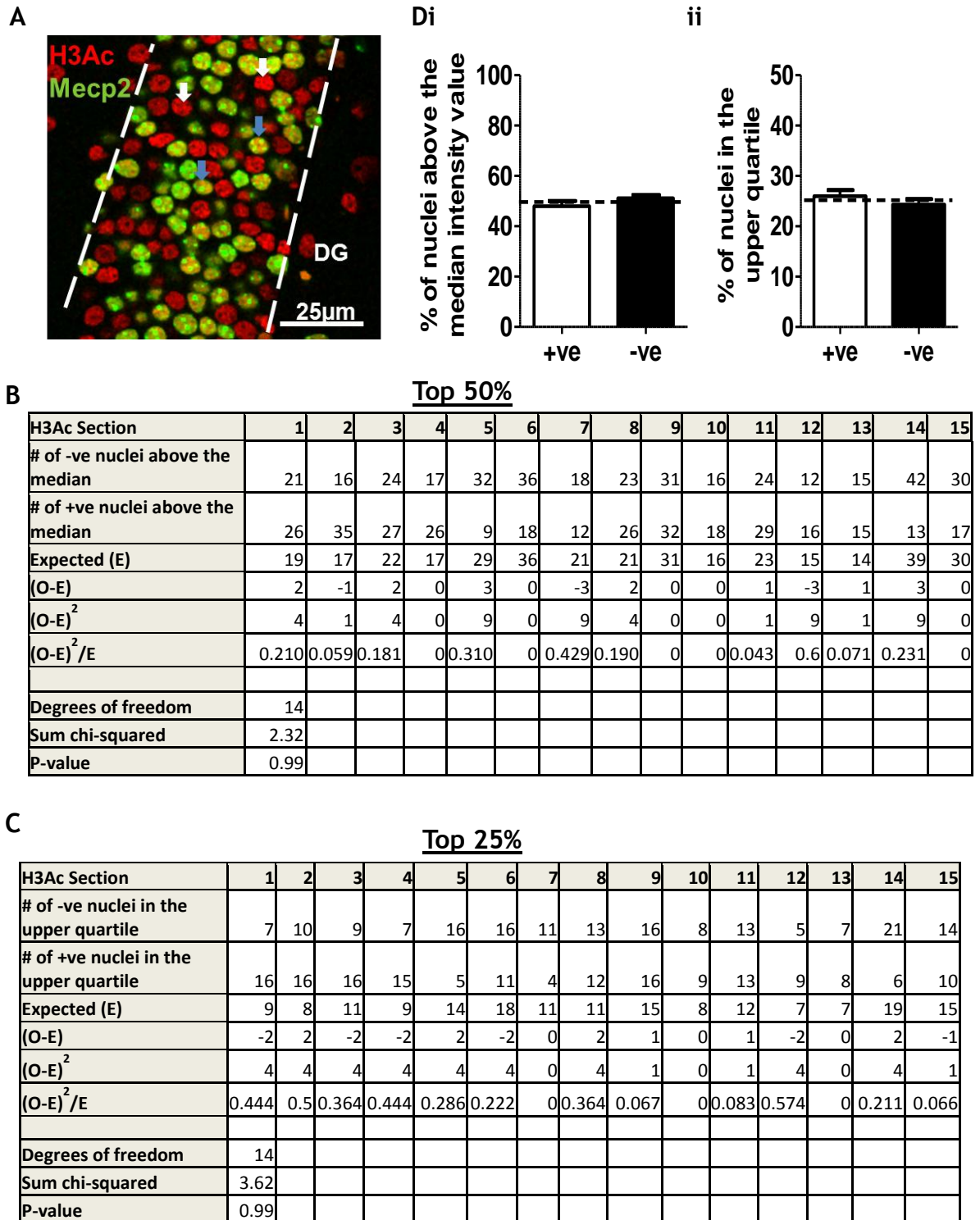


**Figure 5-4 Unaltered H3Ac levels in DG granule cell nuclei of the hippocampal formation between Mecp2 nuclei type after kainic acid application**

(A) Representative image of DG granule cell nuclei immunostained for H3Ac and Mecp2 status displayed through fluorescence of the EGFP fusion protein following neuronal activity. White arrows highlight example nuclei which do not contain Mecp2 and blue arrows indicate those that do. (B-C) Tables showing the number of Mecp2 positive and negative nuclei above the overall median (B) and upper quartile (C) for H3Ac intensity values from sections used for chi-square analysis. Chi-squared statistic is derived from the expected and observed number of Mecp2 negative nuclei present. The number of observed nuclei was not different to the expected number in both cases ( $p=0.99$  for (B) and (C), chi-square test,  $n=15$  sections from 4 mice). (Di-ii) Summary plots showing the percentage of each nuclei type above the median (Di) and in the upper quartile (Dii) H3Ac intensity values. Data expressed as mean  $\pm$  SEM in the bar graphs. Scale bar = 25 $\mu$ M; +ve = positive nuclei and -ve = negative nuclei.

Equally, there was no difference in the observed number of *Mecp2* negative nuclei above the median H3Ac intensity value and expected 50% of the total *MeCP2* negative nuclei number in the CA1 following neuronal activity induction (Figure 5-5B;  $p=0.98$ , chi-square test;  $n = 14$  sections from four mice). As this chi-square statistic was not significant there was no difference in the percentage of *Mecp2* positive nuclei ( $43 \pm 2.2\%$ ) above the median H3Ac intensity value compared to *Mecp2* negative nuclei ( $54.9 \pm 2.1\%$ ; Figure 5-5Di).

Finally, there was no difference in the observed number of *Mecp2* negative nuclei in the upper quartile H3Ac intensity values and the expected number of *Mecp2* negative nuclei following induction of neuronal activity (Figure 5-5C;  $p=0.85$ , chi-square test). Therefore the percentage of *Mecp2* positive nuclei ( $20.2 \pm 2.5\%$ ) compared to *Mecp2* negative nuclei ( $29.4 \pm 1.9\%$ ) nuclei in the upper quartile H3Ac intensity values was also due to random chance as the chi-square analysis was not significant (Figure 5-5Dii).

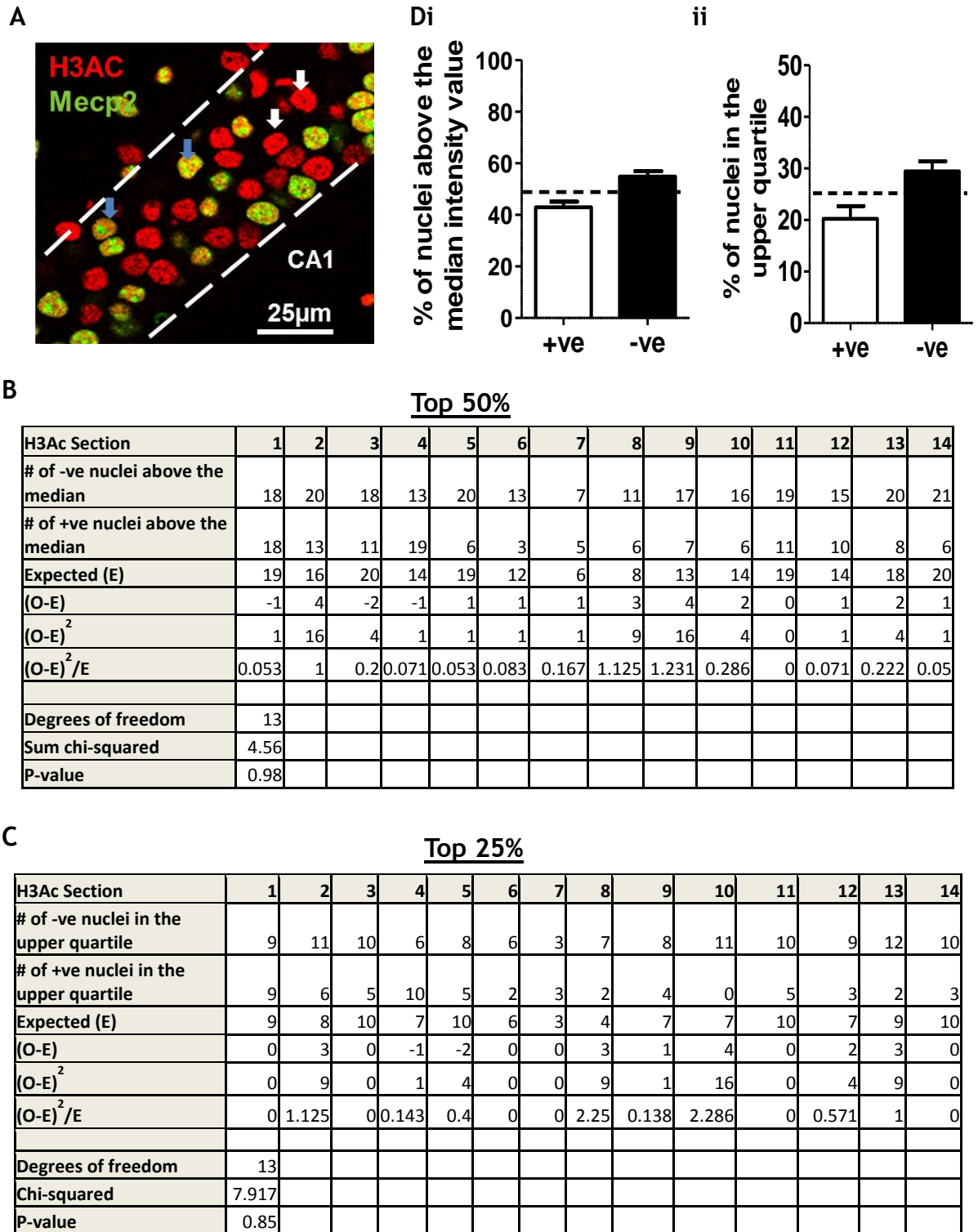


**Figure 5-5 Unaltered H3Ac levels in CA1 pyramidal cell nuclei of the hippocampal formation between Mecp2 nuclei type after kainic acid application**

(A) Representative image of CA1 pyramidal cell nuclei immunostained for H3Ac and Mecp2 status displayed through fluorescence of the GFP fusion protein following neuronal activity. White arrows highlight example nuclei which do not contain Mecp2 and blue arrows indicate those that do. (B-C) Tables showing the number of Mecp2 positive and negative nuclei above the overall median (B) and upper quartile (C) for H3Ac intensity values from sections used for chi-square analysis. Chi-square statistic is derived from the expected and observed number of Mecp2 negative nuclei present. The number of observed nuclei was not different to the expected number in both cases ( $p=0.98$  for (B) and  $p=0.85$  for (C), chi-square test,  $n=14$  sections from 4 mice). (Di-ii) Summary plots showing the percentage of each nuclei type above the median (Di) and in the upper quartile (Dii) H3Ac intensity values. Data expressed as mean  $\pm$  SEM in the bar graphs. Scale bar = 25 $\mu$ M; +ve = positive nuclei and -ve = negative nuclei.

### **5.4.3 Levels of total histone H3 was unaltered between Mecp2 containing and Mecp2-deficient nuclei in the hippocampal formation**

As a set of control experiments, I also examined levels of total Histone H3 protein to establish whether Mecp2 deficiency affects basal histone levels. I investigated the difference in the proportion of Mecp2 positive and negative nuclei with total histone H3 in the hippocampus under saline control conditions as well as following induction of neuronal activity using kainic acid as described previously. An example image of the nuclei immunostained with total histone H3 and Mecp2 status displayed through fluorescence of the EGFP fusion protein in the DG of the hippocampus under saline control conditions is shown in Figure 5-6A. Chi-square analysis revealed that there was no difference in the number of observed Mecp2 negative nuclei above 50% (Figure 5-6B;  $p=0.55$ , chi-square test;  $n= 8$  sections from 3 mice) or 25% (Figure 5-6C;  $p=0.64$ , chi-square test) of the highest histone H3 intensities and expected numbers. The lack of significance in these tests confirmed that there was no difference in the percentage of Mecp2 positive above the median ( $47.6 \pm 4.3\%$ ) and in the upper quartile ( $24.3 \pm 2.4\%$ ) H3Ac intensity values compared to Mecp2 negative nuclei ( $53.6 \pm 1.3\%$  for above median;  $26.8 \pm 2.6\%$  for in the upper quartile) as the results were due to random chance (Figure 5-6Di-Dii).

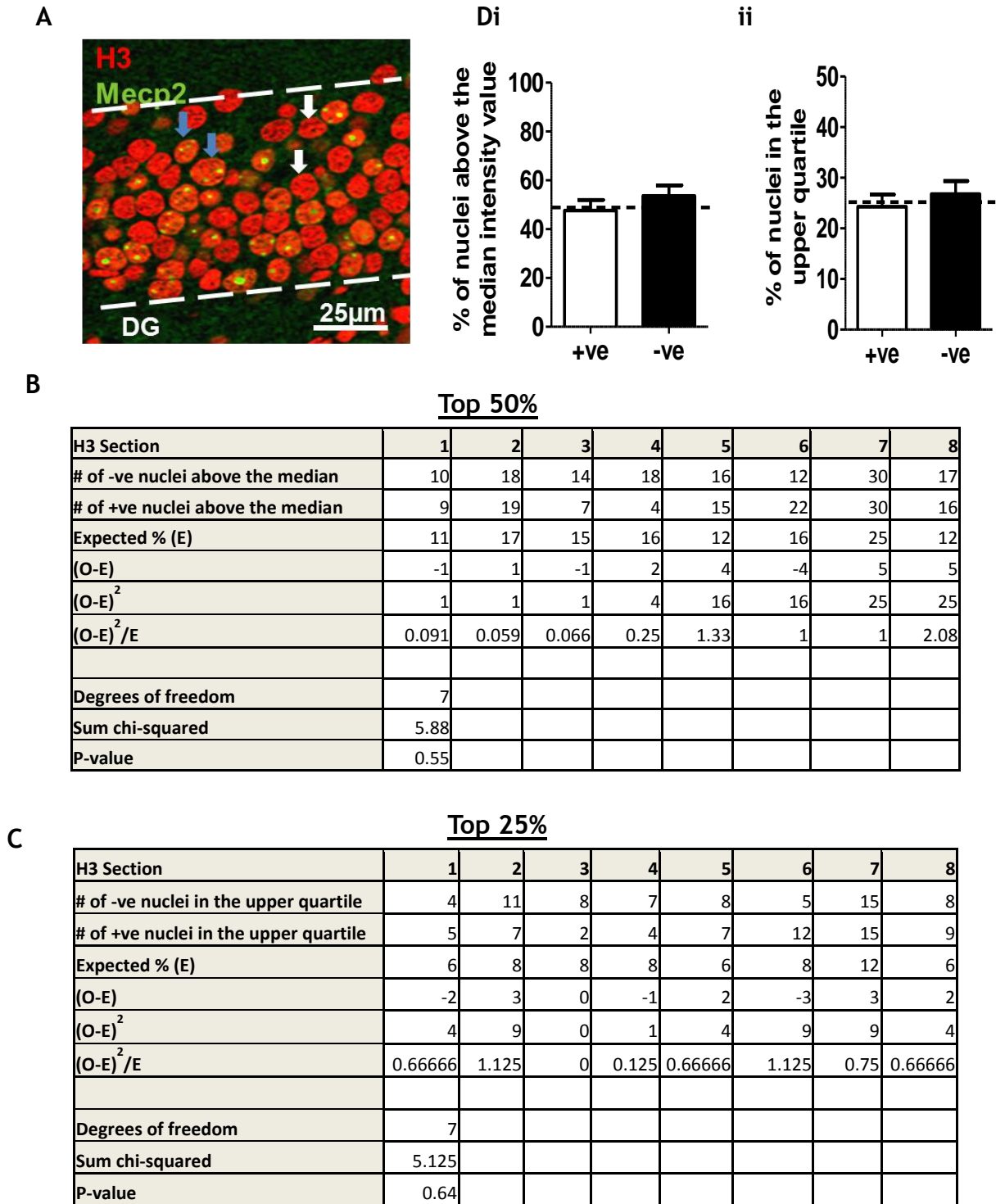


**Figure 5-6 Unaltered total histone H3 levels in DG granule cell nuclei of the hippocampal formation between Mecp2 nuclei type under saline control conditions**

(A) Representative image of DG granule cell nuclei immunostained for total histone H3 and Mecp2 status displayed through fluorescence of the EGFP fusion protein. White arrows highlight example nuclei which do not contain Mecp2 and blue arrows indicate those that do. (B-C) Tables showing the number of Mecp2 positive and negative nuclei above the overall median (B) and upper quartile (C) for total histone H3 intensity values from sections used for chi-square analysis. Chi-square statistic is derived from the expected and observed number of Mecp2 negative nuclei present. The number of observed nuclei was not different to the expected number in both cases ( $p=0.55$  for (B) and  $p=0.64$  (C), chi-square test,  $n = 8$  sections from 3 mice). (Di-ii) Summary plots showing the percentage of each nuclei type above the median (Di) and in the upper quartile (Dii) total histone H3 intensity values. Data expressed as mean  $\pm$  SEM in the bar graphs. Scale bar = 25 $\mu$ m; +ve = positive nuclei and -ve = negative nuclei.

To investigate basal levels of total histone H3 intensity further, I extended my analysis to hippocampal area CA1. Similarly there was no difference in the observed number of *Mecp2* negative nuclei above 50% of total histone H3 intensities and expected numbers in the CA1 under saline control conditions (Figure 5-7B;  $p=0.96$ , chi-square test;  $n=6$  sections from 3 mice). Additionally there was no variation in the number of observed *Mecp2* negative nuclei and expected numbers in the upper quartile (Figure 5-7C;  $p=0.97$ , chi-square test;  $n=6$  sections from 3 mice). Collectively there was no difference in percentage of *Mecp2* positive nuclei above the median ( $42.4 \pm 4.5\%$ ) and in the upper quartile ( $24.7 \pm 4.5\%$ ) total histone H3 intensity values compared to *Mecp2* negative nuclei ( $53.9 \pm 2.6\%$  for above the median;  $25.3 \pm 1.6\%$  for in the upper quartile) as no significance was observed in either chi-square (Figure 5-7Di-Dii).

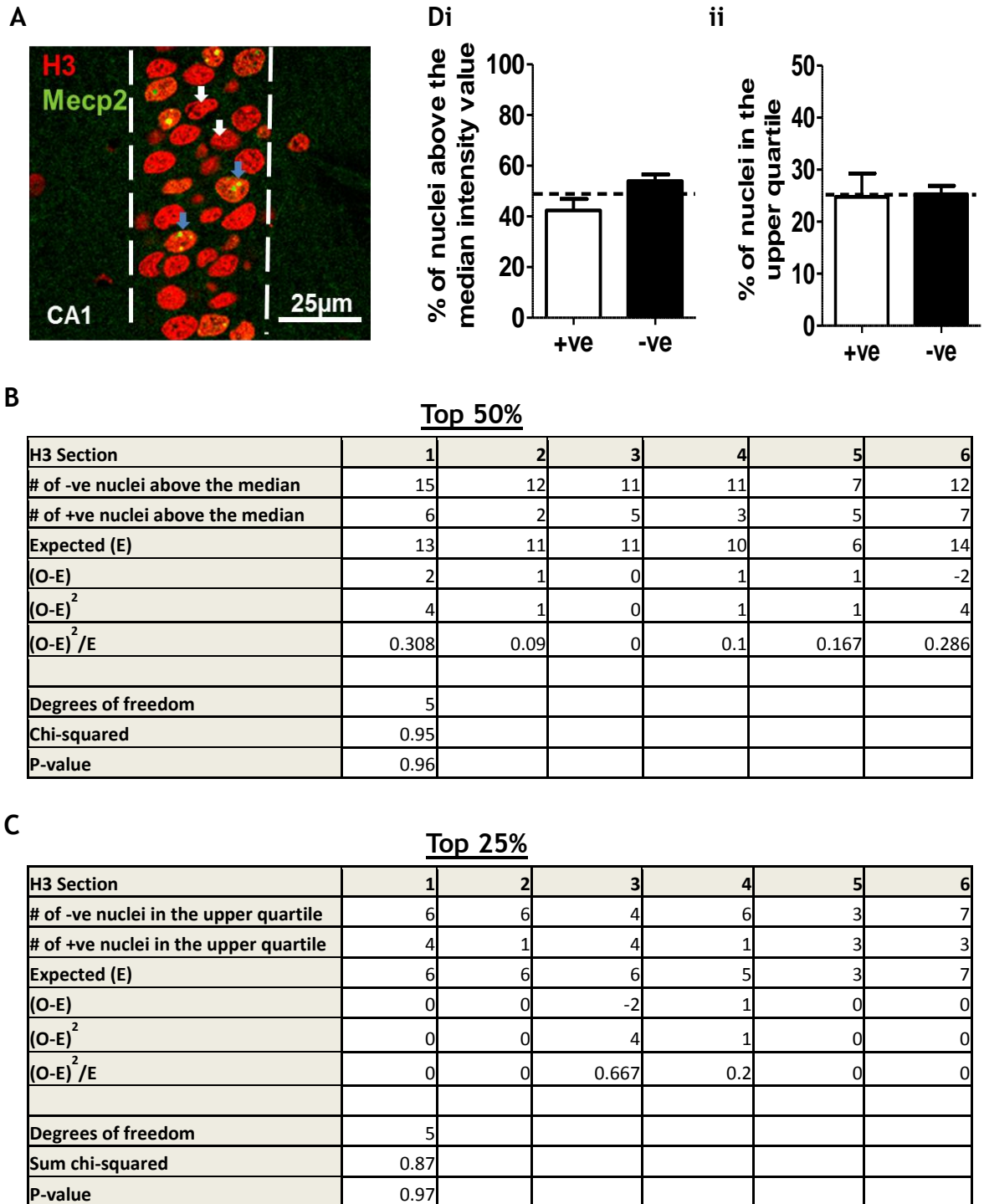


**Figure 5-7 Unaltered total histone H3 levels in CA1 pyramidal cell nuclei of the hippocampal formation between Mecp2 nuclei type under saline control conditions**

(A) Example micrograph of CA1 pyramidal cell nuclei immunostained for total histone H3 and Mecp2 status displayed through fluorescence of the EGFP fusion protein following neuronal activity. White arrows highlight example nuclei which do not contain Mecp2 and blue arrows indicate those that do. (B-C) Tables showing the number of Mecp2 positive and negative nuclei above the overall median (B) and upper quartile (C) for total histone H3 intensity values from sections used for chi-square analysis. Chi-square statistic is derived from the expected and observed number of Mecp2 negative nuclei present. The number of observed nuclei was not different to the expected number in both cases ( $p=0.96$  for (B) and  $p=0.97$  (C), chi-square test,  $n = 6$  sections from 3 mice). (Di-ii) Summary plots showing the percentage of each nuclei type above the median (Di) and in the upper quartile (Dii) total histone H3 intensity values. Data expressed as mean  $\pm$  SEM in the bar graphs. Scale bar = 25 $\mu$ m; +ve = positive nuclei and -ve = negative nuclei.

Following induction of neuronal activity by kainic acid, the immunostaining of total histone H3 and Mecp2 status displayed through fluorescence of the EGFP fusion protein in the cell body layer of the DG can be observed in Figure 5-8A. As before, no difference in the number of observed Mecp2 negative nuclei and expected nuclei above the median total histone H3 intensity was seen (Figure 5-8B;  $p=0.99$ , chi-square test;  $n= 15$  sections from 4 mice) after neuronal activity. Therefore, there was no difference in percentage of Mecp2 negative nuclei ( $45.4 \pm 1.4\%$ ) above the median total histone H3 intensity value compared to Mecp2 positive nuclei ( $53.5 \pm 2\%$ ) and was down to random chance as the chi-square value was not significant (Figure 5-8Di).

Furthermore, there was no difference observed in the number of Mecp2 negative nuclei and expected number in the upper quartile even though a few differ in their number by 4-5 nuclei (Figure 5-8C;  $p=0.76$ , chi-square test). Consequently there was no difference in the percentage of Mecp2 negative nuclei ( $21.4 \pm 2.1\%$ ) in the upper quartile compared to the percentage of Mecp2 positive nuclei ( $30 \pm 2.3\%$ ) as the chi-square was not significant (Figure 5-8Dii).

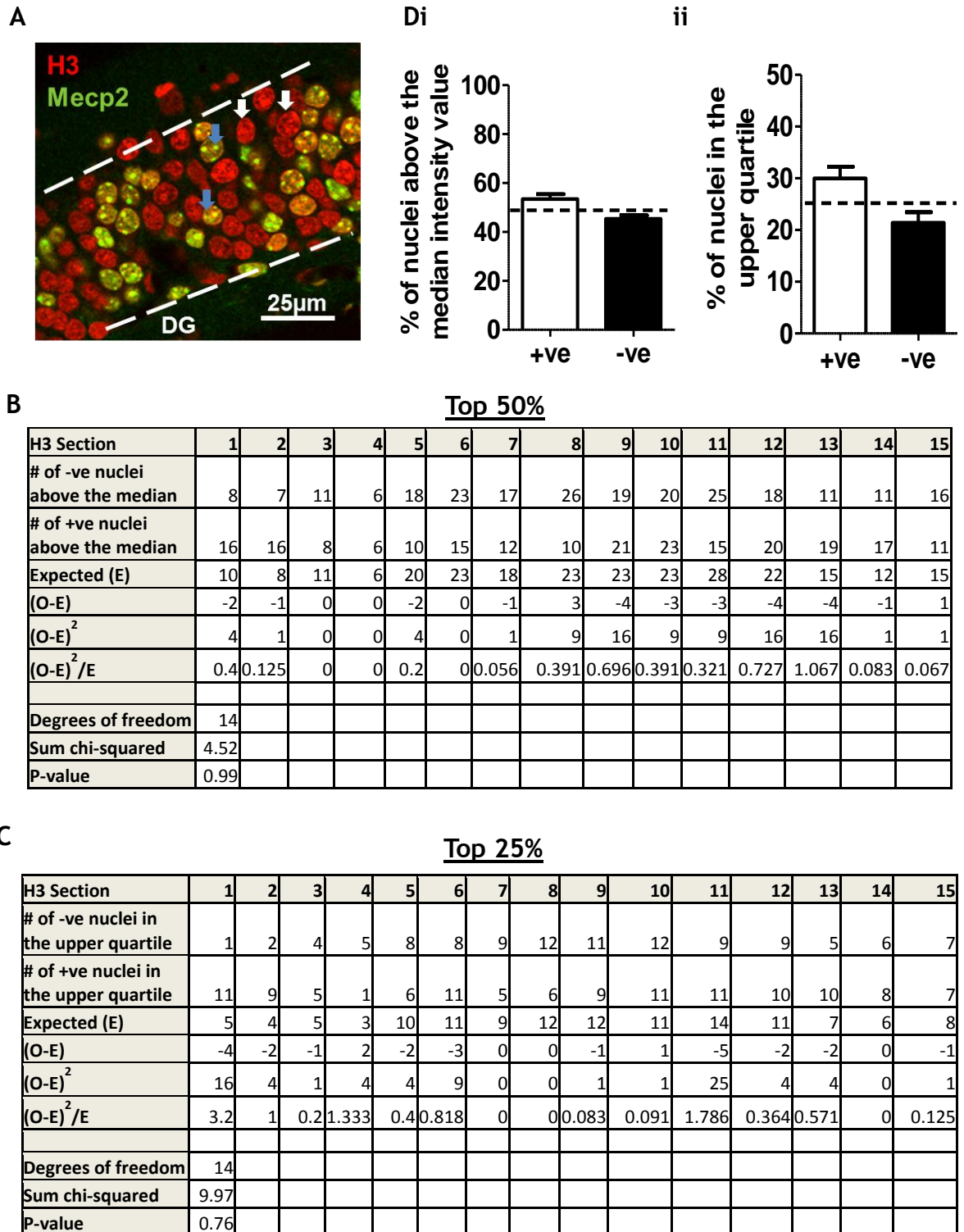


**Figure 5-8 Unaltered total histone H3 levels in DG granule cell nuclei of the hippocampal formation between Mecp2 nuclei type after kainic acid administration**

(A) Example micrograph of DG granule cell nuclei immunostained for total histone H3 and Mecp2 status displayed through fluorescence of the EGFP fusion protein following neuronal activity. White arrows highlight example nuclei which do not contain Mecp2 and blue arrows indicate those that do. (B-C) Tables showing the number of Mecp2 positive and negative nuclei above the overall median (B) and upper quartile (C) for total histone H3 intensity values from sections used for chi-square analysis. Chi-square statistic is derived from the expected and observed number of Mecp2 negative nuclei present. The number of observed nuclei was not different to the expected number in both cases ( $p=0.99$  for (B) and  $p=0.76$  (C), chi-square test,  $n=15$  sections from 4 mice). (Di-ii) Summary plots showing the percentage of each nuclei type above the median (Di) and in the upper quartile (Dii) total histone H3 intensity values. Data expressed as mean  $\pm$  SEM in the bar graphs. Scale bar = 25 $\mu$ M; +ve = positive nuclei and -ve = negative nuclei.

Finally, the immunostaining of total histone H3 and Mecp2 status displayed through fluorescence of the EGFP fusion protein in the cell body layer of the CA1 following initiation of neuronal activity can be seen in Figure 5-9A. There was no difference detected in the number of observed Mecp2 negative nuclei and expected nuclei above the median total histone H3 intensity (Figure 5-9B;  $p=0.99$ , chi-square test;  $n= 12$  sections from 4 mice) after neuronal activity. As a consequence, the percentage of Mecp2 negative nuclei ( $48.5 \pm 1.3\%$ ) above the median total histone H3 intensity value compared to Mecp2 positive nuclei ( $50.2 \pm 1.9\%$ ) was down to random chance as the chi-square value was not significant (Figure 5-9Di). Moreover, there was no significant difference observed in Mecp2 negative nuclei and expected nuclei in the upper quartile (Figure 5-9C;  $p=0.99$ , chi-square test). This confirmed that the overall percentage difference in Mecp2 negative nuclei in the upper quartile ( $24 \pm 1.1$ ) compared to Mecp2 positive nuclei ( $26.3 \pm 1.8\%$ ) was due to random chance (Figure 5-9Dii).

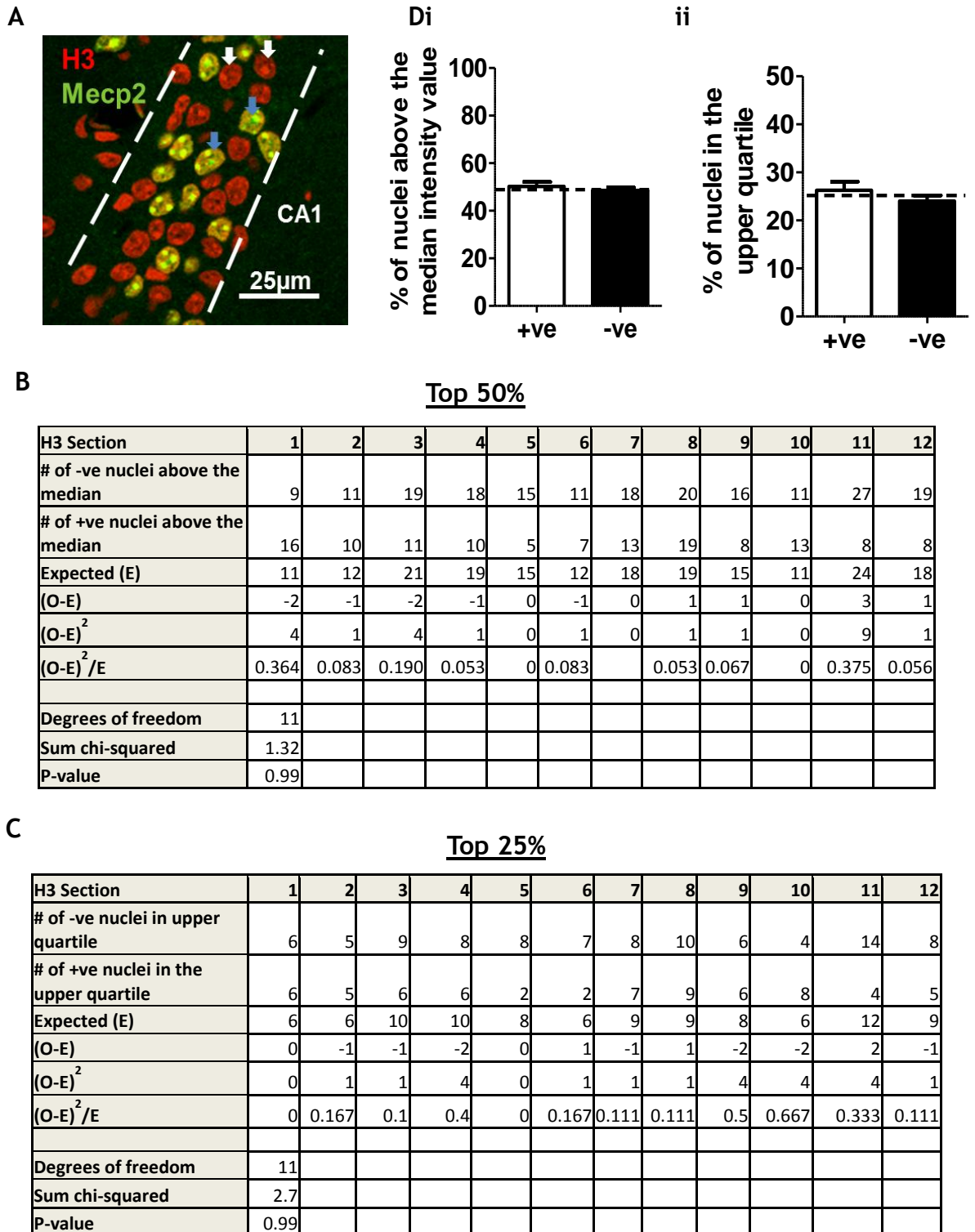


**Figure 5-9 Unaltered total histone H3 levels in CA1 pyramidal cell nuclei of the hippocampal formation between Mecp2 nuclei type after kainic acid application**

(A) Example micrograph of CA1 pyramidal cell nuclei immunostained for total histone H3 and Mecp2 status displayed through fluorescence of the EGFP fusion protein following neuronal activity. White arrows highlight example nuclei which do not contain Mecp2 and blue arrows indicate those that do. (B-C) Tables showing the number of Mecp2 positive and negative nuclei above the overall median (B) and upper quartile (C) for total histone H3 intensity values from sections used for chi-square analysis. Chi-square statistic is derived from the expected and observed number of Mecp2 negative nuclei present. The number of observed nuclei was not different to the expected number in both cases ( $p=0.99$  for (B) and (C), chi-square test,  $n = 12$  sections from 4 mice). (Di-ii) Summary plots showing the percentage of each nuclei type above the median (Di) and in the upper quartile (Dii) total histone H3 intensity values. Data expressed as mean  $\pm$  SEM in the bar graphs. Scale bar = 25 $\mu$ M; +ve = positive nuclei and -ve = negative nuclei.

#### 5.4.4 Levels of histone H4 acetylation was unaltered between Mecp2 containing and Mecp2-deficient nuclei in the hippocampal formation

In Chapter 4, I found the levels of histone H4 acetylation (H4Ac) to be unaltered between Mecp2-deficient mice and their wild-type littermates in the hippocampus under control conditions. To study potential modifications in H4Ac occurring at the single cell level, my quantitative immunofluorescence approach was again used to determine if there were differences in the proportion of H4Ac in Mecp2 positive and negative nuclei after saline (control). An example micrograph showing immunostained H4Ac and Mecp2 status displayed through fluorescence of the EGFP fusion protein in DG granule nuclei of the hippocampal formation under saline control conditions is shown in Figure 5-10A. Although there was no significant change in the observed and expected number of Mecp2 negative nuclei above the median H4Ac intensity, (Figure 5-10B;  $p=0.21$ , chi-square test,  $n=9$  sections from three mice) there appeared to be a trend towards less observed Mecp2 negative nuclei as some sections had up to 10 fewer nuclei. This lower chi-square statistic gave more confidence in the trend that there was a decrease in the percentage of Mecp2 negative nuclei ( $41.8 \pm 3.1\%$ ) compared to Mecp2 positive nuclei ( $55 \pm 2.5\%$ ) however the effect could still be due to random chance as significance was not achieved (Figure 5-10Di).

Correspondingly, there was no significant difference in the number of observed and expected negative Mecp2 nuclei in the upper quartile (Figure 5-10C,  $p=0.32$ , chi-square test) although a trend was present towards a decrease in observed nuclei. This gave a margin of confidence in the trend towards a decline in the percentage of Mecp2 negative nuclei ( $21.4 \pm 2.5\%$ ) in the upper quartile H4Ac intensity compared to Mecp2 positive nuclei ( $26.9 \pm 2.1\%$ ) but the effect could still be due to random chance as the chi-square statistic was not significant (Figure 5-10Dii).

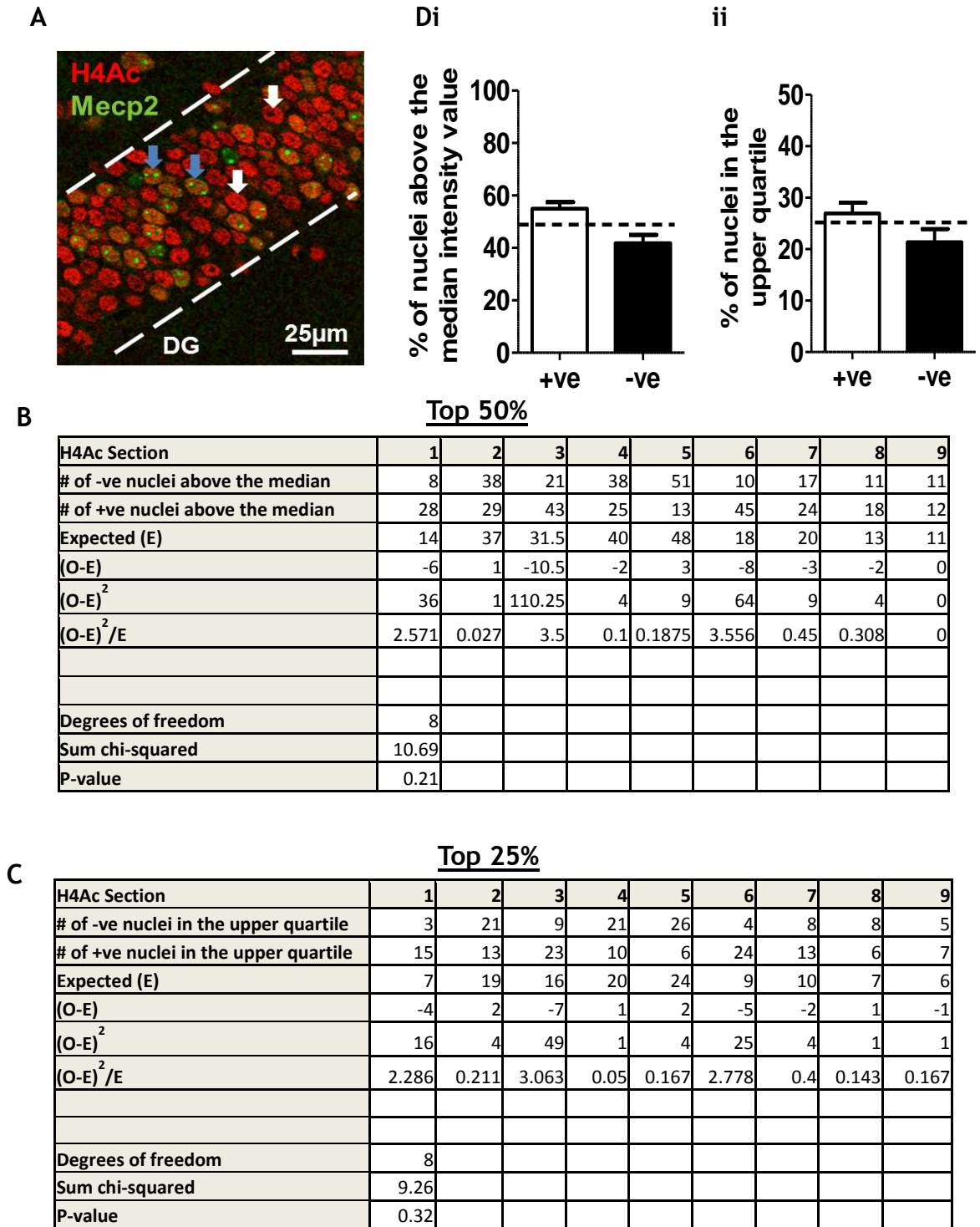
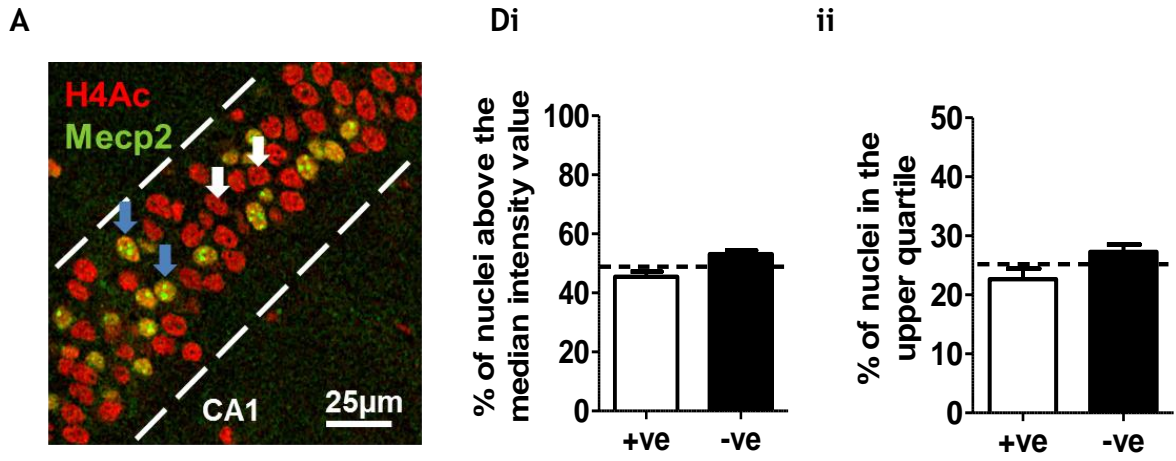


**Figure 5-10 Unaltered H4Ac levels in DG granule cell nuclei of the hippocampal formation between Mecp2 nuclei type under saline control conditions**

(A) Example micrograph of DG granule cell immunostained for H4Ac and Mecp2 status displayed through fluorescence of the EGFP fusion protein. White arrows highlight example nuclei which do not contain Mecp2 and blue arrows indicate those that do. (B-C) Tables showing the number of Mecp2 positive and negative nuclei above the overall median (B) and upper quartile (C) for H4Ac intensity values from sections used for chi-square analysis. Chi-square statistic is derived from the expected and observed number of Mecp2 negative nuclei present. The number of observed nuclei was not different to the expected number in both cases ( $p=0.21$  for (B) and  $p=0.32$  for (C), chi-square test,  $n = 9$  sections from 3 mice). (Di-ii) Summary plots showing the percentage of each nuclei type above the median (Di) and in the upper quartile (Dii) H4Ac intensity values. Data expressed as mean  $\pm$  SEM in the bar graphs. Scale bar = 25 $\mu$ m; +ve = positive nuclei and -ve = negative nuclei.

To verify the distribution of H4Ac intensities, analysis of the CA1 in the hippocampal formation was also investigated. In contrast to the above results, no trend was present in Mecp2 positive nuclei immunostained with H4Ac in the CA1 of the hippocampus (Figure 5-11A) as there was no significant change and values were similar in the observed and expected Mecp2 negative nuclei above the median (Figure 5-11B;  $p=0.99$ , chi-square test,  $n=10$  sections from three mice) and in the upper quartile (Figure 5-11C;  $p=0.93$ , chi-square test) H4Ac intensities. The percentage of positive nuclei above the median ( $45.4 \pm 1.8\%$ ) and in the upper quartile ( $22.7 \pm 1.8\%$ ) H3Ac intensity values compared to the percentage of Mecp2 negative nuclei ( $53.1 \pm 1.2\%$  above the median;  $27.3 \pm 1.2\%$  in the upper quartile) was not different as no significance was achieved in the chi-squares (Figure 5-11Di-Dii).



**B**

Top 50%

H4Ac Section	1	2	3	4	5	6	7	8	9	10
# of -ve nuclei above the median	33	20	22	35	29	18	22	20	22	23
# of +ve nuclei above the median	16	9	8	10	18	17	16	16	14	13
Expected (E)	32	19	23	32	26	18	19	19	23	20
(O-E)	1	1	-1	3	3	0	3	1	-1	3
(O-E) <sup>2</sup>	1	1	1	9	9	0	9	1	1	9
(O-E) <sup>2</sup> /E	0.031	0.0526	0.043	0.281	0.346	0	0.47	0.053	0.043	0.45
Degrees of freedom	9									
Sum chi-squared	1.77									
P-value	0.99									

**C**

Top 25%

H4Ac Section	1	2	3	4	5	6	7	8	9	10
# of -ve nuclei in the upper quartile	16	10	11	20	13	12	12	9	10	11
# of +ve nuclei in the upper quartile	8	5	4	3	11	6	7	9	8	7
Expected (E)	16	9	11	16	13	9	9	9	12	10
(O-E)	0	1	0	4	0	3	3	0	-2	1
(O-E) <sup>2</sup>	0	1	0	16	0	9	9	0	4	1
(O-E) <sup>2</sup> /E	0	0.111	0	1	0	1	1	0	0.333	0.1
Degrees of freedom	9									
Sum chi-squared	3.54									
P-value	0.93									

**Figure 5-11 Unaltered H4AC levels in CA1 pyramidal cell nuclei of the hippocampal formation between Mecp2 nuclei type under saline control conditions**

(A) Example micrograph of CA1 pyramidal cell nuclei immunostained for H4Ac and Mecp2 status displayed through fluorescence of the EGFP fusion protein. White arrows highlight example nuclei which do not contain Mecp2 and blue arrows indicate those that do. (B-C) Tables showing the number of Mecp2 positive and negative nuclei above the overall median (B) and upper quartile (C) for H4Ac intensity values from sections used for chi-square analysis. Chi-square statistic is derived from the expected and observed number of Mecp2 negative nuclei present. The number of observed nuclei was not different to the expected number in both cases ( $p=0.99$  for (B) and  $p=0.99$  for (C), chi-square test,  $n = 10$  sections from 3 mice). (Di-ii) Summary plots showing the percentage of each nuclei type above the median (Di) and in the upper quartile (Dii) H4Ac intensity values. Data expressed as mean  $\pm$  SEM in the bar graphs. Scale bar = 25 $\mu$ M; +ve = positive nuclei and -ve = negative nuclei.

Previously, no difference was observed in H4Ac protein levels between *Mecp2*-deficient mice and their WT littermates following induction of neuronal activity through kainic acid application (Chapter 4). Quantification using my immunostaining approach was thus used to study the level of H4Ac immunoreactivity in the *Mecp2* mosaic brain. A representative micrograph of the immunostaining in the DG following neuronal activity induction can be observed in Figure 5-12A. No difference is evident in the number of observed and expected nuclei above the median H3Ac intensity (Figure 5-12B;  $p=0.99$ , chi-square test;  $n=15$  sections from four mice). As this statistic was not significant, there was no difference in the percentage of *Mecp2* positive and negative ( $49.1 \pm 0.9\%$ ) nuclei above the median (Figure 5-12Di).

Similarly, no significant alterations were shown in the observed and expected number of *Mecp2* negative nuclei in the upper quartile for H4Ac intensities (Figure 5-12C;  $p=0.98$ , chi-square test) thus the percentage difference in *Mecp2* positive nuclei ( $26.1 \pm 1.2\%$ ) compared to the *Mecp2* negative nuclei ( $23.7 \pm 1.1\%$ ) was also due to random chance (Figure 5-12Dii).

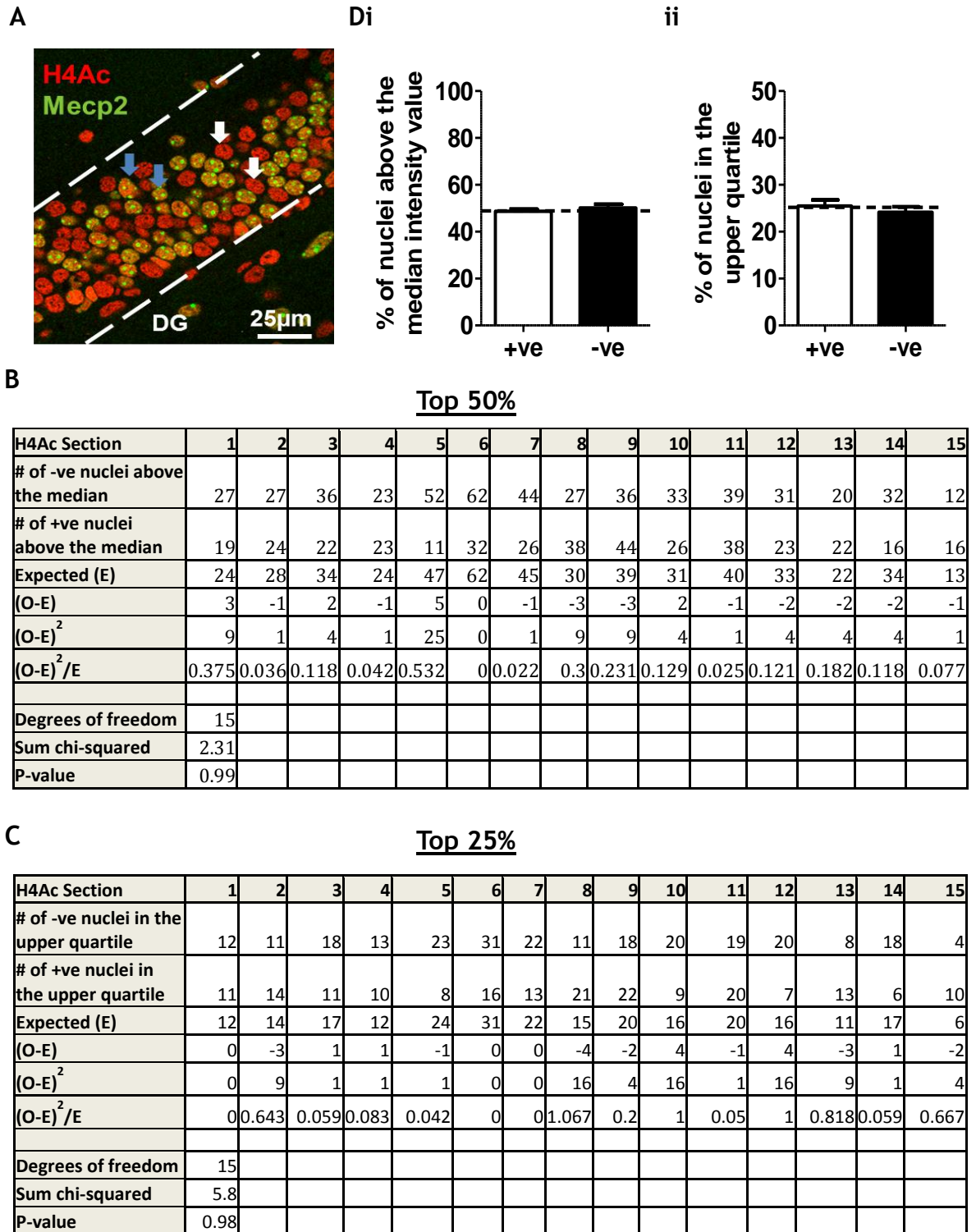


**Figure 5-12 Unaltered H4Ac levels in DG granule cell nuclei of the hippocampal formation between Mecp2 nuclei type after kainic acid application**

(A) Representative micrograph of DG granule cell nuclei immunostained for H4Ac and Mecp2 status displayed through fluorescence of the EGFP fusion protein following neuronal activity. White arrows highlight example nuclei which do not contain Mecp2 and blue arrows indicate those that do. (B-C) Tables showing the number of Mecp2 positive and negative nuclei above the overall median (B) and upper quartile (C) for H4Ac intensity values from sections used for chi-square analysis. Chi-square statistic is derived from the expected and observed number of Mecp2 negative nuclei present. The number of observed nuclei was not different to the expected number in both cases ( $p=0.99$  for (B) and  $p=0.98$  for (C), chi-square test,  $n = 15$  sections from 4 mice). (Di-ii) Summary plots showing the percentage of each nuclei type above the median (Di) and in the upper quartile (Dii) H4Ac intensity values. Data expressed as mean  $\pm$  SEM in the bar graphs. Scale bar = 25 $\mu$ M; +ve = positive nuclei and -ve = negative nuclei.

Finally an immunostained micrograph of H4Ac in the CA1 of the hippocampus can be seen in Figure 5-13A. As above no difference is evident in the expected and observed *Mecp2* negative nuclei number above the median (Figure 5-13B;  $p=0.99$ , chi-square test;  $n=15$  sections from four mice) and upper quartile (Figure 5-13C,  $p=0.97$ , chi-square test) H4Ac intensity values. Considering no significance is achieved in either chi-square test, there was no difference between *Mecp2* positive nuclei above the median ( $47.5 \pm 1.9\%$ ) and in the upper quartile ( $21.8 \pm 1.6\%$ ) H3Ac intensity values compared to *Mecp2* negative nuclei ( $51.8 \pm 1.4\%$  for above the median;  $28.6 \pm 1.55$  in the upper quartile).

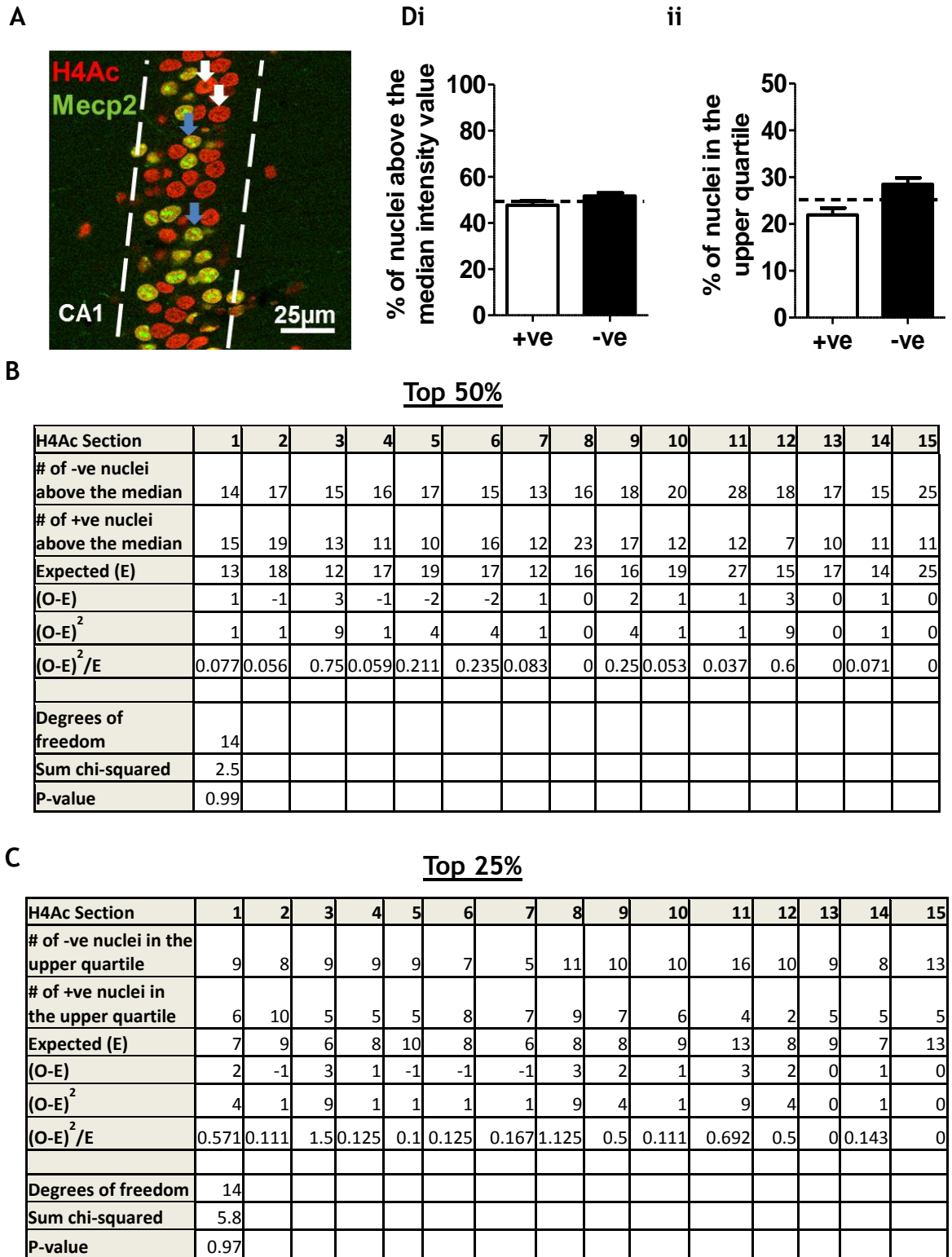


**Figure 5-13 Unaltered H4AC levels in CA1 pyramidal cell nuclei of the hippocampal formation between Mecp2 nuclei type after kainic acid application**

(A) Representative micrograph of CA1 pyramidal cell nuclei immunostained for H4Ac and Mecp2 status displayed through fluorescence of the EGFP fusion protein following neuronal activity. White arrows highlight example nuclei which do not contain Mecp2 and blue arrows indicate those that do. (B-C) Tables showing the number of Mecp2 positive and negative nuclei above the overall median (B) and upper quartile (C) for H4Ac intensity values from sections used for chi-square analysis. Chi-square statistic is derived from the expected and observed number of Mecp2 negative nuclei present. The number of observed nuclei was not different to the expected number in both cases ( $p=0.99$  for (B) and  $p=0.97$  for (C), chi-square test,  $n = 15$  sections from 4 mice). (Di-ii) Summary plots showing the percentage of each nuclei type above the median (Di) and in the upper quartile (Dii) H4Ac intensity values. Data expressed as mean  $\pm$  SEM in the bar graphs. Scale bar = 25 $\mu$ M; +ve = positive nuclei and -ve = negative nuclei.

#### **5.4.5 Levels of total histone H4 was unaltered between Mecp2 containing and Mecp2-deficient nuclei in the hippocampal formation**

I also included control experiments to rule out potential changes as a consequence of cellular Mecp2 deficiency. The differences in the proportion of total histone H4 between Mecp2 positive and negative nuclei in the hippocampus were investigated under saline control conditions and after the induction of neuronal activity by kainic acid. Figure 5-14A shows the staining of total histone H4 and Mecp2 status displayed through fluorescence of the EGFP fusion protein in the DG of saline control mice. No difference in the number of observed and expected Mecp2 negative nuclei above the median total histone H4 intensity value was seen (Figure 5-14B;  $p=0.56$ , chi-square test;  $n=9$  sections from 3 mice). As a result there was no difference in the percentage of Mecp2 positive nuclei ( $54 \pm 1.9\%$ ) above the median total histone H4 intensity value compared to Mecp2 negative nuclei ( $42.9 \pm 2.5\%$ ) and was due to random chance (Figure 5-14Di).

Conversely, there was a trend towards a decrease in the number of observed Mecp2 negative nuclei in the DG in the upper quartile intensity values for total histone H4 as shown in nearly half of sections and the chi-squared being close to significance (Figure 5-14C;  $p=0.18$ , chi-square test). Therefore more confidence can be given in the decrease in the percentage of Mecp2 negative nuclei ( $19.6 \pm 2.5\%$ ) in the top 25% of total histone H4 intensity values compared to the percentage of Mecp2 positive nuclei ( $29.1 \pm 1.9\%$ ). Nonetheless as the overall chi-square statistic was not significant the result could still be due random variation (Figure 5-14Dii).

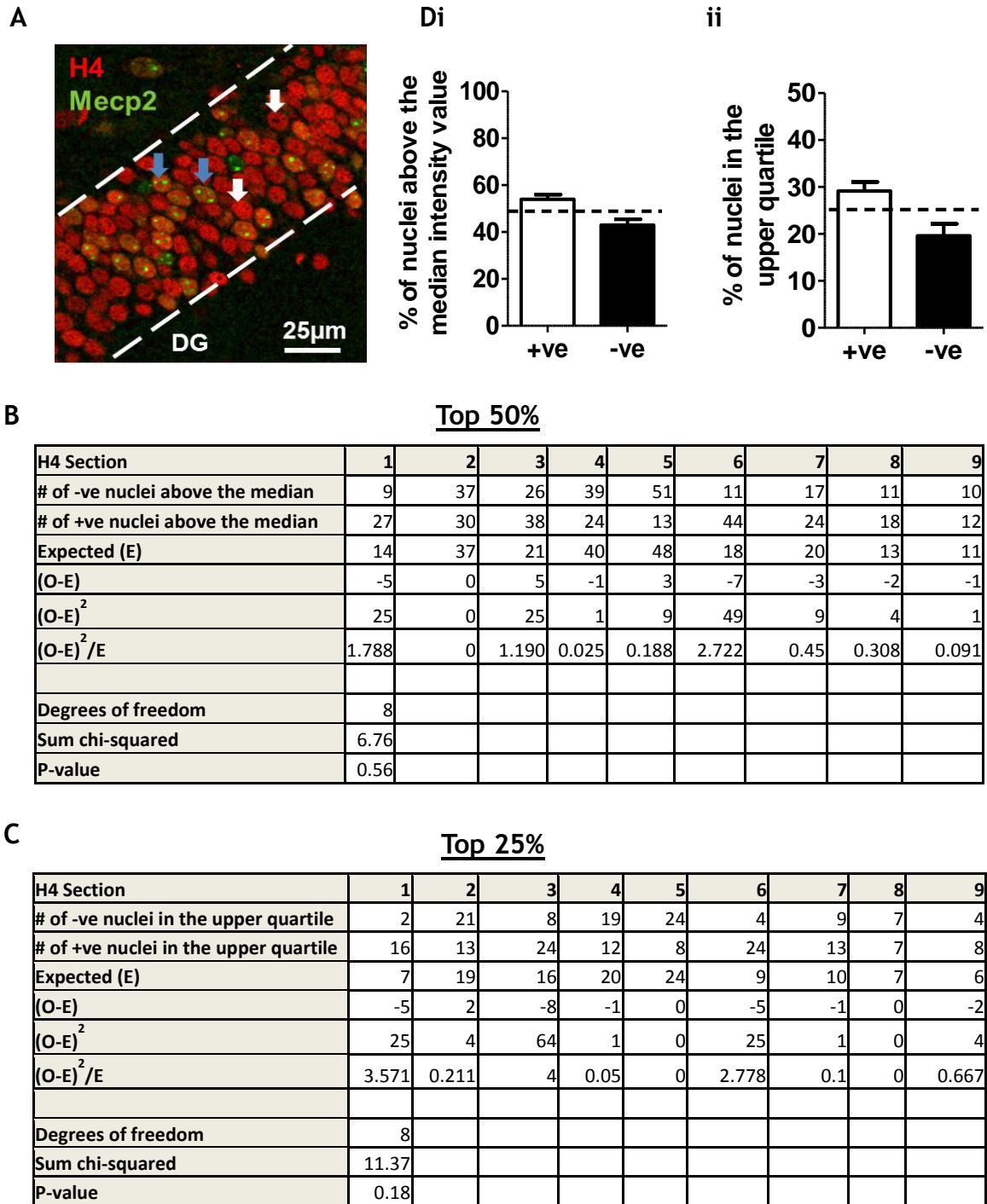


**Figure 5-14 Unaltered total histone H4 levels in DG granule cell nuclei of the hippocampal formation between Mecp2 nuclei type under saline control conditions**

(A) Example micrograph of DG granule cell nuclei immunostained for total histone H4 and Mecp2 status displayed through fluorescence of the EGFP fusion protein. White arrows highlight example nuclei which do not contain Mecp2 and blue arrows indicate those that do. (B-C) Tables showing the number of Mecp2 positive and negative nuclei above the overall median (B) and upper quartile (C) for total histone H4 intensity values from sections used for chi-square analysis. Chi-square statistic is derived from the expected and observed number of Mecp2 negative nuclei present. The number of observed nuclei was not different to the expected number in both cases ( $p=0.56$  for (B) and  $p=0.18$  for (C), chi-square test,  $n = 9$  sections from 3 mice). (Di-ii) Summary plots showing the percentage of each nuclei type above the median (Di) and in the upper quartile (Dii) total histone H4 intensity values. Data expressed as mean  $\pm$  SEM in the bar graphs. Scale bar = 25 $\mu$ M; +ve = positive nuclei and -ve = negative nuclei.

The micrograph showing total histone H4 and Mecp2 status displayed through fluorescence of the EGFP fusion protein in the CA1 region of the hippocampus is shown in Figure 5-15A. No difference was determined in observed and expected Mecp2 negative nuclei either above the median (Figure 5-15B;  $p=0.99$ , chi-square test,  $n=10$  sections from three mice) or upper quartile (Figure 5-15C,  $p=0.98$ , chi-square test) total histone H4 intensity values. As no significance was observed in these chi-square values, the percentage change in Mecp2 positive nuclei above the median ( $46.9 \pm 1.6\%$ ) and in the upper quartile ( $27.6 \pm 2.6\%$ ) total histone H4 intensity values compared to Mecp2 negative nuclei ( $52.1 \pm 1.2\%$  for above the median;  $24.2 \pm 1.2\%$  in the upper quartile) was due to random chance (Figure 5-15D-Dii).

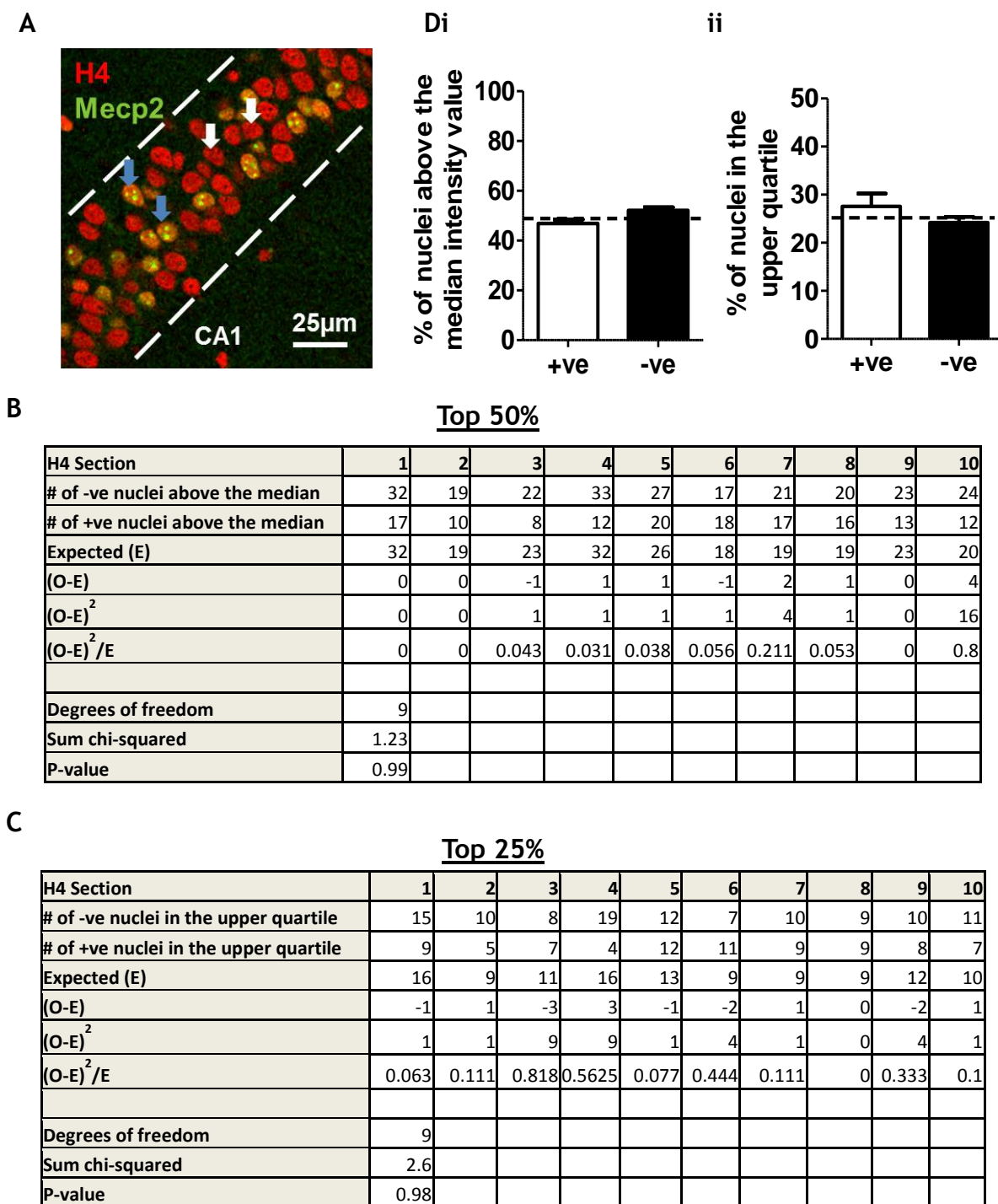


**Figure 5-15 Unaltered total histone H4 levels in CA1 pyramidal cell nuclei of the hippocampal formation between Mecp2 nuclei type under saline control conditions**

(A) Example micrograph of CA1 pyramidal cell nuclei immunostained for total histone H4 and Mecp2 status displayed through fluorescence of the EGFP fusion protein. White arrows highlight example nuclei which do not contain Mecp2 and blue arrows indicate those that do. (B-C) Tables showing the number of Mecp2 positive and negative nuclei above the overall median (B) and upper quartile (C) for total histone H4 intensity values from sections used for chi-square analysis. Chi-square statistic is derived from the expected and observed number of Mecp2 negative nuclei present. The number of observed nuclei was not different to the expected number in both cases ( $p=0.99$  for (B) and  $p=0.98$  for (C), chi-square test,  $n = 10$  sections from 3 mice). (Di-ii) Summary plots showing the percentage of each nuclei type above the median (Di) and in the upper quartile (Dii) total histone H4 intensity values. Data expressed as mean  $\pm$  SEM in the bar graphs. Scale bar = 25 $\mu$ m; +ve = positive nuclei and -ve = negative nuclei.

To investigate the effect neuronal activity has on total histone H4, kainic acid was applied as detailed before and tissues assessed at three hours post seizure induction. The immunostaining of this histone and Mecp2 status displayed through fluorescence of the EGFP fusion protein in the DG following this treatment is shown in Figure 5-16A. There was no overall difference between observed and expected Mecp2 negative nuclei above the median total histone H4 intensity value with variable increases and decreases in sections (Figure 5-16B;  $p=0.93$ , chi-square test,  $n= 15$  sections from four mice). As a result, there was no difference in the percentage of Mecp2 negative cells ( $45.4 \pm 1.3\%$ ) and Mecp2 positive cells ( $54.2 \pm 1.9\%$ ) above the median total histone H4 intensity value (Figure 5-16Di). Similarly there was no difference in the observed and expected nuclei in the upper quartile of total histone H4 intensity value (Figure 5-16C;  $p=0.92$ , chi-square test). Therefore there was no difference detected between the percentage of Mecp2 positive ( $29.2 \pm 0.9\%$ ) and negative ( $22 \pm 0.8\%$ ) nuclei in the upper quartile (Figure 5-16Dii).

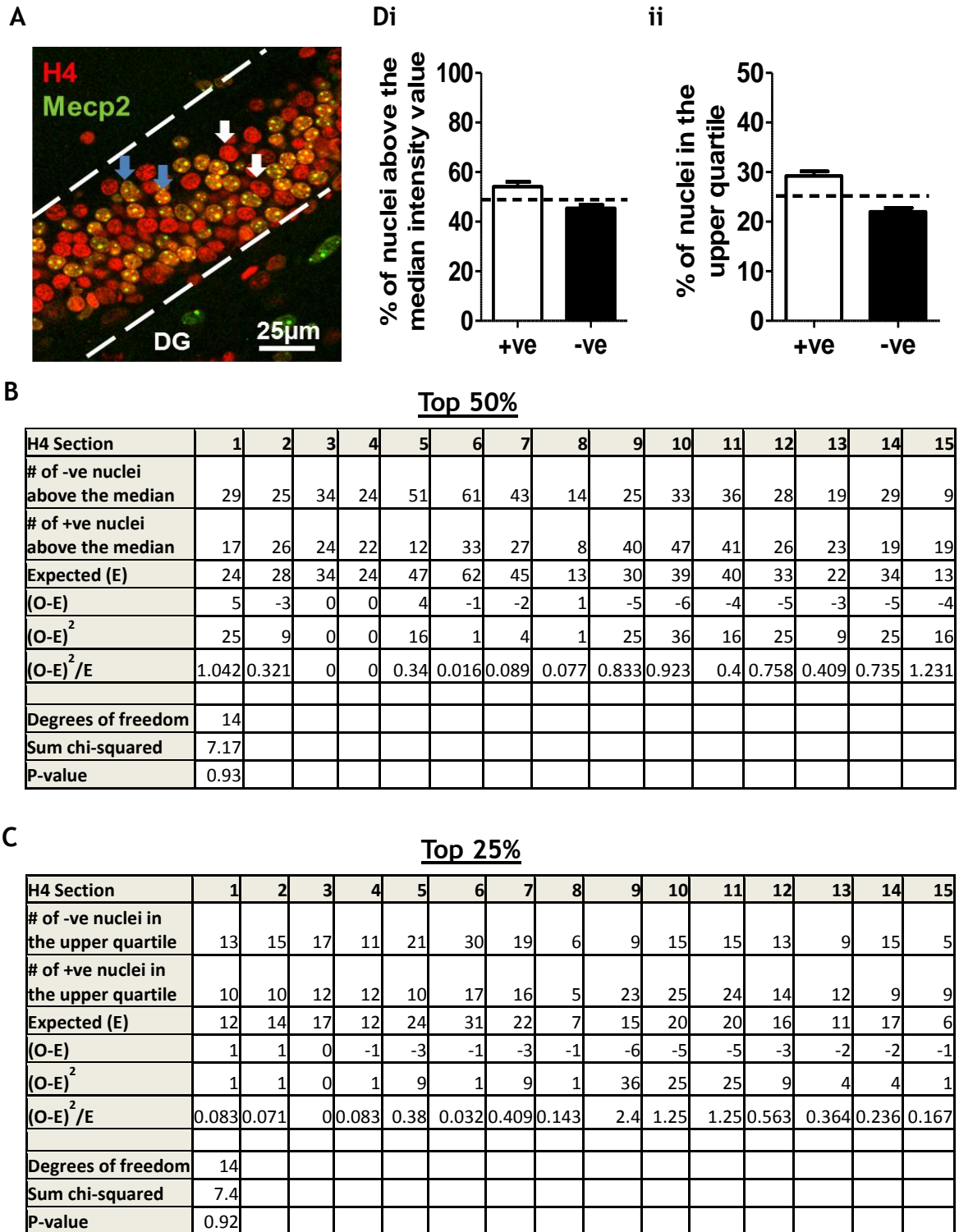


**Figure 5-16 Unaltered total histone H4 levels in DG granule cell nuclei of the hippocampal formation between Mecp2 nuclei type after kainic acid application**

(A) Representative micrograph of DG granule cell nuclei immunostained for total histone H4 and Mecp2 status displayed through fluorescence of the EGFP fusion protein following neuronal activity. White arrows highlight example nuclei which do not contain Mecp2 and blue arrows indicate those that do. (B-C) Tables showing the number of Mecp2 positive and negative nuclei above the overall median (B) and upper quartile (C) for total histone H4 intensity values from sections used for chi-square analysis. Chi-square statistic is derived from the expected and observed number of Mecp2 negative nuclei present. The number of observed nuclei was not different to the expected number in both cases ( $p=0.93$  for (B) and  $p=0.92$  for (C), chi-square test,  $n = 15$  sections from 4 mice). (Di-ii) Summary plots showing the percentage of each nuclei type above the median (Di) and in the upper quartile (Dii) total histone H4 intensity values. Data expressed as mean  $\pm$  SEM in the bar graphs. Scale bar = 25 $\mu$ M; +ve = positive nuclei and -ve = negative nuclei.

Finally, the immunostaining of total histone H4 and Mecp2 status displayed through fluorescence of the EGFP fusion protein in the CA1 of the hippocampus is shown in Figure 5-17A. As in the DG no difference was noted in the observed and expected number of Mecp2 negative nuclei above the median total histone H4 intensity value in the CA1 (Figure 5-17B;  $p=0.99$ , chi-square test;  $n= 15$  sections from four mice). Consequently, there was no difference in the percentage of Mecp2 negative ( $45.2 \pm 1.4\%$ ) and positive ( $54.7 \pm 1.6\%$ ) Mecp2 nuclei above the median intensity value (Figure 5-17Di). Equally there was no difference in observed and expected number of Mecp2 negative nuclei in the upper quartile total histone H4 intensity values (Figure 5-17C;  $p=0.96$ , chi-square test). As a result, there was no difference in percentage of Mecp2 negative ( $21.4 \pm 1.1\%$ ) and positive ( $30.4 \pm 1.2\%$ ) nuclei in the upper quartile intensity (Figure 5-17Dii).

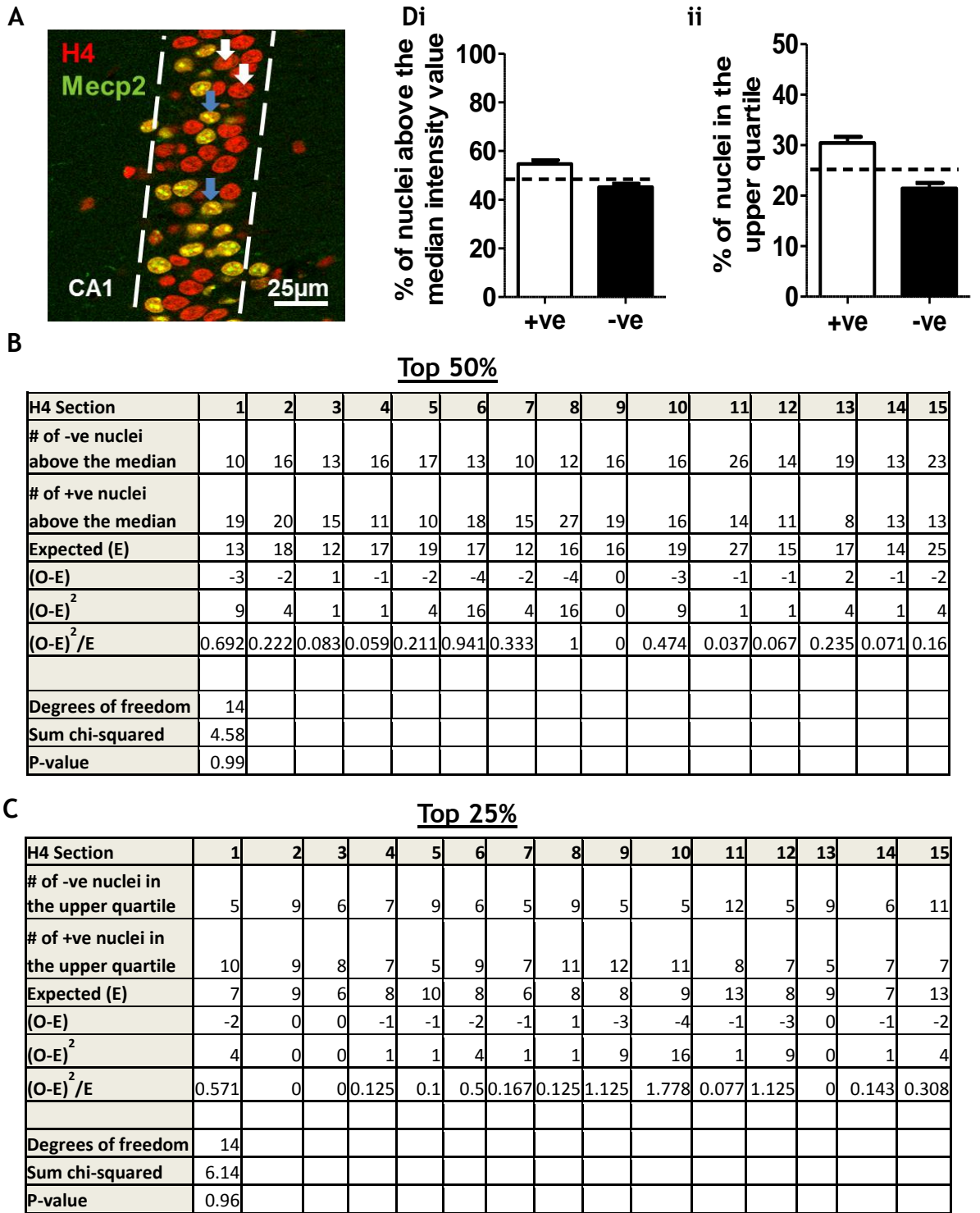


**Figure 5-17 Unaltered total histone H4 levels in CA1 pyramidal cell nuclei of the hippocampal formation between Mecp2 nuclei type after kainic acid administration**  
 (A) Representative micrograph of CA1 pyramidal cell nuclei immunostained for total histone H4 and Mecp2 status displayed through fluorescence of the EGFP fusion protein following neuronal activity. White arrows highlight example nuclei which do not contain Mecp2 and blue arrows indicate those that do. (B-C) Tables showing the number of Mecp2 positive and negative nuclei above the overall median (B) and upper quartile (C) for total histone H4 intensity values from sections used for chi-square analysis.. Chi-square statistic is derived from the expected and observed number of Mecp2 negative nuclei present. The number of observed nuclei was not different to the expected number in both cases ( $p=0.99$  for (B) and  $p=0.96$  for (C), chi-square test,  $n = 15$  sections from 4 mice). (Di-ii) Summary plots showing the percentage of each nuclei type above the median (Di) and in the upper quartile (Dii) total histone H4 intensity values. Data expressed as mean  $\pm$  SEM in the bar graphs. Scale bar = 25 $\mu$ m; +ve = positive nuclei and -ve = negative nuclei.

## 5.5 Discussion

A large number of studies suggest *Mecp2* acts in part through recruitment of histone deacetylase enzymes (Adachi et al. 2009; Bird and Wolffe 1999; Nan et al. 1998; Jones et al., 1998; Nelson, Kavalali, and Monteggia 2006). In order to accurately investigate the role MeCP2 has in controlling levels of histone protein acetylation, and thus gene expression, with a high degree of specificity and resolution, I developed a quantitative immunohistochemistry method to compare levels of histone acetylation at a single nuclei resolution. I utilised mice which were heterozygous for the *Mecp2* knockout mutation to compare the possible differential effects on various histone proteins in cells which were either positive or negative for *Mecp2* expression. This method enabled me to sample many neurons and use the cells positive for *Mecp2* as an internal control to minimise technical variables that can be present with quantitative immunofluorescence imaging. The major finding from this chapter was that there was a modest but significant (5%;  $p < 0.001$ ) reduction in the nuclear volume in *Mecp2*-deficient cells compared to cells expressing a functional *Mecp2*. However there was no significant difference in total histone H3, total histone H4, H3Ac and H4Ac between *Mecp2* positive and negative cells within the hippocampal formation. Whilst there was a trend towards a reduction in the percentage of *Mecp2*-deficient nuclei in the CA1 of the hippocampus to be in the top 25% of H4Ac and total histone H4 intensities within each brain section, this never achieved statistical significance.

The decrease in nuclear volume reported in this chapter (Figure 5-1) agrees with other studies which also report a reduction in nuclear volume in the hippocampus of *Mecp2*-deficient mice compared to WT mice (Giacometti et al. 2007; Johnson et al. 2011; Yazdani et al. 2012). Since *Mecp2* is a highly abundant nuclear protein (Skene et al., 2010) it is perhaps not surprising that its absence causes a reduction in the volume of the nucleus. Correspondingly, work performed on the Embryonic Stem (ES) cell-derived neurons derived from WT mice correlate the size of neuronal nuclei during maturation with the levels of *Mecp2* and that lack of *Mecp2* disrupts this process (Yazdani et al., 2012).

A decrease in the soma size has also been documented in neurons in *Mecp2*-deficient male and heterozygous female mice (Fukuda et al. 2005; Robinson et al. 2012; Taneja et al. 2009). As the size of the nucleus is directly proportional to the size of the cytoplasm, a decrease in the nucleus and cytoplasm volume with age was attributed to potential loss of DNA or a cytoplasmic influence on nuclear size (Ledda et al., 2000). Similarly *Mecp2*-deficient cells could have a reduced nuclear volume because there is a loss of DNA or cytoplasm volume is reduced. Interestingly, transcriptional rates are reduced in nuclei isolated from ES cell driven neurons from *Mecp2*-deficient mice (Yazdani et al., 2012). Furthermore nucleoli have been shown to be smaller in *Mecp2*-deficient neuronal cells and as these structures are formed by transcriptionally active ribosomal DNA in the nucleus, measurements of their size give an approximation of active ribosomal DNA transcription (Singleton et al., 2011). A decrease in their size could be attributed to a decrease in ribosomal DNA transcription in *Mecp2*-deficient cells. This group also documented a decrease in the size of chromocenters, transcriptionally silent DNA positioned around nucleoli (Singleton et al., 2011). Collectively, the functional consequences of these differences observed in neuronal nuclei and cell volume are still unknown but it could relate to the size of the area of the brain composed of that specific neuron type. For example the adrenal medulla of *Mecp2*-deficient mice have been shown to be reduced compared to WT mice (Ladas et al., 2009) thus potentially contributing to the abnormal catecholamine function in this brain region observed in RTT. It could even relate to the microcephaly phenotype associated with RTT patients (Schultz et al., 1993).

Some of the main structures in the nucleus such as heterochromatin and euchromatin (compact and non-tightly packed DNA respectively) undergo dynamic changes throughout maturation (Martou and De Boni 2000). Histone proteins are the main components of chromatin around which DNA is wrapped and are amenable to a variety of modifications (as detailed in chapter one and four) which will contribute to these alterations during maturation (reviewed by MacDonald and Roskams, 2009). One such modification involves histone deacetylase proteins which *Mecp2* has been shown to recruit (Jones et al., 1998; Nan et al., 1998) to repress gene transcription. As activity-dependent regulation of gene expression plays an important role in postnatal neuronal maturation

(reviewed by West and Greenberg, 2011), the interaction Mecp2 has with histone proteins to control gene expression may also be influenced by activity (Guy et al., 2011). I initially investigated this theory in chapter four by quantifying the differences in H3Ac and H4Ac under basal conditions and following induction of neuronal activity (kainic acid treatment) in WT and Mecp2-deficient mice by western blot. However the results obtained were variable and subtle therefore the quantitative immunostaining method used in this chapter was devised and the differences in histone proteins measured in nuclei from mice heterozygous for Mecp2. This enabled the quantification of large number of cells and also had the advantage of providing an internal standard (Mecp2 positive and negative cells in the same brain).

The effects of H3Ac under basal conditions and following induction of neuronal activity were observed first. If Mecp2 recruited histone deacetylase proteins under normal conditions (Jones et al., 1998; Nan et al., 1998), lack of Mecp2 could disrupt this interaction leading to an increase in acetylated histones. Furthermore the levels of total histone H3 were quantified to determine if there were any differences as this would have a direct effect on alterations in acetylation. No difference in the proportion of Mecp2 positive and negative nuclei above the median or in the upper quartile H3Ac (lysine 9 and 14; key regulatory sites as documented by Roh et al., 2005) and total histone H3 intensity levels under any experimental conditions was detected in the hippocampus. Therefore, no overall difference in the levels of these histone proteins was evident between nuclei types (Figure 5-2-Figure 5-9). These results in H3Ac under basal conditions agree with my results in chapter 4 but are contradictory to other published data in which a 2.6 fold increase in H3Ac (lysine 9 and 14) from FACS sorted neuronal nuclei in Mecp2-deficient mice whole brain (Skene et al., 2010). One explanation for this might be that the effects on acetylation are restricted to specific brain regions or to discrete/ other acetylated lysine residues. For example there was an increase in acetylation specifically at histone H3 lysine 9 from nuclei in the cerebral cortex of *Mecp2*<sup>-/-</sup> mice (Thatcher and LaSalle, 2006). Skene et al studied the effects in whole brain but there could be specific cells types which have large acetylation changes thus accounting for the differences observed in the entire brain. My result showing no difference in H3Ac in the hippocampus may be specific to this brain region.

Furthermore, levels of H3Ac have also been shown to differ depending on the mutation type in mouse models and human tissue samples specific for a certain mutation. For example, an increase in the H3Ac (lysine 9 and 14) protein was observed in *Mecp2*<sup>308/y</sup> mice in the cerebellum and cortex compared to WT littermates (Shahbazian et al., 2002). An increase in H3Ac (lysine 9 and 14) protein was also detected at specific promoters, namely *Arc* and *Tubb5* in the striatum of *Mecp2*<sup>308/y</sup> mice compared to WT littermates (Su et al., 2012). Additionally, human cerebral cortex tissue samples from females (*Mecp2*-deficient cells) with a R138X mutation exhibit an increase in acetylation specifically at histone H3 lysine 9 (Thatcher and LaSalle, 2006). Conversely, no difference in H3Ac (lysine 9 and 14) were seen in cell cultures from RTT patients with truncated mutations R168X and 803delG (Wan et al., 2001) and a decrease in H3Ac (lysine 9 and 14; although driven by a decrease in histone H3 lysine 14) was observed from RTT patients lymphocyte lysates with nonsense mutations (Kaufmann et al., 2005). Collectively the above studies from *Mecp2*<sup>-/y</sup> and *Mecp2*<sup>308/y</sup> mice and RTT with specific mutations focus on alterations in histone acetylation under basal conditions. Uniquely in this study, I investigated the effects of H3Ac following induction of neuronal activity. However the lack of alteration in H3Ac observed between *Mecp2* positive and negative nuclei suggests that neuronal activity has no effect on the interaction *Mecp2* has with H3Ac and control of gene expression in the hippocampus. An increase (0.5 fold) in H3Ac was observed in *Mecp2*<sup>stop/y</sup> mice compared to WT littermates from my results in chapter four but these effects were subtle. Moreover the difference in total histone H3 between WT and mutant cells under basal or following neuronal activity has not been observed before and only used as a loading control for western blot experiments in one study mentioned above (Shahbazian et al. 2002). They were used in this context as it is assumed the levels of total histone H3 are not affected by lack of *Mecp2* and my results do not contradict this theory.

Similarly to the effects of H3Ac under basal conditions and following induction of neuronal activity, no significant difference in the proportion of *Mecp2* positive and negative nuclei above the median or in the upper quartile H4Ac (lysines 5, 8, 12 and 16 key regulatory sites as documented by Clarke et al., 1993) and total histone H4 intensity levels under any experimental conditions was detected in

the hippocampus. Therefore, no overall difference in these histone proteins was evident between nuclei types (Figure 5-10-Figure 5-17). These results, under basal conditions, agree with my results from chapter four and also with studies performed in other regions of the brain; no difference was detected in H4Ac (lysine 5, 8, 12 and 16) in protein extracts from the whole cortex, midbrain and cerebellum in WT and *Mecp2*<sup>-/-</sup> mice (Urduingio et al., 2007). These results suggest the absence of *Mecp2* has no effect on H4Ac. However mice with specific mutations in *Mecp2* in mouse models and human tissue samples show varied results. For example no difference was detected in H4Ac (lysines 5, 8, 12 and 16) protein in *Mecp2*<sup>308/y</sup> mice in the cerebellum and cortex compared to WT littermates (Shahbazian et al., 2002) or in H4Ac (lysines 5, 8, 12 and 16; although driven by histone H4 lysine 16) from RTT patients lymphocyte lysates with nonsense mutations (Kaufmann et al., 2005). Conversely an increase in H4Ac (lysines 5, 8, 12 and 16) was seen in cell cultures from RTT patients with truncated mutations R168X and 803delG (Wan et al., 2001). These studies suggest specific mutation types in *Mecp2* could be affecting the levels of H4Ac.

Although no significant difference was observed in H4Ac under basal conditions, there was a trend towards a reduction in the percentage of *Mecp2*-deficient nuclei in the CA1 of the hippocampus to be in the top 25% of H4Ac and total histone H4 intensities within each section. This would imply that the decrease in histone acetylation was attributed to the reduction in total histone H4 and that cell types can be differentially regulated by *Mecp2* even in the same region of the brain. Additionally, as with H3Ac, investigating the effects of H4Ac following induction of neuronal activity in my model was unique. Nonetheless the lack of alteration in H4Ac observed between *Mecp2* positive and negative nuclei suggests that neuronal activity has no effect on the interaction of *Mecp2* with H4Ac and control of gene expression in the hippocampus. This agrees with results obtained from chapter four. Moreover, the difference in total histone H4 between WT and mutant cells under basal or following neuronal activity has not been observed before. It is assumed that the levels of total histone H4 are not affected by lack of *Mecp2* and overall my data does not contradict this.

Another phenomenon that needs to be taken into consideration and could explain why no difference was observed in all the histone proteins from my results is non-cell autonomous effects. In multicellular organisms, if only cells

with a specific mutation exhibit the mutant phenotype then the effects are referred to as cell autonomous. However if the mutant cells also have a direct influence on adjacent cells with a normal genotype, they are referred to as non-cell autonomous. In the case of mice and patients with RTT that are heterozygous for *Mecp2*, this would mean negative *Mecp2* cells inflicting their mutant trait onto *Mecp2* positive cells.

Studies have previously described non-cell autonomous effects. For instance one group has shown non-cell autonomous effects in dendritic arborization from cortical pyramidal neurons in WT mice transfected with *Mecp2*<sup>-/-y</sup> cortical neuroblasts (Kishi and Macklis, 2010). Furthermore another study has shown dendritic abnormalities in *Mecp2* positive cells in the cerebral cortex of heterozygous female mice (Belichenko et al., 2009a). Interestingly, glial cells deficient in MeCP2 have also been shown to display a non-cell autonomous trait. For example having co-cultured WT and *Mecp2* mutated hippocampal neurons in astrocyte conditioned media (ACM) from WT or *Mecp2* mutated astrocytes, one group discovered that the ACM from mutant neurons was unable to support the growth of WT or mutant hippocampal neurons but WT ACM could (Ballas et al., 2009). Moreover, another group have shown a similar finding but with the conditioned media from microglia (Maezawa and Jin, 2010). With regards to my data non-cell autonomous effects on *Mecp2* negative cells could lead to deficits in histone protein levels in *Mecp2* positive cells thus preventing accurate assessment of the direct effect of *Mecp2* on histone proteins. In future studies comparisons could be made between WT cells and *Mecp2* positive cells from heterozygous females to investigate this phenomenon further.

In conclusion, my quantitative immunostaining method enabled me to investigate in what I consider a robust manner, the influence of the presence or absence of cellular *Mecp2* in determining levels of acetylated histone H3 and H4 protein levels in the hippocampus and dentate gyrus principal cells. This method enabled a higher degree of specificity and resolution than in Chapter four. However my results show that whilst there is a 5% reduction in the nuclear volume of *Mecp2*-deficient cells, there is no difference in H3Ac, H4Ac, total histone H3 and total histone H4 between *Mecp2* positive and negative nuclei in the hippocampus under control and also following the induction of neuronal activity which is largely in agreement with my previous results in chapter four.

This result for histone proteins might be dependent on the brain region, specific acetylated histones or mutation type investigated and even influenced by non-cell autonomous effects. There could also be possible adaptive mechanisms occurring that are regulating the effects of histone acetylation as seen in adaptive physiological mechanisms in response to stress (reviewed by McEwen, 2000). Therefore further experiments using models in which *Mecp2* is knocked down genetically (Cheval et al., 2012) or through RNA interference in cultured systems at specific time points in development instead of from birth might reveal different results.

## Chapter 6

# Altered regulation of immediate early genes levels in neurons deficient in *Mecp2* in the *Mecp2*<sup>+/-</sup> mosaic brain

### 6.1 Introduction

Activity-dependent transcription in the brain is important because it is correlated with and directly required for experience-dependent synaptic changes which underlie maturation of neural networks (Dragunow et al. 2000; Marek, Kurtz, and Spitzer 2010; West and Greenberg, 2011). For example, visual input shapes synaptic organisation of the visual cortex during a critical period of development in postnatal life (Hubel, 1982). Nuclear proteins, such as immediate early genes (IEGs) are important regulators in coupling extracellular stimuli with intracellular adaptations in neurons. The principal action of these genes first became clear in experiments conducted in fibroblasts, in which the IEG *Fos* became rapidly upregulated in response to growth factors (Greenberg and Ziff, 1984). Since these key experiments, many IEG families have been identified comprising members of the *Fos*, *Jun*, early growth response (*Egr*) and nuclear receptor families of transcription factors (Herdegen and Leah, 1998) which are rapidly and transiently induced in response to a variety of environmental stimuli. Additionally, cell type and stimulus specificity have been shown to govern the functional consequences of IEG induction (Hill and Treisman, 1999).

The proto-oncogene *c-Fos*, from the *Fos* IEG family, can be rapidly induced by neurotransmitters (Greenberg et al., 1986), nerve growth factor (Curran and Morgan, 1985) and high concentrations of potassium (Morgan and Curran, 1986) in neuronal cultures. Kainic acid-induced seizures have also been shown to induce *c-Fos* in the hippocampus (Ben-Ari 1985; Popovici et al. 1990). Mice in which *c-Fos* was knocked out in the hippocampus (Tsien et al., 1996) displayed more severe seizures in response to kainic acid application (Zhang et al., 2002) suggesting that *c-Fos* can regulate cellular mechanisms mediating neuronal

excitability. Interestingly I have shown that *Mecp2*-deficient mice and heterozygous female mice display a hyperexcitability phenotype following induction of neuronal activity using the convulsant drug kainic acid (chapter three). Additionally, as *Mecp2* can be dynamically regulated through phosphorylation at specific residues (Chen et al., 2003; Tao et al., 2009; Zhou et al. 2006; chapter four) in response to neuronal activity, there could be a role for phosphorylated MeCP2 protein to regulate IEGs levels such as c-Fos in an activity dependent manner. This interaction might be dysfunctional in *Mecp2*-deficient mice thus contributing to the hyperexcitability phenotype observed in my mice. To investigate this phenomenon further I utilised the quantitative immunohistochemistry method previously used to analyse histone proteins (chapter five) to investigate whether *Mecp2* positive and negative nuclei in heterozygous female mice differ in their expression of IEGs following induction of neuronal activity.

## 6.2 Study aims

The overall objective of this chapter was to establish whether IEGs are altered depending on the presence or absence of functional *Mecp2* in the nucleus. The specific aims were to:

- i. Determine whether the expression of two different IEGs, c-Fos and Egr-1 vary in their intensity levels in nuclei positive and negative for *Mecp2* under saline control (quiescent) conditions and following induction of neuronal activity (kainic acid).
- ii. Conduct further analysis to ask the related question whether *Mecp2* positive and negative nuclei differ in the number of nuclei that express detectable c-Fos or Egr1 in a quiescent and activity induced environment.

## 6.3 Methods

Pre-symptomatic *Mecp2*<sup>+/-</sup> and *Mecp2*<sup>GFP/-</sup> female mice aged 10-13 weeks were administered kainic acid (25mg/kg) or saline (controls) intraperitoneally in the absence of anaesthesia (Chapter 2). Mice were monitored for a 0-3 hour observation period after which they were given an overdose of sodium

pentobarbital (Euthatal) and fixed by intracardiac perfusion (4% PFA) with the brain subsequently removed and processed for immunohistochemistry as described in Chapter two. Alternatively, a subset of mice was culled by cervical dislocation and the hippocampi removed and processed for western blot as described in Chapter two.

Hippocampal proteins were probed over night with the following primary antibodies: rabbit anti-c-Fos (1/1000), rabbit anti-Egr-1 (1/1000) or rabbit anti-histone H3 (1/20,000) as a loading control. Subsequently anti-rabbit HRP-conjugated secondary antibodies were applied to membranes and results visualized using ECL. Additionally immunohistochemistry was completed as described in chapter two whereby brain sections were incubated with primary antibody rabbit anti-c-Fos (1/4500), rabbit anti-Egr-1 (1/100) or mouse anti-Mecp2 (1/500). Afterward, fluorescent secondary antibodies (Alexa fluor 488 goat anti-mouse and Alexa fluor 647 goat anti-rabbit) were added to sections in the dark, prior to incubation with the nuclei marker DAPI (1/1000) and mounted onto coverslips.

Following immunohistochemistry, at least two randomly selected and non-overlapping image stacks of the hippocampal formation in the DG and CA1 region for each section were captured using a Leica SP5 Confocal microscope (Dr David Kelly, University of Edinburgh). Nuclei intensity differences in IEGs between Mecp2 positive and negative nuclei were quantified using an automated script in Image-pro Plus 6.0 described in detail in Chapters two and Chapter five. Only a few nuclei were clearly immunostained for c-Fos under saline control conditions (Figure 6-1) and following 0.5 hour of kainic acid treatment therefore the majority of nuclei selected from the automated script are background signal (identifies nuclei based on the DAPI staining). Consequently, a frequency distribution of all raw c-Fos intensities for each section was performed (Figure 6-1) before any analysis was carried out to distinguish nuclei genuinely expressing c-Fos from background fluorescence signal. A larger peak with low intensity values would form which represents nuclei containing background signal. There would be fewer genuinely c-Fos expressing nuclei which represent smaller peaks in the distribution with higher intensities. Typically there is a clear separation between these two intensity types (as shown in Figure 6-1 by the dotted line) thus the background signalling can be identified and excluded from the analysis.

The accuracy of this method for determining genuinely expressing nuclei were confirmed by manually counting the c-Fos expression in several sections.

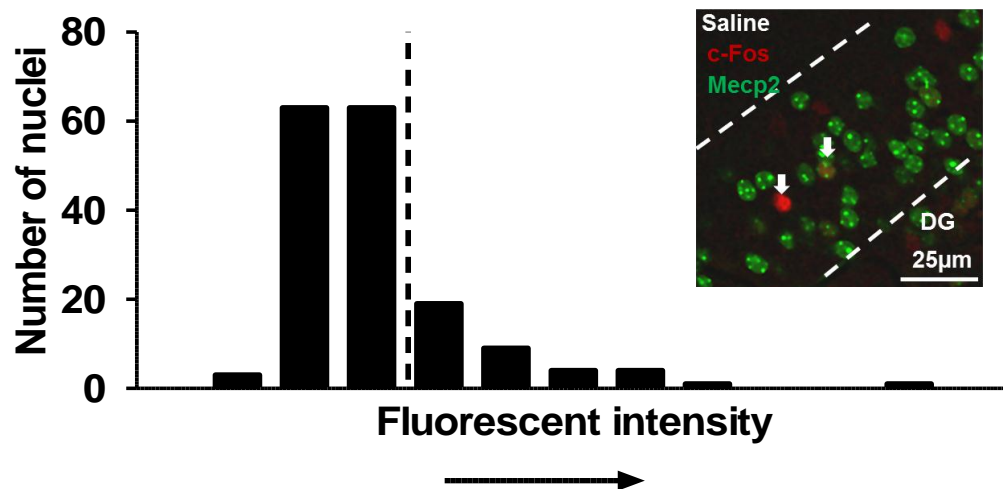


**Figure 6-1 Example distribution of c-Fos fluorescent intensities and identification of background signal.**

An example of the frequency fluorescent intensity distribution from nuclei in a saline control section immunostained for c-Fos. Examples of genuinely expressing c-Fos nuclei are indicated in the micrograph by white arrows. There are fewer nuclei immunostained with c-Fos, represented by the small higher intensity peaks. The background signal will be all the remaining nuclei with no c-Fos expression thus forming a larger lower intensity peak. The dotted line in the distribution graph indicates the clear division between the two.

Subsequently, a chi-square analysis was performed for each immediate early gene as described in Chapter five to determine whether there was a change in the distribution of positive and negative nuclei above the median or upper quartile immediate early gene intensity values. As done previously, the statistics were done on the raw number counts and not percentages to ensure that sections with smaller numbers of nuclei do not disproportionately affect the overall chi-squared value. Furthermore the difference between the total numbers of nuclei immunostained for c-Fos in Mecp2 positive and negative nuclei were quantified manually using Image J software as described in chapter two. A 2x2 contingency table chi-square test was carried out for each animal comparing the total number of Mecp2 positive and negative nuclei immunostained against the total number of each nuclei type immunostained for c-Fos.

## 6.4 Results

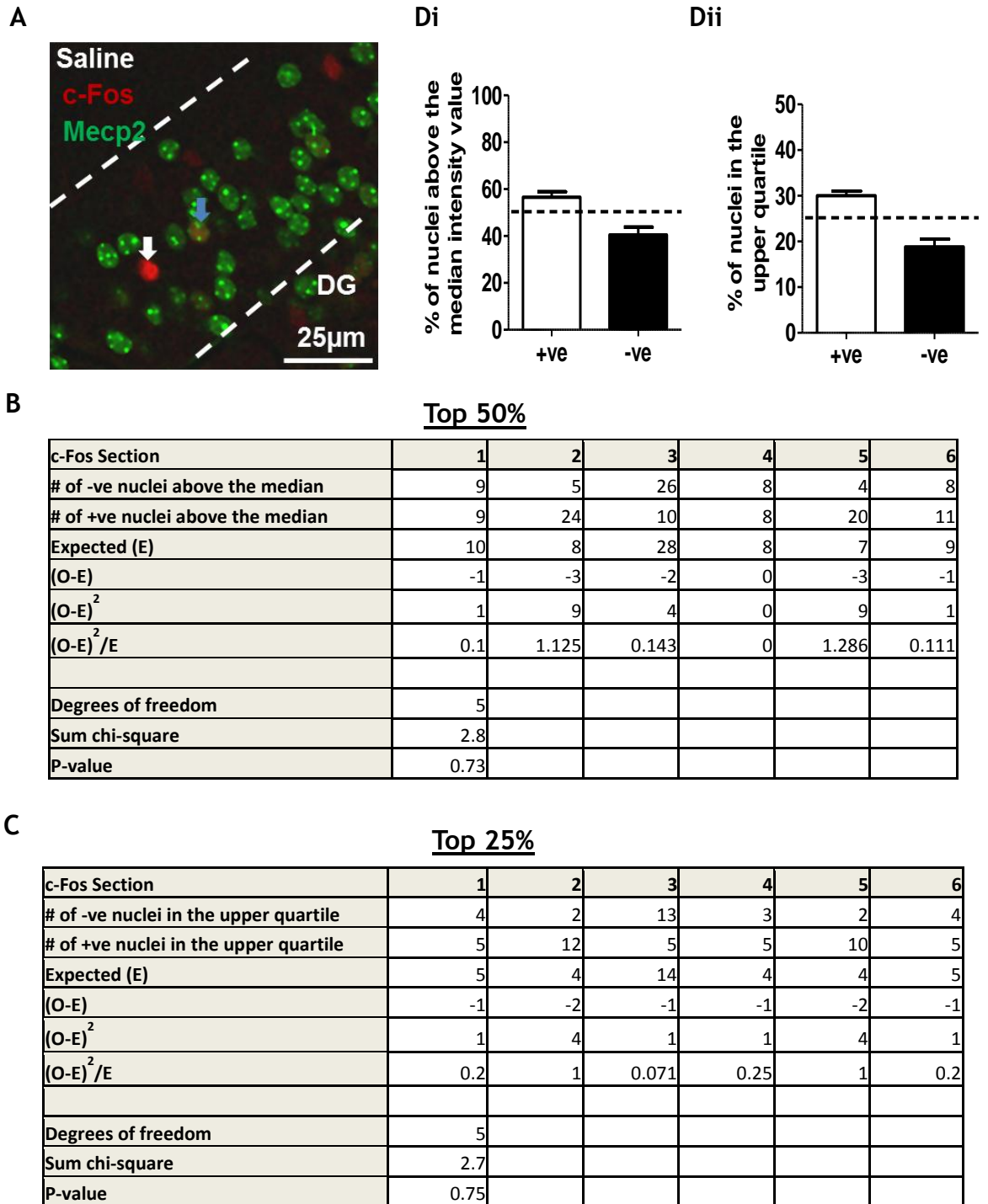
### 6.4.1 *Mecp2*<sup>+/-</sup> mice display an increase in c-Fos expression following induction of neuronal activity compared to saline controls

The induction of c-Fos expression has been shown to occur in the DG of the hippocampus within 90 minutes of intraperitoneal injection of the convulsant drug kainic acid in rats (Popovici et al., 1990). The authors showed that c-Fos staining was maximal at three hours post kainic acid with labelling in other regions of the hippocampus (CA1 and CA3) only occurring after three hours. Furthermore, the authors reported that elevated c-Fos was still detectable 12 hours after kainic acid treatment. As the expression of c-Fos in the hippocampus of *Mecp2*<sup>+/-</sup> heterozygous female mice has not been documented before, I studied the expression of c-Fos in the hippocampal formation during saline control conditions and at 0.5, 1.5 and 3 hours following application of the convulsant drug kainic acid. Within minutes after kainic acid treatment, mice develop seizures similar to *Mecp2*<sup>stop/y</sup> male mice (Chapter 3). No detectable c-Fos signal was observed by western blot under saline control conditions but a strong band of c-Fos was detected after 1.5 and 3 hours following induction of kainic acid treatment (Figure 6-2A). However the micrographs in Figure 6-2B showed a small selection of nuclei were immunostained for c-Fos in the DG under saline control conditions (Figure 6-2Bi) and after 0.5 hours of kainic acid (Figure 6-2Bii). A few nuclei in the CA1 were also immunostained for c-Fos after 0.5 hours but every nucleus in the cell body layer of the hippocampus became brightly immunostained with c-Fos following 3 hours of kainic acid administration (Figure 6-2Biii).



positive ( $56.5 \pm 2.4\%$ ) and negative nuclei ( $40.5 \pm 3.3\%$ ) above the c-Fos median intensity value (Figure 6-3Di).

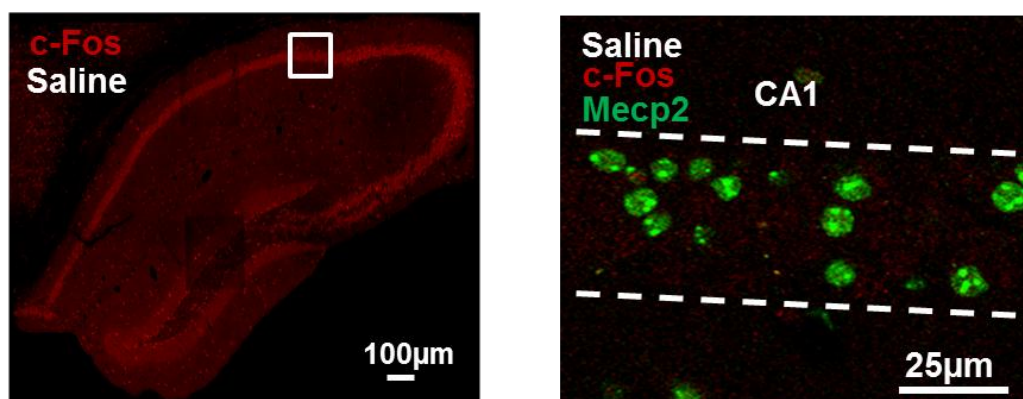
Similarly, there was no difference in the observed and expected number of Mecp2 negative nuclei in the top quartile of c-Fos intensities (Figure 6-3C;  $p=0.75$ , chi-square test). Although there appears to be a decrease in the percentage of Mecp2 negative nuclei ( $18.8 \pm 1.7\%$ ) in the upper quartile c-Fos intensities compared to Mecp2 positive nuclei ( $30 \pm 1\%$ ), this was not significant as the chi-square value for the raw number counts was not significant (Figure 6-3Dii).



**Figure 6-3 Unaltered c-Fos levels in DG granule cell nuclei of the hippocampal formation between Mecp2 nuclei type under saline control conditions**

(A) Representative image of DG granule cell nuclei immunostained for c-Fos and Mecp2 status displayed through fluorescence of the GFP fusion protein. White arrows highlight example nuclei which do not contain Mecp2 and blue arrows indicate those that do. (B-C) Tables showing the number of Mecp2 positive and negative nuclei above the overall median (B) and upper quartile (C) for c-Fos intensity values from sections used for chi-square analysis. Chi-square statistic is derived from the expected and observed number of Mecp2 negative nuclei present. The number of observed nuclei was not different to the expected number in both cases ( $p=0.73$  for (B) and  $p=0.75$  (C), chi-square test,  $n=6$  sections from 3 mice). (Di-ii) Summary plots showing the percentage of each nuclei type above the median (Di) and in the upper quartile (Dii) c-Fos intensity values. Data expressed as mean  $\pm$  SEM in the bar graphs. Scale bar = 25µm; +ve = positive nuclei and -ve = negative nuclei.

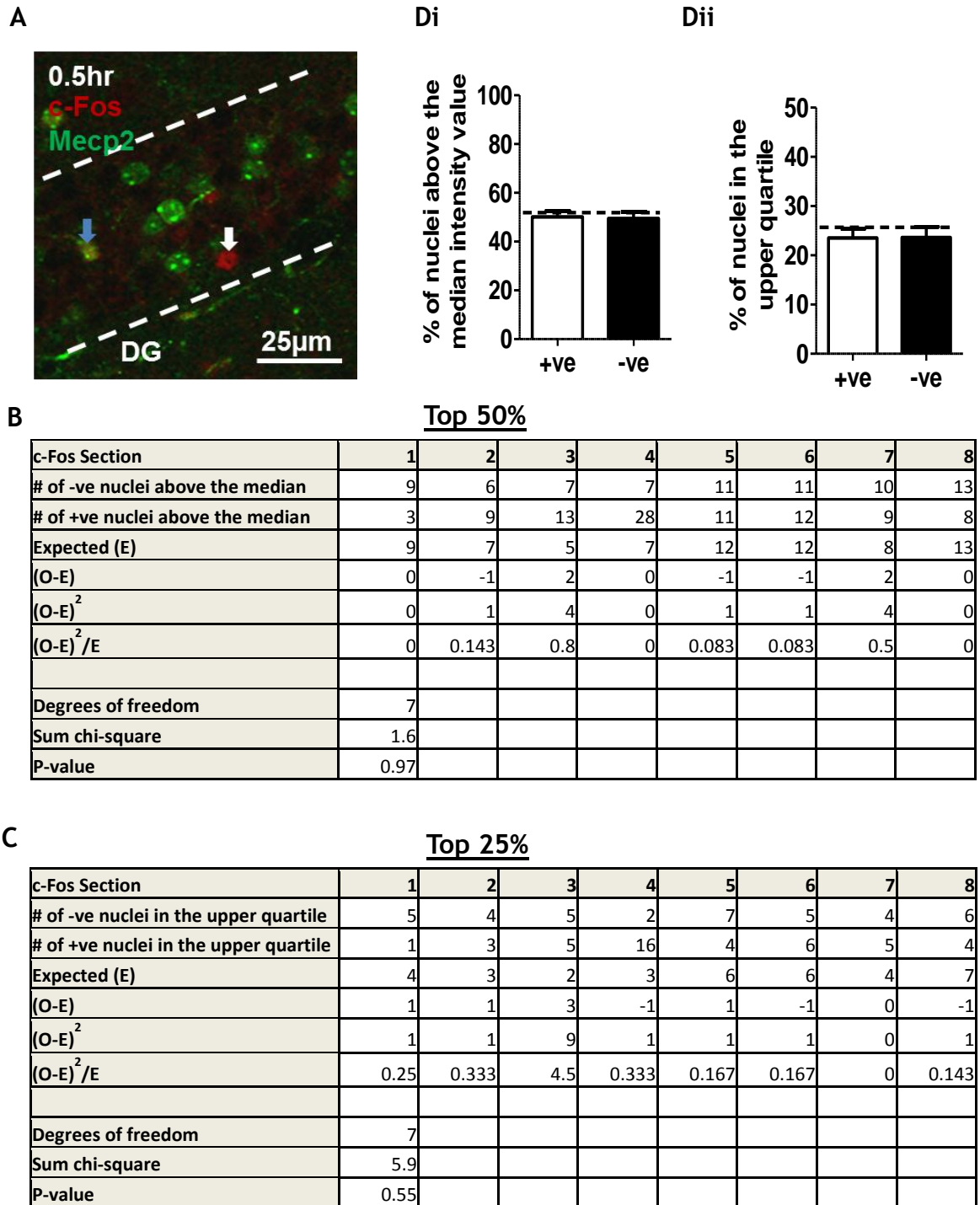
As initially observed in the lower power image (20x objective) in Figure 6-2B, there was no detectable c-Fos immunostaining in the CA1 region of the hippocampus under control conditions therefore the distribution of c-Fos intensities in Mecp2 positive and negative nuclei could not be analysed. A higher power image (63x objective) showing a lack of detectable c-Fos expression in the CA1 can be seen in Figure 6-4.



**Figure 6-4 Lack of c-Fos expression in Mecp2 positive and negative nuclei in the CA1 region of the hippocampus under saline control conditions.**

High (20x objective; left) and low (63x objective; right) micrograph images displaying the lack of c-Fos expression in Mecp2 positive and negative nuclei in the CA1 region of the hippocampus under control conditions. Scale bar = 100µm for 20x objective image and 25µm for 63x objective image.

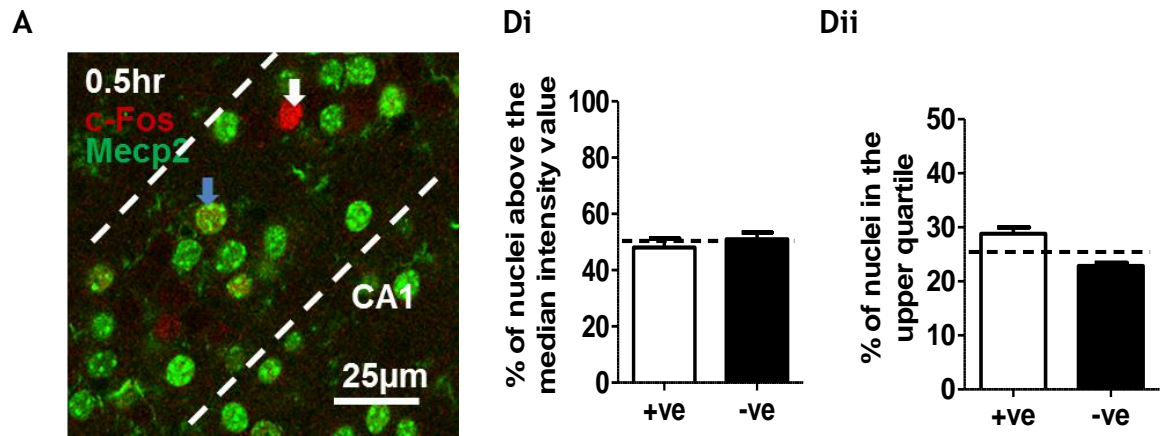
Subsequently, I also determined whether there was a difference in the distribution of c-Fos intensities in nuclei positive and negative for Mecp2 at 0.5 and 3 hours following application of kainic acid treatment. An example micrograph of the nuclei immunostained with c-Fos and Mecp2 in the DG of the hippocampal formation after 0.5 hour of kainic acid administration is shown in Figure 6-5A. Chi-square analysis revealed that there was no difference in the number of observed and expected Mecp2 negative nuclei within the top 50% (Figure 6-5B;  $p=0.97$ , chi-square test;  $n= 8$  sections from 3 mice) or 25% (Figure 6-5C;  $p=0.55$ , chi-square test) of the highest c-Fos intensities. The percentage of Mecp2 positive nuclei above the median ( $50.1 \pm 2.4\%$ ) and in the upper quartile ( $23.5 \pm 1.9\%$ ) c-Fos intensity values compared to Mecp2 negative nuclei ( $49.4 \pm 2.8\%$  for above the median;  $23.6 \pm 2.2\%$  for above in the upper quartile) was likely due to random chance as no significance was observed in either chi-square (Figure 6-5Di-Dii).



**Figure 6-5 Unaltered c-Fos levels in DG granule cell nuclei of the hippocampal formation between Mecp2 nuclei type following 0.5 hour of kainic acid application.**

(A) Representative image of DG granule cell nuclei immunostained for c-Fos and Mecp2 following 0.5 hours of neuronal activity. White arrows highlight example nuclei which do not contain Mecp2 and blue arrows indicate those that do. (B-C) Tables showing the number of Mecp2 positive and negative nuclei above the overall median (B) and upper quartile (C) for c-Fos intensity values from sections used for chi-square analysis. Chi-square statistic is derived from the expected and observed number of Mecp2 negative nuclei present. The number of observed nuclei was not different to the expected number in both cases ( $p=0.97$  for (B) and  $p=0.55$  (C), chi-square test,  $n=8$  sections from 3 mice). (Di-ii) Summary plots showing the percentage of each nuclei type above the median (Di) and in the upper quartile (Dii) c-Fos intensity values. Data expressed as mean  $\pm$  SEM in the bar graphs. Scale bar = 25µm; +ve = positive nuclei and -ve = negative nuclei.

Analysis of immunostaining in the putative pyramidal cells of area CA1 after 0.5 hour of kainic acid treatment (Figure 6-6A), showed that there was no difference in the number of observed and expected Mecp2 negative nuclei above the median c-Fos intensity (Figure 6-6B;  $p=0.95$ , chi-square test;  $n=7$  sections from 3 mice). As a result there was no significant difference in the percentage of Mecp2 positive ( $48 \pm 3.2\%$ ) and Mecp2 negative nuclei ( $51 \pm 2.4\%$ ) above the median (Figure 6-6Di). Similarly, there was no difference in the number of expected and observed Mecp2 negative nuclei in the upper quartile c-Fos intensities (Figure 6-6C;  $p=0.58$ , chi-square test). Therefore there was no difference in the percentage of Mecp2 negative nuclei ( $22.9 \pm 0.6\%$ ) and Mecp2 positive nuclei ( $28.8 \pm 1.2\%$ ) in the upper quartile c-Fos intensities (Figure 6-6Dii).

**B****Top 50%**

c-Fos Section	1	2	3	4	5	6	7
# of -ve nuclei above the median	8	4	6	9	13	3	14
# of +ve nuclei above the median	8	15	10	7	3	10	13
Expected (E)	10	5	6	7	11	3	13
(O-E)	-2	-1	0	2	2	0	1
(O-E) <sup>2</sup>	4	1	0	4	4	0	1
(O-E) <sup>2</sup> /E	0.4	0.2	0	0.571	0.364	0	0.077
Degrees of freedom	6						
Sum chi-square	1.6						
P-value	0.95						

**C****Top 25%**

c-Fos Section	1	2	3	4	5	6	7
# of -ve nuclei in the upper quartile	4	2	3	4	5	3	6
# of +ve nuclei in the upper quartile	4	8	5	4	3	3	8
Expected (E)	5	2	3	3	6	1	6
(O-E)	-1	0	0	1	-1	2	0
(O-E) <sup>2</sup>	1	0	0	1	1	4	0
(O-E) <sup>2</sup> /E	0.2	0	0	0.333	0.167	4	0
Degrees of freedom	6						
Sum chi-square	4.7						
P-value	0.58						

**Figure 6-6 Unaltered c-Fos levels in CA1 pyramidal cell nuclei of the hippocampal formation between Mecp2 nuclei type following 0.5 hour of kainic acid application**

(A) Representative image of CA1 pyramidal cell nuclei immunostained for c-Fos and Mecp2 following 0.5 hours of neuronal activity. White arrows highlight example nuclei which do not contain Mecp2 and blue arrows indicate those that do. (B-C) Tables showing the number of Mecp2 positive and negative nuclei above the overall median (B) and upper quartile (C) for c-Fos intensity values from sections used for chi-square analysis. Chi-square statistic is derived from the expected and observed number of Mecp2 negative nuclei present. The number of observed nuclei was not different to the expected number in both cases ( $p=0.95$  for (B) and  $p=0.58$  (C), chi-square test,  $n=7$  sections from 3 mice). (Di-ii) Summary plots showing the percentage of each nuclei type above the median (Di) and in the upper quartile (Dii) c-Fos intensity values. Data expressed as mean  $\pm$  SEM in the bar graphs. Scale bar = 25 $\mu$ m; +ve = positive nuclei and -ve = negative nuclei.

Finally, an example micrograph of the nuclei immunostained with c-Fos and Mecp2 status displayed through fluorescence of the EGFP fusion protein in the DG of the hippocampal formation after three hours of kainic acid administration is shown in Figure 6-7A. Similar to the effects after 0.5 hours, there was no difference in the observed and expected numbers of Mecp2 negative nuclei above the median c-Fos intensity (Figure 6-7B;  $p=0.77$ , chi-square test;  $n= 15$  sections from four animals). Subsequently, as the chi-square value was not significant, there was no difference in the percentage of Mecp2 positive ( $51.3 \pm 0.9\%$ ) and negative ( $48.1 \pm 1.3\%$ ) nuclei observed above the median c-Fos intensity value (Figure 6-7Di). Furthermore, there was no difference in the number of expected and observed Mecp2 negative nuclei in the upper quartile c-Fos intensities (Figure 6-7B;  $p=0.92$ , chi-square test). Thus overall, there was no significant difference in the percentage of Mecp2 positive ( $25.9 \pm 0.5\%$ ) and negative nuclei ( $23.9 \pm 0.9\%$ ; Figure 6-7Dii).

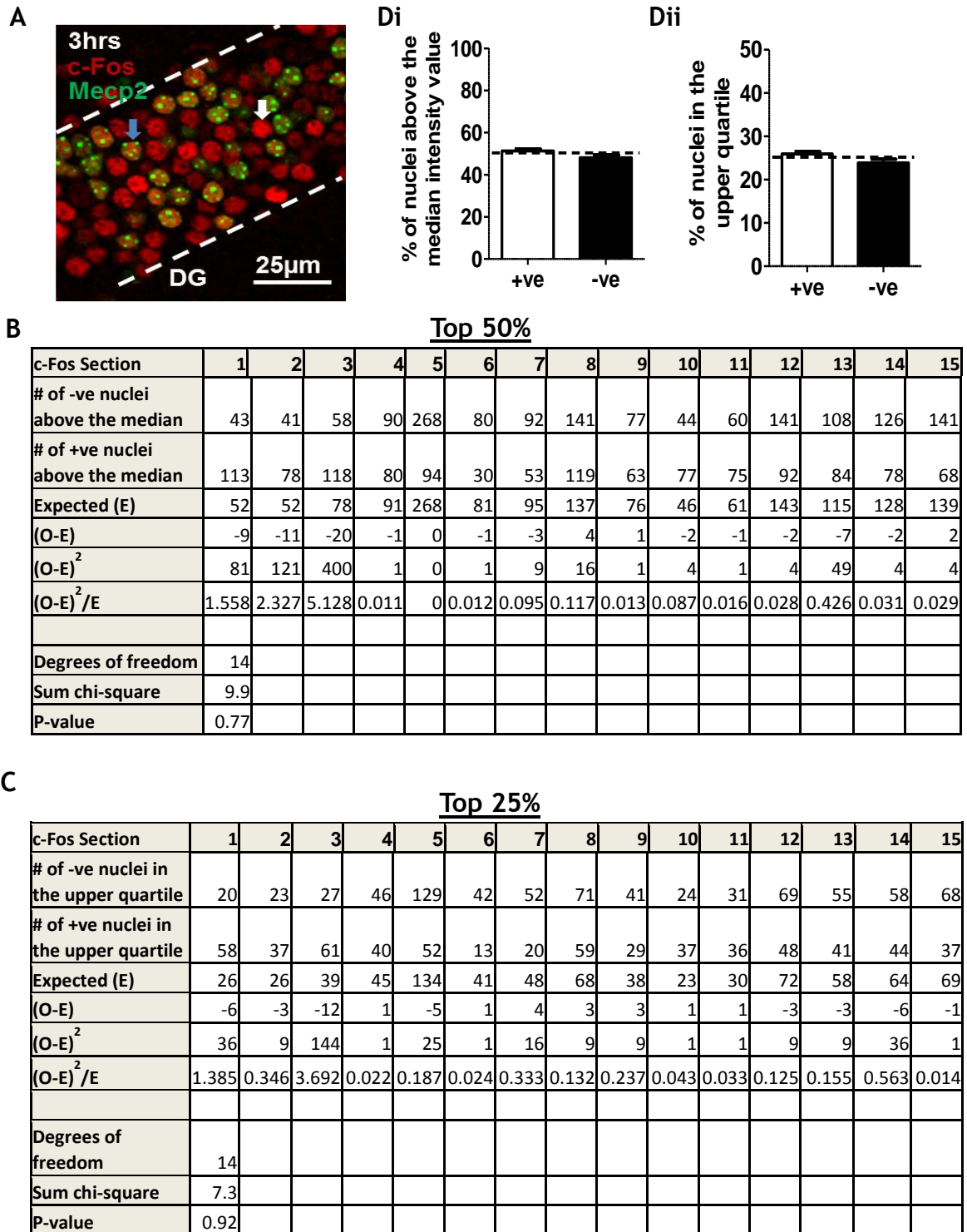


**Figure 6-7 c-Fos expression is elevated following 3 hours of kainic acid induced seizures but is not different between Mecp2 nuclei type in DG granule cell nuclei**

(A) Representative image of nuclei in DG granule cell nuclei immunostained for c-Fos and Mecp2 status displayed through fluorescence of the EGFP fusion protein following 3 hours of neuronal activity. White arrows highlight example nuclei which do not contain Mecp2 and blue arrows indicate those that do. (B-C) Tables showing the number of Mecp2 positive and negative nuclei above the overall median (B) and upper quartile (C) for c-Fos intensity values from sections used for chi-square analysis. Chi-square statistic is derived from the expected and observed number of Mecp2 negative nuclei present. The number of observed nuclei was not different to the expected number in both cases ( $p=0.77$  for (B) and  $p=0.92$  (C), chi-square test,  $n=15$  sections from 4 mice). (Di-ii) Summary plots showing the percentage of each nuclei type above the median (Di) and in the upper quartile (Dii) c-Fos intensity values. Data expressed as mean  $\pm$  SEM in the bar graphs. Scale bar = 25 $\mu$ m; +ve = positive nuclei and -ve = negative nuclei.

Analysis of immunostaining in the CA1 after three hours of kainic acid treatment (Figure 6-8A), showed there was no difference in the number of observed and expected Mecp2 negative nuclei above the median (Figure 6-8B;  $p=0.95$ , chi-square test;  $n= 14$  sections from 4 mice) or upper quartile (Figure 6-8C;  $p=0.89$ , chi-square test) c-Fos intensity values. Therefore, there was no significant difference in the percentage of Mecp2 positive nuclei above the median ( $53.4 \pm 1.5\%$ ) and upper quartile ( $26.9 \pm 1.3\%$ ) c-Fos intensity values compared to Mecp2 negative nuclei ( $46.3 \pm 1.4\%$  for above the median;  $22.7 \pm 1.4\%$  in the upper quartile) (Figure 6-8Di-Dii).

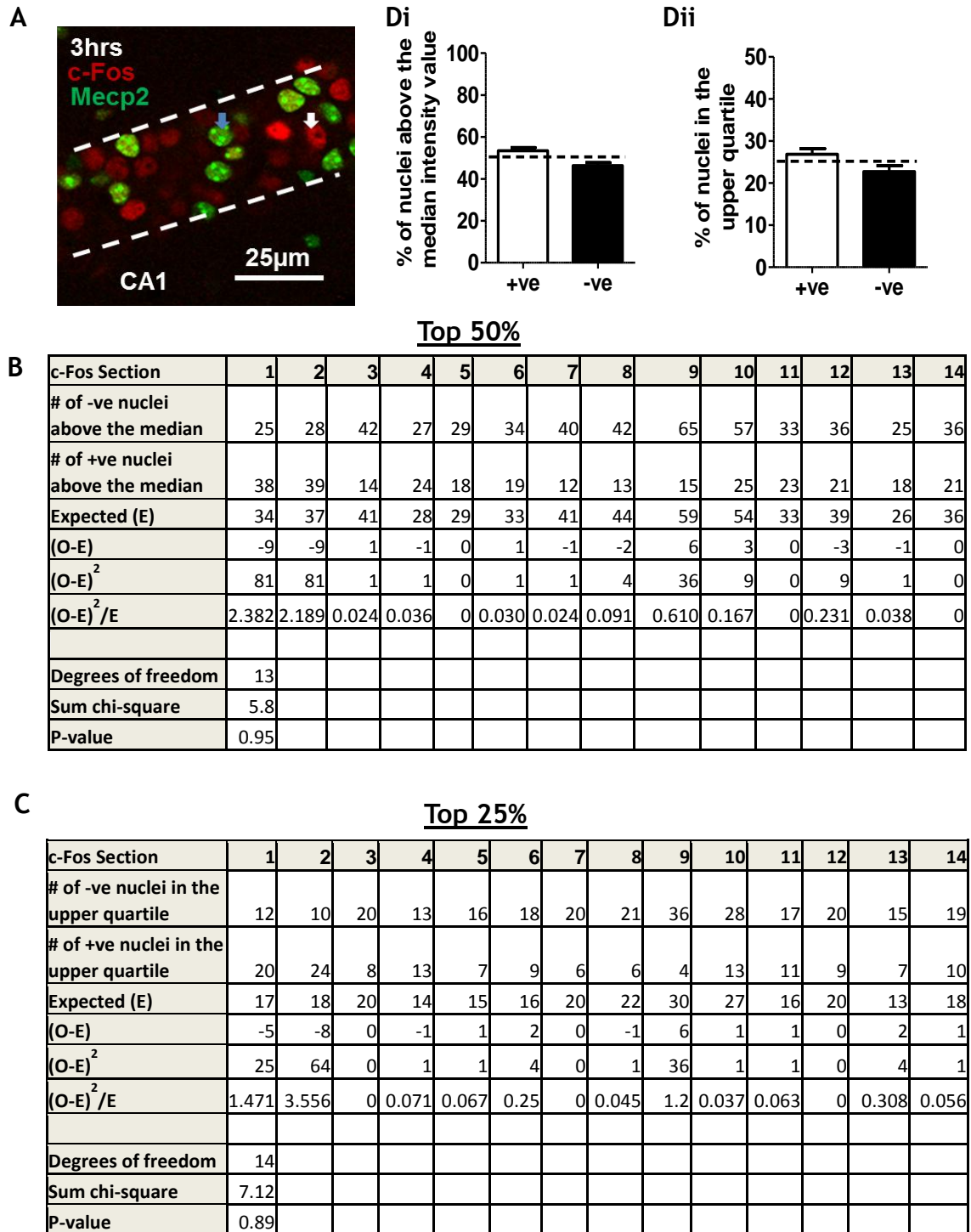


**Figure 6-8 c-Fos expression is elevated following 3 hours of kainic acid induced seizures but is not different between Mecp2 nuclei type in CA1 pyramidal cell nuclei**

(A) Representative image of CA1 pyramidal cell nuclei immunostained for c-Fos and Mecp2 status displayed through fluorescence of the EGFP fusion protein following 3 hours of neuronal activity. White arrows highlight example nuclei which do not contain Mecp2 and blue arrows indicate those that do. (B-C) Tables showing the number of Mecp2 positive and negative nuclei above the overall median (B) and upper quartile (C) for c-Fos intensity values from sections used for chi-square analysis. Chi-square statistic is derived from the expected and observed number of Mecp2 negative nuclei present. The number of observed nuclei was not different to the expected number in both cases ( $p=0.95$  for (B) and  $p=0.89$  (C), chi-square test,  $n=14$  sections from 4 mice). (Di-ii) Summary plots showing the percentage of each nuclei type above the median (Di) and in the upper quartile (Dii) c-Fos intensity values. Data expressed as mean  $\pm$  SEM in the bar graphs. Scale bar = 25µm; +ve = positive nuclei and -ve = negative nuclei.

### 6.4.3 Greater proportion of Mecp2-deficient nuclei express c-Fos in the hippocampal formation

An alternative theory to variations in c-Fos intensity between nuclei types is the presence of a disproportionate number of Mecp2 negative nuclei expressing c-Fos regardless of intensity. At three hours, following the induction of kainic acid treatment, every nucleus in the cell body layer of the DG and CA1 of the hippocampal formation shows detectable c-Fos expression. However, under control conditions in the DG and following 0.5 hour of kainic acid application (CA1 and DG), there are only a subpopulation of nuclei labelled. As a result, it is possible there could be variations in the number of nuclei that have c-Fos depending on nuclei type Mecp2-status. A chi-square test was used to determine whether there was a significant difference in the proportion of Mecp2 positive and Mecp2 negative nuclei immunostaining positively for c-Fos in the DG under saline control. This difference was found to be significant (Figure 6-9Aiv;  $p < 0.0001$ , chi-square test,  $n = 9$  sections from three mice) and this pattern was observed in the majority of mice analysed (Figure 6-9Ai-iii). Overall, 61% of Mecp2 negative nuclei contained c-Fos compared to 39% of Mecp2 positive nuclei (Figure 6-9B). This result was not influenced by the total number of each nuclei type present in each section as the total number of Mecp2 positive and negative nuclei immunostained were significantly different from the total number of each nuclei type immunostained for c-Fos.

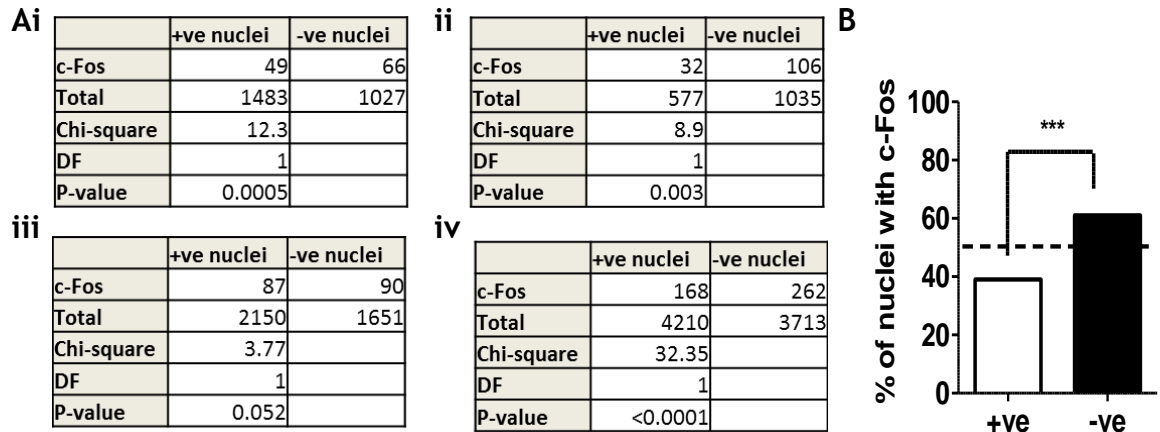


**Figure 6-9 Increased percentage of MeCP2 negative nuclei expressing c-Fos in the DG of the hippocampal formation under saline control conditions.**

(Ai-iv) Chi-square analysis of the total number (labelled total in table) of MeCP2 positive and MeCP2 negative nuclei immunostained in the DG under saline control conditions compared to the number of each nuclei type immunostained for c-Fos (labelled c-Fos in the table). The first three tables represent the data from a different animal whereby a significant difference was observed in two (Ai-ii) out of three (Aiii) mice ( $p < 0.05$ , chi-square test,  $n =$  three sections per animal). The fourth table represents the pooled data for all three mice ( $p < 0.0001$ , chi-square test). (B) Summary plot from the pooled data showing an increase in the percentage of MeCP2 negative nuclei (61%) expressing c-Fos compared to MeCP2 positive nuclei (39%).

A similar analysis was conducted for the effects observed in the DG and CA1 of the hippocampal formation following 0.5 hour of kainic acid treatment. Once again there was a significant difference in the proportion of MeCP2 positive and MeCP2 negative nuclei staining positively for c-Fos (Figure 6-10Bi;  $p < 0.0001$ , chi-square test,  $n =$  12 sections from four mice). This difference was seen in all four mice analysed (Figure 6-10Ai-iv). Overall, 62% of MeCP2 positive nuclei contain c-Fos compared to 38% of MeCP2 positive nuclei (Figure 6-10Bii).

Ai

	+ve nuclei	-ve nuclei
c-Fos	40	75
Total	1622	1386
Chi-square	13.3	
DF	1	
P-value	<0.0001	

ii

	+ve nuclei	-ve nuclei
c-Fos	32	83
Total	2011	1063
Chi-square	68	
DF	1	
P-value	<0.0001	

Bi

	+ve nuclei	-ve nuclei
c-Fos	154	253
Total	5843	6071
Chi-square	19.8	
DF	1	
P-value	<0.0001	

iii

	+ve nuclei	-ve nuclei
c-Fos	29	62
Total	1118	1398
Chi-square	5.6	
DF	1	
P-value	0.01	

iv

	+ve nuclei	-ve nuclei
c-Fos	53	33
Total	1092	2224
Chi-square	30.9	
DF	1	
P-value	<0.0001	

Bii

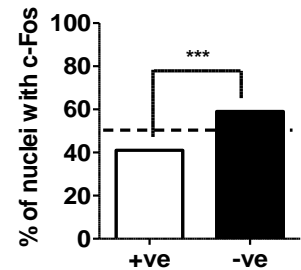


**Figure 6-10 Increased percentage of MeCP2 negative nuclei expressing c-Fos in the DG of the hippocampal formation after 0.5 hour of kainic acid application.**

(Ai-iv) Chi-square analysis of the total number (labelled total in table) of MeCP2 positive and MeCP2 negative nuclei immunostained in the DG after 0.5 hour of kainic acid treatment compared to the number of each nuclei type immunostained for c-Fos (labelled c-Fos in the table). Each table represents a different animal whereby a significant difference was observed in all mice ( $p < 0.05$ , chi-square test,  $n =$  three sections per animal). (Bi) Pooled data for all four mice ( $p < 0.0001$ , chi-square test). (Bii) Summary plot from the pooled data showing an increase in the percentage of MeCP2 negative nuclei (62%) expressing c-Fos compared to MeCP2 positive nuclei (38%).

Pooled data mouse data from the CA1 showed a significant difference in the proportion of MeCP2 positive and MeCP2 negative nuclei staining positively for c-Fos (Figure 6-11Bi;  $p < 0.0001$ , chi-square test,  $n =$  12 sections from four mice). This difference was observed in three (Figure 6-11Ai, iii and iv) out of four (Figure 6-11Aii) mice analysed. Overall, 59% of MeCP2 negative nuclei contain c-Fos compared to 41% of MeCP2 positive nuclei (Figure 6-11Bii).

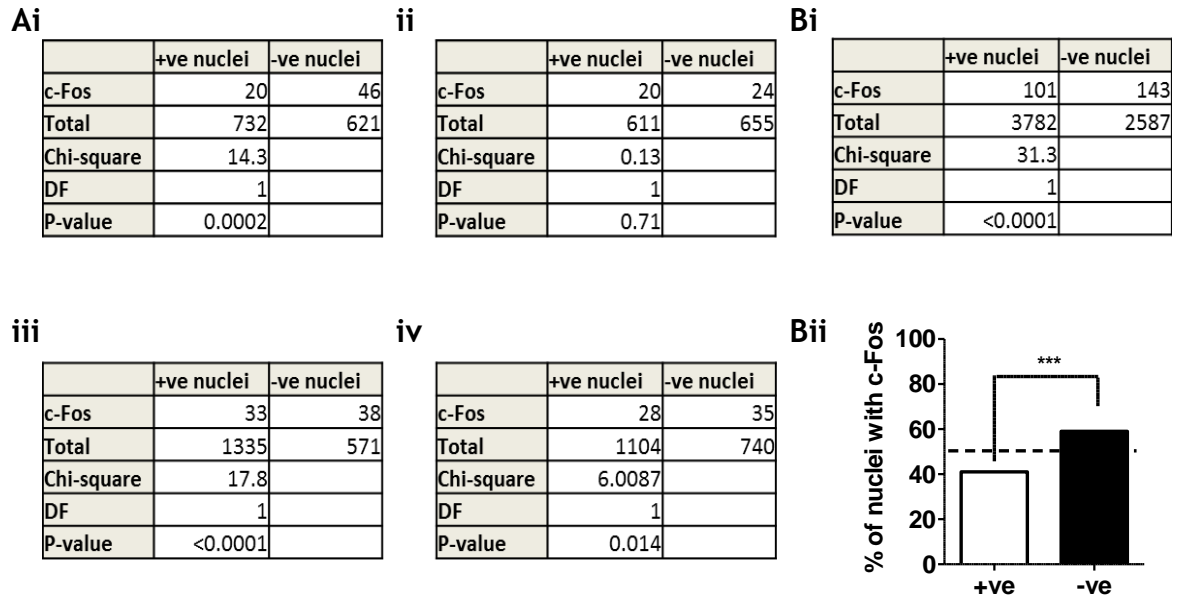


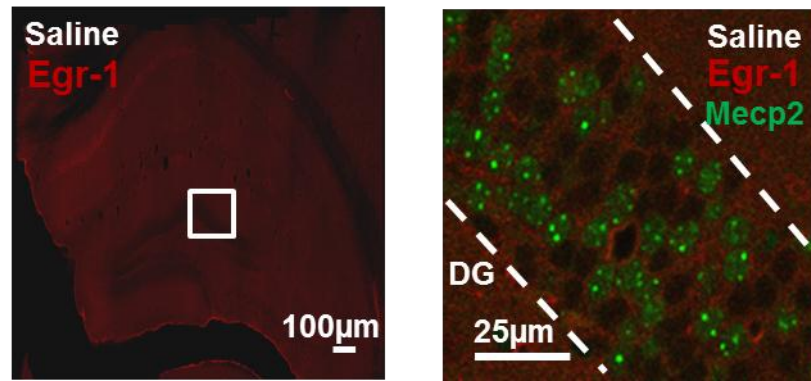
**Figure 6-11 Increased percentage of *Mecp2* negative nuclei expressing c-Fos in the CA1 of the hippocampal formation after 0.5 hour of kainic acid application.**

(Ai-iv) Chi-square analysis of the total number (labelled total in table) of *Mecp2* positive and *Mecp2* negative nuclei immunostained in the CA1 after 0.5 hour of kainic acid treatment compared to the number of each nuclei type immunostained for c-Fos (labelled c-Fos in the table). Each table represents a different animal whereby a significant difference was observed three (Ai, iii and iv) out of four (Aii) mice ( $p < 0.05$ , chi-square test,  $n = 3$  sections per animal). (Bi) Pooled data for all four mice ( $p < 0.0001$ , chi-square test). (Bii) Summary plot from the pooled data showing an increase in the percentage of *Mecp2* negative nuclei (59%) expressing c-Fos compared to *Mecp2* positive nuclei (41%).

#### 6.4.4 *Mecp2*<sup>+/-</sup> mice display an increase in *Egr-1* expression following induction of neuronal activity compared to saline controls

In order to investigate whether other IEG families have altered expression in the hippocampal formation of *Mecp2*-deficient nuclei, the early growth response (*Egr*) family of transcription factors, specifically *Egr1*, was also studied. In comparison to c-Fos, *Egr-1* has been shown to have a high basal expression in the hippocampus (Waters et al., 1990). However the expression of *Egr-1* in the hippocampal formation of *Mecp2*<sup>+/-</sup> heterozygous female mice has not been documented before. Therefore, I investigated the expression of *Egr-1* in the hippocampal formation during saline control conditions and after 0.5, 1.5 and 3 hours of the convulsant drug kainic acid. Low levels of *Egr-1* expression were detected by western blot under saline control conditions and following 0.5 hour of kainic acid treatment but a clear increase was observed after 1.5 hour and three hours of kainic acid administration (Figure 6-12A). The micrographs in Figure 6-12B showed that nuclei in the CA1 express *Egr-1* under saline control conditions (Figure 6-12Bi) and following 0.5 hour of kainic acid treatment (Figure 6-12Bii) but no detectable immunostaining was present in the DG. However, all

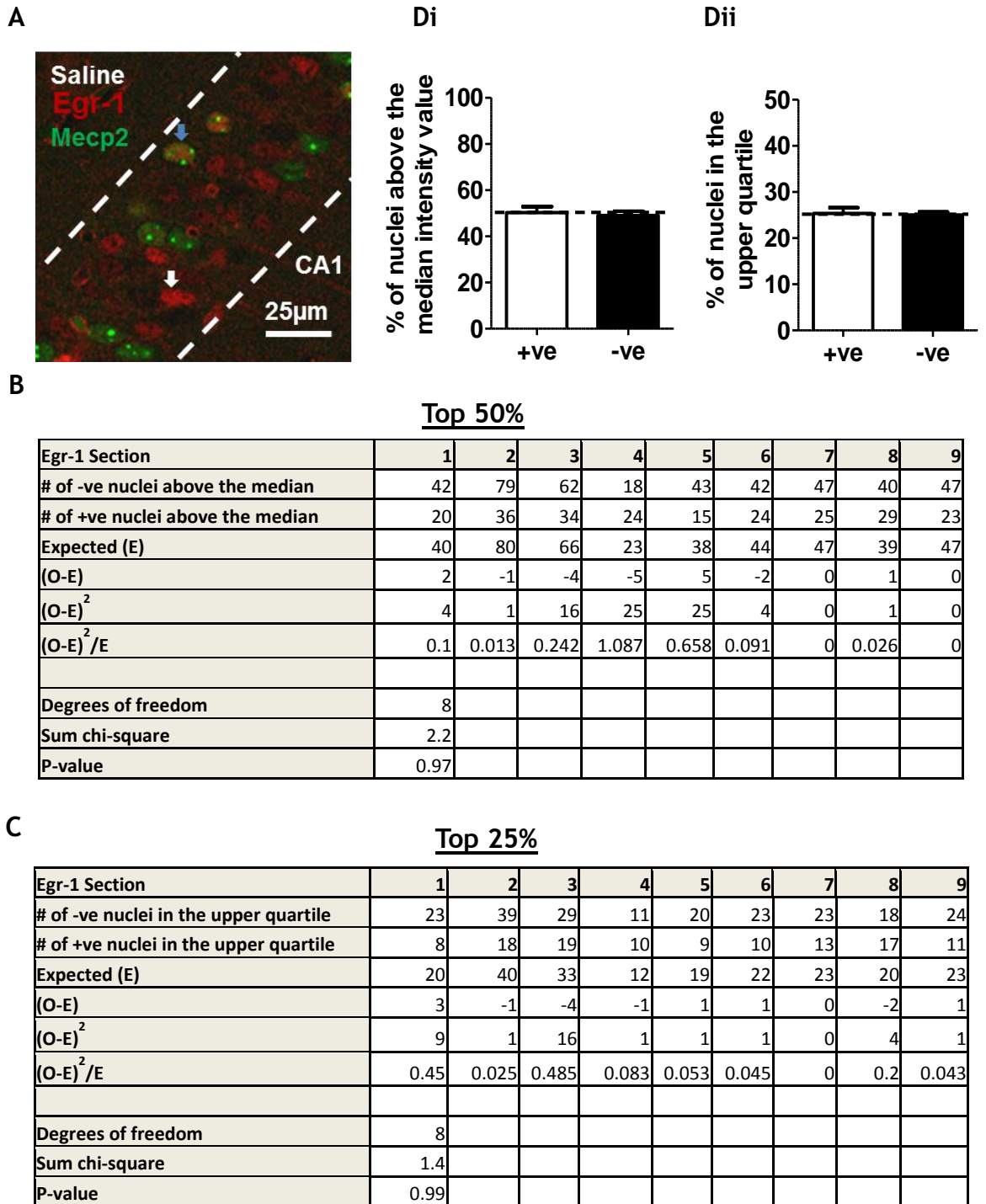




**Figure 6-13 Lack of Egr-1 expression in Mecp2 positive and negative nuclei in the DG region of the hippocampal formation under saline control conditions.**

High (20x objective; left) and low (63x objective; right) micrograph images displaying the lack of Egr-1 expression in Mecp2 positive and negative nuclei in the DG region of the hippocampal formation under control conditions. Scale bar = 100µm for 20x objective image and 25µm for 63x objective image.

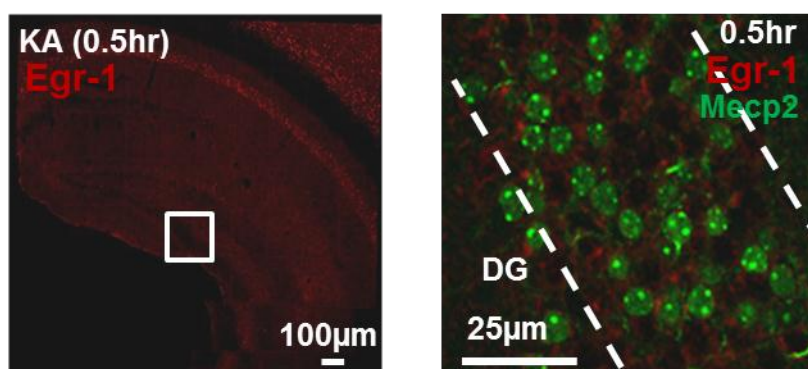
Conversely, all nuclei within the CA1 of the hippocampus under saline control conditions are immunostained with Egr-1 as shown in Figure 6-14A. However, there was no difference in the number of observed and expected Mecp2 negative nuclei above the median Egr-1 intensity value (Figure 6-14B;  $p=0.97$ , chi-square test;  $n=9$  sections from 3 mice). As a result there was no significant difference in the percentage of Mecp2 positive ( $50 \pm 2.6\%$ ) and negative nuclei ( $49.1 \pm 1.8\%$ ) with Egr-1 intensity values above the median (Figure 6-14Di). Additionally, there was no difference in the number of expected and observed Mecp2 negative nuclei in the upper quartile Egr-1 intensities (Figure 6-14C;  $p=0.99$ , chi-square test). Therefore there was no significant difference in the percentage of Mecp2 negative nuclei ( $25 \pm 0.6\%$ ) and positive nuclei ( $25.3 \pm 1.3\%$ ) in the upper quartile Egr-1 intensities (Figure 6-14Dii).



**Figure 6-14 Unaltered Egr-1 levels in CA1 pyramidal cell nuclei of the hippocampal formation between Mecp2 nuclei type under saline control conditions**

(A) Representative image of CA1 pyramidal cell nuclei immunostained for Egr-1 and Mecp2 status displayed through fluorescence of the EGFP fusion protein. White arrows highlight example nuclei which do not contain Mecp2 and blue arrows indicate those that do. (B-C) Tables showing the number of Mecp2 positive and negative nuclei above the overall median (B) and upper quartile (C) for Egr-1 intensity values from sections used for chi-square analysis. Chi-square statistic is derived from the expected and observed number of Mecp2 negative nuclei present. The number of observed nuclei was not different to the expected number in both cases ( $p=0.97$  for (B) and  $p=0.99$  (C), chi-square test,  $n=9$  sections from 3 mice). (Di-ii) Summary plots showing the percentage of each nuclei type above the median (Di) and in the upper quartile (Dii) Egr-1 intensity values. Data expressed as mean  $\pm$  SEM in the bar graphs. Scale bar = 25µm; +ve = positive nuclei and -ve = negative nuclei.

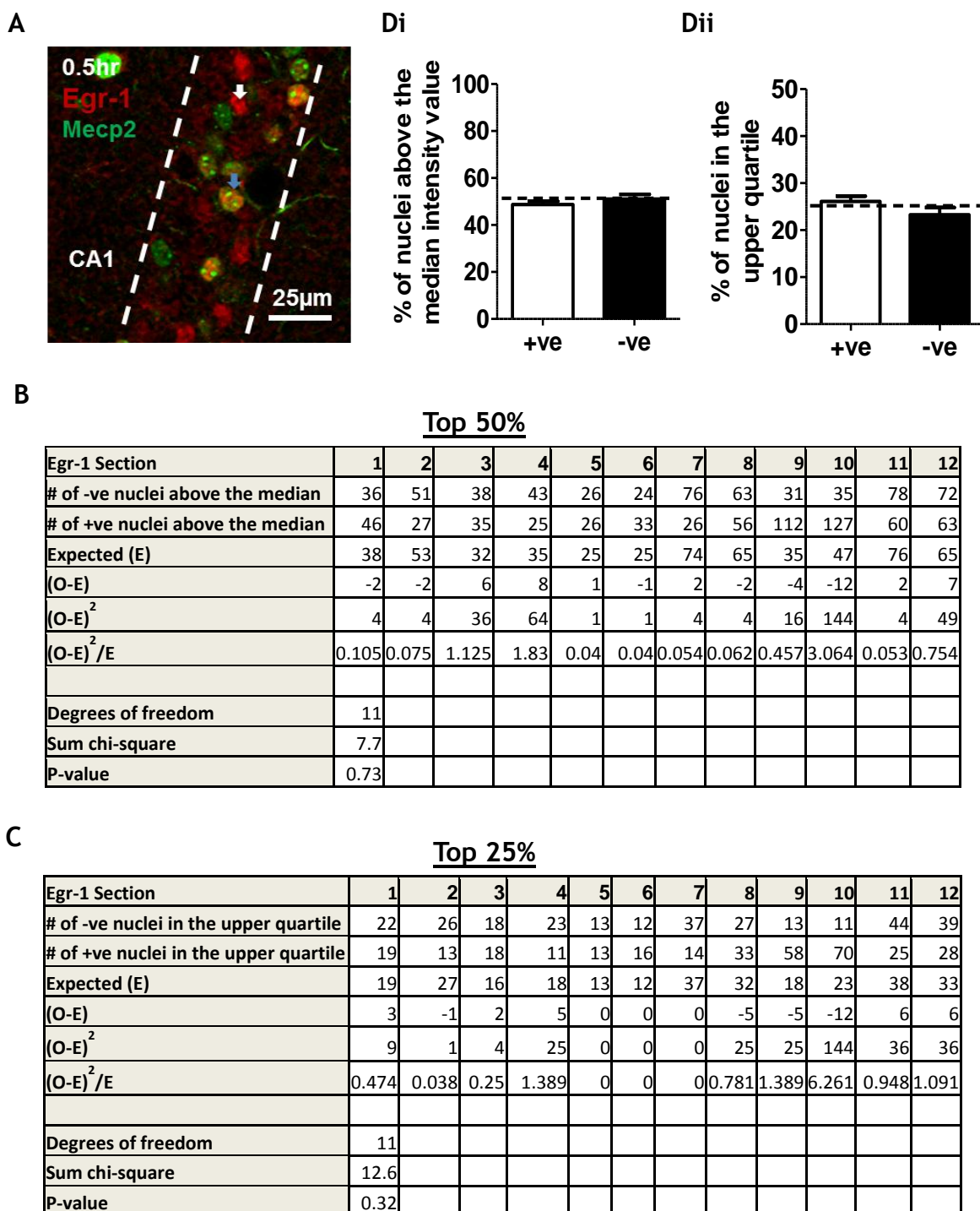
Subsequently, I also determined whether there was a difference in the distribution of Egr-1 intensities in nuclei positive and negative for Mecp2 following 0.5 and 3 hours of treatment with the convulsant drug kainic acid. Similarly to saline control conditions in the DG at 0.5 hour following kainic acid application, no detectable Egr-1 expression was evident and therefore distribution analysis was not performed in this area. This is demonstrated in the high power (63x objective) image in Figure 6-15.



**Figure 6-15 Lack of Egr-1 expression in Mecp2 positive and negative nuclei in the DG region of the hippocampal formation following 0.5 hour of kainic acid treatment**

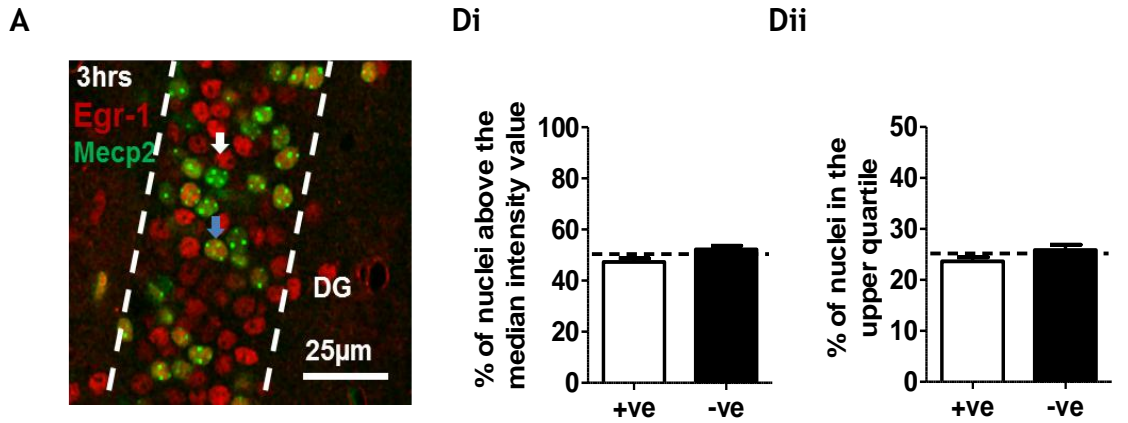
High (20x objective; left) and low (63x objective; right) micrograph images displaying the lack of Egr-1 expression in Mecp2 positive and negative nuclei in the DG region of the hippocampal formation after 30 minutes of kainic acid (KA) treatment. Scale bar = 100µm for 20x objective image and 25µm for 63x objective image.

Immunostaining of nuclei in CA1 of the hippocampus following 0.5 hour kainic acid treatment can be observed in Figure 6-16A. Similarly to saline control conditions, no difference was evident in the number of observed and expected Mecp2 negative nuclei above the median Egr-1 intensity value (Figure 6-15B;  $p=0.73$ , chi-square test;  $n= 12$  sections from 3 mice). There was no significant difference in the percentage of positive nuclei ( $48.7 \pm 1.5\%$ ) compared to negative nuclei ( $51 \pm 2.1\%$ ) above the median Egr-1 intensity (Figure 6-169Di). Furthermore, although there were a few sections with less than expected negative nuclei above the 3<sup>rd</sup> quartile Egr-1 intensity, the overall chi-square value was not significant (Figure 6-16C;  $p=0.32$ , chi-square test). Therefore, there was no significant difference in the percentage of Mecp2 negative nuclei ( $23.3 \pm 1.6\%$ ) positive nuclei ( $26.1 \pm 1.1\%$ ) with intensities in the upper quartile (Figure 6-16Dii).



**Figure 6-16 Unaltered Egr-1 levels in CA1 pyramidal cell nuclei of the hippocampal formation between Mecp2 nuclei type following 0.5 hour of kainic acid administration**  
 (A) Representative image of CA1 pyramidal cell nuclei immunostained for Egr-1 and Mecp2 following 0.5 hour of neuronal activity. White arrows highlight example nuclei which do not contain Mecp2 and blue arrows indicate those that do. (B-C) Tables showing the number of Mecp2 positive and negative nuclei above the overall median (B) and upper quartile (C) for Egr-1 intensity values from sections used for chi-square analysis. Chi-square statistic is derived from the expected and observed number of Mecp2 negative nuclei present. The number of observed nuclei was not different to the expected number in both cases ( $p=0.73$  for (B) and  $p=0.32$  (C), chi-square test,  $n=12$  sections from 3 mice). (Di-ii) Summary plots showing the percentage of each nuclei type above the median (Di) and in the upper quartile (Dii) Egr-1 intensity values. Data expressed as mean  $\pm$  SEM in the bar graphs. Scale bar = 25 $\mu$ m; +ve = positive nuclei and -ve = negative nuclei.

Following three hours of kainic acid application, 100% of nuclei express Egr-1 in the DG of the hippocampal formation. A high power (63x objective) image of this can be observed in Figure 6-17A. However analysis of the number of observed and expected Mecp2 negative nuclei above the median (Figure 6-17B;  $p=0.96$ , chi-square test;  $n= 12$  sections from 4 mice) or in the upper quartile (Figure 6-17C;  $p=0.84$ , chi-square test) Egr-1 intensity values showed no difference between the two. Therefore there was no significant difference in the percentage of Mecp2 positive nuclei above the median ( $47.3 \pm 1.5\%$ ) and upper quartile ( $23.7 \pm 0.8\%$ ) Egr-1 intensity values compared to Mecp2 negative nuclei ( $52.2 \pm 1.4\%$  for above the median;  $25.8 \pm 1.1\%$  in the upper quartile) (Figure 6-17Di-Dii).

**B****Top 50%**

Egr-1 Section	1	2	3	4	5	6	7	8	9	10	11	12
# of -ve nuclei above the median	37	38	20	14	189	108	97	67	23	49	31	57
# of +ve nuclei above the median	68	95	65	103	126	51	50	46	61	85	44	74
Expected (E)	40	40	18	13	182	107	86	66	21	41	29	55
(O-E)	-3	-2	2	1	7	1	11	1	2	8	2	2
(O-E) <sup>2</sup>	9	4	4	1	49	1	121	1	4	64	4	4
(O-E) <sup>2</sup> /E	0.225	0.1	0.222	0.077	0.269	0.009	1.407	0.015	0.190	1.561	0.138	0.073
Degrees of freedom	11											
Sum chi-square	4.3											
P-value	0.96											

**C****Top 25%**

Egr-1 Section	1	2	3	4	5	6	7	8	9	10	11	12
# of -ve nuclei in the upper quartile	18	22	11	8	99	62	51	36	12	25	13	29
# of +ve nuclei in the upper quartile	34	45	32	50	59	18	23	20	30	42	25	37
Expected (E)	20	20	9	7	91	53	43	33	10	21	15	28
(O-E)	-2	2	2	1	8	9	8	3	2	4	-2	1
(O-E) <sup>2</sup>	4	4	4	1	64	81	64	9	4	16	4	1
(O-E) <sup>2</sup> /E	0.2	0.2	0.444	0.143	0.703	1.528	1.488	0.273	0.4	0.762	0.267	0.036
Degrees of freedom	11											
Sum chi-square	6.4											
P-value	0.84											

**Figure 6-17 Egr-1 expression is elevated following 3 hours of kainic acid induced seizures but is not different between Mecp2 nuclei type in DG granule cell nuclei**

(A) Representative image of DG granule cell nuclei immunostained for Egr-1 and Mecp2 status displayed through fluorescence of the EGFP fusion protein following 3 hours of neuronal activity. White arrows highlight example nuclei which do not contain Mecp2 and blue arrows indicate those that do. (B-C) Tables showing the number of Mecp2 positive and negative nuclei above the overall median (B) and upper quartile (C) for Egr-1 intensity values from sections used for chi-square analysis. Chi-square statistic is derived from the expected and observed number of Mecp2 negative nuclei present. The number of observed nuclei was not different to the expected number in both cases ( $p=0.96$  for (B) and  $p=0.84$  (C), chi-square test,  $n=12$  sections from 4 mice). (Di-ii) Summary plots showing the percentage of each nuclei type above the median (Di) and in the upper quartile (Dii) Egr-1 intensity values. Data expressed as mean  $\pm$  SEM in the bar graphs. Scale bar = 25 $\mu$ m; +ve = positive nuclei and -ve = negative nuclei.

Finally, the expression of Egr1 between Mecp2 positive and negative nuclei in the CA1 following three hours of kainic acid treatment can be observed in the micrograph in Figure 6-18A. Although there was no significant difference in the observed and expected number of Mecp2 negative nuclei above the median Egr-1 intensity, (Figure 6-18B;  $p=0.17$ , chi-square test,  $n= 16$  sections from four mice) there appeared to be a trend towards less than expected nuclei as a number of sections had up to half the amount of nuclei as expected. This lower chi-square p-value gave more confidence in the trend that there was a decrease in the percentage of Mecp2 negative nuclei ( $40.8 \pm 2\%$ ) compared to Mecp2 positive nuclei ( $61.8 \pm 1.9\%$ ) however the effect could still be due to random chance as significance was not achieved (Figure 6-18Di).

Interestingly, there was a significant difference in the number of observed and expected Mecp2 negative nuclei in the upper quartile Egr-1 intensity values (Figure 6-18C;  $p=0.03$ , chi-square test). This suggest that there is a significant difference the percentage of Mecp2 negative nuclei ( $19.1 \pm 1.7\%$ ) in the upper quartile Egr1 intensity values compared to the percentage of Mecp2 positive nuclei ( $33.5 \pm 2.3\%$ ; Figure 6-18Dii).

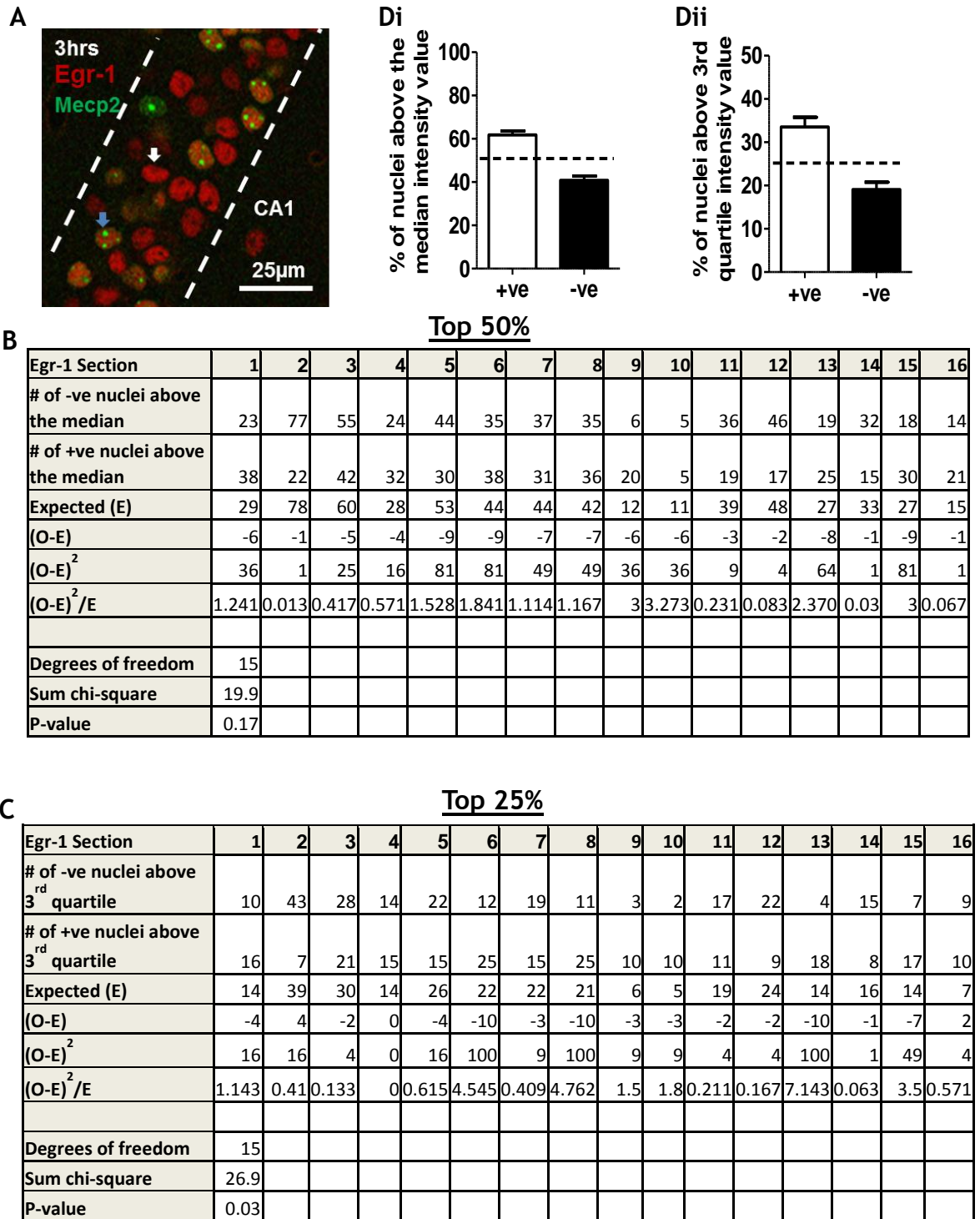


**Figure 6-18 Decreased Egr-1 levels in CA1 pyramidal cell nuclei deficient in Mecp2 following 3 hours of kainic acid administration**

(A) Representative image of CA1 pyramidal cell nuclei immunostained for Egr-1 and Mecp2 status displayed through fluorescence of the EGFP fusion protein following 3 hours of neuronal activity. White arrows highlight example nuclei which do not contain Mecp2 and blue arrows indicate those that do. (B-C) Tables showing the number of Mecp2 positive and negative nuclei above the overall median (B) and upper quartile (C) for Egr-1 intensity values from sections used for chi-square analysis. Chi-square statistic is derived from the expected and observed number of Mecp2 negative nuclei present. The number of observed nuclei was not different to the expected number above the median intensity ( $p=0.17$  chi-square test,  $n=16$  sections from 4 mice). However there was a significant difference in the number of observed and expected nuclei in the upper quartile. (Di-ii) Summary plots showing the percentage of each nuclei type above the median (Di) and in the upper quartile (Dii) Egr-1 intensity values. Data expressed as mean  $\pm$  SEM in the bar graphs. Scale bar = 25µm; +ve = positive nuclei and -ve = negative nuclei.

## 6.5 Discussion

Activity-dependent regulation of genes is important for the precise maturation and maintenance of neuronal networks in the brain during development and adulthood (reviewed by West and Greenberg, 2011). As the onset of neurological symptoms occur early (4-6 weeks) in the development of the *Mecp2* mutant male mice (Chen et al. 2001; Guy et al. 2001) and the levels of *Mecp2* increase greatly in postnatal life (Kishi and Macklis 2004; Skene et al. 2010) this would suggest an important role for MeCP2 during neuronal maturation too. Indeed recent studies show that MeCP2 may be more important in the mature nervous system rather than during neurodevelopment per se (McGraw et al., 2011; Cheval et al., 2012). *Mecp2* has been shown to be dynamically regulated by neuronal activity (Chen et al., 2003; Tao et al., 2009; Zhou et al. 2006; Chapter four) however the downstream effects of this event on gene regulation is still debatable.

Considering IEGs are induced rapidly in response to neuronal activity and regulate the transcription of genes (Herdegen and Leah, 1998), there could be an association between the activity dependent regulation of MeCP2 and IEGs in the control of gene expression during maturation. To investigate this in greater detail, I used the quantitative immunofluorescence method (explained in chapter two and five) to determine whether there were any alterations in the expression of two IEGs, c-Fos and Egr-1, between *Mecp2* positive and negative nuclei under saline control conditions and in response to neuronal activity. The results from this chapter showed there was an elevation of c-Fos levels in the entire hippocampal formation of *Mecp2*<sup>+/-</sup> heterozygous female mice following induction of neuronal activity, but no difference in the distribution of c-Fos intensities between *Mecp2* positive and negative nuclei. However there was a greater proportion of *Mecp2*-deficient nuclei expressing c-Fos under saline control conditions and following neuronal activity. This might suggest that c-Fos has a lower threshold for induction in *Mecp2*-deficient cells. In addition to c-Fos, there was also an activity-dependent increase in Egr-1 levels in the whole hippocampal formation of *Mecp2*<sup>+/-</sup> heterozygous female mice following kainic acid. However, this was accompanied by a reduction in the percentage of *Mecp2* negative nuclei in the top 25% of Egr-1 intensities in the CA1 following three hours of neuronal activity. This result suggests that Egr-1 may have a higher threshold for induction in *Mecp2*-deficient cells.

There are at least 30-40 neuronal IEG (Lanahan and Worley, 1998) which can be referred to as biomarkers of activity as they are the first response elements following neuronal activity induction into a cell with Egr-1 and c-Fos amongst the best characterised. Upon activity-dependent stimulation, c-Fos proteins dimerize with c-Jun, from Jun IEG family, and form a complex with activator protein (AP-1) transcription factor to regulate gene expression through binding promoters containing AP-1 activation elements (Halazonetis et al., 1988). In contrast, Egr-1 proteins (also known as NGFI-A, krox-24, zif268 and TIS8) are a subclass of zinc finger motif-containing proteins which act as interaction modules that bind DNA, RNA and proteins (Lemaire et al., 1988). As these two IEGs have different structural properties and DNA binding motifs it is anticipated that they will differentially regulate gene expression and potentially interact with Mecp2.

From my results I have shown that although there was no difference in the distribution of intensities of c-Fos between nuclei types (Figure 6-2 to 6-7) in the hippocampal formation, there was an increased percentage (~20%) of Mecp2 negative nuclei expressing c-Fos in the CA1 and DG under saline control conditions and following 0.5 hour of the convulsant drug kainic acid (Figure 6-8 to 6-10). These results suggest that there is an overall upregulation of c-Fos expression but no difference in c-Fos intensity between Mecp2 containing and Mecp2-deficient nuclei. Interestingly, as Mecp2 can be phosphorylated upon induction of neuronal activity and at low levels in basal conditions (Chen et al., 2003; Tao et al., 2009; Zhou et al., 2006; chapter four) there could be a link between the two whereby MeCP2 regulates the expression of c-Fos upon phosphorylation of its protein. Other studies have shown that *Mecp2*<sup>308</sup> mutant mice have normal intensity levels of c-Fos mRNA expression in the striatum following cocaine induction (Su et al., 2012). This agrees with my studies in terms of c-Fos intensity differences. Furthermore hippocampal cultures with mutations in phosphorylated S421 on Mecp2 had comparable c-Fos mRNA expression levels to WT controls in response to 55mM KCl (Zhou et al., 2006). However my study was unique in determining the differences in the number of cells expressing c-Fos suggesting that c-Fos has a lower threshold for induction in Mecp2-deficient cells.

Stimulation with kainic acid *in vivo* generates a range of epileptic seizures (Chapter three). Application of this convulsant drug to mutant mice in which *c-Fos* knocked out in the hippocampus (Tsien et al., 1996) resulted in mice displaying more severe seizures (Zhang et al., 2002). Interestingly I have shown that *Mecp2*-deficient mice also display increased severity of kainic-induced seizures (chapter three). These combined results suggest that *c-Fos* can regulate neuronal excitability and that a reduction in *c-Fos* in *Mecp2* mutant mice could contribute to the hyperexcitability phenotype observed. However, I detected the opposite in this chapter in which a greater proportion of *Mecp2*-deficient nuclei expressed *c-Fos* in the hippocampus. One explanation for this could be expression of *c-Fos* needs to be tightly regulated for the appropriate control of cellular mechanisms involved in neuronal excitability, with too much just as detrimental as too little. This could be similar to the requirement for tightly regulated MeCP2 expression with overexpression of *Mecp2* being shown to be just as detrimental as its absence (Collins et al. 2004; Na et al. 2012). Alternatively, instead of *c-Fos* contributing to the hyperexcitable phenotype, it could be the opposite in *Mecp2*-deficient mice. As the neurons are already hyperexcitable, they are more likely to respond to environmental influences. I have shown that *Mecp2*-deficient nuclei are 20% more likely to express *c-Fos* under control conditions and that this percentage difference is the same after induction of neuronal activity. Therefore there is a possibility that this increase in *c-Fos* expression is due to *Mecp2*-deficient nuclei being highly excitable and more likely to respond to subtle changes in the environment, even background activity under basal conditions.

In contrast to *c-Fos*, there was a reduction in the percentage of *Mecp2* negative nuclei in the top 25% of *Egr-1* intensities in the CA1 following three hours of neuronal activity (Figure 6-17) but not at any other time point (Figure 6-12 to 6-16). This suggests that following neuronal activity, *Egr-1* expression in *Mecp2*-deficient nuclei becomes desensitized. As with *c-Fos*, there could be a link between phosphorylation of MeCP2 and regulation of *Egr-1* levels, except instead of increasing levels under WT conditions, there is a decrease in *Egr-1* protein in nuclei deficient in MeCP2. Interestingly a recent study has highlighted the type of phosphorylation of *Mecp2* and exact gene being studied are important for determining whether *Mecp2* acts as a repressor or activator of gene transcription

(Gonzales et al., 2012). This could be the case here whereby MeCP2 phosphorylation could activate Egr-1 expression but repress c-Fos in response to neuronal activity. A study has shown that another member of the IEG Egr family, Egr-2, displays reduced protein expression levels in the cortex of *Mecp2*-deficient mice, cultured human neuroblastoma cells in which MeCP2 is knocked down by RNA interference and in RTT post-mortem cortex samples (Swanberg et al., 2009). This suggests a dysregulation in the expression of Egr-1 and Egr-2 may be a common feature in MeCP2-deficient cells.

Egr-1 also has high basal expression in the hippocampus (Waters et al., 1990) especially in the CA1 region of *Mecp2*<sup>+/-</sup> heterozygous female mice (Figure 6-10 and Figure 6-13) which is likely due to on-going synaptic input in the brain (Worley et al., 1991). This expression can be abolished by NMDA receptor antagonists (Worley et al., 1991) and L-type voltage-gated calcium channel antagonists (Murphy et al., 1991). These studies suggest that basal levels of Egr-1 expression could be maintained by synaptic plasticity as the above receptors are key components in this physiological event. Furthermore there is an increase in Egr-1 expression following induction of LTP in the hippocampus (Cole et al. 1989; Wisden et al. 1990). As *Mecp2*-deficient mice have been shown to have an impairment in LTP in the hippocampus (Moretti et al. 2006; Weng et al. 2011), the decrease I observed in Egr-1 expression in the CA1 following induction of neuronal activity would be consistent with this model.

In conclusion I have shown that there is a dysregulation in the expression of two IEGs, c-Fos and Egr-1, in the hippocampal formation within *Mecp2*-deficient nuclei. These effects could be correlated to alterations in activity-dependent phosphorylation of *Mecp2*. Further experiments immunostaining for the effects of phosphorylated *Mecp2* in the hippocampus of *Mecp2*<sup>+/-</sup> heterozygous female mice would enable a more direct association to be made between IEGs. However my results could also be secondary to the hyperexcitability or LTP defects seen in *Mecp2*-deficient neurons. Either way, my results show that there are alterations in neuronal activity and IEG protein expression in *Mecp2*-deficient neurons. Importantly, the strength, stimulus type (Hardingham, Fukunaga, and Bading 2002; Traverse et al. 1994), structural DNA binding properties of each IEG and cell type will all contribute to the cellular

response generated and functional consequences of the absence of MeCP2 from cells.

## Chapter 7

### General discussion

#### 7.1 Major and novel findings

The general theme of this project was to examine how the presence or absence of MeCP2 affects neuronal activity and how in turn neuronal activity affects MeCP2 actions. For this I chose to focus my attention on aspects of hyperexcitability (epileptiform activity) and how neuronal activity can influence post translational modifications of MeCP2 and histone acetylation. Whilst many of my results were negative, this thesis nevertheless gives important novel insights into a number of areas.

##### 7.1.1 Reduced seizure threshold and altered oscillatory properties in *Mecp2* knockout mice

In Chapter three the major and novel findings I report are a reduction in seizure threshold and an increase in the power of gamma oscillations in *Mecp2*-deficient mice. Seizures are a major RTT phenotype (Glaze et al., 2010), and are a feature of mice models overexpressing *Mecp2* (Collins et al., 2004) and those with a truncated *Mecp2* mutation (Shahbazian et al., 2002). Constitutive knockout mice models of *Mecp2* do not express an overt epileptic phenotype, displaying only a slight tremor that increases in severity with age (Chen et al. 2001; Guy et al. 2001). This is also true of the functional knockout model I used in my epileptic studies (Guy et al., 2007). Few other studies have investigated, in a systematic way, the changes behind generation of seizures *in vivo* using mouse models of RTT. Therefore, my experiments in which I applied the convulsant drug kainic acid to mice deficient in *Mecp2* and their WT littermates to investigate, in quantitative terms, their epileptic phenotype was unique. I discovered that *Mecp2*<sup>stop/y</sup> mice display a more severe seizure score and have a quicker onset of seizures compared to their WT littermates. This is consistent with a lack of functional *Mecp2* resulting in a compromised nervous system that is predisposed to seizure generation. Furthermore, this phenotype was supported by observed increases in frequency of spontaneous epileptiform

field events and longer duration of evoked field potentials in *Mecp2*<sup>stop/y</sup> mice following application of bicuculline *in vitro* to hippocampal slices. Collectively, these results imply that *Mecp2* mutant mice have an inherent reduced epileptiform threshold which contributes to an increased susceptibility to seizure generation.

Application of kainic acid *in vivo* is commonly considered a model for temporal lobe epilepsy (Nadler, 1981). In contrast, application of kainic acid to hippocampal slices *in vitro* produces rhythmic gamma frequency oscillations consistent with normal physiological hippocampal rhythms (Fisahn, 2005). Gamma rhythms are present during waking and sleeping states and are important for timing of action potential firing in the brain. In my studies, I found that mice deficient in *Mecp2* display a more powerful (high power) gamma oscillation in the presence of kainic acid compared to WT controls. Normal generation and maintenance of physiological gamma rhythm is highly dependent on inhibitory neurotransmission (GABA mediated) in the brain, namely fast spiking interneurons (Hasenstaub et al., 2005; Whittington et al., 1995). Furthermore, a recent study has shown that axo-axonic cells are important in generating tonic levels of inhibition during gamma activity (Dugladze et al., 2012). Most intrinsic properties of principal cells in the hippocampus/cortex of *Mecp2*-deficient mice are reported to be normal (Dani et al., 2005; Wood et al., 2009; Zhang et al., 2008). This is consistent with the fact that I observed no difference in the frequency of gamma oscillations in my studies. However, other studies have shown alterations in GABAergic release and kinetics (Chao et al., 2010; Medrihan et al., 2008). Whatever the case, the heightened gamma power may be indicative of a hippocampal network brought closer to a pathological network hyperexcitability/hypersynchrony threshold by MeCP2 deficiency.

### **7.1.2 No alteration in histone protein levels in *Mecp2* positive and negative neurons in the *Mecp2*<sup>+/-</sup> mosaic brain.**

In Chapters four and five, I demonstrated that phosphorylation of *Mecp2* is not associated with alterations in histone acetylation levels following induction of neuronal activity. To understand the alterations in network excitability I observed in *Mecp2*-deficient mice further, I wanted to investigate the molecular

pathways associated with MeCP2 function that could contribute to this dysfunction. Acetylation sites on histone proteins have been shown to be amenable to alterations in neuronal activity (reviewed by Riccio, 2010). Furthermore, an increase in H3Ac was detected in whole brains from *Mecp2*-deficient mice compared to WT controls under basal conditions suggesting that the effects of *Mecp2* are more global (Skene et al., 2010). However I was never able to replicate this finding using either a western blot approach or a quantitative immunostaining method. By using whole brains to do their analysis, Skene et al could have been picking up a variety of cell types in which some possibly non-neuronal populations had big changes in histone acetylation. My results showed no difference in histone acetylation between *Mecp2* containing and *Mecp2*-deficient neurons in saline control conditions and following induction of activity. This could reflect alterations in histone acetylation that are specific to regions of the brain or MeCP2 mutation type. For example an increase in acetylation at specifically histone H3 lysine 9 from nuclei in the cerebral cortex of *Mecp2*<sup>-/y</sup> mice has been reported (Thatcher and LaSalle, 2006) but no difference in H3Ac (lysine 9 and 14) were seen in cell cultures from RTT patients with truncated mutations (Wan et al., 2001). Furthermore there could possibly be adaptive mechanisms compensating for deficiencies in MeCP2.

The effect of MeCP2 deficiency on histone acetylation could also be influenced by non-cell autonomous effects, in which cells negative for MeCP2 can have deleterious effects on neighbouring MeCP2 positive cells. This has been shown to occur in cortical pyramidal neurons in WT mice transfected with *Mecp2*<sup>-y</sup> cortical neuroblasts (Kishi and Macklis, 2010), with these cells displaying deficits in dendritic arborization. Glial cells deficient in MeCP2 have also been shown to display a non-cell autonomous trait in which *Mecp2*-deficient glial cells were unable to support the growth of WT neurons (Ballas et al., 2009; Maezawa and Jin, 2010). However, in this study I observed cell-autonomous effects in the hippocampus of *Mecp2*<sup>+/-</sup> heterozygous mice in which I document a robust and reliable reduction in nuclear volume in cells that lack *Mecp2*. Although this has been documented in the hippocampus of *Mecp2*-deficient mice (Giacometti et al. 2007; Johnson et al. 2011; Yazdani et al. 2012) and in neurons of the locus ceruleus of *Mecp2*<sup>+/-</sup> heterozygous mice (Taneja et al., 2009), this has never been shown in the hippocampal formation in these mice. These effects

argue against a role for non-cell autonomous effects of MeCP2. Overall, the quantitative immunofluorescence approach I used to study the effect of MeCP2 on histone acetylation levels was unique and sensitive enough to determine subtle changes in histone levels. My results are predominantly negative findings but are nevertheless important as they help to rule out particular mechanisms and models of MeCP2 function. Furthermore no other study has attempted to see whether neuronal activity affects the levels of histone acetylation in *Mecp2*-deficient mice.

### **7.1.3 Altered regulation of immediate early gene levels in neurons deficient in *Mecp2* in the *Mecp2*<sup>+/-</sup> mosaic brain**

In Chapter six I demonstrated that at the cellular level, neurons deficient in *Mecp2* in the *Mecp2*<sup>+/-</sup> mosaic brain have a greater proportion of nuclei containing the immediate early gene (IEG) c-Fos under basal conditions. Furthermore *Mecp2* negative nuclei display a reduction in the levels of another IEG, Egr-1, in the CA1 of the hippocampal formation following kainic acid administration. These results suggest c-Fos and Egr-1 have differential threshold levels for induction in *Mecp2*-deficient cells. Activity-dependent changes in gene expression in response to external stimuli are important for normal development and function of the maturing nervous system (Dragunow et al. 2000; Marek et al., 2010; West and Greenberg, 2011). Therefore, as I observed an increase in the excitability of hippocampal neurons deficient in *Mecp2* in my physiology studies, this could result in or be the result of a dysfunction in the regulation of gene expression. IEGs are nuclear transcription factors which are usually the first response elements induced following neuronal activity and are thus useful targets to test this hypothesis. Additionally, few studies have defined the behaviour of these genes in RTT or *Mecp2* knockout mice.

My results are the first to document alterations in c-Fos and Egr-1 in the hippocampal formation of *Mecp2*<sup>+/-</sup> heterozygous mice. C-Fos and Egr-1 have differential structural properties and binding motifs (Halazonetis et al., 1988; Lemaire et al., 1988) which could explain why there is an increase in c-Fos but a decrease in Egr-1. Furthermore, I have shown in Chapter four, *Mecp2* can become phosphorylated in response to the convulsant drug kainic acid. This is in agreement with previous studies (Chen et al., 2003; Tao et al., 2009;

Zhou et al., 2006) and may represent a link between phosphorylation of MeCP2 and regulation of IEGs, in a similar manner to the transcription of c-Fos in response to activity induced CREB phosphorylation (Greenberg et al., 1986). Potentially, phosphorylation of MeCP2 interacts with various transcription factors and result in the regulated expression of genes in in a manner dependent on the specific gene and the region of the brain/cell involved.

## 7.2 Significance of this study

My physiology experiments are significant because the *in vivo* kainic acid seizure model could be beneficial in future studies to test novel pharmacological and genetic approach therapies in RTT. Reversal of the symptoms of RTT was first established in 2007 (Guy et al., 2007) and other groups since then have tried to improve the phenotypes of RTT by numerous means (Derecki et al., 2012; Gadalla et al., 2011; Liroy et al., 2011; Tropea et al., 2009; Weng et al., 2011). A common requirement of these phenotype reversal studies is the need to validate successful symptom reversal, including in the epilepsy domain. My *in vivo* kainic acid seizure model is a quantitative behavioural assay of hypersensitivity to drug-induced epilepsy which produces a distinctive phenotype and could be used to establish the extent of symptom rescue.

The reduction in seizure threshold and increased oscillatory activity observed in *Mecp2* mutant mice in my study are important because they help to clarify the underlying features leading to a disruption in network excitability in this disease model. A particularly surprising finding is that intrinsic excitability of pyramidal neurons is relatively unaltered (Dani et al., 2005; Wood et al., 2009; Zhang et al., 2008) whereas at the network level aberrant excitability is very clear. It is possible that this results from altered synaptic balance or structural changes at the level of the network. The dysfunction in IEG regulation and lack of histone acetylation following neuronal activity provides greater detail as to the effects of MeCP2 deficiency at the cellular level. My histone acetylation results, whilst predominantly negative, are nevertheless important as they help to rule out particular mechanisms and models of MeCP2 function. The differential alterations in IEGs in *Mecp2*-deficient mice I report could also suggest a more gene specific role for MeCP2.

Additionally, the effects I observed using a mouse model of RTT could potentially transfer to other neurodevelopmental disorders. External stimuli in the brain following birth is important for neurite outgrowth, synapse formation and elimination to create an accurate balance of inhibitory and excitatory synapses in the adult brain (reviewed by West and Greenberg, 2011). Interestingly, a vast number of other neurodevelopmental disorders have deficits during neuronal maturation including disorders such as Fragile-X syndrome (FRAX; 300624) and Angelman syndrome (AS; OMIM 105830). Furthermore these two disorders are the result of mutations in genes involved in epigenetic mechanisms. FRAX results from DNA methylation of an expanded CGC sequence within the *FMR1* gene. This gene encodes for the fragile-X mental retardation protein, FMRP on the X chromosome (Sutcliffe et al., 1992). Most cases of AS are caused by deletions in an imprinted gene, *Ube3A* on the maternal allele (Matsuura et al., 1997). Normally genomic imprinting requires DNA methylation and histone modifications to silence the expression of a gene on one paternal or maternal allele. FRAX, AS and RTT also exhibit similar phenotypes such as a dendritic spine loss and abnormalities (reviewed by Fiala et al., 2002). The commonalities between these disorders suggest a link between the pathology of these disorders whereby information gained on one could translocate to another.

### 7.3 Technical considerations and future studies

There are some technical considerations that need to be addressed from the experiments conducted in this thesis which would be incorporated into future studies. Firstly, a negative effect of using the convulsant drug kainic acid to induce epilepsy is cell death in the hippocampal formation (Sperk et al., 1983b) which could potentially complicate the analysis of my physiology and immunohistochemistry work. To minimise this occurrence, the strain of mice used in all experiments were on a C57BL/6 background strain which display a higher resistance to neuronal death (Schauwecker and Steward, 1997). Secondly, the ages of male mice used in all physiology experiments in chapter three were symptomatic for RTT phenotypes making it more complex to decipher whether the deficits I observe are the cause directly by *Mecp2* deficiency or are secondary pathological changes. Future experiments that could aid clarification of this would be to repeat the experiments in pre-symptomatic mice *Mecp2* knockout male and *Mecp2*<sup>+/-</sup> heterozygous mice. However, I did observe an

increase in seizure severity to kainic acid induced seizures in pre-symptomatic *Mecp2*<sup>+/-</sup> heterozygous mice giving an indication that the effects would also be present earlier in development.

Thirdly, an issue with the automated script developed to determine differences in IEG and acetylated histone proteins levels between *Mecp2* positive and negative nuclei in *Mecp2*<sup>+/-</sup> heterozygous mice was that it did not automatically count the total number of nuclei that were in an optical image stack therefore some analysis had to be quantified manually. To minimise human error, in future it would be better to redesign the script to include this function allowing the process to be fully automated. Fourthly, a variety of studies investigating the role of histone acetylation administer histone deacetylase inhibitors in the first instance. I added the histone deacetylase inhibitor sodium butyrate to my nuclear preparation; however this might not have been the most optimal method. Studies have shown that intraperitoneal injection of the histone deacetylase inhibitor trichostatin A (TSA) prior to kainic acid, can lead to an increase in acetylated histone levels (Sng et al., 2005). In future experiments, incorporating this into the protocol could make it easier to decipher differences in histone acetylation between *Mecp2* positive and negative nuclei if there was a more pronounced increase present from the start.

Other studies that could also be conducted to build upon the findings of this thesis include the specification of which neuronal types in the hippocampal formation contribute to the deficits I observe. For example in chapter three, altering the input of inhibitory neurotransmission when conducting kainic acid experiments *in vitro* will help clarify the mechanisms involved in the enhanced gamma oscillations in *Mecp2*-deficient mice. Furthermore, in my quantification of IEG and histone acetylation levels in nuclei in chapter five and six, it would be interesting to determine whether the effects observed are specific to neuronal subtypes or if glia cells are involved. Immunostaining for these cell types in the hippocampus and in other brain regions could answer this question. Immunostaining for phosphorylated *Mecp2* proteins in *Mecp2*<sup>+/-</sup> heterozygous female mice would also enable a better association between IEG regulation and MeCP2 phosphorylation following induction of neuronal activity into cells.

Finally conducting experiments using an animal model in which *Mecp2* is conditionally knocked down (Cheval et al., 2012) will enable the role of *Mecp2* in the regulation of activity-dependent gene expression to be assessed at different developmental stages. A related question is whether the germline knockout mouse models of *Mecp2* are masking possible effects in histone acetylation due to possible adaptive mechanism present. Rapid inactivation or knockdown of *Mecp2* might reveal undiscovered associations between presence/absence of *Mecp2* and histone acetylation.

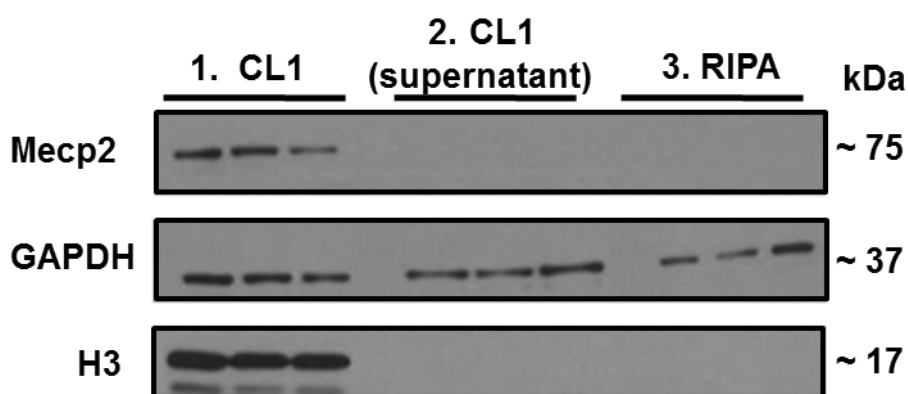
## 7.4 Summary

Focussing on the hippocampus, the aim of this thesis was to investigate the role of MeCP2 in activity-dependent brain processes. At the network level I have shown that lack of *Mecp2* leads to a reduction in seizure threshold and enhancement in the power of gamma frequency network oscillations thus altering network level excitability in the brain to promote epileptogenesis. At the molecular level, I demonstrate that *Mecp2* can become phosphorylated following the induction of neuronal activity using the convulsant drug kainic acid and that this is not associated with global alterations in histone acetylation. However, I do report a reduction in nuclear volume and alterations in the levels of two IEGs, c-Fos and Egr-1, in *Mecp2*-deficient nuclei from *Mecp2*<sup>+/-</sup> heterozygous mice. These results propose a cell-autonomous role for *Mecp2* and the activity-dependent control *Mecp2* exerts on gene transcription. Overall, I believe my work contributes to the understanding of how neuronal activity affects the function of MeCP2 in neurons at the network and cellular levels thus providing further insight in to the pathogenesis of RTT.

## Appendix A

### Cell lysate preparation optimisation

Three cell lysate techniques were optimised to decipher which method gave a clear nuclear protein expression for western blot experiments. The decision to proceed with homogenising hippocampal tissue in a cell lysate buffer (CL1) in which none of the tissue was discarded from the final product was taken as the other two methods (CL1 supernatant and RIPA) resulted in an absence of nuclear proteins Mecp2 and total histone H3 (see Supplementary Figure 1-1 below).



#### Supplementary Figure 1-1 Comparison of three cell lysate methods for western blot analysis

Representative western blots comparing three nuclear extract techniques 1. Hippocampal tissue is homogenised in a cell lysate buffer (CL1) in which none of the tissue is discarded from the final product. 2. Hippocampal tissue is homogenised in the same CL1 buffer but the samples are spun down (13000rpm for 5 minutes at 4°C) and the supernatant tissue used for western blot analysis (CL1 supernatant). 3. Hippocampal tissue is homogenised in a different nuclear extract buffer (50mM TRIS, 150mM NaCl, 1% IGEPAL, 0.5% Triton-X-100 and 0.1% SDS) with the samples then spun down and the protein supernatant tissue used for western blot analysis (RIPA). The loading control GAPDH is present in all three methods but Mecp2 and total histone H3 (H3) are only observed in the CL1 method.

## Appendix B

### Automated Script

An annotated automated script developed by Dr David Kelly at the University of Edinburgh for quantifying cell intensity differences between Mecp2 positive and negative nuclei in Chapters four and five can be observed below.

```
Option Explicit
Public RedId As Integer, GreenId As Integer, DAPIId As Integer, DAPIBinary As Integer
Public DAPIMaskId(200) As Integer
Public TotalCount As Integer, RowCount As Integer, pos As Integer
Public seqinfo As Long
Public GetTheVal As String
Public NObjects As Double

'*****
'*****
'*****
'***      Macro Written For Use In Image Pro Plus 7.0.1.658 with 3D Constructor
'***      Author David Kelly
'***      Final Version 8-11-2011
'***
'***      DESCRIPTION
'***
'***      Takes 3 colour Z stack Leica .lif images. Turns Dapi image into a 3D thresholded binary mask, the mask is applied
'***      to the green (GFP) image to check for the presence/absence of GFP labelling. The masks are used because its far
'***      easier to threshold a 2D image.
'***
'***      The DAPI mask is then applied to the red image to measure total intensity of red within single cells.
'***      All results are then passed to Excel for later analysis.
'*****
'*****
Sub StartHere()
'*****
'*      Starting point of the macro, Each command calls a different subroutine in the correct order
'*****
IdImages                                'Subroutine to identify which image is which

MakeDAPIMask                            'Subroutine to make 3D Dapi mask count number of nuclei

MakeMeasurements                        'Main measurement subroutine for volume, intensity and colocalisation

ret = MsgBox("Macro Finished")          'Lets user know that macro has finished

End Sub

Sub IdImages()
```

```

*****
'*      Instructs user to open and image and then to manually click on each image in turn to
'*      identify which channel is which
*****

ret = MsgBox("Open Image")
ret = MsgBox("Select Red Image")
ret = IpDocGet(GETACTDOC, 0, RedId)           'Assigns red image id to variable for later use
ret = MsgBox("Select Green Image")
ret = IpDocGet(GETACTDOC, 0, GreenId)        'Assigns green image id to variable for later use
ret = MsgBox("Select DAPI Image")
ret = IpDocGet(GETACTDOC, 0, DAPIId)        'Assigns blue image id to variable for later use
ret = MsgBox("Make Sure Excel is Open")     'Warning for user to open up Excel

End Sub
Sub MakeDAPIMask()

Dim FromVal As Single, ToVal As Single, MaxIntensity(10) As Single
Dim x As Integer, RedBinaryTemp As Integer, TempNum As Integer

*****
'*      User thresholds the blue (DAPI) intensity image to highlight the whole cell nucleus, cells/objects
'*      which fall below the size threshold are excluded from any measurements. Objects are split using the
'*      watershed split function and any undersize objects ignored. A binary mask is then created for each
'*      layer in the Z stack and combined into a binary copy of the original with only the nuclei selected.
*****

ret = IpAppSelectDoc(DAPIId)
ret = IpSeqGet(SEQ_NUMFRAMES, seqinfo)
ret = IpSMPlay(0)
ret = IpSeqPlay(0)
ret = IpBlbSetAttr(BLOB_FILLHOLES,1)

**      Section to subtract Background from blue intensity image using an area
**      of the image with no objects in it on any z plane.

ret = IpBlbEnableMeas(BLBM_DENSITY, 1)       'Enable mean intensity
ret = IpBlbEnableMeas(BLBM_DENSMAX, 1)      'Enable max intensity
ret = IpAoiShow(FRAME_RECTANGLE)           'Show rectangle AOI
ret = MsgBox("Draw AOI to area not containing a DAPI nucleus") 'Prompt for user to draw region on area of background
ret = IpSegSetRange(0, 0, 4095)            'Set threshold to entire range
ret = IpSegPreview(CURRENT_C_T)
ipICal(0) = 0
ipICal(1) = 4095
ret = IpBlbMultiRanges(ipICal(0), 1)
ret = IpBlbCount()                         'Measure intensity
ret = IpBlbUpdate(0)
ret = IpBlbData(BLBM_DENSMAX, 0, 0, MaxIntensity(0)) 'Retrieve Max intensity value
ret = IpAoiShow(FRAME_NONE)               'Remove AOI
ret = IpBlbDelete()                       'Delete intensity measurement from count size dialogue

```

```

ret = IpOpNumberArithmetics(MaxIntensity(0), OPA_SUB, 1)          'Subtract Max BkGrd intensity from Dapi image
ret = IpDocGet(GETACTDOC, 0, TempNum)
ret = IpAppSelectDoc(DAPIId)
ret = IpDocClose()                                             'Close original DAPI image as its now useless.
DAPIId = TempNum

***      Section to make binary image from BkGrd
***      subtracted dapi image

ret = IpAppSelectDoc(DAPIId)                                  'Application selects Dapi Image
ret = MsgBox("Draw region around cells of interest")          'Draw a region around a subset of cells as image too big to
                                                                process as a whole

ret = IpSegShow(1)
ret = MsgBox("Threshold the DAPI Image")                      'User prompt to threshold the image
ret = IpSegGetRange(0, FromVal, ToVal)                        'Gets the threshold values to apply to each plane in image
ipICal(0) = FromVal
ipICal(1) = ToVal
ret = IpBlbMultiRanges(ipICal(0), 1)
ret = IpSegShow(0)

*        Loop 1 to identify cells based on intensity in each layer
*        and then produce a binary from each layer
For x = 0 To seqinfo -1
    ret = IpAppSelectDoc(DAPIId)
    ret = IpSMPlay(x)
    ret = IpSeqPlay(x)
    ret = IpBlbCount()
    ret = IpBlbUpdate(0)
    ret = IpBlbSplitObjects(1)
    ret = IpBlbSetFilterRange(BLBM_AREA, 55.43291855, 10000000.0) 'Sets filter range to stop too small objects from
                                                                    being counted.
    ret = IpBlbCreateMask()
    ret = IpDocGet(GETACTDOC, 0, DAPIMaskId(x))
Next x

*        Loop 2 Takes all the binaries created in loop 1 and
*        re-assembles the z stack made of binaries
For x = 1 To seqinfo -1
    ret = IpAppSelectDoc(DAPIMaskId(0))
    ret = IpSeqMergeDoc(DAPIMaskId(x), 0, -1)
Next x

ret = IpSCalSetLong(0, SCAL_UNIT_CONVERT, 1)
ret = IpSCalSetUnitName("um")                                'Sets the units to microns instead of the default nm
ret = IpSCalSetLong(SCAL_CURRENT_CAL, SCAL_APPLY, 0)
ret = IpPcTint(TINT_BLUE)                                    'Applies blue tint to binary
ret = IpDocGet(GETACTDOC, 0, DAPIBinary)                      'Assigns the binary image id to variable for later use

* Loop 3 closes all the single binaries made by loop 1      *
* which are no longer need to free up system memory        *
For x = 1 To seqinfo -1

```

```

        ret = IpAppSelectDoc(DAPIMaskId(x))
        ret = IpDocClose()
    Next x
End Sub
Sub MakeMeasurements

    Dim x As Integer, y As Integer, SingleDAPIBinary As Integer
    Dim Filesave As String, Answer As String
    Dim MeanIntensity(10) As Single, TotalMean As Single
    Dim Count As Integer, MeanCount As Integer

    '*****
    '**      Sub-routine makes a 3D image using the dapi binary created in MakeDapiMask. The 3D image      **
    '**      is watershed split to separate any touching objects, objects which are too firmly joined      **
    '**      and can't be separated have to be ignored using the object size filters. A single cell      **
    '**      is extracted from the 3D image and compared slice by slice with the exact same position      **
    '**      in the green image to see if any GFP was present in the cell. 3 consecutive GFP positive      **
    '**      slices counts as colocalised. The individual cells are then labelled as colocalised (GFP      **
    '**      positive) or non-colocalised (GFP negative). The extracted single dapi nucleus is then      **
    '**      applied slice by slice to the red image to get the total red intensity for that cell.      **
    '*****

    '**      Load DAPI binary stack into 3d Constructor      **
    ret = IpRendShow(REND_OPTIONS,REND_HIDE)
    ret = IpRendSet(REND_VOXELSIZE, 0.480000, 0.480000, 0.250000)      'Set voxel size
    ret = IpRendSet(REND_SUBSAMPLING, 1, 1, 1)
    ret = IpRendSet(REND_ACTIVE_PORTION, 1, 0, 0)
    ret = IpRendSet(REND_HI_COLOR, 0, 0, 0)
    ret = IpRendSet(REND_RESET_OPTIONS, 0, 0, 0)
    ret = IpRendLoad()

    '***      Make 3D volume image of DAPI Binary Stack Image      ****
    ret = IpAppSelectDoc(DAPIBinary)      'Select Dapi Binary Stack
    ret = IpRendSet(REND_ISO_SUBSAMPLING, 1, 1, 1)      'Turn off subsampling to increase accuracy
    ret = IpRendSet(REND_ISO_FILTER, FLT_3D_None, 0, 0)      'Set No Filtering
    ret = IpRendSet(REND_ISO_CLOSE_EDGES, 0, 0, 0)
    ret = IpRendSet(REND_ISO_COUNT, 1, 0, 0)
    ret = IpRendSet(REND_ISO_SIMPL, ISO_SIMPL_NONE, 0, 0)      'No Simplification
    ret = IpRendElem(ELEM_ADD,IP_REND_ISO_SURF,0,IPNULL)
    ret = IpRendElemSet(ELEM_ISO_LEVEL,IP_REND_ISO_SURF,0,250.000000)      'Set Iso-Surface
    ipDArray(0)=150.000000      'Lower Volume Limit
    ipDArray(1)=500.000000      'Upper Volume Limit
    ret = IpRendVMeas(M_FILTER_RANGES_SET,IVM_SurfVolume,ipDArray(0))
    ret = IpRendVMeasSet(M_UPDATE,0,0)
    ret = IpDcSelect("3D_Vol_Measurements", "IVM_SurfVolume", 1)      'Turn on Cell Volume Measurement

    ret = IpFlt3DWatershed(127.500000,-1,0)      'Watershed split joined objects
    ret = IpRendSet(REND_VOXELSIZE, 0.480000, 0.480000, 0.250000)      'Set voxel size
    ret = IpRendSet(REND_SUBSAMPLING, 1, 1, 1)      'Turn off subsampling to increase accuracy

```

```

ret = IpRendSet(REND_ACTIVE_PORTION, 1, 0, 0)
ret = IpRendSet(REND_HI_COLOR, 0, 0, 0)
ret = IpRendSet(REND_RESET_OPTIONS, 0, 0, 0)
ret = IpRendReload() 'Load image into 3D Constructor

ret = IpRendVMeas(M_NUM_OBJECTS_GET,0,NObjects) 'Gets number of Objects in the 3D data table from dapi image

ReDim TheVol(NObjects) As Double
ReDim ReportVol(NObjects) As Double
ReDim CellType(NObjects) As String
ReDim TheMean (NObjects) As Single

*** For Loop Iterates through every identified Dapi nucleus and extracts it to a single 1 cell image
*** Each Nuclear outline applied to green to check if colocalised (ie GFP positive)
*** Each Nuclear Outline used to measure intensity in Red image

ret = IpBlbSetAttr(BLOB_AUTORANGE, 1) 'Set measurements to Bright Objects
ret = IpBlbSetAttr(BLOB_BRIGHTOBJ, 1)
ret = IpBlbEnableMeas(BLBM_DENSITY, 1) 'Enable intensity measurements
For x = 0 To NObjects -1
    ret = IpRendVMeasSet(M_SEL_SET,x,1) 'Selects the next measurement in the 3D data table list
    ret = IpRendVMeasSet(M_SHOW_SELECTED,0,1) 'Show only selected volume measurements
    Answer = InputBox("Is Cell OK y/n","Cell Check","y")
    If Answer = "y" Then
        ret = IpRendVMeasSet(M_CREATE_MASK_IMAGE,0,0) 'Create a binary mask of that selected volume
        ret = IpDocGet(GETACTDOC, 0, SingleDAPIBinary) 'Get ID of the cells mask image so that it can be
        applied to others
        ret = IpSMPlay(0) 'Select First position in stack
        ret = IpSeqPlay(0)
        'Loop to produce outlines from cell selected from 3D volume
        For y = 0 To seqinfo -1
            ret = IpBlbCount()
            ret = IpBlbUpdate(0)
            ret = IpSeqPlay(SEQ_NEXT)
            ret = IpBlbCount()
            ret = IpBlbUpdate(0)
            Filesave = "C:\Temp\Data_" + CStr(y) + ".scl"
            ret = IpBlbSaveOutline(Filesave)
        Next y
        'Loop applies the outline from the dapi to the green image to check for co-localisation
        ret = IpAppSelectDoc(GreenId) 'Select Green Image Stack
        Count = 0
        For y = 0 To seqinfo -1
            ret = IpSMPlay(y) 'Select First position in stack
            ret = IpSeqPlay(y)
            Filesave = "C:\Temp\Data_" + CStr(y) + ".scl"
            ret = IpBlbLoadOutline(Filesave)
            ret = IpBlbData(BLBM_DENSITY, 0, 0, MeanIntensity(0)) 'Retrieve Mean intensity value

```

```

If MeanIntensity(0) > 750 Then 'Sets mean intensity for cell to be considered colocalised
    Count = Count + 1
    If Count = 3 Then
        CellType(x) = "Colocalised"
    End If
End If
If y = seqinfo -2 And Count < 3 Then
    CellType(x) = "Non-Colocalised"
End If
ret = IpBlbDelete
MeanIntensity(0) = 0
Next y

ret = IpAppSelectDoc(RedId) 'Select Red Image Stack
MeanCount = 0
For y = 0 To seqinfo -1
    ret = IpSMPlay(y) 'Select First position in stack
    ret = IpSeqPlay(y)
    Filesave = "C:\Temp\Data_" + CStr(y) + ".scl"
    ret = IpBlbLoadOutline(Filesave)
    ret = IpBlbData(BLBM_DENSITY, 0, 0, MeanIntensity(0)) 'Retrieve Mean intensity value
    If MeanIntensity(0) > 0 Then
        MeanCount = MeanCount + 1
        TotalMean = TotalMean + MeanIntensity(0)
    End If
    ret = IpBlbDelete
    MeanIntensity(0) = 0
Next y
If TotalMean > 0 Then
    TheMean(x) = TotalMean/MeanCount
End If
TotalMean = 0
ret = IpRendVMeas(M_MEAS_GET, IVM_SurfVolume, TheVol(0))
ReportVol(x) = TheVol(x) 'Gets cell volume for measured cell
ret = IpAppSelectDoc(SingleDAPIBinary)
ret = IpDocClose() 'Closes the image of the single dapi labelled cell
End If

ret = IpRendVMeasSet(M_SHOW_ALL,0,0)
ret = IpRendVMeasSet(M_SEL_SET,x,0) 'Selects the next measurement in the 3D data table list

Next x
ret = IpRendElem(ELEM_DELETE,IP_REND_ISO_SURF,0,IPNULL) 'Delete volume measurement 1 at end of macro run
ret = IpRendElem(ELEM_DELETE,IP_REND_ISO_SURF,1,IPNULL) 'Delete volume measurement 2 at end of macro run
DDE(ReportVol,CellType,TheMean) 'Send data to DDE module for export to excel
End Sub

Sub DDE(ReportVol,CellType,TheMean)
Dim x As Integer

```

```

*****

```

```

** Sub-routine to take all the outputs from MakeMeasurements such as cell volume, whether

```

```

**      or not its GFP positive and the cells red intensity measurement and sends it to Excel
**      so that the user can analyse the numbers.
*****

ret = IpDde(DDE_OPEN, "excel", "sheet1")           'Opens Sheet1 within excel
RowCount = 2

DoEvents

'Loop iterates through the array variables passed from MakeMeasurements
'so that each extracted cell measurements are applied to the correct cell
For x = 0 To NObjects - 1
    GetTheVal = "R" + CStr(RowCount) + "C1"
    ret = IpDde(DDE_PUT, GetTheVal, CStr(x))        'Cell Number
    GetTheVal = "R" + CStr(RowCount) + "C2"
    ret = IpDde(DDE_PUT, GetTheVal, CStr(TheMean(x))) 'Mean Red intensity
    GetTheVal = "R" + CStr(RowCount) + "C3"
    ret = IpDde(DDE_PUT, GetTheVal, CStr(ReportVol(x))) 'Cell Volume
    GetTheVal = "R" + CStr(RowCount) + "C4"
    ret = IpDde(DDE_PUT, GetTheVal, CStr(CellType(x))) 'GFP positive/Negative
    RowCount = RowCount + 1
Next x

DoEvents

'Section sets the column labels so user can identify measurements
ret = IpDde(DDE_PUT, "R1C1", "Measurement Number")
ret = IpDde(DDE_PUT, "R1C2", "Mean Intensity")
ret = IpDde(DDE_PUT, "R1C3", "Cell Volume")
ret = IpDde(DDE_PUT, "R1C4", "Status")
ret = IpRendVMeasSet(M_SHOW_ALL,0,0)              'Show All Volume Measurements

End Sub

```

## References

- Adachi M, Autry AE, Covington HE, Monteggia LM (2009) MeCP2-mediated transcription repression in the basolateral amygdala may underlie heightened anxiety in a mouse model of Rett syndrome. *J Neurosci* 29:4218-4227.
- Aldrich MS, Garofalo EA, Drury I (1990) Epileptiform abnormalities during sleep in Rett syndrome. *Electroencephalogr Clin Neurophysiol* 75:365-370.
- Amir RE, Van den Veyver IB, Wan M, Tran CQ, Francke U, Zoghbi HY (1999) Rett syndrome is caused by mutations in X-linked MECP2, encoding methyl-CpG-binding protein 2. *Nat Genet* 23:185-188.
- Armstrong D, Dunn JK, Antalffy B, Trivedi R (1995) Selective dendritic alterations in the cortex of Rett syndrome. *J Neuropathol Exp Neurol* 54:195-201.
- Asaka Y, Jugloff DG, Zhang L, Eubanks JH, Fitzsimonds RM (2006) Hippocampal synaptic plasticity is impaired in the Mecp2-null mouse model of Rett syndrome. *Neurobiol Dis* 21:217-227.
- Bale TL, Lee K-F, Vale WW (2002) The Role of Corticotropin-Releasing Factor Receptors in Stress and Anxiety. *Integr Comp Biol* 42:552-555.
- Ballas N, Liroy DT, Grunseich C, Mandel G (2009) Non-cell autonomous influence of MeCP2-deficient glia on neuronal dendritic morphology. *Nat Neurosci* 12:311-317.
- Bauman ML, Kemper TL, Arin DM (1995) Pervasive neuroanatomic abnormalities of the brain in three cases of Rett's syndrome. *Neurology* 45:1581-1586.
- Belichenko NP, Belichenko PV, Mobley WC (2009a) Evidence for both neuronal cell autonomous and nonautonomous effects of methyl-CpG-binding protein 2 in the cerebral cortex of female mice with Mecp2 mutation. *Neurobiol Dis* 34:71-77.
- Belichenko PV, Oldfors A, Hagberg B, Dahlstrom A (1994) Rett syndrome: 3-D confocal microscopy of cortical pyramidal dendrites and afferents. *Neuroreport* 5:1509-1513.
- Belichenko PV, Wright EE, Belichenko NP, Masliah E, Li HH, Mobley WC, Francke U (2009b) Widespread changes in dendritic and axonal morphology in Mecp2-mutant mouse models of Rett syndrome: evidence for disruption of neuronal networks. *J Comp Neurol* 514:240-258.
- Ben-Ari Y (1985) Limbic seizure and brain damage produced by kainic acid: mechanisms and relevance to human temporal lobe epilepsy. *Neuroscience* 14:375-403.
- Benito E, Barco A (2010) CREB's control of intrinsic and synaptic plasticity: implications for CREB-dependent memory models. *Trends Neurosci* 33:230-240.
- Bird A (2007) Perceptions of epigenetics. *Nature* 447:396-398.

- Bird AP, Wolffe AP (1999) Methylation-Induced Repression— Belts, Braces, and Chromatin. *Cell* 99:451-454.
- Blue ME, Naidu S, Johnston MV (1999) Development of amino acid receptors in frontal cortex from girls with Rett syndrome. *Ann Neurol* 45:541-545.
- Burgoyne RD (2007) Neuronal Calcium Sensor Proteins: Generating Diversity in Neuronal Ca<sup>2+</sup> Signalling. *Nat Rev Neurosci* 8:182-193.
- Calfa G, Hablitz JJ, Pozzo-Miller L (2011) Network hyperexcitability in hippocampal slices from *Mecp2* mutant mice revealed by voltage-sensitive dye imaging. *J Neurophysiol* 105:1768-1784.
- Cardoza B, Clarke A, Wilcox J, Gibbon F, Smith PEM, Archer H, Hryniewiecka-Jaworska A, Kerr M (2011) Epilepsy in Rett syndrome: association between phenotype and genotype, and implications for practice. *Seizure* 20:646-649.
- Carlà V, Moroni F (1992) General anaesthetics inhibit the responses induced by glutamate receptor agonists in the mouse cortex. *Neurosci Lett* 146:21-24.
- Carrión AM, Link WA, Ledo F, Mellström B, Naranjo JR (1999) DREAM is a Ca<sup>2+</sup>-regulated transcriptional repressor. *Nature* 398:80-84.
- Chahrour M, Jung SY, Shaw C, Zhou X, Wong STC, Qin J, Zoghbi HY (2008) MeCP2, a key contributor to neurological disease, activates and represses transcription. *Science* 320:1224-1229.
- Chahrour M, Zoghbi HY (2007) The story of Rett syndrome: from clinic to neurobiology. *Neuron* 56:422-437.
- Chang BS, Lowenstein DH (2003) Epilepsy. *N Engl J Med* 349:1257-1266.
- Chang Q, Khare G, Dani V, Nelson S, Jaenisch R (2006) The disease progression of *Mecp2* mutant mice is affected by the level of BDNF expression. *Neuron* 49:341-348.
- Chao HT, Chen H, Samaco RC, Xue M, Chahrour M, Yoo J, Neul JL, Gong S, Lu HC, Heintz N, Ekker M, Rubenstein JL, Noebels JL, Rosenmund C, Zoghbi HY (2010) Dysfunction in GABA signalling mediates autism-like stereotypies and Rett syndrome phenotypes. *Nature* 468:263-269.
- Chao HT, Zoghbi HY, Rosenmund C (2007) MeCP2 controls excitatory synaptic strength by regulating glutamatergic synapse number. *Neuron* 56:58-65.
- Chapleau CA, Calfa GD, Lane MC, Albertson AJ, Larimore JL, Kudo S, Armstrong DL, Percy AK, Pozzo-Miller L (2009) Dendritic spine pathologies in hippocampal pyramidal neurons from Rett syndrome brain and after expression of Rett-associated MECP2 mutations. *Neurobiol Dis* 35:219-233.
- Chen RZ, Akbarian S, Tudor M, Jaenisch R (2001) Deficiency of methyl-CpG binding protein-2 in CNS neurons results in a Rett-like phenotype in mice. *Nat Genet* 27:327-331.

- Chen WG, Chang Q, Lin Y, Meissner A, West AE, Griffith EC, Jaenisch R, Greenberg ME (2003) Derepression of BDNF transcription involves calcium-dependent phosphorylation of MeCP2. *Science* 302:885-889.
- Cheung P, Tanner KG, Cheung WL, Sassone-Corsi P, Denu JM, Allis CD (2000) Synergistic coupling of histone H3 phosphorylation and acetylation in response to epidermal growth factor stimulation. *Mol Cell* 5:905-915.
- Cheval H, Guy J, Merusi C, De Sousa D, Selfridge J, Bird A (2012) Postnatal inactivation reveals enhanced requirement for MeCP2 at distinct age windows. *Hum Mol Genet* 21:3806-3814.
- Christodoulou J, Grimm A, Maher T, Bennetts B (2003) RettBASE: The IRSA MECP2 variation database—a new mutation database in evolution. *Human Mutation* 21:466-472.
- Chrivia JC, Kwok RP, Lamb N, Hagiwara M, Montminy MR, Goodman RH (1993) Phosphorylated CREB binds specifically to the nuclear protein CBP. *Nature* 365:855-859.
- Chwang WB, O’Riordan KJ, Levenson JM, Sweatt JD (2006) ERK/MAPK regulates hippocampal histone phosphorylation following contextual fear conditioning. *Learn Mem* 13:322-328.
- Clarke DJ, O’Neill LP, Turner BM (1993) Selective use of H4 acetylation sites in the yeast *Saccharomyces cerevisiae*. *Biochem J* 294 ( Pt 2):557-561.
- Cobb S, Guy J, Bird A (2010) Reversibility of functional deficits in experimental models of Rett syndrome. *Biochem Soc Trans* 38:498-506.
- Cohen S, Gabel HW, Hemberg M, Hutchinson AN, Sadacca LA, Ebert DH, Harmin DA, Greenberg RS, Verdine VK, Zhou Z, Wetsel WC, West AE, Greenberg ME (2011) Genome-wide activity-dependent MeCP2 phosphorylation regulates nervous system development and function. *Neuron* 72:72-85.
- Cole AJ, Saffen DW, Baraban JM, Worley PF (1989) Rapid increase of an immediate early gene messenger RNA in hippocampal neurons by synaptic NMDA receptor activation. *Nature* 340:474-476.
- Colic S, Wither R, Eubanks JH, Zhang L, Bardakjian BL (2011) EEG analysis for estimation of duration and inter-event intervals of seizure-like events recorded in vivo from mice. In: 2011 Annual International Conference of the IEEE Engineering in Medicine and Biology Society, EMBC, pp 2570 - 2573.
- Collingwood TN, Urnov FD, Wolffe AP (1999) Nuclear receptors: coactivators, corepressors and chromatin remodeling in the control of transcription. *J Mol Endocrinol* 23:255-275.
- Collins AL, Levenson JM, Vilaythong AP, Richman R, Armstrong DL, Noebels JL, David Sweatt J, Zoghbi HY (2004) Mild overexpression of MeCP2 causes a progressive neurological disorder in mice. *Hum Mol Genet* 13:2679-2689.

- Crosio C, Cermakian N, Allis CD, Sassone-Corsi P (2000) Light induces chromatin modification in cells of the mammalian circadian clock. *Nature Neuroscience* 3:1241-1247.
- Curran T, Morgan JI (1985) Superinduction of c-fos by nerve growth factor in the presence of peripherally active benzodiazepines. *Science* 229:1265-1268.
- D'Cruz JA, Wu C, Zahid T, El-Hayek Y, Zhang L, Eubanks JH (2010) Alterations of cortical and hippocampal EEG activity in MeCP2-deficient mice. *Neurobiol Dis* 38:8-16.
- Dani VS, Chang Q, Maffei A, Turrigiano GG, Jaenisch R, Nelson SB (2005) Reduced cortical activity due to a shift in the balance between excitation and inhibition in a mouse model of Rett syndrome. *Proc Natl Acad Sci U S A* 102:12560-12565.
- Derecki NC, Cronk JC, Lu Z, Xu E, Abbott SB, Guyenet PG, Kipnis J (2012) Wild-type microglia arrest pathology in a mouse model of Rett syndrome. *Nature* 484:105-109.
- Dolmetsch RE, Pajvani U, Fife K, Spotts JM, Greenberg ME (2001) Signaling to the nucleus by an L-type calcium channel-calmodulin complex through the MAP kinase pathway. *Science* 294:333-339.
- Dragunow M, Xu R, Walton M, Woodgate A, Lawlor P, MacGibbon GA, Young D, Gibbons H, Lipski J, Muravlev A, Pearson A, During M (2000) c-Jun promotes neurite outgrowth and survival in PC12 cells. *Brain Res Mol Brain Res* 83:20-33.
- Dugladze T, Schmitz D, Whittington MA, Vida I, Gloveli T (2012) Segregation of axonal and somatic activity during fast network oscillations. *Science* 336:1458-1461.
- Dulac C (2010) Brain function and chromatin plasticity. *Nature* 465:728-735.
- Fiala JC, Spacek J, Harris KM (2002) Dendritic spine pathology: cause or consequence of neurological disorders? *Brain Res Brain Res Rev* 39:29-54.
- Fisahn A (2005) Kainate receptors and rhythmic activity in neuronal networks: hippocampal gamma oscillations as a tool. *J Physiol (Lond)* 562:65-72.
- Free A, Wakefield RI, Smith BO, Dryden DT, Barlow PN, Bird AP (2001) DNA recognition by the methyl-CpG binding domain of MeCP2. *J Biol Chem* 276:3353-3360.
- Fukuda T, Itoh M, Ichikawa T, Washiyama K, Goto Y (2005) Delayed maturation of neuronal architecture and synaptogenesis in cerebral cortex of Mecp2-deficient mice. *J Neuropathol Exp Neurol* 64:537-544.
- Fyffe SL, Neul JL, Samaco RC, Chao HT, Ben-Shachar S, Moretti P, McGill BE, Goulding EH, Sullivan E, Tecott LH, Zoghbi HY (2008) Deletion of Mecp2 in Sim1-expressing neurons reveals a critical role for MeCP2 in feeding behavior, aggression, and the response to stress. *Neuron* 59:947-958.

- Gadalla KK, Bailey ME, Cobb SR (2011) MeCP2 and Rett syndrome: reversibility and potential avenues for therapy. *Biochem J* 439:1-14.
- Giacometti E, Luikenhuis S, Beard C, Jaenisch R (2007) Partial rescue of MeCP2 deficiency by postnatal activation of MeCP2. *Proc Natl Acad Sci USA* 104:1931-1936.
- Glaze DG (2005) Neurophysiology of Rett syndrome. *J Child Neurol* 20:740-746.
- Glaze DG, Frost JD Jr, Zoghbi HY, Percy AK (1987) Rett's syndrome. Correlation of electroencephalographic characteristics with clinical staging. *Arch Neurol* 44:1053-1056.
- Glaze DG, Percy AK, Skinner S, Motil KJ, Neul JL, Barrish JO, Lane JB, Geerts SP, Annese F, Graham J, McNair L, Lee H-S (2010) Epilepsy and the natural history of Rett syndrome. *Neurology* 74:909-912.
- Goffin D, Allen M, Zhang L, Amorim M, Wang I-TJ, Reyes A-RS, Mercado-Berton A, Ong C, Cohen S, Hu L, Blendy JA, Carlson GC, Siegel SJ, Greenberg ME, Zhou Z (2012) Rett syndrome mutation MeCP2 T158A disrupts DNA binding, protein stability and ERP responses. *Nat Neurosci* 15:274-283.
- Gonzales ML, Adams S, Dunaway KW, Lasalle JM (2012) Phosphorylation of Distinct Sites in MeCP2 Modifies Cofactor Associations and the Dynamics of Transcriptional Regulation. *Mol Cell Biol* 32:2894-2903.
- Greenberg ME, Ziff EB, Greene LA (1986) Stimulation of neuronal acetylcholine receptors induces rapid gene transcription. *Science* 234:80-83.
- Guy J, Cheval H, Selfridge J, Bird A (2011) The Role of MeCP2 in the Brain. *Annual Review of Cell and Developmental Biology* 27:631-652.
- Guy J, Gan J, Selfridge J, Cobb S, Bird A (2007) Reversal of neurological defects in a mouse model of Rett syndrome. *Science* 315:1143-1147.
- Guy J, Hendrich B, Holmes M, Martin JE, Bird A (2001) A mouse *Mecp2*-null mutation causes neurological symptoms that mimic Rett syndrome. *Nat Genet* 27:322-326.
- Hagberg B (2002) Clinical manifestations and stages of Rett syndrome. *Ment Retard Dev Disabil Res Rev* 8:61-65.
- Hagberg B (2005) Rett syndrome: long-term clinical follow-up experiences over four decades. *J Child Neurol* 20:722-727.
- Hagberg B, Aicardi J, Dias K, Ramos O (1983) A progressive syndrome of autism, dementia, ataxia, and loss of purposeful hand use in girls: Rett's syndrome: report of 35 cases. *Ann Neurol* 14:471-479.
- Hagberg B, Hanefeld F, Percy A, Skjeldal O (2002) An update on clinically applicable diagnostic criteria in Rett syndrome. Comments to Rett Syndrome Clinical Criteria Consensus Panel Satellite to European Paediatric Neurology Society Meeting, Baden Baden, Germany, 11 September 2001. *Eur J Paediatr Neurol* 6:293-297.

- Hagne I, Witt-Engerström I, Hagberg B (1989) EEG development in Rett syndrome. A study of 30 cases. *Electroencephalogr Clin Neurophysiol* 72:1-6.
- Halazonetis TD, Georgopoulos K, Greenberg ME, Leder P (1988) c-Jun dimerizes with itself and with c-Fos, forming complexes of different DNA binding affinities. *Cell* 55:917-924.
- Hardingham GE, Fukunaga Y, Bading H (2002) Extrasynaptic NMDARs oppose synaptic NMDARs by triggering CREB shut-off and cell death pathways. *Nat Neurosci* 5:405-414.
- Harrison NL, Kugler JL, Jones MV, Greenblatt EP, Pritchett DB (1993) Positive modulation of human gamma-aminobutyric acid type A and glycine receptors by the inhalation anesthetic isoflurane. *Mol Pharmacol* 44:628-632.
- Hasenstaub A, Shu Y, Haider B, Kraushaar U, Duque A, McCormick DA (2005) Inhibitory postsynaptic potentials carry synchronized frequency information in active cortical networks. *Neuron* 47:423-435.
- Hendrich B, Abbott C, McQueen H, Chambers D, Cross S, Bird A (1999) Genomic structure and chromosomal mapping of the murine and human Mbd1, Mbd2, Mbd3, and Mbd4 genes. *Mamm Genome* 10:906-912.
- Hendrich B, Bird A (1998) Identification and characterization of a family of mammalian methyl-CpG binding proteins. *Mol Cell Biol* 18:6538-6547.
- Herdegen T, Leah JD (1998) Inducible and constitutive transcription factors in the mammalian nervous system: control of gene expression by Jun, Fos and Krox, and CREB/ATF proteins. *Brain Res Brain Res Rev* 28:370-490.
- Hill CS, Treisman R (1999) Growth Factors and Gene Expression: Fresh Insights from Arrays. *Sci STKE* 1999:pe1.
- Horike S, Cai S, Miyano M, Cheng J-F, Kohwi-Shigematsu T (2005) Loss of silent-chromatin looping and impaired imprinting of DLX5 in Rett syndrome. *Nat Genet* 37:31-40.
- Hubel DH (1982) Exploration of the primary visual cortex, 1955-78. , Published online: 07 October 1982; | doi:10.1038/299515a0 299:515-524.
- Hutchinson AN, Deng JV, Aryal DK, Wetsel WC, West AE (2012) Differential regulation of MeCP2 phosphorylation in the CNS by dopamine and serotonin. *Neuropsychopharmacology* 37:321-337.
- Ishizaki A, Inoue Y, Sasaki H, Fukuyama Y (1989) Longitudinal observation of electroencephalograms in the Rett syndrome. *Brain Dev* 11:407-412.
- Jaenisch R, Bird A (2003) Epigenetic regulation of gene expression: how the genome integrates intrinsic and environmental signals. *Nat Genet* 33 Suppl:245-254.
- Jan MM, Dooley JM, Gordon KE (1999) Male Rett syndrome variant: application of diagnostic criteria. *Pediatr Neurol* 20:238-240.

- Johnson RA, Lam M, Punzo AM, Li H, Lin BR, Ye K, Mitchell GS, Chang Q (2011) 7,8-dihydroxyflavone (7,8-DHF) exhibits therapeutic efficacy in a mouse model of Rett syndrome. *J Appl Physiol* Available at: <http://www.ncbi.nlm.nih.gov/pubmed/22194327>.
- Jones PL, Veenstra GJ, Wade PA, Vermaak D, Kass SU, Landsberger N, Strouboulis J, Wolffe AP (1998) Methylated DNA and MeCP2 recruit histone deacetylase to repress transcription. *Nat Genet* 19:187-191.
- Kaludov NK, Wolffe AP (2000) MeCP2 driven transcriptional repression in vitro: selectivity for methylated DNA, action at a distance and contacts with the basal transcription machinery. *Nucleic Acids Res* 28:1921-1928.
- Katan-Khaykovich Y, Struhl K (2002) Dynamics of global histone acetylation and deacetylation in vivo: rapid restoration of normal histone acetylation status upon removal of activators and repressors. *Genes Dev* 16:743-752.
- Kaufmann WE, Jarrar MH, Wang JS, Lee Y-JM, Reddy S, Bibat G, Naidu S (2005) Histone modifications in Rett syndrome lymphocytes: a preliminary evaluation. *Brain Dev* 27:331-339.
- Kim HJ, Kim SH, Kim HD, Lee JS, Lee Y-M, Koo KY, Lee JS, Kang H-C (2012) Genetic and Epileptic Features in Rett Syndrome. *Yonsei Med J* 53:495-500.
- Kishi N, Macklis JD (2004) MECP2 is progressively expressed in post-migratory neurons and is involved in neuronal maturation rather than cell fate decisions. *Mol Cell Neurosci* 27:306-321.
- Kishi N, Macklis JD (2010) MeCP2 functions largely cell-autonomously, but also non-cell-autonomously, in neuronal maturation and dendritic arborization of cortical pyramidal neurons. *Exp Neurol* 222:51-58.
- Kouzarides T (2007) Chromatin modifications and their function. *Cell* 128:693-705.
- Kuo MH, Brownell JE, Sobel RE, Ranalli TA, Cook RG, Edmondson DG, Roth SY, Allis CD (1996) Transcription-linked acetylation by Gcn5p of histones H3 and H4 at specific lysines. *Nature* 383:269-272.
- Ladas T, Chan SA, Ogier M, Smith C, Katz DM (2009) Enhanced dense core granule function and adrenal hypersecretion in a mouse model of Rett syndrome. *Eur J Neurosci* 30:602-610.
- Lanahan A, Worley P (1998) Immediate-Early Genes and Synaptic Function. *Neurobiology of Learning and Memory* 70:37-43.
- LaSalle JM (2007) The Odyssey of MeCP2 and Parental Imprinting. *Epigenetics* 2:5-10.
- Ledda M, Barni L, Altieri L, Pannese E (2000) Decrease in the nucleo-cytoplasmic volume ratio of rabbit spinal ganglion neurons with age. *Neuroscience Letters* 286:171-174.

- Lemaire P, Revelant O, Bravo R, Charnay P (1988) Two mouse genes encoding potential transcription factors with identical DNA-binding domains are activated by growth factors in cultured cells. *Proc Natl Acad Sci USA* 85:4691-4695.
- Lewis JD, Meehan RR, Henzel WJ, Maurer-Fogy I, Jeppesen P, Klein F, Bird A (1992) Purification, sequence, and cellular localization of a novel chromosomal protein that binds to methylated DNA. *Cell* 69:905-914.
- Li E, Beard C, Jaenisch R (1993) Role for DNA methylation in genomic imprinting. *Nature* 366:362-365.
- Li H, Zhong X, Chau KF, Williams EC, Chang Q (2011) Loss of activity-induced phosphorylation of MeCP2 enhances synaptogenesis, LTP and spatial memory. *Nat Neurosci* 14:1001-1008.
- Liao W, Gandal MJ, Ehrlichman RS, Siegel SJ, Carlson GC (2012) MeCP2<sup>+/-</sup> mouse model of RTT reproduces auditory phenotypes associated with Rett syndrome and replicate select EEG endophenotypes of autism spectrum disorder. *Neurobiol Dis* 46:88-92.
- Lioy DT, Garg SK, Monaghan CE, Raber J, Foust KD, Kaspar BK, Hirrlinger PG, Kirchhoff F, Bissonnette JM, Ballas N, Mandel G (2011) A role for glia in the progression of Rett's syndrome. *Nature* 475:497-500.
- Luikenhuis S, Giacometti E, Beard CF, Jaenisch R (2004) Expression of MeCP2 in postmitotic neurons rescues Rett syndrome in mice. *Proc Natl Acad Sci U S A* 101:6033-6038.
- Ma DK, Jang M-H, Guo JU, Kitabatake Y, Chang M, Pow-anpongkul N, Flavell RA, Lu B, Ming G, Song H (2009) Neuronal Activity-Induced Gadd45b Promotes Epigenetic DNA Demethylation and Adult Neurogenesis. *Science* 323:1074-1077.
- MacDonald JL, Roskams AJ (2009) Epigenetic regulation of nervous system development by DNA methylation and histone deacetylation. *Prog Neurobiol* 88:170-183.
- Maezawa I, Jin LW (2010) Rett syndrome microglia damage dendrites and synapses by the elevated release of glutamate. *J Neurosci* 30:5346-5356.
- Maliszewska-Cyna E, Bawa D, Eubanks JH (2010) Diminished prevalence but preserved synaptic distribution of N-methyl-d-aspartate receptor subunits in the methyl CpG binding protein 2(MeCP2)-null mouse brain. *Neuroscience* 168:624-632.
- Mao L-M, Horton E, Guo M-L, Xue B, Jin D-Z, Fibuch EE, Wang JQ (2011) Cocaine increases phosphorylation of MeCP2 in the rat striatum in vivo: a differential role of NMDA receptors. *Neurochem Int* 59:610-617.
- Marek KW, Kurtz LM, Spitzer NC (2010) cJun integrates calcium activity and tlx3 expression to regulate neurotransmitter specification. *Nat Neurosci* 13:944-950.

- Matsui T, Segall J, Weil PA, Roeder RG (1980) Multiple factors required for accurate initiation of transcription by purified RNA polymerase II. *J Biol Chem* 255:11992-11996.
- Matsuura T, Sutcliffe JS, Fang P, Galjaard RJ, Jiang YH, Benton CS, Rommens JM, Beaudet AL (1997) De novo truncating mutations in E6-AP ubiquitin-protein ligase gene (UBE3A) in Angelman syndrome. *Nat Genet* 15:74-77.
- McEwen BS (2000) The neurobiology of stress: from serendipity to clinical relevance. *Brain Res* 886:172-189.
- McGill BE, Bundle SF, Yaylaoglu MB, Carson JP, Thaller C, Zoghbi HY (2006) Enhanced anxiety and stress-induced corticosterone release are associated with increased Crh expression in a mouse model of Rett syndrome. *Proc Natl Acad Sci U S A* 103:18267-18272.
- McGraw CM, Samaco RC, Zoghbi HY (2011) Adult Neural Function Requires MeCP2. *Science* Available at: <http://www.ncbi.nlm.nih.gov/pubmed/21636743>.
- McIntyre J, Moral MA, Bozzo J (2007) Combination therapy with valproic acid in cancer: Initial clinical approach. *Drugs of the Future* 32:45.
- Medrihan L, Tantalaki E, Aramuni G, Sargsyan V, Dudanova I, Missler M, Zhang W (2008) Early defects of GABAergic synapses in the brain stem of a MeCP2 mouse model of Rett syndrome. *J Neurophysiol* 99:112-121.
- Meehan RR, Lewis JD, McKay S, Kleiner EL, Bird AP (1989) Identification of a mammalian protein that binds specifically to DNA containing methylated CpGs. *Cell* 58:499-507.
- Meffert MK, Baltimore D (2005) Physiological functions for brain NF-kappaB. *Trends Neurosci* 28:37-43.
- Meffert MK, Chang JM, Wiltgen BJ, Fanselow MS, Baltimore D (2003) NF-kappaB functions in synaptic signaling and behavior. *Nature Neuroscience* 6:1072-1078.
- Mehler MF (2008) Epigenetic principles and mechanisms underlying nervous system functions in health and disease. *Progress in Neurobiology* 86:305-341.
- Mercurio F, Zhu H, Murray BW, Shevchenko A, Bennett BL, Li J, Young DB, Barbosa M, Mann M, Manning A, Rao A (1997) IKK-1 and IKK-2: cytokine-activated I-kappaB kinases essential for NF-kappaB activation. *Science* 278:860-866.
- Mnatzakanian GN, Lohi H, Munteanu I, Alfred SE, Yamada T, MacLeod PJ, Jones JR, Scherer SW, Schanen NC, Friez MJ, Vincent JB, Minassian BA (2004) A previously unidentified MECP2 open reading frame defines a new protein isoform relevant to Rett syndrome. *Nat Genet* 36:339-341.
- Moretti P, Levenson JM, Battaglia F, Atkinson R, Teague R, Antalffy B, Armstrong D, Arancio O, Sweatt JD, Zoghbi HY (2006) Learning and memory and

- synaptic plasticity are impaired in a mouse model of Rett syndrome. *J Neurosci* 26:319-327.
- Moretti P, Zoghbi HY (2006) MeCP2 dysfunction in Rett syndrome and related disorders. *Curr Opin Genet Dev* 16:276-281.
- Morgan JI, Curran T (1986) Role of ion flux in the control of c-fos expression. *Nature* 322:552-555.
- Murphy TH, Worley PF, Baraban JM (1991) L-type voltage-sensitive calcium channels mediate synaptic activation of immediate early genes. *Neuron* 7:625-635.
- Na ES, Nelson ED, Adachi M, Autry AE, Mahgoub MA, Kavalali ET, Monteggia LM (2012) A mouse model for MeCP2 duplication syndrome: MeCP2 overexpression impairs learning and memory and synaptic transmission. *J Neurosci* 32:3109-3117.
- Nagai K, Miyake K, Kubota T (2005) A transcriptional repressor MeCP2 causing Rett syndrome is expressed in embryonic non-neuronal cells and controls their growth. *Brain Res Dev Brain Res* 157:103-106.
- Nan X, Campoy FJ, Bird A (1997) MeCP2 is a transcriptional repressor with abundant binding sites in genomic chromatin. *Cell* 88:471-481.
- Nan X, Ng HH, Johnson CA, Laherty CD, Turner BM, Eisenman RN, Bird A (1998) Transcriptional repression by the methyl-CpG-binding protein MeCP2 involves a histone deacetylase complex. *Nature* 393:386-389.
- Nelson ED, Kavalali ET, Monteggia LM (2006) MeCP2-dependent transcriptional repression regulates excitatory neurotransmission. *Curr Biol* 16:710-716.
- Neul JL, Fang P, Barrish J, Lane J, Caeg EB, Smith EO, Zoghbi H, Percy A, Glaze DG (2008) Specific mutations in methyl-CpG-binding protein 2 confer different severity in Rett syndrome. *Neurology* 70:1313-1321.
- Neul JL, Kaufmann WE, Glaze DG, Christodoulou J, Clarke AJ, Bahi-Buisson N, Leonard H, Bailey ME, Schanen NC, Zappella M, Renieri A, Huppke P, Percy AK (2010) Rett syndrome: revised diagnostic criteria and nomenclature. *Ann Neurol* 68:944-950.
- Nguyen MVC, Du F, Felice CA, Shan X, Nigam A, Mandel G, Robinson JK, Ballas N (2012) MeCP2 Is Critical for Maintaining Mature Neuronal Networks and Global Brain Anatomy during Late Stages of Postnatal Brain Development and in the Mature Adult Brain. *J Neurosci* 32:10021-10034.
- Niedermeyer E, Naidu SB, Plate C (1997) Unusual EEG theta rhythms over central region in Rett syndrome: considerations of the underlying dysfunction. *Clin Electroencephalogr* 28:36-43.
- Nikitina T, Shi X, Ghosh RP, Horowitz-Scherer RA, Hansen JC, Woodcock CL (2007) Multiple modes of interaction between the methylated DNA binding protein MeCP2 and chromatin. *Mol Cell Biol* 27:864-877.

- Noma K, Allis CD, Grewal SI (2001) Transitions in distinct histone H3 methylation patterns at the heterochromatin domain boundaries. *Science* 293:1150-1155.
- Nuber UA, Kriaucionis S, Roloff TC, Guy J, Selfridge J, Steinhoff C, Schulz R, Lipkowitz B, Ropers HH, Holmes MC, Bird A (2005) Up-regulation of glucocorticoid-regulated genes in a mouse model of Rett syndrome. *Hum Mol Genet* 14:2247-2256.
- Okano M, Bell DW, Haber DA, Li E (1999) DNA methyltransferases Dnmt3a and Dnmt3b are essential for de novo methylation and mammalian development. *Cell* 99:247-257.
- Patel AJ, Honoré E, Lesage F, Fink M, Romey G, Lazdunski M (1999) Inhalational anesthetics activate two-pore-domain background K<sup>+</sup> channels. *Nat Neurosci* 2:422-426.
- Peltier SJ, Kerssens C, Hamann SB, Sebel PS, Byas-Smith M, Hu X (2005) Functional connectivity changes with concentration of sevoflurane anesthesia. *Neuroreport* 16:285-288.
- Percy AK, Lane JB, Childers J, Skinner S, Annese F, Barrish J, Caeg E, Glaze DG, MacLeod P (2007) Rett syndrome: North American database. *J Child Neurol* 22:1338-1341.
- Popovici T, Represa A, Crépel V, Barbin G, Beaudoin M, Ben-Ari Y (1990) Effects of kainic acid-induced seizures and ischemia on c-fos-like proteins in rat brain. *Brain Res* 536:183-194.
- Racine RJ (1972) Modification of seizure activity by electrical stimulation. II. Motor seizure. *Electroencephalogr Clin Neurophysiol* 32:281-294.
- Rett A (1966) [On a unusual brain atrophy syndrome in hyperammonemia in childhood]. *Wien Med Wochenschr* 116:723-726.
- Riccio A (2010) Dynamic epigenetic regulation in neurons: enzymes, stimuli and signaling pathways. *Nat Neurosci* 13:1330-1337.
- Robinson L, Guy J, McKay L, Brockett E, Spike R, Selfridge J, De Sousa D, Merusi C, Riedel G, Bird A, Cobb SR (2012) Morphological and functional reversal of phenotypes in a mouse model of Rett syndrome. *Brain* In press.
- Roh T-Y, Cuddapah S, Zhao K (2005) Active chromatin domains are defined by acetylation islands revealed by genome-wide mapping. *Genes Dev* 19:542-552.
- Salomão Schwartzman J, Zatz M, dos Reis Vasquez L, Ribeiro Gomes R, Koiffmann CP, Fridman C, Guimarães Otto P (1999) Rett syndrome in a boy with a 47,XXY karyotype. *Am J Hum Genet* 64:1781-1785.
- Samaco RC, Mandel-Brehm C, Chao H-T, Ward CS, Fyffe-Maricich SL, Ren J, Hyland K, Thaller C, Maricich SM, Humphreys P, Greer JJ, Percy A, Glaze DG, Zoghbi HY, Neul JL (2009) Loss of MeCP2 in aminergic neurons causes

cell-autonomous defects in neurotransmitter synthesis and specific behavioral abnormalities. *Proc Natl Acad Sci USA* 106:21966-21971.

- Schauwecker PE, Steward O (1997) Genetic determinants of susceptibility to excitotoxic cell death: Implications for gene targeting approaches. *Proc Natl Acad Sci U S A* 94:4103-4108.
- Schüle B, Li HH, Fisch-Kohl C, Purmann C, Francke U (2007) DLX5 and DLX6 Expression Is Biallelic and Not Modulated by MeCP2 Deficiency. *Am J Hum Genet* 81:492-506.
- Schultz RJ, Glaze DG, Motil KJ, Armstrong DD, del Junco DJ, Hubbard CR, Percy AK (1993) The pattern of growth failure in Rett syndrome. *Am J Dis Child* 147:633-637.
- Shahbazian M, Young J, Yuva-Paylor L, Spencer C, Antalffy B, Noebels J, Armstrong D, Paylor R, Zoghbi H (2002) Mice with truncated MeCP2 recapitulate many Rett syndrome features and display hyperacetylation of histone H3. *Neuron* 35:243-254.
- Shaywitz AJ, Greenberg ME (1999) CREB: a stimulus-induced transcription factor activated by a diverse array of extracellular signals. *Annu Rev Biochem* 68:821-861.
- Singleton MK, Gonzales ML, Leung KN, Yasui DH, Schroeder DI, Dunaway K, LaSalle JM (2011) MeCP2 is required for global heterochromatic and nucleolar changes during activity-dependent neuronal maturation. *Neurobiol Dis* 43:190-200.
- Skene PJ, Illingsworth RS, Webb S, Kerr A, James KD, Turner DJ, Andrews R, Bird A (2010) Neuronal MeCP2 is expressed at near histone-octamer levels and globally alters the chromatin state. *Mol Cell* In press.
- Smeets E, Terhal P, Casaer P, Peters A, Midro A, Schollen E, van Roozendaal K, Moog U, Matthijs G, Herbergs J, Smeets H, Curfs L, Schrandt-Stumpel C, Fryns JP (2005) Rett syndrome in females with CTS hot spot deletions: a disorder profile. *Am J Med Genet A* 132A:117-120.
- Smrt RD, Eaves-Egenes J, Barkho BZ, Santistevan NJ, Zhao C, Aimone JB, Gage FH, Zhao X (2007) Mecp2 deficiency leads to delayed maturation and altered gene expression in hippocampal neurons. *Neurobiol Dis* 27:77-89.
- Sng JCG, Taniura H, Yoneda Y (2005) Inhibition of histone deacetylation by trichostatin A intensifies the transcriptions of neuronal c-fos and c-jun genes after kainate stimulation. *Neurosci Lett* 386:150-155.
- Sng JCG, Taniura H, Yoneda Y (2006) Histone modifications in kainate-induced status epilepticus. *Eur J Neurosci* 23:1269-1282.
- Sperk G, Lassmann H, Baran H, Kish SJ, Seitelberger F, Hornykiewicz O (1983) Kainic acid induced seizures: neurochemical and histopathological changes. *Neuroscience* 10:1301-1315.

- Steffenburg U, Hagberg G, Hagberg B (2001) Epilepsy in a representative series of Rett syndrome. *Acta Paediatr* 90:34-39.
- Su D, Cha YM, West AE (2012) Mutation of MeCP2 alters transcriptional regulation of select immediate-early genes. *Epigenetics* 7:146-154.
- Sutcliffe JS, Nelson DL, Zhang F, Pieretti M, Caskey CT, Saxe D, Warren ST (1992) DNA methylation represses FMR-1 transcription in fragile X syndrome. *Human Molecular Genetics* 1:397-400.
- Swanberg SE, Nagarajan RP, Peddada S, Yasui DH, LaSalle JM (2009) Reciprocal co-regulation of EGR2 and MECP2 is disrupted in Rett syndrome and autism. *Hum Mol Genet* 18:525-534.
- Taneja P, Ogier M, Brooks-Harris G, Schmid DA, Katz DM, Nelson SB (2009) Pathophysiology of locus ceruleus neurons in a mouse model of Rett syndrome. *J Neurosci* 29:12187-12195.
- Tao J, Hu K, Chang Q, Wu H, Sherman NE, Martinowich K, Klose RJ, Schanen C, Jaenisch R, Wang W, Sun YE (2009) Phosphorylation of MeCP2 at Serine 80 regulates its chromatin association and neurological function. *Proc Natl Acad Sci USA* 106:4882-4887.
- Tao S, Yang X, Chen Y, Wang X, Xiao Z, Wang H, Wu Q, Wang X (2012) Up-Regulated Methyl CpG Binding Protein-2 in Intractable Temporal Lobe Epilepsy Patients and a Rat Model. *Neurochemical research* Available at: <http://www.ncbi.nlm.nih.gov/pubmed/22707285> [Accessed July 10, 2012].
- Thatcher KN, LaSalle JM (2006) Dynamic changes in Histone H3 lysine 9 acetylation localization patterns during neuronal maturation require MeCP2. *Epigenetics* 1:24-31.
- Trappe R, Laccone F, Cobilanschi J, Meins M, Huppke P, Hanefeld F, Engel W (2001) MECP2 Mutations in Sporadic Cases of Rett Syndrome Are Almost Exclusively of Paternal Origin. *Am J Hum Genet* 68:1093-1101.
- Traub RD, Cunningham MO, Gloveli T, LeBeau FEN, Bibbig A, Buhl EH, Whittington MA (2003) GABA-enhanced collective behavior in neuronal axons underlies persistent gamma-frequency oscillations. *PNAS* 100:11047-11052.
- Traub RD, Jefferys JG (1994) Are there unifying principles underlying the generation of epileptic afterdischarges in vitro? *Prog Brain Res* 102:383-394.
- Traub RD, Spruston N, Soltesz I, Konnerth A, Whittington MA, Jefferys GR (1998) Gamma-frequency oscillations: a neuronal population phenomenon, regulated by synaptic and intrinsic cellular processes, and inducing synaptic plasticity. *Prog Neurobiol* 55:563-575.
- Traverse S, Seedorf K, Paterson H, Marshall CJ, Cohen P, Ullrich A (1994) EGF triggers neuronal differentiation of PC12 cells that overexpress the EGF receptor. *Curr Biol* 4:694-701.

- Tropea D, Giacometti E, Wilson NR, Beard C, McCurry C, Fu DD, Flannery R, Jaenisch R, Sur M (2009) Partial reversal of Rett Syndrome-like symptoms in MeCP2 mutant mice. *Proc Natl Acad Sci U S A* 106:2029-2034.
- Tsien JZ, Chen DF, Gerber D, Tom C, Mercer EH, Anderson DJ, Mayford M, Kandel ER, Tonegawa S (1996) Subregion- and cell type-restricted gene knockout in mouse brain. *Cell* 87:1317-1326.
- Tudor M, Akbarian S, Chen RZ, Jaenisch R (2002) Transcriptional profiling of a mouse model for Rett syndrome reveals subtle transcriptional changes in the brain. *PNAS* 99:15536-15541.
- Turner BM (1991) Histone acetylation and control of gene expression. *J Cell Sci* 99:13-20.
- Urduingio RG, Pino I, Ropero S, Fraga MF, Esteller M (2007) Histone H3 and H4 modification profiles in a Rett syndrome mouse model. *Epigenetics* 2:11-14.
- van Nimwegen E (2003) Scaling laws in the functional content of genomes. *Trends in Genetics* 19:479-484.
- Victor Nadler J (1981) Kainic acid as a tool for the study of temporal lobe epilepsy. *Life Sciences* 29:2031-2042.
- Wan M, Zhao K, Lee SS, Francke U (2001) MECP2 truncating mutations cause histone H4 hyperacetylation in Rett syndrome. *Hum Mol Genet* 10:1085-1092.
- Waters CM, Hancock DC, Evan GI (1990) Identification and characterisation of the *egr-1* gene product as an inducible, short-lived, nuclear phosphoprotein. *Oncogene* 5:669-674.
- Wei Y, Yu L, Bowen J, Gorovsky MA, Allis CD (1999) Phosphorylation of histone H3 is required for proper chromosome condensation and segregation. *Cell* 97:99-109.
- Weng SM, McLeod F, Bailey ME, Cobb SR (2011) Synaptic plasticity deficits in an experimental model of Rett syndrome: long term potentiation saturation and its pharmacological reversal. *Neuroscience* 180:314-21.
- West AE, Greenberg ME (2011) Neuronal activity-regulated gene transcription in synapse development and cognitive function. *Cold Spring Harb Perspect Biol* 3 Available at: <http://www.ncbi.nlm.nih.gov/pubmed/21555405> [Accessed July 21, 2012].
- Whittington MA, Traub RD, Jefferys JG (1995) Synchronized oscillations in interneuron networks driven by metabotropic glutamate receptor activation. *Nature* 373:612-615.
- Wisden W, Errington ML, Williams S, Dunnett SB, Waters C, Hitchcock D, Evan G, Bliss TV, Hunt SP (1990) Differential expression of immediate early genes in the hippocampus and spinal cord. *Neuron* 4:603-614.

- Wither RG, Colic S, Wu C, Bardakjian BL, Zhang L, Eubanks JH (2012) Daily Rhythmic Behaviors and Thermoregulatory Patterns Are Disrupted in Adult Female MeCP2-Deficient Mice. *PLoS ONE* 7:e35396.
- Wood L, Gray NW, Zhou Z, Greenberg ME, Shepherd GMG (2009) Synaptic circuit abnormalities of motor-frontal layer 2/3 pyramidal neurons in an RNA interference model of methyl-CpG-binding protein 2 deficiency. *J Neurosci* 29:12440-12448.
- Worley PF, Christy BA, Nakabeppu Y, Bhat RV, Cole AJ, Baraban JM (1991) Constitutive expression of zif268 in neocortex is regulated by synaptic activity. *Proc Natl Acad Sci USA* 88:5106-5110.
- Xiang F, Zhang Z, Clarke A, Joseluiz P, Sakkubai N, Sarojini B, Delozier-Blanchet CD, Hansmann I, Edström L, Anvret M (1998) Chromosome mapping of Rett syndrome: a likely candidate region on the telomere of Xq. *J Med Genet* 35:297-300.
- Xu M, Long C, Chen X, Huang C, Chen S, Zhu B (2010) Partitioning of histone H3-H4 tetramers during DNA replication-dependent chromatin assembly. *Science* 328:94-98.
- Yasui DH, Peddada S, Bieda MC, Vallero RO, Hogart A, Nagarajan RP, Thatcher KN, Farnham PJ, Lasalle JM (2007) Integrated epigenomic analyses of neuronal MeCP2 reveal a role for long-range interaction with active genes. *Proc Natl Acad Sci USA* 104:19416-19421.
- Yazdani M, Deogracias R, Guy J, Poot RA, Bird A, Barde Y-A (2012) Disease Modeling Using Embryonic Stem Cells: MeCP2 Regulates Nuclear Size and RNA Synthesis in Neurons. *STEM CELLS*:N/A-N/A.
- Yoder JA, Soman NS, Verdine GL, Bestor TH (1997) DNA (cytosine-5)-methyltransferases in mouse cells and tissues. Studies with a mechanism-based probe. *J Mol Biol* 270:385-395.
- Yusufzai TM, Wolffe AP (2000) Functional consequences of Rett syndrome mutations on human MeCP2. *Nucleic Acids Res* 28:4172-4179.
- Zhang J, Zhang D, McQuade JS, Behbehani M, Tsien JZ, Xu M (2002) c-fos regulates neuronal excitability and survival. *Nat Genet* 30:416-420.
- Zhang L, He J, Jugloff DG, Eubanks JH (2008) The MeCP2-null mouse hippocampus displays altered basal inhibitory rhythms and is prone to hyperexcitability. *Hippocampus* 18:294-309.
- Zhang Z-W, Zak JD, Liu H (2010) MeCP2 is required for normal development of GABAergic circuits in the thalamus. *J Neurophysiol* 103:2470-2481.
- Zhou Z, Hong EJ, Cohen S, Zhao WN, Ho HY, Schmidt L, Chen WG, Lin Y, Savner E, Griffith EC, Hu L, Steen JA, Weitz CJ, Greenberg ME (2006) Brain-specific phosphorylation of MeCP2 regulates activity-dependent Bdnf transcription, dendritic growth, and spine maturation. *Neuron* 52:255-269.